UNIVERSITE D'AIX-MARSEILLE

ECOLE DOCTORALE 352 – PHYSIQUE ET SCIENCE DE LA MATIERE

Laboratoire d'accueil : CEA / DEN / CAD / DER / SPRC / Laboratoire d'Etudes Physique

THÈSE PRÉSENTÉE POUR L'OBTENTION DU GRADE DE DOCTEUR
Discipline : Énergie, Rayonnement, Plasma

Paul DUFAY

Quantification des biais et incertitudes sur l'effet en réactivité de vidange sodium dans le cœur d'ASTRID à l'aide des mesures intégrales

Soutenue le 18/10/2018 devant le jury :

Gilles BAN	Professeur (ENSICAEN/LPC)	Président de jury
Andrei RINEISKI	Directeur de Recherche (KIT/TRANS)	Rapporteur
Nuria GARCIA HERRANZ	Professeur associé (UPM/ETSI)	Rapporteur
Adrien BIDAUD	Professeur (GRENOBLE INP)	Examinateur
José BUSTO	Professeur (CNRS/CPPM)	Examinateur
Gérald RIMPAULT	Directeur de recherche (CEA/SPRC)	Directeur de thèse

Numéro national de thèse/suffixe local : 2018AIXM0334/043ED352

This page has been left blank intentionally

Résumé

Le 21ème siècle a vu le boom économique de pays comme la Chine, l'Inde et le Brésil et doit faire face au réchauffement climatique qui menace l'écosystème et les populations côtières. L'énergie nucléaire est l'une des plus propres en matière d'émission de gaz à effet de serre et, malgré ses atouts, n'est développée que dans quelques pays du monde. La sûreté reste une question ouverte pour l'avenir de cette énergie après l'accident de Fukushima. En France, la loi de 2006 sur la gestion des déchets soutient le développement d'une nouvelle génération de réacteurs nucléaires et du prototype de Réacteur Technologiquement Avancé au Sodium pour la Démonstration Industrielle (projet ASTRID) qui vise à apporter une réponse industrielle et technologique à de nombreux enjeux de ce siècle. En effet, cette nouvelle génération doit être économiquement compétitive, transmuter les déchets radioactifs, faciliter la gestion du combustible en utilisant tout le minerai d'uranium et obtenir des normes de sûreté identiques ou supérieures à celles des réacteurs les plus récents, c'est-à-dire EPR.

L'une des préoccupations de la technologie du Réacteur à Neutrons Rapides et caloporteur sodium (RNR Na) est la perte de ce dernier car elle pourrait entraîner un emballement de la réaction en chaîne si l'effet en réactivité de vidange sodium (SVRE) est positif. Lorsque le sodium est retiré du cœur, deux effets antagonistes se produisent qui affectent l'équilibre neutronique: l'un augmente la réactivité du cœur et est appelé la composante centrale (CC) et l'autre est la composante de fuite (LC) avec un effet négatif sur la réactivité. Maximiser la dernière composante est l'une des réponses pour augmenter la sûreté inhérente aux RNR-Na. C'est pourquoi le CEA a développé un concept de cœur innovant: le «Cœur à Faible Vidange» (CFV) qui donne un SVRE négatif. Cependant, de telles innovations doivent être validées expérimentalement et l'incertitude sur cet effet en réactivité doit être maîtrisée. En soutien au développement des RNR Na : la base de données expérimentale existante est assez importante avec, par exemple, dans les installations expérimentales de MASURCA au CEA de Cadarache (France), les programmes expérimentaux PRE-RACINE et CIRANO avec de nombreuses configurations différentes. De plus, dans l'installation expérimentale BFS à Obninsk (Russie), deux programmes expérimentaux dédiés aux spécificités du cœur CFV ont été réalisés en collaboration entre le CEA.

L'objectif de cette thèse est de maîtriser les différentes sources d'incertitudes dans le calcul de l'effet de réactivité de vidange sodium et d'utiliser les expériences intégrales pour prédire l'effet de réactivité de vidange sodium du cœur CFV d'ASTRID ainsi que son incertitude.

Dans les différents programmes expérimentaux considérés, l'effet en réactivité de vidange sodium (SVRE) est mesuré pour des zones de tailles différentes afin de faire varier l'importance relative des composantes centrales et de fuites. Les réglettes ou les plaquettes de sodium sont remplacées progressivement par des réglettes ou des plaquettes vides. La réactivité est mesurée par la position de la barre de pilotage et/ou par l'ajout d'assemblages périphériques. Une chute de barre et l'utilisation de l'équation de Nordheim assurent l'étalonnage de la réactivité. Cette réactivité est mesurée sur une échelle en β_{eff} qui est la fraction neutronique retardée du cœur. Une nouvelle analyse des β_{eff} mesurés dans le programme BERENICE (dans l'installation MASURCA) a donc été faite en utilisant le code Monte Carlo TRIPOLI4® avec la méthode de probabilité de fission (IFP) nouvellement développée pour le calcul des intégrales. Ces intégrales ont été utilisées pour réévaluer la valeur calculée mais également les corrections calculées des valeurs mesurées. Le code TRIPOLI-4® donne du crédit aux codes déterministes tels que ERANOS pour le calcul de β_{eff}. Cependant, l'atout de TRIPOLI-4® est la possibilité d'obtenir une

meilleure représentation des cœurs expérimentaux, en particulier le cœur expérimental ZONA2 qui présente de larges canaux expérimentaux pour l'hébergement de grandes chambres à fission. Pour JEFF-3.2, les ratios C/E revisités sont de 1,2% ± 3,6% pour le cœur ZONA2 lors de l'utilisation de la technique de mesure du bruit. La propagation de l'incertitude des données nucléaires a conduit à une incertitude de 2,6% pour le cœur U-Pu, les principaux contributeurs étant le rendement de fission de neutrons retardés et la section efficace de fission des valeurs U238. Ceci permet de revisiter plus précisément les expériences dédiées aux mesures de réactivité de vidange sodium.

Pour analyser l'effet en réactivité des vidanges sodium, nous le séparons en deux composantes: la composante centrale (CC) qui est un effet en réactivité positif dû aux changements de spectre et la composante de fuite (LC) qui est un effet en réactivité négatif dû à l'augmentation du libre parcours moyen des neutrons. Afin d'étudier en détail l'incertitude associée au calcul du SVRE, on a développé une procédure innovante basée sur la théorie des perturbations généralisées pour calculer les sensibilités de la CC et de la LC indépendamment. Avec de telles sensibilités et l'utilisation de la matrice de covariance COMAC-V2, nous sommes capables de calculer les incertitudes dues aux données nucléaires sur chaque composante en utilisant des données nucléaires JEFF-3.2. L'utilisation de cette méthode sur le cœur CFV d'ASTRID montre une incertitude de 2,6% sur la CC, une incertitude de 2,0% sur la LC et un effet de 18% sur la réactivité totale du vide de sodium avec très peu de corrélation entre les deux ($-0{,}002$).

Cette approche a permis d'étudier des programmes expérimentaux réalisés dans des installations critiques comme MASURCA. L'analyse indépendante de chaque composante (CC et LC) de la SVRE a été développée dans le cadre de ce travail de thèse. L'utilisation d'une approche déterministe et stochastique est obligatoire car même si le code Monte-Carlo TRIPOLI-4® donne des résultats de référence en utilisant les géométries «exactes » des cœurs, la perturbation généralisée n'a pas encore été implémentée dans ce code. Le code déterministe ERANOS du CEA est donc utilisé en complément pour le calcul des sensibilités et incertitudes sur l'effet de vidange global mais aussi sur la composante centrale (CC) et la composante de fuites (LC).

Une fois les simulations effectuées pour chaque configuration des divers programmes expérimentaux, il est possible d'évaluer la représentativité de différents programmes expérimentaux avec le cœur CFV d'ASTRID mais aussi d'ajuster les résultats d'ERANOS et de TRIPOLI-4® avec l'expérience grâce à un jeu de paramètre (α,β) et d'obtenir des incertitudes sur ces paramètres. Ce travail a été conduit pour l'ensemble des programmes expérimentaux considérés et a montré que les résultats de TRIPOLI-4® surestiment la composante centrale des zones combustibles lorsqu'elles sont vidangées de 11,3% et aussi la composante de fuites lorsque le plenum sodium est vidangé de 6%. Ces écarts ne sont pas cohérents lorsque l'on regarde les incertitudes expérimentales et statistiques à 1σ (qui sont respectivement pour la CC et la LC de 4,8% en zone combustible et de 1,8% en zone plenum) et aussi celles dues aux données nucléaires qui sont de 3,1% sur la CC et de 2,1% sur la LC. On suspecte une sous-estimation des incertitudes sur les données nucléaires en particulier pour le sodium avec COMAC-V2.

Abstract

The 21st century has seen the economic boom of countries like China, India and Brazil and has to face a new issue: the global warming which is threatening the ecosystem and coastal population. The nuclear energy is one of the cleanest energy with respect to greenhouse gas emissions and despite its assets is only developed in few countries in the world. Safety remains an open issue for the future of this energy after the Fukushima accident[1]. In France the 2006 act on the waste management ensures the development of a new generation of nuclear reactors and has lead to the Advanced Sodium Technology Reactor for Industrial Demonstration (ASTRID) which aims at bringing an industrial and technological advanced answer to many issues of this century. Indeed this new generation has to: be economically competitive, burn radioactive waste, make the material management easier by using the whole uranium ore as fuel and get the same or higher safety standards than most recent reactors i.e. EPR…

One of the concerns in the sodium cooled fast reactor (SFR) technology is the loss of sodium coolant accident because it might lead to a snowball effect in the chain reaction if the sodium void reactivity effect (SVRE) is positive. When the sodium is removed from the core, two antagonistic effects arise that affect the neutron balance: one increases the reactivity of the core and is called the central component (CC) and the other is the leakage component (LC) with a negative feedback on the reactivity. Maximizing the last component is one of the answer to increase the inherent safety of the SFRs. That is why the CEA has developed an innovative core design: the "Cœur à Faible Vidange" (CFV : Core with low void effect) which exhibits a negative SVRE. However, such innovations have to be experimentally validated and the uncertainty on this reactivity effect has to be mastered. In support of SFRs the existing experimental data base is quite large with for instance, in the MASURCA experimental facility at CEA Cadarache (France), the PRE-RACINE and the CIRANO experimental programmes with many different voided configurations. Furthermore, in the BFS experimental at Obninsk (Russia) two dedicated experimental programmes have been done in collaboration between the CEA and IPPE in support to the specificities of the CFV core.

The objective of this PhD thesis is to master the different sources of uncertainties in calculating the sodium void reactivity effect and use the integral experiments to predict the sodium void reactivity effect of the CFV core of ASTRID as well as its uncertainty.

In the various experimental programmes considered, the sodium void reactivity effect (SVRE) is measured for zones of different sizes in order to vary the relative importance of central and leakage components. The sodium rodlets or platelets are substituted step by step by voided rodlets or platelets. Reactivity is measured by the position of shim rod or/and the addition of peripheral assemblies. A rod drop and the use of the Nordheim equation insure calibration of the reactivity. This reactivity is measured on a β_{eff} scale which is the delayed neutron fraction of the core. A new analysis of β_{eff} measured in the BERENICE programme (in the MASURCA facility) has been made using the TRIPOLI4® Monte Carlo with the newly Iterated Fission Probability (IFP) method for calculating integrals. These integrals have been used for reassessing the calculated value but also the calculated corrections of the measured values.

[1] ranked at the level 7 of the INES scale

Abstract

The TRIPOLI-4® code gives credit to deterministic codes such as ERANOS for calculating β_{eff}. However, the asset of TRIPOLI-4® is the possibility to get a better representation of experimental cores, especially the ZONA2 experimental core which exhibits more experimental channels for hosting large fission chambers. For JEFF3.2, the revised C/E ratios for β_{eff} are of 1.2% ± 3.6% for the ZONA2 core when using the Noise measurement technique. The nuclear data uncertainty propagation has been leading to a 2.6% uncertainty for the U-Pu core with main contributors being the delayed neutron fission yield and the fission cross section of U238 values. It allows revisiting more precisely the experiments dedicated to sodium void reactivity measurements.

For analysing the sodium void reactivity effect, we split it into two components: the central component (CC) which is a positive reactivity effect due to spectrum changes and the leakage component (LC) which is a negative reactivity effect due to the increase of the neutron mean free path. In order to study in details the uncertainty associated to the SVRE, a development of an innovative generalised perturbation theory procedure for computing sensitivities of the CC and the LC has been conducted. With such sensitivities and the use of the COMAC-V2 covariance matrix, we are able to calculate the uncertainties due to nuclear data on each component using JEFF-3.2 nuclear data. The application of the method to the ASTRID CFV core shows a 2.6% uncertainty on the CC, a 2.0% uncertainty on the LC and a 18% on the total sodium void reactivity effect. There is a low correlation factor of -0.002 between the LC and CC uncertainties.

This approach gives the possibility of studying experimental programmes performed in zero power facilities such as MASURCA. Either the deterministic or the stochastic methods used to solve the Boltzmann equation which rules the neutron balance in a core requires nuclear data as inputs (cross-section, fission spectrum …) which are known with significant uncertainties. These uncertainties induce an overall uncertainty on the calculation result which is often more important than the experimental uncertainty. The independent analysis of each component (CC and LC) of the SVRE was developed within this PhD work. Using both deterministic and stochastic approach is mandatory because even if the Monte-Carlo code such as TRIPOLI-4® gives reference results by using "as-built" geometry of the core the generalised perturbation has not been implemented yet in this code. ERANOS allows developing procedures to get the CC and the LC and the nuclear data uncertainties associated to each component.

Once simulations have been run for each experimental programme it is possible to adjust the results from ERANOS and TRIPOLI-4® to experimental ones. Independent adjustment according to the fuel composition, the core geometry lead to a set of parameter (α,β) to correct the CC and LC. The results show that TRIPOLI-4® overestimate the CC by 11.3% when the fuel area is voided and that the LC is overestimated by 6% when the sodium plenum is voided. These discrepancies are not consistent within 1σ uncertainty when we consider the experimental and statistical uncertainty (which is about 4.8% in the fuel area for the CC and about 1.8% for the LC of the sodium plenum) and also the nuclear data uncertainties which are about 3.1% for the CC and about 2.1% for the LC. An underestimation of the nuclear data uncertainty is suspected in particular the one of sodium in COMAC-V2.

Content

Chapter I: Introduction: motivation and objectives

Introduction

A general introduction to the nuclear energy is given in this Chapter I, an historical recap is done in the first section and it reminds the pioneer role of French researchers in this field. Then the evolution of nuclear energy in the world during the cold war is described with a focus on the French situation. The future of nuclear energy is discussed in respect to the 21st century challenges: economic growth, global warming … The second section presents the international collaboration about the development of a new generation of nuclear reactors taking into account economic, safety, non-proliferation and sustainability issues. The 6 designs of reactors chosen by the Generation IV International Forum (GIF IV) are briefly described and the assets of Fast Reactors considering the sustainability and non-proliferation issues are presented. Research in France is lead by the CEA with the Advanced Sodium Technological reactor for Industrial Demonstration (ASTRID) project to build a Sodium cooled Fast Reactor (SFR) prototype. The advantages of this technology and the design of this reactor prototype are given in the third section. The development of such a technology means also a development in numerical simulations in the different nuclear reactor fields. The proof of the developed tools must go under the Verification, Validation and Uncertainty Quantification (VV&UQ) processes. In these series of processes, the innovative features (but also the more standard ones) of nuclear reactors need to be experimentally validated.

Contents

I.1 Nuclear energy around the world

I.1.1 Historical development of nuclear energy

Since Chadwick has discovered the neutron in 1932 and since the fission process has been discovered by Lise Meitner and Otto Hahn in 1938, some scientists have planned to use the high amount of energy released during this process to produce electricity. The French physician Joliot-Curie lead a team of researchers of the "Collège de France" and they protected the idea of nuclear reactor power plant with a patent in 1939 describing a system to produce energy: "Two ways are recommended for the production of energy : the method of thermal neutrons using enriched Uranium-235; or the one of fast neutrons with the hope that the capture of neutrons by Uranium-238 leads after all to a new fissionable nucleus[1]."

However it is the Italian physicist Fermi who emigrated to USA in 1939 who built the first atomic "pile"[2] in the underground of the Chicago stadium realising the product of Joliot-Curie's patent in 1942.

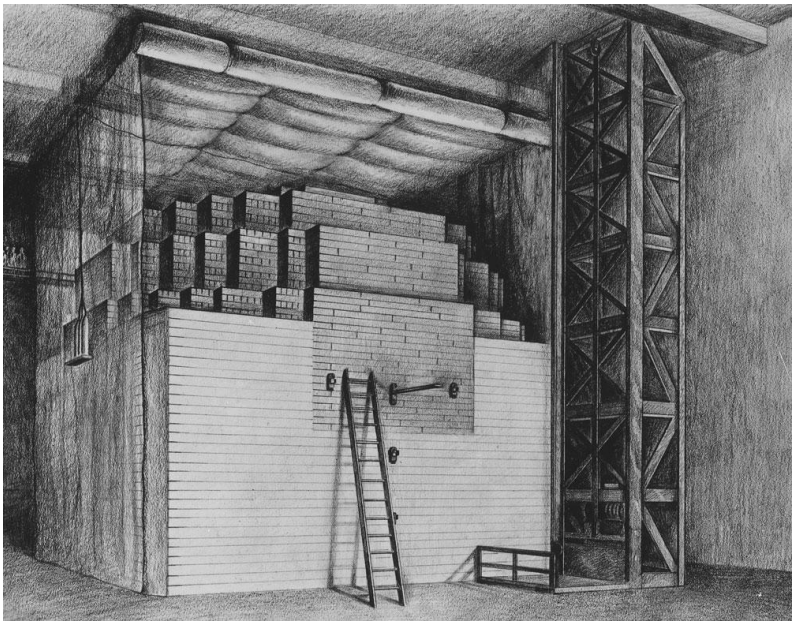

Figure I.1.1: illustration of Fermi's pile

Credit: Melvin A. Miller of the Argonne National Laboratory

In the context of the Second World War, the USA launched the Manhattan project to develop the atomic bomb. The Hiroshima (6 august 1945) and Nagasaki (9 august 1945) bombs have proved to the world that the nuclear power is so strong that it has to be controlled in order to ensure the survival of the life on Earth: the treaty on the non-proliferation of nuclear weapons has been signed in 1968. Nevertheless the Cold War has seen USSR, Great-Britain, France and China developing their own atomic and H-bombs. In the same times, nuclear reactors have taken advantage of this arms race and have been developed to produce the Plutonium (which cannot be found in the environment) needed to develop nuclear bomb. In France, the CEA[3] is created in 1945 and has developed the UNGG (Natural Uranium moderated by Graphite and cooled by Gas see "Sidebar 1") reactors which is really

[1] This new fissionable nucleus is ^{239}Pu that will be discovered in Berkeley in 1941
[2] Literally a pile of bricks of natural uranium and graphite.
[3] "Commissariat à l'énergie atomique" for atomic energy commission

proliferating because these reactors were able to produce enough Plutonium for the French military nuclear project [1] (due to the use of natural uranium (99.3% of Uranium 238 [2])). Feeling the opportunity the public electricity provider of France: EDF[1] invested in this generation of nuclear reactor. Near Chinon, 3 reactors prototypes are built with a growing power between 1963 and 1966 (see Table 1.1 [3]).

Table 1.1: Power of UNGG prototypes

	Chinon A1 (1963)	Chinon A2 (1965)	Chinon A3 (1966)
Electric power (MWe)	70	210	480

However with the increase of power the UNGG reactors have reached their design limit. Then in 1969 it is decided to develop a new generation of nuclear reactors: the Pressurised Water Reactors (PWR) with the Westinghouse licence, using enriched uranium and water as a moderator and coolant.

Sidebar 1 : Thermal reactors

To build a nuclear reactor you need :
-a fuel (natural uranium, enriched uranium, plutonium, thorium)
-a moderator (water (H_2O), heavy water (D_2O), graphite, sodium)
-a coolant (water, heavy water, sodium, gas (air, helium))

The nuclear fission process of a fuel nucleus is initialised by the absorption of a thermal neutron (energy around 0.025 eV) and it produced 2 or more fast neutrons (energy around 2 MeV).

Table 1.2 : Thermal neutrons yield by type of fuel

nucleus	U235	Pu239	U233
Thermal yield	2.42	2.87	2.49

To get a chain reaction these fast neutrons have to be slowed down to make efficient fissions. The fast neutrons which can run some 10 cm between two interactions will go from the fuel zone to the moderator zone in the core and be scattered by colliding on moderator nucleus. Collision after collision the fast neutron will lose energy and become thermal. The less the number of collisions needed to thermalize the neutrons the more efficient the moderator will be.

A little kinetic exercise can be done here to understand the impact of atomic mass in scattering power [4]. In the laboratory referential there is a neutron (with A_n=1) running at a speed of $\overrightarrow{V_n}$ into a moderator atom (with an atomic mass $A_M = A$) and the neutron is scattered with an angle Ω. Neglecting potential energy due to gravitation we can write that the neutrons is running forward with an a speed: $\overrightarrow{V_n'}$. In the centre of mass referential the collision is assumed isotropic and this referential is running with a speed $\overrightarrow{V_g}$ in the laboratory referential. In order to go from one referential to another we write:

$$\vec{V} = \vec{v} + \overrightarrow{V_g}$$

We also introduce the relative speed:

$$\overrightarrow{V_r} = \overrightarrow{V_n} - \overrightarrow{V_M} \quad \text{and} \quad \overrightarrow{V_r'} = \overrightarrow{V_n'} - \overrightarrow{V_M'}$$

[1] "Electricité de France" for Electricity of France

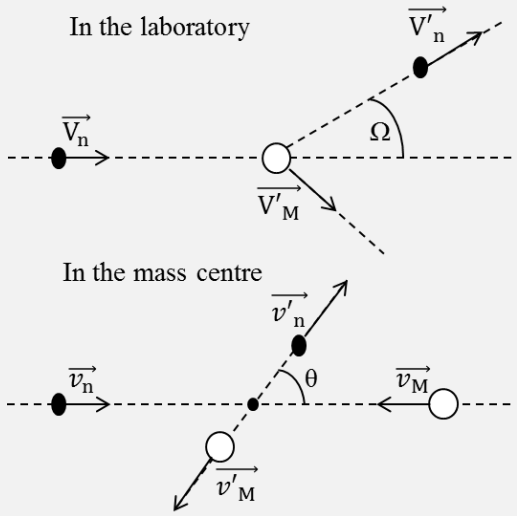

Using the conservation of the impulsion law we can write:

$$\overrightarrow{V_n} + A\overrightarrow{V_M} = \overrightarrow{V'_n} + A\overrightarrow{V'_M} = (A+1)\overrightarrow{V_g}$$

$$\begin{cases} \overrightarrow{V_n} = \overrightarrow{V_g} + \dfrac{A}{A+1}\overrightarrow{V_r} \\ \overrightarrow{V_M} = \overrightarrow{V_g} - \dfrac{1}{A+1}\overrightarrow{V_r} \end{cases} \quad (\mathbf{1.1})$$

$$\begin{cases} \overrightarrow{V'_n} = \overrightarrow{V'_g} + \dfrac{A}{A+1}\overrightarrow{V'_r} \\ \overrightarrow{V'_M} = \overrightarrow{V'_g} - \dfrac{1}{A+1}\overrightarrow{V'_r} \end{cases} \quad (\mathbf{1.2})$$

Using the conservation of the kinetic energy law we can write:

$$V_n^2 + AV_M^2 = V_n'^2 + AV_M'^2$$

$$(A+1)V_g^2 + \frac{A}{A+1}V_r^2 = (A+1)V_g'^2 + \frac{A}{A+1}V_r'^2$$

As $\overrightarrow{V_g} = \overrightarrow{V'_g}$ (no external forces applied on the system) we deduce that: $V_r = V'_r$ during a collision. The relative speed not modified but the angle of the relative speed has changed, in the mass centre this deviation is characterised by: θ such as: $\overrightarrow{V_r} \cdot \overrightarrow{V'_r} = V_r^2 \cos\,\theta$. Now we consider that the nucleus is still before the collision that is quite true when considering fast neutrons: $\overrightarrow{V_M} = \vec{0}$ and we look at the $(\mathbf{1.1})$ equations:

$$\begin{cases} \overrightarrow{V_n} = \overrightarrow{V_r} \\ \overrightarrow{V_g} = \dfrac{1}{A+1}\overrightarrow{V_n} \end{cases}$$

The first equation of the $(\mathbf{1.2})$ system becomes:

$$\overrightarrow{V'_n} = \overrightarrow{V_g} + \frac{A}{A+1}\overrightarrow{V'_r} \Rightarrow \overrightarrow{V'_n} = \frac{1}{A+1}\overrightarrow{V_n} + \frac{A}{A+1}\overrightarrow{V'_r}$$

Then we square the equation:

$$V_n'^2 = \left(\frac{1}{A+1}\right)^2 V_n^2 + \left(\frac{A}{A+1}\right)^2 V_r'^2 + 2A\frac{V'_r V'_n}{(A+1)^2}\cos\,\theta$$

We get the new energy of the neutrons :

$$\frac{E'_n}{E_n} = \frac{A^2 + 2A\cos\theta + 1}{(A+1)^2}$$

An efficient moderator will minimise the $A^2 + 2A\cos\theta + 1$ value which is done for a angle of deviation equals to π: $A^2 - 2A + 1 = (A-1)^2$ and for A=1, the best moderator is then the Hydrogen and by extension the ones **with low mass number**: helium (A=4), carbon (A=12), etc.

I.1.2 450 nuclear reactors are operated all around the globe

Since this decision in France, 58 PWR have been built on behalf of energetic independence which becomes relevant due to successive oil shocks occurring in 1973 and 1979. In fact the French energetic bill was multiplied by 2.6 between 1972 and 1973 and by 4 between 1972 and 1981 because it was mainly based on oil import. In 2016 these reactors have produced 384 TWh representing 72.3% of the total electric production [5] when oil, gas and coal represent less than 10% of the energetic mix. Then the energetic independence can be considered as successfully achieved.

According to the International Atomic Energy Agency (IAEA) 450 nuclear reactors are operational all around the globe in 2018 [6] for an electric capacity of 393.7 TWe. Furthermore 60% of these plants have been built in the countries of the security council of the United Nations Organisation (UNO) as a legacy of the cold war (taking into account all reactors of the countries of the former USSR).

The world energy demand should increase in the next decades considering that developing countries such India and China have a mean GDP growth of respectively 8.56% and 9.45% since 2010 [7] and those increases have implied an increase of the electric production of respectively 39.3% and 41.2% since 2010 in China and India [8]. This growing need of energy lead these countries to build nuclear plants, 18 are under construction in China and 6 in India. In western countries 5 nuclear reactors are under construction in Russia, 2 in USA and 1 in France. In the case of France the replacement of old reactors built between the years 1970 and 2000 has already begun with the construction of the Evolutionary Power Reactor (EPR) by EDF in Flamanville. The United-Kingdom is also interested in this technology as 2 EPR are planned to be built at Hinkley Point. Even though the public opinion is skeptical (47% for closing nuclear plants in France and 53% against [9]) the nuclear energy is still an asset for France and for the planet as the world energy demand increases and this needs to be achieved without increasing the greenhouse gases emission.

I.1.3 Sustainable and clean energy

The global warming is one of the main concerns of this century and has been enlighten thanks to the work of the intergovernmental panel on climate change (IPCC). The physical phenomenon of greenhouse gases increasing the average temperature of the globe is well known but the amplitude of the negative feedback is still debated in the IPCC, that is why simulations predict an increase of the average temperature by 2100 between +1°C and +2°C [10] in a optimistic scenario where the radiative forcing is limited to 4.5W/m².

In 2015 in Paris took place the COP21 (21st conference of parties) where 197 countries agreed to limit the rise of the average temperature of the globe to 2°C by 2100, this is the most important agreement on climate change since the one signed in Kyoto in 1997. This commitment implies a reduction of greenhouse gases emission especially in developed countries because USA and European Union are responsible of 24% of these emissions [11]. One answer is the development of renewable energies (solar, wind, ...) which are among the lowest CO_2 emitter for electric production. Nevertheless, these sources are intermittent while the electricity consumption respect a pattern well defined. Another issue is the storage of their production for more than few hours for 30,000 houses consumption [12]. Furthermore the NEA report points out [13] that the nuclear energy produces less CO_2 per GWh than solar energy (see Figure I.1.2). Then nuclear energy allows a large scale production of electricity (up to 23 MWe/m² when solar is about 1 MWe/m² [14]) with low emission of CO_2.

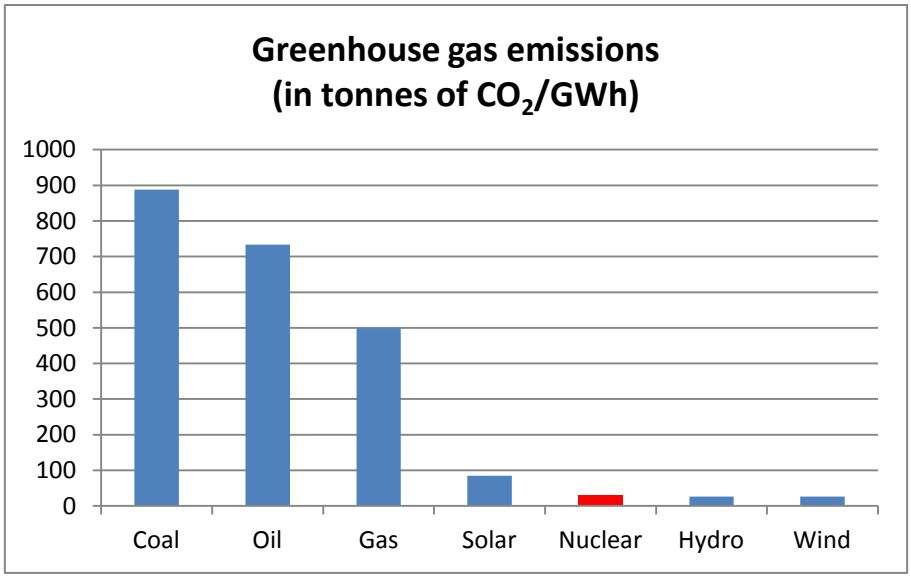

Figure I.1.2: Greenhouse gas emissions by energy source

However the uranium resource is also limited: according to the IAEA if the electric production by nuclear plants remains stable, the uranium proven stocks guarantees 100 years of supply. As seen before the number of countries interested in nuclear energy to meet their increase of electricity consumption is important meaning that the nuclear production will remain stable or will increase making these 100 years of supply an upper limit for proven stock. Nevertheless only 99% of uranium is exploited in current reactors then the development of another technology is needed to push back this limit.

I.2 Important challenges of the 4th generation

I.2.1 The Generation IV International Forum challenges

In order to develop a new technology of nuclear reactors some countries have decided to launch a research cooperation called the Generation IV International Forum (GIF). In 2000, on the initiative of the US department of energy (DOE) 9 countries have decided to form a group of experts in order to make recommendations on research and development of this new generation of nuclear reactors. Nowadays this is 13 countries: South-Africa, Argentina, Australia, Brazil, Canada, China, South-Korea, France, Japan, United Kingdom, Russia, Swiss, USA and the EU (with EURATOM) which are pooling their effort to get an industrial deployment of this technology by 2040.

Four major challenges have been identified [15]:

- The **sustainability**: the system has to provide energy for a long-term, to efficiently use the fuel and to minimise the waste produced.
- The **economic competitiveness**: the financial cost has to be similar with other energy sources.
- The **safety** and **reliability**: the probability of core damage and accident consequences without the need of an offsite emergency response have to be the lowest possible.
- The **proliferation resistance**: these systems have to consume transuranic as fuel.
- The **physical protection** of people and the environment have to be ensured.

The panel of experts have selected 6 designs to meet these challenges and countries have picked among them where invest research and funds.

I.2.2 Designs studied for the 4th generation

In these 6 designs selected: two projects are using thermal neutrons, the Very High Temperature Reactor system (VHTR) and the Super Critical Water Reactor (SCWR). The VHTR uses graphite for neutron moderation and helium at high temperature as coolant. Due to this high temperature (>800°C compared to 320°C in PWR) when exiting the reactor core it enables high thermal efficiency for electricity production. The SCWR is a high temperature and high pressure water-cooled reactor operated above the thermodynamic critical point (374°C, 22.1 MPa) of water. The main advantage of the SCWR is also a higher thermal efficiency for electricity production.

The 4 other designs use fast neutrons, the Gas cooled Fast Reactor (GFR), the Sodium cooled Fast Reactor (SFR), the Lead cooled Fast Reactor (LFR) and Molten Salt Fast Reactor (MSFR). The GFR is a high temperature gas-cooled reactor, it allows a higher thermal efficiency. The LFR uses lead as coolant which has excellent properties for cooling and safety (its density, high boiling point, shielding gamma-ray, …). The MSFR uses liquid fuel dissolved in molten fluoride salt at low pressure, the main benefit is the good cooling properties of molten salt and for its promotors its high level of safety. The SFR is a low pressure reactor using the sodium as coolant which has also good cooling properties (thermal capacity, …).

All systems using fast neutrons have the same benefits: the sustainability and the proliferation resistance. As seen before, the uranium resources are limited but PWR only use Uranium 235 as fuel representing less than 1% of the uranium ore and Pu from the first PWR UOX recycled fuel. Fast reactors are an answer to use the whole uranium ore, as under irradiation, the Uranium 238, a fertile isotope, turns into Plutonium 239, a fissile isotope. In order to sustain a chain reaction it is needed to get: 1 neutron for another fission plus 1 neutron to transmute ^{238}U into ^{239}Pu plus a fraction of neutrons to balance sterile capture by other isotopes or the neutrons leaking out of the core and this is only possible with fast neutrons. Then fast reactors can produce as much fissile materials as they burn making it a sustainable source of energy. Burning plutonium decreases the radiotoxicity of waste produced by operating PWR: in fact the uranium oxide fuel produce plutonium and minor quantities of actinides (neptunium, curium, americium) which are the main contributors of long term radiotoxicity (see Figure I.2.1). Thus burning plutonium and minor actinides would minimise the volume of waste produced and decrease the cost of storage of nuclear waste in a geological deposit.

The French parliament has passed a law on the management of nuclear waste in 2006 [16], the 3rd article states the researchers have to work on:

> "*The separation and transmutation of long-life radioactive elements. The corresponding studies and research will be developed in relation with the ones on the new generation of nuclear reactor*"

The CEA launched in 2010 the Advanced Sodium Technological Reactor for Industrial Demonstration (ASTRID) project to fulfil this legal obligation.

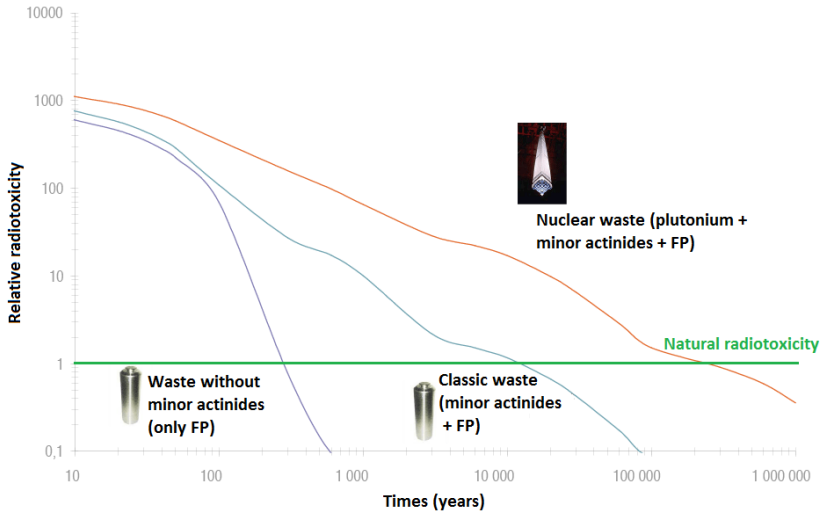

Figure I.2.1: Radiotoxicity of nuclear waste (FP: fission products)

I.3 The ASTRID project

I.3.1 Choice of Sodium Fast Reactor

As seen in section **2.2** there are numerous choices of coolant to develop the 4th generation of nuclear reactors but they have to meet important specifications. Indeed the choice of the coolant structures the whole project because:

-the heat removal has to be ensured even in case of accident so efficient thermal conductivity and capacity are required.

-the coolant in the system can have an important thermal inertia which increases the safety of the core.

-the coolant must not absorb and scatter neutrons in contrast to the thermal neutron reactor using a moderator.

-the coolant must not corrode structural elements of the core or as less as possible.

The technology developed by the CEA for the 4th generation of nuclear reactor is the SFR. The sodium coolant has many assets in regards of these important specifications:

-Its thermal capacity and conductivity are excellent and it is liquid in a large range of temperatures with a high margin before boiling (around 350°C) at atmospheric pressure.

-Its hydraulic properties allow natural convection in the primary circuit even in case of loss of pumps.

-Due to its atomic mass (A=23) the sodium is a poor moderator.

-Sodium has few interactions with steel structure.

Table 3.1: Sodium and Lead-Bismuth properties comparison

	Sodium	Lead-Bismuth
Density (g/cm³)	0.847	10.45
Melting point (°C)	98	125
Boiling point (°C)	883	1670
Thermal conductivity	70	13
Corrosive power	Medium	High
Atomic mass	23	208

All these properties allow operation of a SFR at atmospheric pressure which is important for building the vessel with important savings thanks to its thin thickness. Furthermore in case of accident no depressurization is feared. Nevertheless sodium has also inconveniences, in contrast to water, the sodium opacity forbids an easy optical checking of the vessel or fuel meaning that other methods using acoustic waves or conductivity measurements have to be developed to inspect the structure integrity. In addition to that, the sodium is highly reactive with air and water and hence a secondary loop of sodium between the primary circuit and the water of the energy conversion systems is needed.

Sodium is already a proven technology especially in Russia (with BOR60, BN350, BN 600 and BN 800) and France (with, Rapsodie, Phénix andSuperphénix) so the industrial feedback is important and is an asset for SFR development.

-The first French experimental SFR has been built in the CEA Cadarache site and was called RAPSODIE (20 MWth). It has been operated from 1967 to 1983. Many technology choices have been set at this time such as: the oxide uranium-plutonium fuel, hexagonal assemblies, etc. Irradiations of materials have been realised and results showed a swelling phenomenon of the fuel pellet.

-The next step has been the construction of a demonstrator called PHENIX (563 MWth, 250 MWe) which has been operated from 1973 to 2010 in the CEA Marcoule site. Its operation has to prove the ability of the SFR to produce electricity before going on industrial scale. Thanks to PHENIX a better understanding of fuel pellet-clad interactions brought significant improvements since any clad rupture events will be reported after 1988. Furthermore irradiations experiments have been conducted by CEA in PHENIX to study the transmutation of spent fuel.

-The industrial prototype SUPERPHENIX has been built in Creys-Malville with European financial contribution (France 51%, Italy 33% and Germany 16%) and has been first operated in 1985. Because of the prototype size some incidents have lead to many stops in its operations but none of them could prevent the demonstration to go further. However due to political decisions SUPERPHENIX has been stopped in 1997.

I.3.2 Design of the reactor

Within the GIF and the strategy defined by the 2006 law, France develops once again the SFR technology. But safety rules have changed since the end of SUPERPHENIX especially since the accident of Fukushima in 2011 meaning going back to old core configurations is not realistic. The challenges of the ASTRID project are:

-proving that SFR have an equivalent or enhanced safety compared to PWR;

-demonstrating the economic competitiveness of SFR;

-building a prototype by 2025 before the deployment of an industrial fleet of SFR by 2040.

The current design is a 1500 MWth prototype for a 600 MWe production, this power ensures the representativity with the future industrial SFR and the electric production should recover the financial cost of the prototype operation. The management of depleted uranium resources and the multi-recycling of plutonium will be optimised with this prototype and it will allow experiments such as the transmutation of minor actinides and irradiation of materials. The onload development methods of inspections at CEA will also be tested. Last but not least, the core design should minimise the risk of severe accidents especially in case of loss of coolant as we will see in chapter 4.

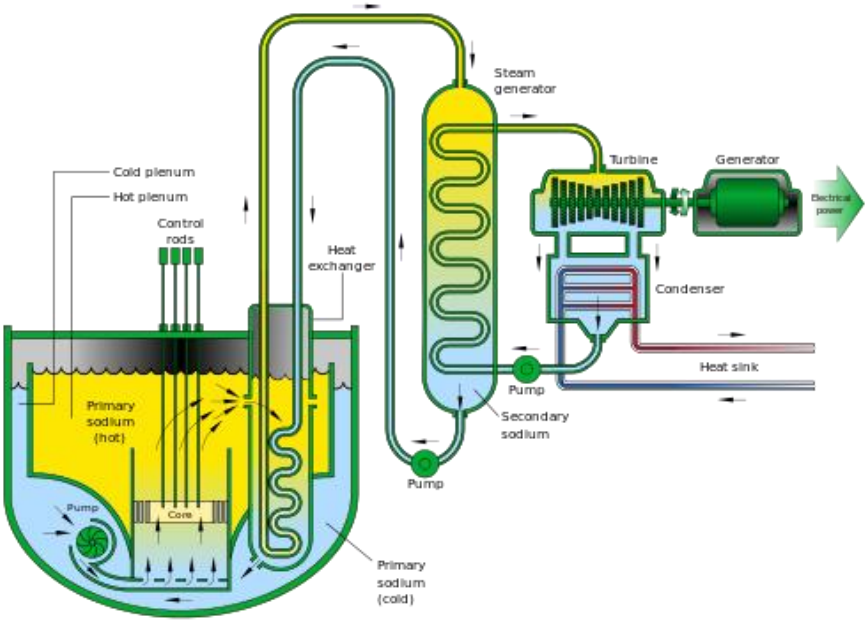

Figure I.3.1: ASTRID plan

I.3.3 VV&UQ process

The development of such a prototype is done using calculation softwares such as ERANOS or APOLLO3 which calculate the characteristics of a core. These software have to go through the Verification, Validation and Uncertainties Quantification process (VV&UQ).

The verification step ensures that algorithms are correctly implemented without programming errors and bugs. The numerical validation compares the results of the code with the ones given by a reference code (most of the times a stochastic code such as MCNP or TRIPOLI-4®), the ability of the code to represent physical phenomena is also verified. The experimental validation compares the results with experimental measurements. Possible computational errors are a combination of model biases and nuclear data ones. Then the uncertainty quantification step has to quantify the nuclear data uncertainties and technical uncertainties and model biases.

This PhD work is part of the VV&UQ process associated to the use of neutronic codes evolved in the development of the ASTRID core. As we will see in Chapter IV an innovative design for the core, the "Cœur à Faible Vidange" (CFV[1]) has been proposed by CEA with the objective of being more resilient to unprotected transients. Such an innovative design has to be validated by comparing

[1] CFV: Core with low void reactivity effect in French

simulations results with representative experimental ones. A detailed analysis of past and recent experimental programmes such as PRE-RACINE[1], CIRANO[1] and BFS[2] is needed for a better understanding of the two antagonistic reactivity effects (the central component CC and the leakage component LC, see Chapter IV) competing in the core when the sodium coolant is removed. Two complementary approaches to do neutronic simulations have been used: the stochastic method (to get reference results) and the deterministic approach (which allows the use of perturbation theory) detailed in the Chapter II. Furthermore the experimental results of sodium void reactivity measurements are given on a β_{eff}[3] scale. It is the reason for which a new analysis of the β_{eff} measurements made in the BERENICE programme[1] in Chapter III has been conducted. In the end the Chapter V analyses the uncertainties due to nuclear data on each component of the Sodium Void Reactivity Effect (SVRE). This allows making recommendation for each component of the SVRE when the sodium is removed from the CFV core.

[1] in the MASURCA facility at CEA Cadarache
[2] made in collaboration with the IPPE in the BFS facilities at Obninsk
[3] the delayed neutron fraction

References

[1] L'épopée de l'énergie nucléaire - Une histoire scientifique et industrielle, Paul Reuss, p119

[2] www.webelements.com/uranium

[3] Haut comité pour la transparence et l'information sur la sécurité nucléaire, www.hctisn.fr

[4] Introduction au génie nucléaire, Jacques Ligou, 1996

[5] Nuclear energy data 2017, NEA, n°7365

[6] Power reactor information system database, IAEA, www.iaea.org

[7] World bank database, www.worldbank.org

[8] International Energy Agency database, www.iea.org

[9] IFOP, Les français et l'énergie nucléaire, avril 2016

[10] IPCC, WG1 5th assessment report, Chapter 11, Figure 11.9 page 981

[11] World Resources Institute, CAIT Climate Data Explorer. 2015. Washington, DC.

[12] "Explainer: What the Tesla big battery can and cannot do", www.reneweconomy.com.au

[13] The role of nuclear energy in a low-carbon energy future, NEA report 2012

[14] "ISE, Total et SunPower mettent en service une centrale solaire à Nanao au Japon", www.total.com

[15] Y. Sagayama, "GIF, 2009 annual report"

[16] Loi n°2006-739 du 28 juin 2006 de programme relative à la gestion durable des matières et déchets radioactifs, www.legifrance.gouv.fr

This page has been left blank intentionally

Chapter II: Neutronic

Abstract

The neutronic is the study of neutrons behaviour in nuclear reactor cores based on the Boltzmann equation as the neutron population is that large that a statistical treatment is possible. This equation is presented in the first section of this Chapter II and also the two solutions developed to numerically solve it. Indeed this problem has too many unknowns to be analytically solved except in very simplified cases and geometries. The first approach is the deterministic one which requires approximations in order to decouple as much as possible the variables of energy, angle, space and time. This calculation is done in two steps: the cell and the core calculations. A reactor core is made of repeated pattern of small cells for instance the ASTRID core is built with thousands of hexagon cells for the fuel, the fertile slab, the reflector, etc. Then the first calculation is made for one cell of each pattern, this refined calculation in energy and space allows getting average values for cross-sections which will be used in the core calculation. Hence once the cross-sections are homogenised and condensed in few groups of energy the neutron flux can be calculated for the whole core using the transport theory. The second approach is the stochastic[1] one which allows using "as-built" geometries and gives reference results because it needs no approximations. This method consists in selecting random events for the neutron history and using the law of large numbers and the central limit theorem. The simulation converges on the value of interest searched by simulating a high number of particles. This last method is "exact" but the time needed to get accurate results is penalising. Deterministic methods use approximations but the simulations are fast and post-treatment analysis[2] treatments are much easier.. The second section presents the perturbation theory which is a post-treatment of data given by the core calculation. Indeed the development of an innovative core design needs parametric studies and to avoid many calculations sensitivity analysis can be done using the perturbation theory at the post-treatment stage. In ERANOS the deterministic code used in this PhD for fast-reactors calculations three methods have been implemented and they are detailed in this section.

[1] Also called "Monte-Carlo" in reference of the Monte-Carlo project developed by the USA to get the atomic bomb.

[2] It also could be used in Monte-Carlo code such as in Serpent but it has not been implemented yet in TRIPOLI-4, the code developed at CEA.

Contents

II.1 Boltzmann equation and its solution

II.1.1 The Boltzmann equation

The operation of nuclear reactors needs to load new fuels assemblies or to remove spent fuel assemblies from the core, these maintenance operations have to be done with sub-criticality conditions for obvious safety reasons. Then the industrial operator has to know the reactivity of the core during these processes and it is done using computer calculations which solve the Boltzmann equation. This equation states that the neutron flux behaviour: Φ in an elementary volume is close to a perfect gas and the balance is given by different terms:

- The disappearance of neutrons leaving the elementary volume:

$$-\vec{\Omega}\cdot\vec{\nabla}\Phi(\vec{r},E,\vec{\Omega},t)\,d^3r\,dE\,d^2\Omega\,dt$$

- The removal of neutrons by absorption or scattering to another energy or angle:

$$-\Sigma_t(\vec{r},E,\vec{\Omega},t)\Phi(\vec{r},E,\vec{\Omega},t)\,d^3r\,dE\,d^2\Omega\,dt$$

- The inflow of neutrons by scattering:

$$\int_0^\infty dE'\int_{4\pi}d^2\Omega'\,\Sigma_s\left(\vec{r},E'\to E,\overrightarrow{\Omega'}\to\vec{\Omega},t\right)\Phi\left(\vec{r},E',\overrightarrow{\Omega'},t\right)\,d^3r\,dE\,d^2\Omega\,dt$$

- The creation of neutrons by fissions

$$\frac{\chi(\vec{r},E)}{4\pi}\int_0^\infty dE'\int_{4\pi}d^2\Omega'\;\upsilon(\vec{r},E')\Sigma_f\left(\vec{r},E',\overrightarrow{\Omega'},t\right)\Phi\left(\vec{r},E',\overrightarrow{\Omega'},t\right)\,d^3r\,dE\,d^2\Omega\,dt$$

- The external sources of neutrons:

$$S(\vec{r},E,\vec{\Omega},t)$$

The Boltzmann equation may be written as [1]:

$$\frac{1}{v}\frac{\partial\Phi}{\partial t}+\vec{\Omega}\cdot\vec{\nabla}\Phi+\Sigma_t\Phi=\int_0^\infty dE'\int_{4\pi}d^2\Omega'\,\Sigma_s(\vec{r},E'\to E,\overrightarrow{\Omega'}\to\vec{\Omega},t)\Phi(\vec{r},E',\overrightarrow{\Omega'},t)+\frac{\chi}{4\pi}\int_0^\infty dE'\int_{4\pi}d^2\Omega'\;\upsilon\Sigma_f(\vec{r},E',\overrightarrow{\Omega'},t)\Phi(\vec{r},E',\overrightarrow{\Omega'},t)+S(\vec{r},E,\vec{\Omega},t) \quad \textbf{1.1}$$

Where Σ_t,Σ_s and $\upsilon\Sigma_f$ are the total, scattering and production macroscopic cross sections, $\chi(\vec{r},E)$ is the isotropic fission spectrum and S is an external source density. This equation is often written using two operators: **A** the transport, removal and scattering operator and **F** the fission source operator.

$$\mathbf{A}\Phi\to\vec{\Omega}\cdot\vec{\nabla}\Phi+\Sigma_t\Phi-\int_0^\infty dE'\int_{4\pi}d^2\Omega'\,\Sigma_s(\vec{r},E'\to E,\overrightarrow{\Omega'}\to\vec{\Omega},t)\Phi(\vec{r},E',\overrightarrow{\Omega'},t) \quad \textbf{1.2}$$

$$\mathbf{F}\Phi\to\frac{\chi}{4\pi}\int_0^\infty dE'\int_{4\pi}d^2\Omega'\;\upsilon\Sigma_f(\vec{r},E',\overrightarrow{\Omega'},t)\Phi(\vec{r},E',\overrightarrow{\Omega'},t) \quad \textbf{1.3}$$

Thus the Boltzmann equation becomes:

$$\frac{1}{v}\frac{\partial \Phi}{\partial t} = (\mathbf{F} - \mathbf{A})\Phi + S \qquad \mathbf{1.4}$$

In core design, we mostly use the time-independent equation meaning that in such steady-state condition the time derivative term vanishes and for most reactors there is no external source and the equation becomes "homogeneous". In order to keep the balance we need to introduce the "effective multiplication factor" which is the multiplication factor of the neutron density between generation i and $i+1$. The equation (1.1) becomes:

$$\begin{aligned}\vec{\Omega}\cdot\vec{\nabla}\Phi + \Sigma_t\Phi = \int_0^\infty dE' \int_{4\pi} d^2\Omega'\, \Sigma_s\left(\vec{r}, E' \to E, \overrightarrow{\Omega'} \to \vec{\Omega}, t\right)\Phi\left(\vec{r}, E', \overrightarrow{\Omega'}, t\right) \\ + \frac{1}{k}\frac{\chi}{4\pi}\int_0^\infty dE' \int_{4\pi} d^2\Omega'\ \upsilon\Sigma_f\left(\vec{r}, E', \overrightarrow{\Omega'}, t\right)\Phi\left(\vec{r}, E', \overrightarrow{\Omega'}, t\right)\end{aligned} \qquad \mathbf{1.5}$$

Or simpler:

$$\left(\mathbf{A} - \frac{\mathbf{F}}{k}\right)\Phi = 0 \qquad \mathbf{1.6}$$

This is an "eigenvalue problem" and we assume that there is an infinite countable set of real positive values of k making this steady state equation solvable. The largest value k_0 is called the fundamental multiplication factor and the associated fundamental flux: Φ_0. The other values arranged in decreasing orders ($k_0 > k_1 > \ldots > k_i$) are called the "i-th harmonics". The flux harmonics are only defined in shapes and not in magnitude meaning that if Φ_i is solution of the equation then for any real λ, $\lambda\Phi_i$ is also a solution.

This linear equation **1.6** seems easy to solve but the number of unknowns is huge, there are 3 dimensions of space using different meshes in each direction plus those of angle using other meshes plus energy meshes. There exist two different ways to solve this problem: deterministic and stochastic.

The first one is deterministic and requires approximations to simplify the problem but leads to a rather fast solution. The second one is called stochastic or Monte-Carlo method and requires the tracking of neutrons from birth to death with a statistical treatment of the various solutions, it can be solved for a refined geometry of the core and with continuous energy but leads to very long calculation times in order to achieve sufficiently small statistical uncertainties. For the time being, it is used as a reference since there are much less approximations and modelling errors.

A reactor is about some meters long, the neutron flux gradient is about some millimetres so the number of an elementary volume of the geometry is about $10^6 x 10^3 = 10^9$, a refined energetic discretisation is about 10^4 groups in the range of 0 to 20 MeV and the angular discretisation needs from 10^2 or 10^3 angles to get a good description of the angular flux. Then the problem is to solve the Boltzmann equation on 10^{16} elementary volumes of the phase space which cannot be handle by recent computer even with the latest improvement in power of calculation because of limited memory.

The reactor physicist states that:

- The neutron density in the reactor is small enough to neglect neutron-neutron interactions.
- A heterogeneous medium can be replaced by a homogeneous one with equivalent properties in the neutron balance equation if it does not disturb its environment calculation.

- The solution of the Boltzmann equation on a refined discretised phase space can be used to calculate averaged neutronic parameters in space and energy and these parameters can be used in a homogeneous expression of the Boltzmann equation.

That leads to the deterministic method and the statistic treatment to solve this problem.

II.1.2 The deterministic code ERANOS

The deterministic method consists to discretise the phase space $(\vec{r}, E, \vec{\Omega})$ as refined as possible taking into account times and convergences issues. Many models exist to discretise a given variable and there are associated numerical methods to solve the Boltzmann equation. Nevertheless these discretisations have to meet the variation of reactions cross-section and their dependence in energy, space and angle. The deterministic code ERANOS[1] [2] solves the Boltzmann equation in two step with first step called the "cell calculation" in which refined average broad group self-shielded cross-section are generated for each medium of the core (cell fuel, cell blanket, etc.) and the second step called "core calculation" is solving the transport equation at this broad group level to get the neutrons flux in the full core geometry.
In the ERANOS scheme calculation the cell calculation is done by the ECCO[2] module and the core calculation can be done with different solvers (BISTRO, PARIS) using different methods of solution (P_n, S_n, SP_n, …). In this PhD the solver BISTRO has been selected for its fast solution of the RZ transport equations.

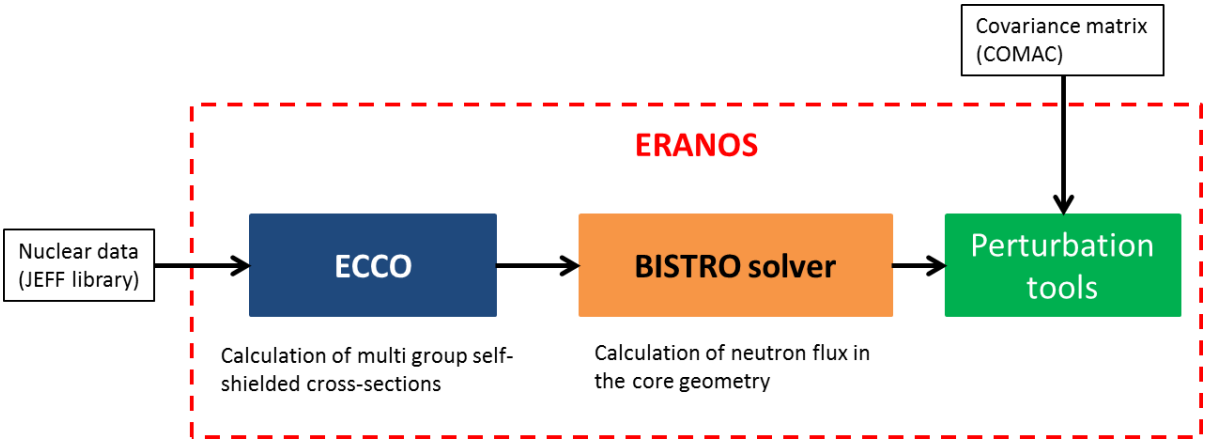

Figure II.1.1: ERANOS platform description

The ERANOS platform uses nuclear data (cross-sections, fission spectrum, …) stored in international libraries such as JEFF, ENDF, etc. It also allows perturbation calculations and sensitivities calculations which lead to nuclear data uncertainties on calculated parameters using covariance matrix data and it is described more in details in part 2 of this chapter.

The flux calculation is rather complex in reactors because the variables of the phase space are not independent then the deterministic approach uses approximations in order to decouple them as much as possible. The deterministic approach considers that refined variations of the flux can be calculated more precisely on an infinite geometry at a sub-assembly scale then self-shielded (see "Sidebar 1") and homogenised cross sections are produced for a third step: the neutron flux calculation at the core scale using homogeneous media.

[1] European Reactor ANalysis Optimised calculation System
[2] European Cell COde

This approach is based on the fundamental mode theory which considers that the space variable behaviour can be split into two step calculations. Indeed reactors are made of large zones of fuel, fertile blanket, etc., compared to the mean free path[1] of fast neutrons. The cell calculation is done using a refined energetic mesh (1968 energy groups in ECCO) and a heterogeneous geometry description of the cell. The core calculation uses homogenised cross section to get the flux using the transport theory at the core level. The **Figure II.1.2** illustrates the smallest variations in green due to the alternating steel and fuel pins at the sub assembly scale and the global shape of the neutron flux in blue.

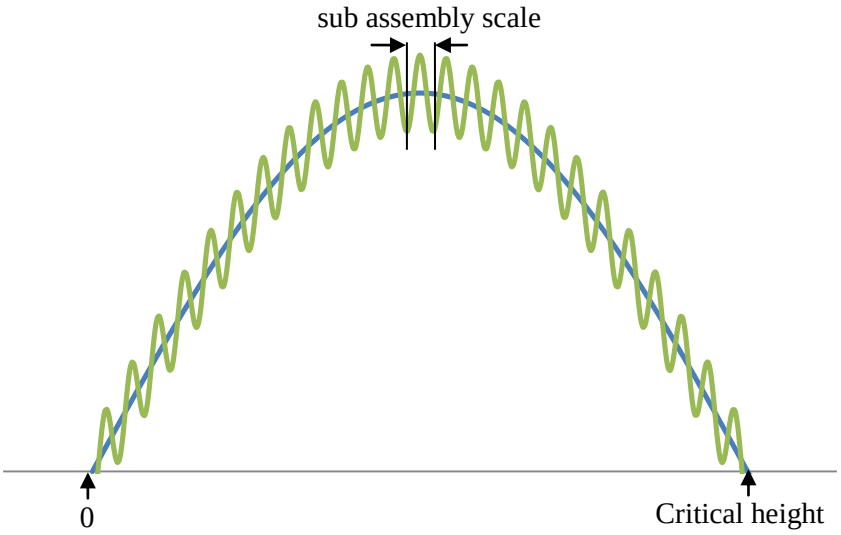

Figure II.1.2: Schematic neutron flux axial traverse of an homogeneous core

(non representative sclae)

The cell calculation is made by the ECCO module when the core calculation is done by the solver BISTRO[2].

II.1.2.1 The ECCO module

As said earlier the ECCO module is used to do refined calculation at the cell scale. The heterogeneous geometry description with the material composition is given to ECCO [3] with nuclear data then it needs between 3 or 5[3] steps to get homogenised and self-shielded cross sections for each cell. The project scheme is made to be faster than the reference scheme with some supplementary approximations. For instance the reference scheme for a fuel cell is presented in **Figure II.1.3**.

[1] The mean free path is the mean distance that a neutron travels between two interactions. About 10 cm for fast neutrons.
[2] BIdimensionnal Sn TRansport Optimised
[3] Dependent on the scheme used (Reference or Project) and the cell type (fuel, fertile or structure)

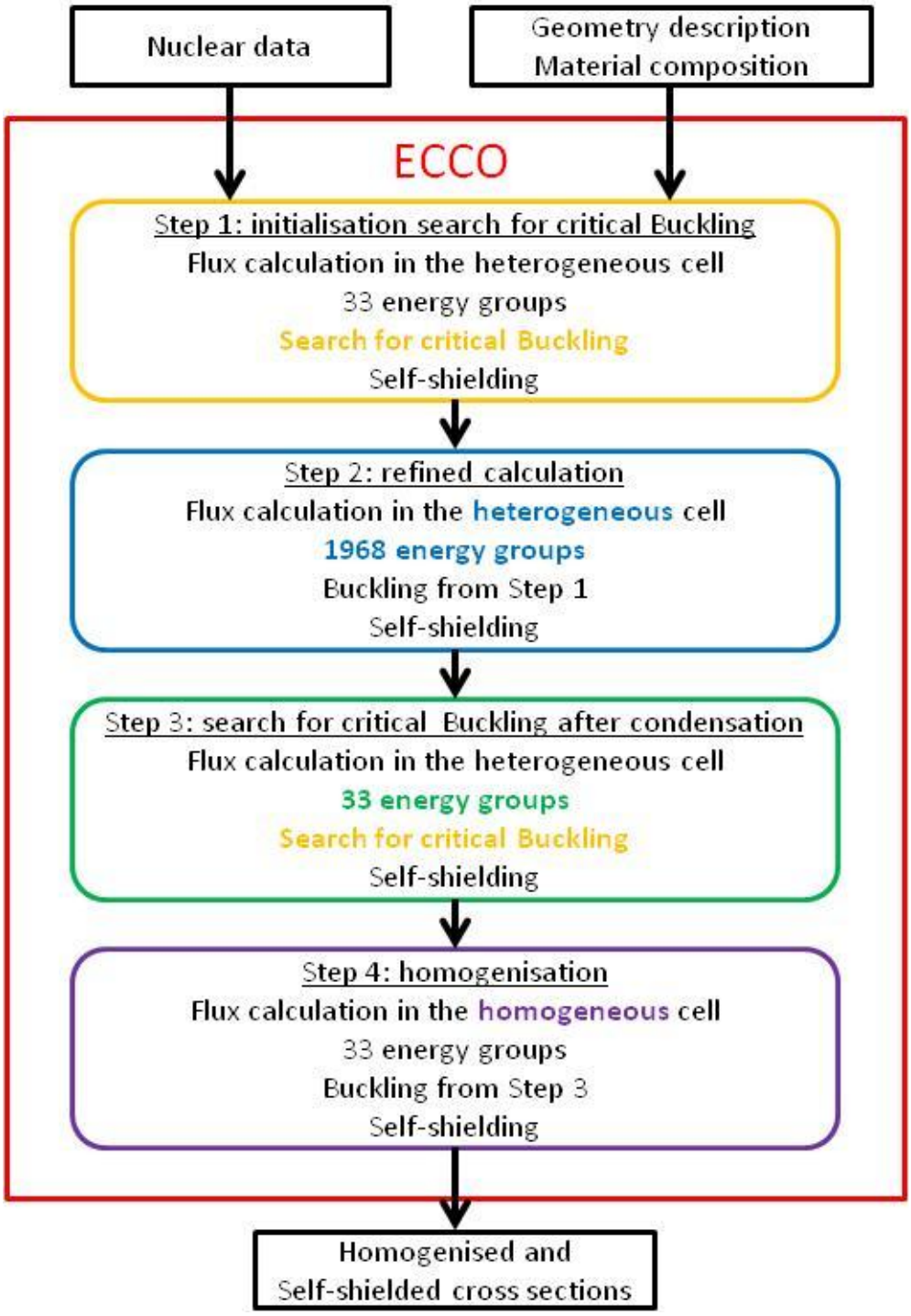

Figure II.1.3: Reference scheme for fuel cell calculation

The homogenised and self-shielded cross-sections are then used by a solver which calculates the neutron flux distribution at the core scale.

Sidebar 1: The self-shielding phenomenon

The discretisation in energy is one of the main issues for developing calculation scheme because the lesser energy groups you get the faster the simulation will be. However some cross-sections have important variations on small energy range, the most famous example is the case of total cross-section of the ^{238}U (see **Figure II.1.4**). From 0.025eV to 5.5 eV the cross-section is almost constant but between 5.5 eV and 20 keV the variations are important and very close from one to another, these variations are called **resonances**. Using a low number of groups to discretise it won't allow a faithful description of these variations and using thousands of groups or more in the core calculation is not an option. Getting a faithful representation in 33 groups of this is handled by the self-shielding process.

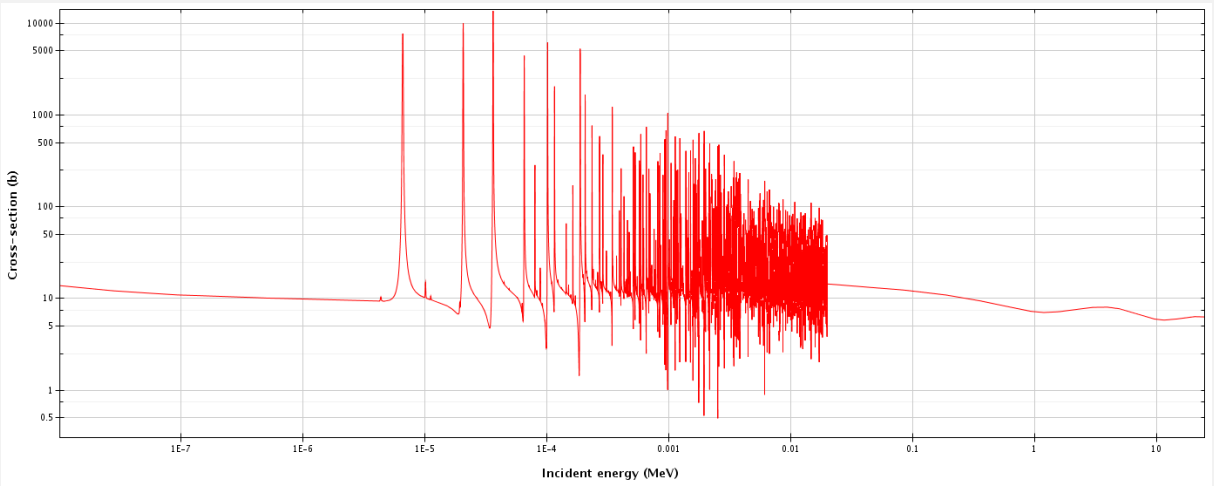

Figure II.1.4: U238 total cross-section

When the total cross-section is important on an energy interval the neutron flux is inversely very low on this interval due to the absorption of neutrons or the high scattering potential. Then the self-shielded cross-sections on the 33 energy groups discretisation have to well represent the neutron flux shape on this group. We define the **multigroup scalar flux**: $\Phi^g(\vec{r})$ such as:

$$\Phi^g(\vec{r}) = \int_g \Phi^g(\vec{r}, E)dE \qquad \textbf{1.7}$$

Then the **multigroup self-shielded cross-sections** are defined such as the multigroup reaction rate is equal to the punctual reaction rate integrated over the energy group. In other words we want to keep the same numbers of reactions by unit of time and volume in a group.

$$\sigma_r^g(\vec{r})\Phi^g(\vec{r}) = \int_g \sigma_r(E)\Phi^g(\vec{r}, E)dE \qquad \textbf{1.8}$$

The self-shielded cross-section is dependent of the space variable because it is weighted by the neutron flux which is calculated with the multigroup Boltzmann equation using the self-shielded cross-sections. This shows how complex the problem is indeed it is hard to get these cross-sections because:

- The punctual reaction rates are unknown because the punctual flux is unknown.
- The cross-section behaviour in the group can be resonant.

The punctual flux can be replaced by a weighting spectrum calculated by solving the slowing-down equation to get the energetic behaviour of the neutron flux. The **sub-group method** [4] used in ECCO calculates the multigroup self-shielded cross-sections without modelling the slowing down operator but by directly solving this equation on each self-shielded region a to get:

$$\sigma_{r,a}^g(\vec{r}) = \frac{\int_g \sigma_r(E)\Phi^g(\vec{r}, E)dE}{\int_g \Phi_a(E)dE} \qquad \textbf{1.9}$$

II.1.2.2 The BISTRO solver

The solver BISTRO [5] is implemented to solve the Boltzmann equation in transport theory which became the standard in neutronic through the improvements in calculation power and numerical methods since the beginning of simulation with the diffusion theory. This solver is able to solve the transport equation on 2D core geometries which is not a big issue since the cores studied can be approximated by a RZ description (see Chapter III and IV), the discrete ordinates method (or S_n method) is used and the angular flux is discretised on a group of directions in 4π steradian.

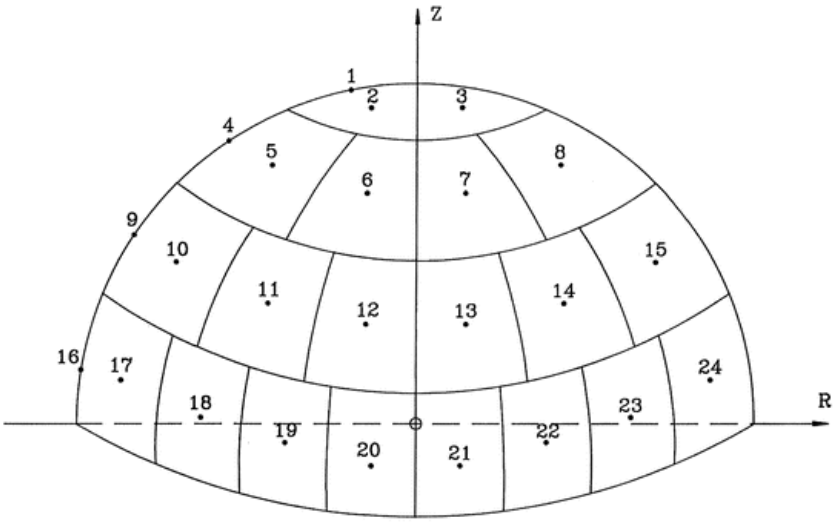

Figure II.1.5: Schematic view of the 24 directions of the S_8 symmetric quadrature

II.1.3 Monte-Carlo code TRIPOLI-4®

The Monte-Carlo approach [6] [7] consists in simulating the "reality" of microscopic phenomenon, the neutrons are tracked (to get their "histories") and their interactions (called "events") are registered and randomly chosen between: diffusion, capture, etc. Simulating a big enough number of particles allows to get the macroscopic values of interest. Typically one billion of histories is enough to get results with an accuracy of some pcm on reactivity or 1% on the power map.

This method is said "exact" compared to the deterministic method because no approximation is used to solve the Boltzmann equation. Another asset is the ability of this method to simulate 3D exact geometries (and not using homogeneous media). Nevertheless the convergence of this method is quite long making it unusable for parametric studies.

The stochastic approach is based on:

- The definition of a statistic "set" from a source: the histories of the particles and their events.
- The definition of a random variable X(Z) associated to the physical value searched R(Z), X is called the estimator. When a particle interacts in the area Z of interest a weight ω is calculated and the estimator is the sum of these weights.
- The random selection of: the path of the particle, the probability of each interaction, the energy of the particle... The probability densities have to be chosen such as: $E(X(Z)) = R(Z)$.
- The "set" has to be repeated independently M times. TRIPOLI-4® in practice repeats M times the set in N batch.

$$\tilde{X}_n(Z) = \frac{1}{M}\sum_{m=1}^{M} \omega_{m,n}(Z)$$

- The law of large numbers states that if N is high enough R(Z) is calculated as:

$$\bar{X}_N(Z) = \frac{1}{N}\sum_{n=1}^{N} \tilde{X}_n(Z)$$

- The "central limit theorem" states that $\tilde{X}_n$ are distributed following a Gaussian law and the variance associated is calculated as follows:

$$\varepsilon^2_{\bar{X}_N} = \frac{1}{N(N-1)}\sum_{n=1}^{N} (X_n(Z) - \bar{X}_N(Z))^2$$

- The trust interval is given as:
  - $1\varepsilon_{\bar{X}_N}$ for 68.9% of trust
  - $2\varepsilon_{\bar{X}_N}$ for 95.4% of trust
  - $3\varepsilon_{\bar{X}_N}$ for 99.7% of trust

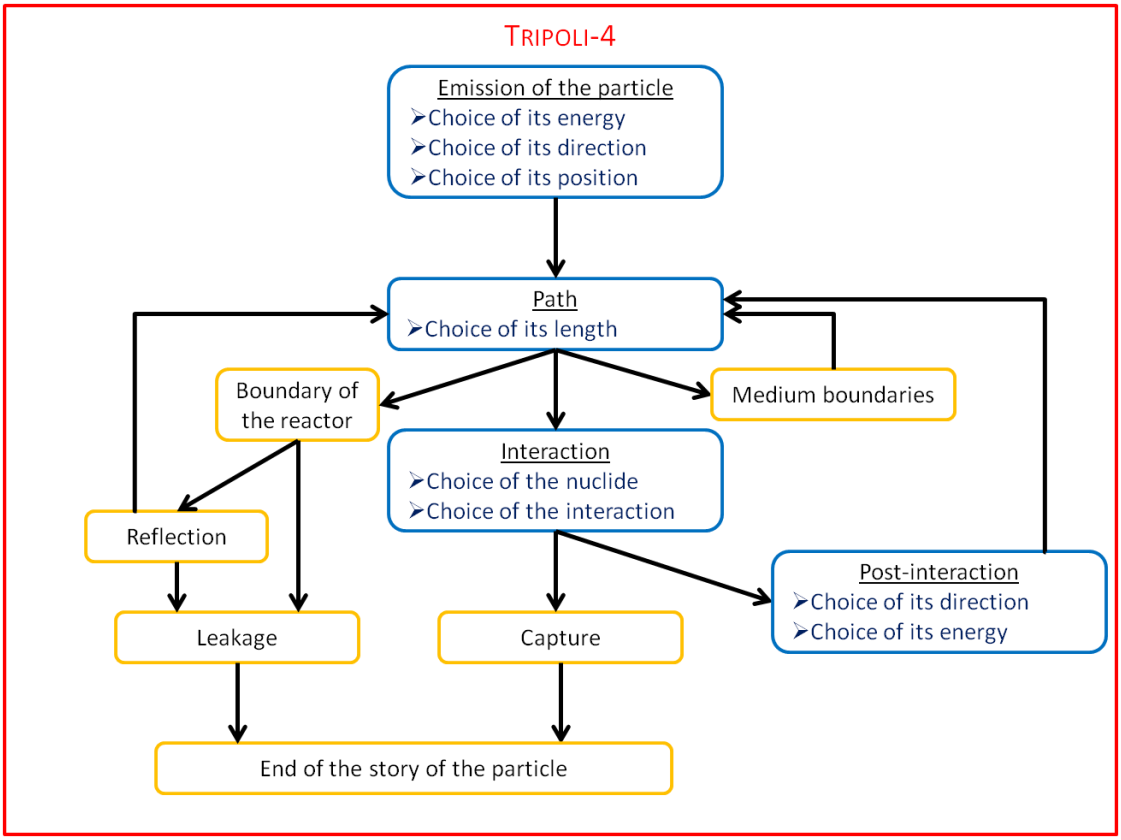

Figure II.1.6: TRIPOLI-4 general algorithm (in blue random sampling)

TRIPOLI-4® [8] is a reference tool for the CEA and its validation has been done according to the NEA standards. An intensive use of this reference tool has been done during this PhD.

II.2 Perturbation theory

The perturbation theory [9] is a powerful tool to analyse the breakdown of reactivity effect by nuclides, reaction and energy groups and also to get the sensitivities of macroscopic values to nuclear data and their associated uncertainties. It allows doing less calculations in parametric studies because the sensitivity to each parameter can be easily calculated using perturbation theory. This section presents the three major theories implemented in ERANOS.

II.2.1 The Standard Perturbation Theory

II.2.1.1 Reactivity variation and the adjoint equation

The reactivity variation $d\rho$ in the core is calculated as a variation of each operator A and F, the variation of the flux has also to be taken into account. In order to access this reactivity variation it is needed to derive the steady-state Boltzmann equation:

$$d\left[\left(\mathbf{A}-\frac{\mathbf{F}}{k}\right)\Phi\right]=0 \qquad \textbf{2.1}$$

The derivation of such equation leads to:

$$\left[\left(d\mathbf{A}-\frac{d\mathbf{F}}{k}\right)\Phi+\left(\mathbf{A}-\frac{\mathbf{F}}{k}\right)d\Phi+\frac{dk}{k^2}\mathbf{F}\Phi\right]=0 \qquad \textbf{2.2}$$

We remind that the reactivity is defined as:

$$\rho=1-\frac{1}{k} \quad \text{then} \quad d\rho=\frac{dk}{k^2} \qquad \textbf{2.3}$$

Meaning that:

$$d\rho\mathbf{F}\Phi=-\left[\left(d\mathbf{A}-\frac{d\mathbf{F}}{k}\right)\Phi+\left(\mathbf{A}-\frac{\mathbf{F}}{k}\right)d\Phi\right] \qquad \textbf{2.4}$$

Usually to get rid of the flux variation dependence this equation is weighted by a function u:

$$d\rho\langle u,\mathbf{F}\Phi\rangle=-\left[\langle u,\left(d\mathbf{A}-\frac{d\mathbf{F}}{k}\right)\Phi\rangle+\langle u,\left(\mathbf{A}-\frac{\mathbf{F}}{k}\right)d\Phi\rangle\right] \qquad \textbf{2.5}$$

The adjoint operators $\mathbf{A}^+$ and $\mathbf{F}^+$ are introduced here, respecting the adjoint equation and vanishing the term in $d\Phi$:

$$\left(\mathbf{A}^+-\frac{\mathbf{F}^+}{k}\right)u=0 \qquad \textbf{2.6}$$

This function u is then referring to the adjoint flux Φ^+ giving for the reactivity variation:

$$d\rho=-\frac{\langle\Phi^+,\left(d\mathbf{A}-\frac{d\mathbf{F}}{k}\right)\Phi\rangle}{\langle\Phi^+,\mathbf{F}\Phi\rangle} \qquad \textbf{2.7}$$

The perturbation theory allows to breakdown a reactivity variation by energy group, by medium and by reaction.

II.2.1.2 Meaning of the adjoint flux

The adjoint flux is a mathematical function obtained by solving the adjoint Boltzmann equation. There is a physical way to read that solution. Considering the case where the system is critical, we introduce a source S of one neutron emitted at t_s, at position $\overrightarrow{r_s}$ with an energy E_s and flying in the direction $\overrightarrow{\Omega_s}$. The time dependent equation is then (see equation **1.4**):

$$\frac{1}{v}\frac{\partial \Phi}{\partial t} = (\mathbf{F} - \mathbf{A})\Phi + S \qquad \textbf{2.8}$$

We define the operator: $\mathbf{H} = \mathbf{F} - \mathbf{A}$ such as before the introduction of S, Ψ is solution of: $\mathbf{H}\Psi = 0$ and Ψ^+ is solution of $\mathbf{H}^+\Psi^+ = 0$. Multiplying the **2.8** equation by Ψ^+ and integrating other all variables leads us to:

$$\langle \Psi^+, \int_{t_s}^{t} \frac{1}{v}\frac{\partial \Phi}{\partial t} dt \rangle = \int_{t_s}^{t} \langle \Psi^+, \mathbf{H}\Phi \rangle dt + \int_{t_s}^{t} \langle \Psi^+, S \rangle dt \qquad \textbf{2.9}$$

As $\mathbf{H}^+\Psi^+ = 0$ the second term vanishes. The third term gives the adjoint flux at t_s: $\Psi^+(\overrightarrow{r_s}, E_s, \overrightarrow{\Omega_s})$. We assume that if we consider a time t long enough, the transients harmonics of the flux Φ will vanish and only the fundamental mode will remain, meaning that for $t \to \infty$ we have: $\Phi \to \lambda\Psi$. The constant λ is then:

$$\lambda = \frac{\Psi^+(\overrightarrow{r_s}, E_s, \overrightarrow{\Omega_s})}{\langle \Psi^+, \frac{1}{v}\Psi \rangle}$$

The asymptotic solution for the neutron flux when we introduce one neutron at t_s, at position $\overrightarrow{r_s}$ with an energy E_s and flying in the direction $\overrightarrow{\Omega_s}$ in a critical system is:

$$\Psi(\vec{r}, E, \vec{\Omega}, t) \xrightarrow[t \to \infty]{} \frac{\Psi^+(\overrightarrow{r_s}, E_s, \overrightarrow{\Omega_s})}{\langle \Psi^+, \frac{1}{v}\Psi \rangle} \Psi(\vec{r}, E, \vec{\Omega})$$

We find there that the adjoint flux is related to the number of fissions that a neutron will produce in a chain reaction, we call it the "importance" of the neutron.

II.2.2 The Generalised Perturbation Theory

The reactivity is not the only interesting physical value in a reactor core, the operation of such a reactor implies the use of detectors such as fission chambers which gives a reaction rate or other kinetic parameter. Then getting the sensitivities of this reaction rate or of this kinetic parameter to nuclear data is important and is done using the Generalised Perturbation Theory [10].

II.2.2.1 Linear function of the forward flux

The reaction rate given by the response of a fission chamber is written as $R = \langle \Sigma_f \Phi \rangle$, the derivation of this value includes variation of flux terms, to get an independent expression of flux variation we introduce a Lagrange multiplier defined as follows:

$$T = \ln(R) - \langle \Psi^+, \left(\mathbf{A} - \frac{\mathbf{F}}{k}\right)\Phi \rangle \qquad \textbf{2.10}$$

The derivation of T gives the sensitivity of the reaction rate to a nuclear data σ: $S(R, \sigma) = \frac{\sigma}{R}\frac{dR}{d\sigma}$

$$dT = \frac{\langle d\Sigma_f \Phi + \Sigma_f d\Phi \rangle}{\langle \Sigma_f \Phi \rangle} - \langle d\Psi^+, \underbrace{\left(\mathbf{A} - \frac{\mathbf{F}}{k}\right)\Phi}_{=0} \rangle - \langle \Psi^+, \left(d\mathbf{A} - \frac{d\mathbf{F}}{k}\right)\Phi \rangle - \langle \Psi^+, \left(\mathbf{A} - \frac{\mathbf{F}}{k}\right) d\Phi \rangle \qquad \textbf{2.11}$$

The adjoint generalised importance Ψ^+ is built as the solution of the following equation (grouping $d\Phi$ terms):

$$\left(\mathbf{A}^{+}-\frac{\mathbf{F}^{+}}{k}\right)\Psi^{+}=\frac{\Sigma_f}{\langle\Sigma_f\,\Phi\rangle} \qquad \textbf{2.12}$$

Finally we get the sensitivity of the reaction rate with a direct and an indirect sensitivity term

$$S(R,\sigma)=\frac{\sigma}{R}\frac{dR}{d\sigma}=\frac{\sigma}{R}\left[\underbrace{\frac{\langle d\Sigma_f\,\Phi\rangle}{\langle\Sigma_f\,\Phi\rangle}}_{\text{direct term}}-\underbrace{\langle\Psi^{+},\left(d\mathbf{A}-\frac{d\mathbf{F}}{k}\right)\Phi\rangle}_{\text{Indirect term}}\right] \qquad \textbf{2.13}$$

II.2.2.2 Bi-linear function of the forward and adjoint flux

It can also be interesting to get the sensitivity of parameters using flux and adjoint flux such as delayed neutron fraction in that case another generalised importance function is added, a forward one: Ψ built as the solution of the equation grouping the $d\Phi^{+}$ terms. The indirect terms is then the sum of two terms:

$$\text{Indirect term}=\langle\Psi^{+},\left(d\mathbf{A}-\frac{d\mathbf{F}}{k}\right)\Phi\rangle+\langle\left(d\mathbf{A}^{+}-\frac{d\mathbf{F}^{+}}{k}\right)\Phi^{+},\Psi\rangle \qquad \textbf{2.14}$$

II.2.3 The Equivalent Generalised Perturbation Theory

In order to study the sensitivities of a reactivity variation: $\Delta\rho=\rho_2-\rho_1$ is calculated using the first order perturbation theory twice.

$$d(\Delta\rho)=d\rho_2-d\rho_1=-\frac{\langle\Phi_2^{+},\left(d\mathbf{A_2}-\frac{d\mathbf{F_2}}{k_2}\right)\Phi_2\rangle}{\langle\Phi_2^{+},\mathbf{F_2}\Phi_2\rangle}+\frac{\langle\Phi_1^{+},\left(d\mathbf{A_1}-\frac{d\mathbf{F_1}}{k_1}\right)\Phi_1\rangle}{\langle\Phi_1^{+},\mathbf{F_1}\Phi_1\rangle} \qquad \textbf{2.15}$$

Then the sensitivities are calculated by normalizing this expression by the reactivity variation:

$$S(\Delta\rho,\sigma)=\frac{\sigma}{\Delta\rho}\frac{d(\Delta\rho)}{d\sigma}=-\frac{1}{\Delta\rho}\left[\frac{\langle\Phi_2^{+},\left(d\mathbf{A_2}-\frac{d\mathbf{F_2}}{k_2}\right)\Phi_2\rangle}{\langle\Phi_2^{+},\mathbf{F_2}\Phi_2\rangle}-\frac{\langle\Phi_1^{+},\left(d\mathbf{A_1}-\frac{d\mathbf{F_1}}{k_1}\right)\Phi_1\rangle}{\langle\Phi_1^{+},\mathbf{F_1}\Phi_1\rangle}\right] \qquad \textbf{2.16}$$

As we will see in the Chapter V this sensitivity is very sensitive to the $\Delta\rho$ value indeed if the two reactivities are very close (i.e. $\Delta\rho\approx 0$) even if the operators **A** and **F** are very different between the two states the $S(\Delta\rho,\sigma)$ will skyrocket due to the $\frac{1}{\Delta\rho}$ factor.

II.3 Nuclear data uncertainties

As seen in the previous section, neutronic codes needs nuclear data such as cross-sections, fission spectrum to solve the Boltzmann equations. These data are coming from international evaluated libraries such as ENDF (USA), JEFF (Europe), JENDL (Japan) … These tabulated values are the results of microscopic experiments or of simulations[1] which model the nucleus and its component to get access to energetic levels. Indeed, as it is impossible to get access to experimental data for each cross-section for each existing isotope then only the most used materials are under experimental studies. Furthermore these values are known with uncertainties which imply an overall uncertainty on the calculated parameters. This uncertainty due to nuclear data (ND) on one parameter p can be

[1] With CONRAD [11] at CEA for instance.

calculated using the sensitivities of this parameter to ND (S_p) and with the help of "Sandwich" law and of a covariance matrix (B):

$$I^2 = S_p^t \, B \, S_p \qquad \textbf{3.1}$$

The covariance matrix takes into account the covariance between energetic distribution of the uncertainty and between cross-sections because their behaviour are not fully independent. The library JEFF is associated to the covariance matrix COMAC [12]. There exist different version of this matrix, the two used in this work are the COMAC-V1 which is the latest version of COMAC produced without an integral assimilation work by CEA whereas the COMAC-V2 incorporates information from some experiments (GODIVA, JEZEBEL and PROFIL). For the main actinides present in nuclear reactors (such as ^{235}U, ^{238}U and ^{239}Pu) the covariance matrices of COMAC-V1 were produced at CEA using the CONRAD code. For the other isotopes, including actinides such as ^{240}Pu or ^{242}Pu, covariance data have been retrieved from COMMARA-V2.0 or the covariance matrices associated to JENDL-4.0. The delayed neutrons data covariance have also been taken from the JENDL-4.0 library. The origin of the covariance matrices present in COMAC-V1 is given in **Table 3.1** for several actinides.

Table 3.1: Origin of the covariance matrices present in COMAC-V1 for the different nuclear of several actinides. PFNS stands for Prompt Fission Neutron Spectrum

Isotope	Cross sections	Neutrons multiplicities	PFNS	
			Thermal	Fast
U-235	CEA	JENDL-4.0-up2	CEA	ENDF/B-VII.1
U-238	CEA	JENDL-4.0-up1	JENDL-4.0-up1	JENDL-4.0-up1
Pu-238	ENDF/B-VII.1	JENDL-4.0-up1	ENDF/B-VII.1	ENDF/B-VII.1
Pu-239	CEA	JENDL-4.0-up1	CEA	JENDL-4.0-up1
Pu-240	CEA	JENDL-4.0	JENDL-4.0	JENDL-4.0
Pu-242	ENDF/B-VII.1	ENDF/B-VII.1	ENDF/B-VII.1	ENDF/B-VII.1
Am-241	CEA (RRR) + ENDF/B-VII.1 (cont.)	ENDF/B-VII.1	JENDL-4.0-up1	JENDL-4.0-up1

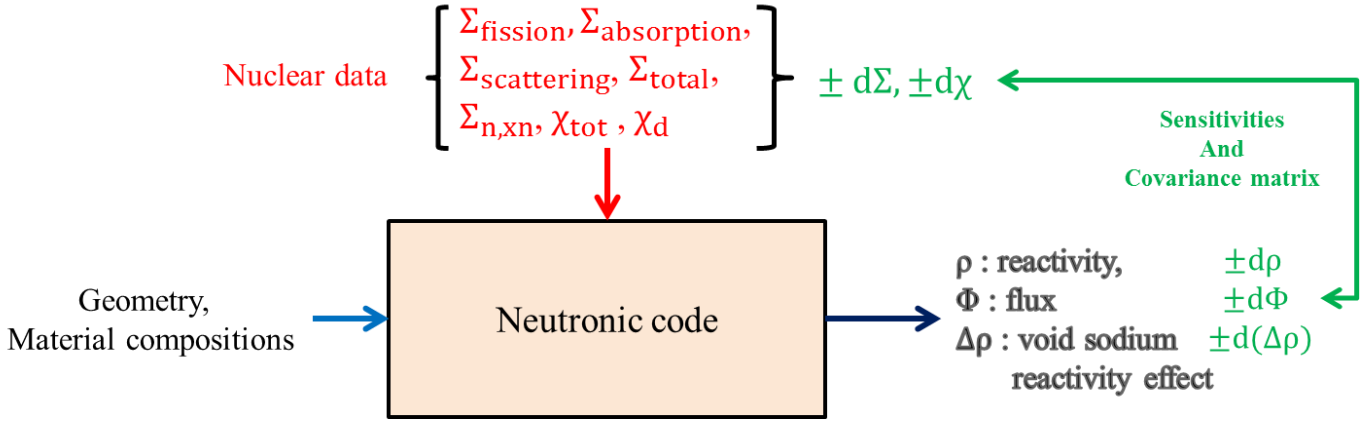

Figure II.3.1: Influence of nuclear data uncertainties on calculated parameters

These uncertainties can be very important and their knowledge is a key challenge for the safety of nuclear reactors. Indeed a better understanding of the source of these uncertainties decreases the gap needed to guarantee the safety margin and then the financial cost of the plant for its construction and its operation.

References

[1] Commissariat à l'énergie atomique (France), *La neutronique*. Paris: le Moniteur : CEA, 2013.

[2] G. Rimpault, D. Plisson, J. Tommasi, and R. Jacqmin, 'The ERANOS code and data system for fast reactor neutronic analyses', presented at the PHYSOR'02, Seoul, KOREA, 2002.

[3] G. Rimpault, 'Algorithmic features of the ECCO Cell Code for treating heterogeneous fast reactor subassemblies', *Proc. Int. Conf. Math. Comput. React. Phys. Environ. Anal.*, vol. 28, 1995.

[4] A. Herbert, 'Development of a subgroup method for the self-shielding of resonant isotopes in arbitrary geometries', *Int. Conf. Phys. React. PHYSOR96*, vol. 1.

[5] G. Palmiotti, J.-M. Rieunier, C. Gho, and M. Salvatores, 'BISTRO Optimized Two Dimensional Sn Transport Code', *Nucl. Sci. Eng.*, vol. 104, no. 1, 1990.

[6] N. Metropolis and S. Ulam, 'The Monte-Carlo Method', *J. Am. Stat. Assoc.*, 1949.

[7] I. Lux and L. Koblinger, 'Monte Carlo Particle Transport Methods : Neutron and Photon Calculations', *CRC Press*, 1991.

[8] E. Brun *et al.*, 'TRIPOLI-4®, CEA, EDF and AREVA reference Monte Carlo code', *Ann. Nucl. Energy*, vol. 82, pp. 151–160, Aug. 2015.

[9] J. Tommasi, 'ERANOS user's manual – applications of perturbation theory with finite difference diffusion and Sn transport flux solvers'. RT 07-003 SPRC/LEPh.

[10] A. Gandini, 'A generalized perturbation method for bi-linear functionals of the real and adjoint neutron fluxes', *J. Nucl. Energy*, vol. 21, no. 10, pp. 755–765, 1967.

[11] P. Archier *et al.*, 'CONRAD Evaluation Code: Development Status and Perspectives', *Nucl. Data Sheets*, vol. 118, pp. 488–490, 2014.

[12] P. Archier, C. De Saint Jean, G. Noguere, O. Litaize, P. Leconte, and C. Bouret, 'COMAC: Nuclear Data Covariance Matrices Library for Reactor Applications', presented at the PHYSOR 2014- The Role of Reactor Physics toward a Sustainable Future, Kyoto, Japan, 2014.

This page has been left blanked intentionally

Chapter III: The delayed neutron fraction

Abstract

In this Chapter, the first section introduces the effective delayed neutron fraction and its importance in the safety and operation of a nuclear reactor. Furthermore in experimental programme the reactivity is measured by the position of shim rod or/and the addition of peripheral assemblies. A rod drop and the use of the Nordheim equation insures the calibration of the reactivity. Then the reactivity is measured in a β_{eff} scale which is the effective delayed neutron fraction of the core. A new analysis of β_{eff} measured in the BERENICE programme (in the MASURCA facility) has been made using different experimental methods which are presented in the second section with the raw experimental values and the parameters calculated through simulations and required to access the measured β_{eff}. The three cores of the BERENICE programme in which these measurements have been conducted are presented in the third section. As the calculated β_{eff} can be obtained with the ERANOS deterministic code or with the stochastic code TRIPOLI-4® using different methods, the fourth section gives an exhaustive recap of these methods and their results for the three studied cores. This section also presents the use of the IFP method recently implemented in TRIPOLI-4® to get adjoint flux integrals and sources importance mandatory to get access to experimental β_{eff}. The last section analyses the uncertainties sources affecting the measurements and the simulations. The use of the Generalised Perturbation Theory allows getting the sensitivities of the β_{eff} to nuclear data and with recent nuclear data covariances and the sandwich formula, we obtain 2.8% of uncertainty for the β_{eff} of R2 cores and 2.6% for the ZONA2 core; values consistent with the C/E values and the experimental uncertainties.

Contents

III.1 The effective delayed neutron fraction

III.1.1 Physics of the chain reaction

In a nuclear reactor, a chain reaction of neutron emissions is maintained for long periods. The fission of an Uranium or Plutonium nuclei produces prompt neutrons[1] and the times interval between two prompt fission in a fast nuclear core is about $\tau = 10^{-7}$s. If only prompt neutrons were existing and if an increase of only one tenth of pcm were occuring during one second, then the neutron population would be multiplied by:

$$1.000001^{10^7} \approx 22000$$

The operation of such a core would be impossible even with computer control. During the fission process, some fission products are produced which are radioactive isotopes[2]. They decay to more stable nuclei by β^- decay. These decays have a longer period and hence they create delayed neutrons because of this late emission after the fission event.

The delayed neutrons are only a fraction of the total of neutrons emitted in the core each second. For instance in enriched Uranium based fuel cores the effective delayed neutrons is about 665 pcm (0.665% !) and around 350 pcm for Plutonium based fuel cores. As it exists hundreds of precursors they have been classified historically in 6 or 8 families according to their decay period [1].

Table III.1.1: Delayed neutrons groups emitted by the Uranium 235

Group	Decay constant λ_i(s^{-1})	β_i (pcm)	Average lifetime τ_i (s)
1	1,247 10^{-2}	22	80,21
2	2,829 10^{-2}	102	35,35
3	4,252 10^{-2}	61	23,52
4	1,330 10^{-1}	31	7,516
5	2,925 10^{-1}	220	3,419
6	6,665 10^{-1}	60	1,500
7	1,635	54	0,6117
8	3,555	15	0,2813
	Average: 7,681 10^{-2}	Total : 665	Average: 13,02

The introduction of these delayed neutrons has a huge impact on the neutron population behaviour in the core because we can calculate the mean time between two generations of neutrons as follow:

$$t = (1 - \beta_{eff}) \times \tau + \sum_i \beta_i \times (\tau_i + \tau) = 0.087 \text{ s}$$

In one second, there are $1/0.087 = 12$ generations of neutrons. If we now consider a reactivity insertion of 100 pcm during one second, the neutron population would be multiplied by:

[1] with an energy of around 2 MeV, there are fast neutrons: see chapter 1.
[2] radioactive isotopes are also produced during the operation of the plant.

$$1.000100^{12} = 1.012$$

The neutron population increases reasonably (compared to possible reactivity insertion by control rods) making the operation of a nuclear reactor possible.

III.1.2 The effective delayed neutron fraction

The cores studied in this chapter are small enough to allow the use of the point kinetic model to describe the neutronic behaviour of the core. The delayed neutrons are emitted by I precursor families and each family i has the following characteristics:

- λ_i the disintegration constant of the precursors family (in s^{-1})
- χ_{di} the delayed neutron spectrum
- ν_{di} the delayed neutron yield
- $C_i(\vec{r}, t)$ the delayed neutrons density emitted by the precursors of the family i, i.e. the product of the precursors density (in cm^{-3}) by the delayed neutron yield ν_{di} divided by 4π, the delayed neutrons emission is isotropic.
- $\beta_i = \frac{\nu_{di}}{\nu_{tot}}$ the delayed neutron fraction associated to the family i, with ν_{tot} the fission yield i.e. the average number of neutrons emitted by fission (prompt and delayed).

The neutron balance is then expressed with the Boltzmann equation dependent on the time (see Chapter II, section 1.1) and the Bateman equations giving the delayed neutron emission by the β^- decay of precursors.

$$\begin{cases} \frac{1}{v}\frac{\partial \Psi}{\partial t} + \mathbf{A}\Psi = \mathbf{F_p}\Psi + \sum_{i=1}^{I} \lambda_i \chi_{di} C_i + S \\ \frac{\partial C_i}{\partial t} + \lambda_i C_i = \beta_i \mathbf{P}\Psi \qquad i = 1, \dots, I \end{cases} \quad \textbf{1.1}$$

With:

- Ψ the neutron flux,
- v the neutron speed,
- S an external source of neutron
- $\mathbf{F_p}$ the prompt fission operator, the neutron yield and spectra are the ones of prompt neutrons,
- $\mathbf{P}$ the production operator such as: $\mathbf{F} = \chi(\vec{r}, E, t)\mathbf{P}$

We do not consider the migration of precursors in the fuel in this work because the fuel used is solid [2]. The neutron flux is factorised such as: $\Psi(\vec{r}, E, \vec{\Omega}, t) = N(t).\Phi(\vec{r}, E, \vec{\Omega}, t)$ in order to split the fast neutron flux magnitude variation $N(t)$ from a shape function $\Phi(\vec{r}, E, \vec{\Omega}, t)$ with slow variation as function of times. To make this factorisation unique we have to add a normalisation condition with the adjoint flux such as:

$$\frac{\partial}{\partial t}\langle \Phi^+, \frac{1}{v}\Phi \rangle = 0$$

The perturbation considered is small enough so that the core remains close to the criticality. Hence, the neutron flux keeps the same spectrum and distribution when adding the delayed neutrons. Weighting the **1.1** system by the adjoint flux we get:

$$\begin{cases} \langle \Phi^+, \frac{1}{v}\frac{\partial \Phi}{\partial t} N\rangle + \langle \Phi^+, \frac{1}{v}\frac{\partial N}{\partial t}\Phi\rangle + \langle \Phi^+, \mathbf{A}\Phi\rangle = \langle \Phi^+, \mathbf{F_p}\Phi\rangle + \langle \Phi^+, \sum_{i=1}^{I} \lambda_i \chi_{di} C_i\rangle + \langle \Phi^+, S\rangle \\ \langle \Phi^+, \frac{\partial C_i}{\partial t}\rangle + \langle \Phi^+, \lambda_i C_i\rangle = \langle \Phi^+, \beta_i \mathbf{P}\Phi\rangle \qquad i = 1, \dots, I \end{cases} \quad \textbf{1.2}$$

By normalising these equations by $\langle \Phi^+, \frac{1}{v}\Phi\rangle$ we get the following system with effective values:

$$\begin{cases} \frac{\partial N}{\partial t} = \frac{\rho_{eff} - \beta_{eff}}{\Lambda_{eff}} N + \sum_{i=1}^{I} \lambda_i C_{eff,i} + S_{eff} \\ \frac{\partial C_{eff,i}}{\partial t} = \frac{\beta_{eff,i}}{\Lambda_{eff}} N - \lambda_i C_{eff,i} \qquad i = 1, \dots, I \end{cases} \quad \textbf{1.3}$$

The effective values are defined as follow:

Table III.1.1: Effective values

$\rho_{eff} = 1 - \frac{1}{k_{eff}} = 1 - \frac{\langle \Phi^+, \mathbf{A}\Phi\rangle}{\langle \Phi^+, \mathbf{F}\Phi\rangle}$	The effective reactivity defined from the effective multiplication factor.
$S_{eff} = \frac{\langle \Phi^+ \vert S\rangle}{\left\langle \Phi^+ \middle\vert \frac{1}{v}\Phi \right\rangle}$	The effective source is the ratio of the importance of the source by the importance of the neutrons of the core.
$C_{eff,i} = \frac{\left\langle \Phi^+ \middle\vert \frac{\chi_{di}}{4\pi} C_i \right\rangle}{\left\langle \Phi^+ \middle\vert \frac{1}{v}\Phi \right\rangle}$	The effective delayed neutrons density is the ratio of the delayed neutron density importance by the importance of the neutrons.
$\Lambda_{eff} = \frac{\left\langle \Phi^+ \middle\vert \frac{1}{v}\Phi \right\rangle}{\langle \Phi^+ \vert \mathbf{F}\Phi\rangle}$	The effective neutrons production time is the ratio of the importance of the neutrons by the importance of the fission production (prompt and delayed)
$\beta_{eff,i} = \frac{\langle \Phi^+ \vert \beta_i \chi_{di} \mathbf{P}\Phi\rangle}{\langle \Phi^+ \vert \mathbf{F}\Phi\rangle}$	The effective delayed neutrons partial fraction is the ratio of the importance of the delayed neutrons production of the i^{th} family by the importance of the fission production.
$\beta_{eff} = \sum_{i=1}^{I} \beta_{eff,i}$	The effective delayed neutron fraction.

The effective delayed neutron fraction is a value of interest for reactor physics, it is also expressed as the weighted delayed neutron production operator ($\mathbf{F_d}$) by the adjoint flux normalized by the total neutron fission operator($\mathbf{F}$):

$$\beta_{eff} = \frac{\langle \Phi^+, \mathbf{F_d}\Phi\rangle}{\langle \Phi^+, \mathbf{F}\Phi\rangle} \quad \textbf{1.4}$$

As it defines the upper limit of prompt criticality, the β_{eff} is used as reference factor for reactivity measurements. Indeed when we study the case of a sub-critical reactor supplied by a neutron stationary source S, the neutron balance is given by:

$$(\mathbf{A} - \mathbf{F})\Phi = S \quad \textbf{1.5}$$

The adjoint homogeneous equation is:

$$\left(\mathbf{A}^{+}-\frac{\mathbf{F}^{+}}{\mathrm{k}}\right)\Phi^{+}=0 \quad \text{or} \quad \mathbf{A}^{+}\Phi^{+}=\frac{\mathbf{F}^{+}\Phi^{+}}{\mathrm{k}} \qquad \textbf{1.6}$$

Multiplying equation **1.5** by the adjoint flux, we get:

$$\langle\Phi^{+},\mathrm{S}\rangle=\langle\Phi^{+},(\mathbf{A}-\mathbf{F})\Phi\rangle=\langle\Phi^{+},\mathbf{A}\Phi\rangle-\langle\Phi^{+},\mathbf{F}\Phi\rangle$$

$$\langle\Phi^{+},\mathrm{S}\rangle=\langle\mathbf{A}^{+}\Phi^{+},\Phi\rangle-\langle\Phi^{+},\mathbf{F}\Phi\rangle=\left(\frac{1}{\mathrm{k}}-1\right)\langle\Phi^{+},\mathbf{F}\Phi\rangle=-\rho\langle\Phi^{+},\mathbf{F}\Phi\rangle$$

$$\rho=-\frac{\langle\Phi^{+},\mathrm{S}\rangle}{\langle\Phi^{+},\mathbf{F}\Phi\rangle} \qquad \textbf{1.7}$$

The static reactivity[1] is then the ratio of the importance of the neutrons emitted by the source, by the importance of the fission production. During rod drop experiments or when introducing a neutron source in the core, the reactivity is measured in dollars which is the ratio of the reactivity of the core by the effective delayed neutrons fraction: $\rho_{\$}=\rho/\beta_{\mathrm{eff}}$.

III.2 Experimental measurements techniques

This section presents two experimental techniques [3] to get access to the β_{eff} thanks to fission chambers located in the experimental core: the Californium source method developed by Mihalczo in 1971 [4] and the noise technique method. There are other techniques but we limit this chapter to those which have been measured in the MASURCA facility during the BERENICE Programme [5].

III.2.1 The Californium source method

This experimental method consists in introducing a punctual source (4x4 mm²) of ^{252}Cf (S_{Cf}) emitting neutrons by spontaneous fission at the core centre and to measure the "apparent" reactivity variation. The counting rate of in-core detectors is directly related to the reactivity level because of the neutron flux levels inverse dependence on the reactivity (see equation **1.7**). Since in a reactor there is always a diffuse source of neutrons S_0 (due to spontaneous fission or from (α,n) reactions on oxygen, …) then the product of the counting rate R by the reactivity gives the level of this source:

$$\mathrm{R}.|\rho|=\mathrm{S}_0=\text{constant} \qquad \textbf{2.1}$$

The neutron balance in the core before (indexed 0) and after (indexed 1) the introduction of the ^{252}Cf source is given by:

$$(\mathbf{A}-\mathbf{F})\Phi_0=\mathrm{S}_0 \quad \text{and} \quad (\mathbf{A}-\mathbf{F})\Phi_1=\mathrm{S}_1 \qquad \textbf{2.2}$$

However the introduction of the ^{252}Cf source is too small to change the reactivity but still impacts the counting rate, the flux change is then seen as an "apparent" reactivity variation to keep the **2.1** relation true.

To define this "apparent" reactivity variation we can write the reactivity expression before and after the introduction of the ^{252}Cf source thanks to equation **1.7**:

$$\rho_0=-\frac{\langle\Phi^{+},\mathrm{S}_0\rangle}{\langle\Phi^{+},\mathbf{F}\Phi_0\rangle}=-\frac{\langle\Phi^{+},\mathrm{S}_1\rangle}{\langle\Phi^{+},\mathbf{F}\Phi_1\rangle} \qquad \textbf{2.3}$$

[1] The reactivity of the core without the source of neutrons.

With: $\langle \Phi^+, S_1 \rangle = \langle \Phi^+, S_0 \rangle + \langle \Phi^+, S_{Cf} \rangle$ and $\langle \Phi^+, \mathbf{F}\Phi_1 \rangle = \langle \Phi^+, \mathbf{F}(\Phi_0 + \Phi_{Cf}) \rangle$

These reactivity expressions imply to know the adjoint flux distribution in the core but this cannot be measured. However, counting rates $\langle \Sigma_d(\Phi_0 + \Phi_{Cf}) \rangle$ have been determined by some detectors located at different places in the core. One detector is chosen as a reference and it is the absolute fission rate of 1g of ^{235}U placed at the core centre $\langle \Sigma_f^{U5}(\Phi_1 + \Phi_0) \rangle$. Then we can develop the **2.3** expression with terms which can be measured or calculated:

$$-\rho \frac{\langle \Sigma_f^{U5} \Phi_1 \rangle}{\langle \Sigma_f^{U5}(\Phi_1 + \Phi_0) \rangle} = \frac{\langle \Phi^+, S_1 \rangle}{\langle \chi_{U5} \Phi^+ \rangle \langle S_1 \rangle} \frac{\langle S_1 \rangle}{\langle \Sigma_d(\Phi_1 + \Phi_0) \rangle} \frac{\langle \Sigma_d(\Phi_1 + \Phi_0) \rangle}{\langle \Sigma_f^{U5}(\Phi_1 + \Phi_0) \rangle} \frac{\langle \chi_{U5} \Phi^+ \rangle \langle \Sigma_f^{U5} \Phi_1 \rangle}{\langle \Phi^+, \mathbf{F}\Phi_1 \rangle} \qquad \textbf{2.4}$$

The first term is a counting rate (R) ratio and according to the approximated multiplication source method [6][7] is equivalent to a reactivity ratio, then multiplied by the reactivity it gives the "apparent" reactivity variation: $\Delta\rho$.

$$-\rho \frac{\langle \Sigma_f^{U5} \Phi_1 \rangle}{\langle \Sigma_f^{U5}(\Phi_1 + \Phi_0) \rangle} = -\rho \left(1 - \frac{\langle \Sigma_f^{U5} \Phi_0 \rangle}{\langle \Sigma_f^{U5}(\Phi_1 + \Phi_0) \rangle} \right) = -\rho \left(1 - \frac{R_{\text{without Cf}}}{R_{\text{with Cf}}} \right) = \Delta\rho$$

The reactivity variation is measured in \$ meaning that: $\Delta\rho = \beta_{eff}.\Delta\rho_{\$}$. The second term of the **2.4** equation is obtained thanks to measured and calculated parameters defined as follow:

$S_{sc} = \langle S_1 \rangle$	The **measured** integrated intensity of the californium 252 source (n/s)
$\varphi_{sc} = \frac{\langle \Phi^+, S_1 \rangle}{\langle \chi_{U5} \Phi^+ \rangle \cdot \langle S_1 \rangle}$	The **calculated** relative importance of the californium 252 source to the neutrons emitted by the fission of 1g of ^{235}U at the core centre (without dimension).
$N = \langle \Sigma_d(\Phi_1 + \Phi_0) \rangle$	The **measured** counting rate of one detector (reactions/s)
$K_e = \frac{\langle \Sigma_f^{U5}(\Phi_1 + \Phi_0) \rangle}{\langle \Sigma_d(\Phi_1 + \Phi_0) \rangle}$	The **measured** counting rate ratio of 1g of ^{235}U at the core centre to the counting rate of the detector (without dimension)
$K_c = \frac{\langle \Phi^+, \mathbf{F}\Phi_1 \rangle}{\langle \chi_{U5} \Phi^+ \rangle \cdot \langle \Sigma_f^{U5} \Phi_1 \rangle}$	The **calculated** importance ratio of the total fission operator to the neutrons emitted by the fission of 1g of the reference nucleus at the core centre (without dimension)

Then we get the effective delayed neutron fraction with one calculated parameter P_c and another one measured P_m:

$$\beta_{eff} = \frac{\varphi_{sc}}{K_c} \frac{S_{sc}}{N.K_e.|\Delta\rho_{\$}|} = P_c.P_m \qquad \textbf{2.5}$$

With:

$P_c = \frac{\varphi_{sc}}{K_c}$	This parameter only needs the calculated value of the importance of the californium source S_1 and the neutron flux due to this source: $(\mathbf{A} - \mathbf{F})\Phi_1 = S_1$ And it also needs the nuclear data of ^{235}U: χ_{U5} and Σ_f^{U5}.
$P_m = \frac{S_{sc}}{N.K_e.\|\Delta\rho_{\$}\|}$	This parameter needs the counting rates of two detectors and the integrated intensity of the source experimentally measured.

III.2.2 The noise technique

In a sub-critical reactor in a stationary state the absorption, the leakage and the production of neutrons are considered as random phenomena ruled by a Poisson distribution creating a noise. These neutronic fluctuations can be studied thanks to a transfer function and thanks to the intercomparating analysis of the signals of two detection chains.

To get the transfer function we look at the spectral density (pulsation ω) of the noise given by:

$$\overline{|\delta s(\omega)|^2} = 2\frac{N}{\Lambda}\frac{\overline{\nu(\nu-1)}}{\bar{\nu}} \qquad \textbf{2.6}$$

With: N the neutron population of the reactor, Λ the production time of prompt neutrons and ν the neutronic yield. Meaning that $^{N}/_{\Lambda}$ is the number of neutrons emitted each second in the reactor also equals to: $\bar{\nu}.F = {}^{N}/_{\Lambda}$. The Diven factor is defined as:

$$D = \frac{\overline{\nu(\nu-1)}}{\bar{\nu}^2}$$

Then we have:

$$\overline{|\delta s(\omega)|^2} = 2\left(\frac{N}{\Lambda}\right)^2\frac{D}{F} \qquad \textbf{2.7}$$

This source of noise is creating fluctuation of neutrons population and in precursors and then in reactivity in **1.3** equations.

$$\begin{cases}\dfrac{\partial \delta N}{\partial t} = \dfrac{\rho_{eff}-\beta_{eff}}{\Lambda_{eff}}\delta N + \displaystyle\sum_{i=1}^{I}\lambda_i \delta C_{eff,i} + \frac{N}{\Lambda}\delta\rho \\ \dfrac{\partial \delta C_{eff,i}}{\partial t} = \dfrac{\beta_{eff,i}}{\Lambda_{eff}}\delta N - \lambda_i \delta C_{eff,i} \qquad i = 1,\dots,I\end{cases} \qquad \textbf{2.8}$$

Using the Fourier transformation on this linear differential system, we get the following transfer function:

$$H(\omega) = \frac{\delta N(\omega)}{\delta s(\omega)} = \frac{\Lambda_{eff}}{i\Lambda_{eff}\omega - (\rho_{eff}-\beta_{eff}) - \sum_{i=1}^{I}\frac{\lambda_i\beta_{eff,i}}{\lambda_i + i\omega}} \qquad \textbf{2.9}$$

Which gives:

$$|\delta N(\omega)|^2 = |\delta s(\omega)|^2.|H(\omega)|^2$$

$$|\delta N(\omega)|^2 = 2\left(\frac{N}{\Lambda}\right)^2\frac{D}{F}\frac{{\Lambda_{eff}}^2}{\left(\beta_{eff}-\rho_{eff}-\sum_{i=1}^{I}\frac{{\lambda_i}^2\beta_{eff,i}}{{\lambda_i}^2+\omega^2}\right)^2 - \omega^2\left(\Lambda_{eff}+\sum_{i=1}^{I}\frac{\lambda_i\beta_{eff,i}}{{\lambda_i}^2+\omega^2}\right)^2} \qquad \textbf{2.10}$$

By choosing a pulsation ω such as:

$$\sum_{i=1}^{I} \frac{{\lambda_i}^2 \beta_{eff,i}}{{\lambda_i}^2 + \omega^2} \ll \rho_{eff} - \beta_{eff} \quad \text{and} \quad \sum_{i=1}^{I} \frac{\lambda_i \beta_{eff,i}}{{\lambda_i}^2 + \omega^2} \ll \Lambda_{eff}$$

The **2.10** expression is simplified as:

$$\frac{|\delta N(\omega)|^2}{N^2} \approx 2\frac{D}{F}\frac{1}{(\beta_{eff} - \rho_{eff})^2 - \omega^2 {\Lambda_{eff}}^2}$$

Furthermore if: $\omega\Lambda_{eff} \ll |\beta_{eff} - \rho_{eff}|$ then:

$$\frac{|\delta N(\omega)|^2}{N^2} \approx 2\frac{D}{F}\frac{1}{(\beta_{eff} - \rho_{eff})^2} \qquad \textbf{2.11}$$

In this case: the first term is the power spectral density (PSD) of the fluctuations of the neutron population which can be measured in the reactor. Two detectors are needed in order to get rid of the detection noise when analysing the signal: the non-correlated events are eliminated and only the simultaneous ones are kept. This is called the intercomparated PSD (IPSD).

$$\frac{IPSD}{V_1 . V_2} = 2\frac{D}{F}\frac{1}{(\beta_{eff} - \rho_{eff})^2}$$

$${\beta_{eff}}^2 = 2\frac{D . V_1 . V_2}{F . IPSD(1 + |\rho_\$|)^2} \qquad \textbf{2.12}$$

With: V_1 and V_2 the voltage of the two detection chains. We get F, the global fission rate in the core, thanks to measured counting rates of two detectors and one calculated parameter:

$$F = \langle \Sigma_f \Phi \rangle = N . K_e . K_c = \langle \Sigma_d \Phi \rangle \frac{\langle \Sigma_{ref} \Phi \rangle}{\langle \Sigma_d \Phi \rangle} \frac{\langle \Sigma_f \Phi \rangle}{\langle \Sigma_{ref} \Phi \rangle}$$

With:

- N the **measured** counting rate of one detector
- K_e the **measured** counting rate ratio of a reference detector to the first one.
- K_c the **calculated** global fission rate in the core core on the counting rate of a reference detector.

Then we have:

$${\beta_{eff}}^2 = \frac{2D}{K_c}\frac{V_1 . V_2}{N . K_e . IPSD(1 + |\rho_\$|)^2} = P_c . P_m \qquad \textbf{2.13}$$

With a calculated parameter P_c and a measured one P_m given by:

$P_c = {2D}/{K_c}$	This **calculated** parameter needs the global fission rate in the core divided by the reference fission rate and the Diven factor.
$P_m = {V_1 . V_2}/{N . K_e . IPSD(1 + \lvert\rho_\$\rvert)^2}$	This **measured** parameter needs the IPSD and the counting rate of two detectors.

III.3 The BERENICE programme

The BERENICE programme is detailed in the Appendix A where all the experimental programmes of the MASURCA facility are presented.

III.3.1 R2 cores

Two different cores with enriched Uranium (20% of ^{235}U) based fuel have been built, the first one is homogeneous and is called "reference" and the other one has some heterogeneities in the inner fuel zone to let a large fission chamber go through the core (which is required for the noise technique measurements). The basic cell of R2 fuel is given (**Figure III.3.1**), it is composed of 32 sodium pins, 16 enriched uranium pins and 16 steel pins.

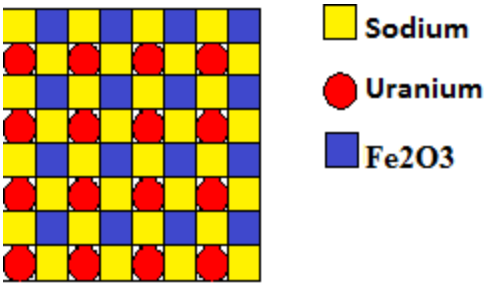

Figure III.3.1: R2 cell

III.3.2 ZONA2 core

The last core built during the BERENICE programme is a U-Pu based fuel core. With the inner fuel zone composed of 90% of PIT pins (with a Pu-vector of 18% of $^{240}Pu/Pu$) and with 10% of POA pins (with a Pu-vector of 8% of $^{240}Pu/Pu$). The basic cell is composed of 32 sodium pins and 32 U-Pu fuel pins.

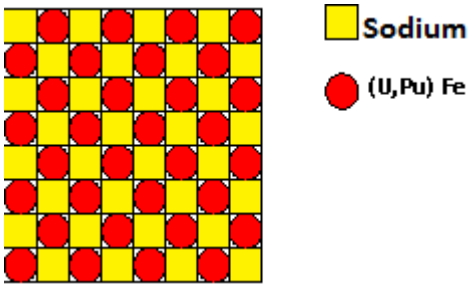

Figure III.3.2: ZONA2 cell

III.4 The new analysis of experimental measurements

III.4.1 Calculated β_{eff} with simulations

III.4.1.1 Deterministic method

The delayed neutron fraction can be calculated with the perturbation theory [8]. Indeed the perturbation at first order is given by the following formula:

$$\frac{dk}{k^2} = -\frac{\langle \Phi^+, \left(d\mathbf{A} - \frac{d\mathbf{F}}{k}\right)\Phi \rangle}{\langle \Phi^+, \mathbf{F}\Phi \rangle} \quad \textbf{4.1}$$

If the perturbation is only on the delayed neutron production operator $\mathbf{F_d}$ then $d\mathbf{F} = -\mathbf{F_d}$ and the **4.1** equation gives:

$$\frac{dk}{k} = \frac{\langle \Phi^+, d\mathbf{F}\Phi \rangle}{\langle \Phi^+, \mathbf{F}\Phi \rangle} = -\frac{\langle \Phi^+, \mathbf{F_d}\Phi \rangle}{\langle \Phi^+, \mathbf{F}\Phi \rangle} \quad \textbf{4.2}$$

The reactivity effect is then only due to delayed neutrons:

$$\beta_{eff} = \frac{\langle \Phi^+, \mathbf{F_d}\Phi \rangle}{\langle \Phi^+, \mathbf{F}\Phi \rangle} \quad \textbf{4.3}$$

For each precursor p [9] the delayed neutron fraction associated to this precursor is calculated with:

$$\beta_{eff}^{p} = \frac{\iiint_r \left(\sum_g \chi_d^p \Phi_g^+\right)\left(\sum_g \nu_d^p \Sigma_{f,g} \Phi_g\right) d^3r}{\iiint_r \left(\sum_g \chi_{tot} \Phi_g^+\right)\left(\sum_g \nu_{tot} \Sigma_{f,g} \Phi_g\right) d^3r} \quad \textbf{4.4}$$

With ν_d and ν_{tot} the delayed and total neutron yield per fission, χ_d and χ_{tot} the delayed and total fission spectrum and $\Sigma_{f,g}$ the fission cross-section of the precursor p. The effective delayed neutron fraction is the sum of these partial delayed neutron fractions. The ERANOS [10] results obtained with this approach are given in Table 4.2.

III.4.1.2 Stochastic methods

In TRIPOLI-4® it exists different methods to calculate the β_{eff} : the Nauchy's method [11][12] and the Iterated Fission Probability method (IFP) [13]. The first one evaluates the β_{eff} as the ratio of the average number of neutrons produced by the fissions induced by the delayed neutrons of a given generation and the average number of neutrons produced by all fissions of this generation. The IFP method evaluates the ratio of the importance of the delayed neutron production operator $\mathbf{F_d}$ and the importance of the total neutron production operator. These two methods have been used to get the β_{eff} of the three experimental cores of the BERENICE programme using the JEFF-3.1.1 nuclear data and results are presented in the following table.

Table III.4.1: Monte-Carlo evaluation of β_{eff} with JEFF-3.1.1

ZONA2	β_{eff} (pcm)	$d\beta_{eff}$ (pcm)
Nauchi	342,7	0,2
IFP	346,7	0,9
R2-A	**β_{eff} (pcm)**	**$d\beta_{eff}$ (pcm)**
Nauchi	720,5	0,8
IFP	736,1	3,2
R2-B	**β_{eff} (pcm)**	**$d\beta_{eff}$ (pcm)**
Nauchi	721,2	0,5
IFP	739,0	1,9

The two methods give consistent results for the β_{eff} (within a 2% discrepancy) the IFP method will be preferred in this work because it is the most recent one implemented in TRIPOLI-4® and the most accurate. Indeed it evaluates the importance of delayed neutrons using more generations of neutrons than the Nauchy's method (see **III.4.2**.1). The Uranium based-fuel of R2 cores gives higher values of β_{eff} due to the more important delayed neutron yield of ^{238}U compared to ^{235}U or Plutonium.

Table III.4.2: calculated β_{eff} comparison with different nuclear data and codes

calculated β_{eff} (pcm)							
Code	Nuclear Data	Cores : ZONA2		R2-ref		R2-exp	
ERANOS	JEFF-3.1.1	357,6		740,5		739,9	
	JEFF-3.2	361,6		748,9		748,2	
TRIPOLI4® (IFP)	JEFF-3.1.1	346.7	± 0.9	736.1	± 3.2	739.0	± 1.9
	JEFF-3.2	349.9	± 0.9	742.4	± 3.2	748.4	± 5.2

The main difference between JEFF-3.1.1 and JEFF-3.2 comes from the better evaluation of fission cross sections of ^{239}Pu and ^{235}U in JEFF-3.2 than in JEFF-3.1.1. ERANOS and TRIPOLI-4® give consistent results (with a 3.3% difference for ZONA2). The main difference from these two results comes from the delayed neutron spectrum that is the same for all nuclides with ERANOS. The statistical uncertainties are given (at 1σ) in the **Table III.4.2** for TRIPOLI-4® results. The influence of the main fissile isotope, ^{235}U and ^{239}Pu, respectively, on β_{eff} is quite evident.

III.4.2 New analysis of the measurements

As seen in **section 2** the experimental results needs calculated parameters (P_c) to get access to the β_{eff} and these parameters are dependent of the nuclear data and methods used, the objective is then to calculate these P_c with JEFF-3.2 nuclear data and stochastic methods.

III.4.2.1 IFP method for adjoint flux integrals

Adjoint flux integrals are needed to get these P_c with the experimental method of the californium 252 source as seen is **section 2.1**. The adjoint flux is related to the "importance" of neutrons as seen in Chapter II. The IFP method [14] consists in calculating the average neutron importance by estimating the number of neutrons produced after L generations, L being called the "length of the IFP cycle". As seen in the **section 2.1.2** of the Chapter II if a simulation is launched with a neutron source at position $\overrightarrow{r_0}$ with an energy E_0 then the importance of the neutrons is related to the number of neutrons produced: N^L, after L cycles and it is calculated as the product of the normalisation factors of each cycle g:

$$N^L(E_0, \vec{r}) = \prod_{g=1}^{L} k_g \qquad \textbf{4.5}$$

These normalisation factors are the estimators called k_{step} in TRIPOLI-4® which allows getting the exact calculation of the number of neutrons. This neutron population is the image of the power injected by the source in the core. If this power is too important the core become overcritical and the neutron population diverges and if the core is still sub-critical, the neutron population tends to 0. As the importance of the source cannot be defined with divergent solutions, these factors have to be normalised by the asymptotic value $k_{g\to\infty}$ [15].

$$I^L(E_0, \vec{r}) = \prod_{g=1}^{L} \frac{k_g}{k_{g\to\infty}} \qquad \textbf{4.6}$$

In this work we use this method to get the importance of a spectrum previously normalised (i.e. $\int_0^\infty \chi(E)dE = 4\pi$):

$$\langle S(E)\, I^{L}(E_0, \vec{r})\rangle = \int_0^{\infty} \chi(E)\mathrm{d}E \prod_{g=1}^{L} \frac{k_g}{k_{g\to\infty}} \qquad \textbf{4.7}$$

In most cases the product of $\prod_{g=1}^{L} \frac{k_g}{k_{g\to\infty}}$ quickly converges and the IFP cycle length which should be theoretically infinite can be chosen between 10 and 20 cycle. The statistical uncertainty associated to this method is the standard deviation of a series of simulations (1000 for each spectrum).

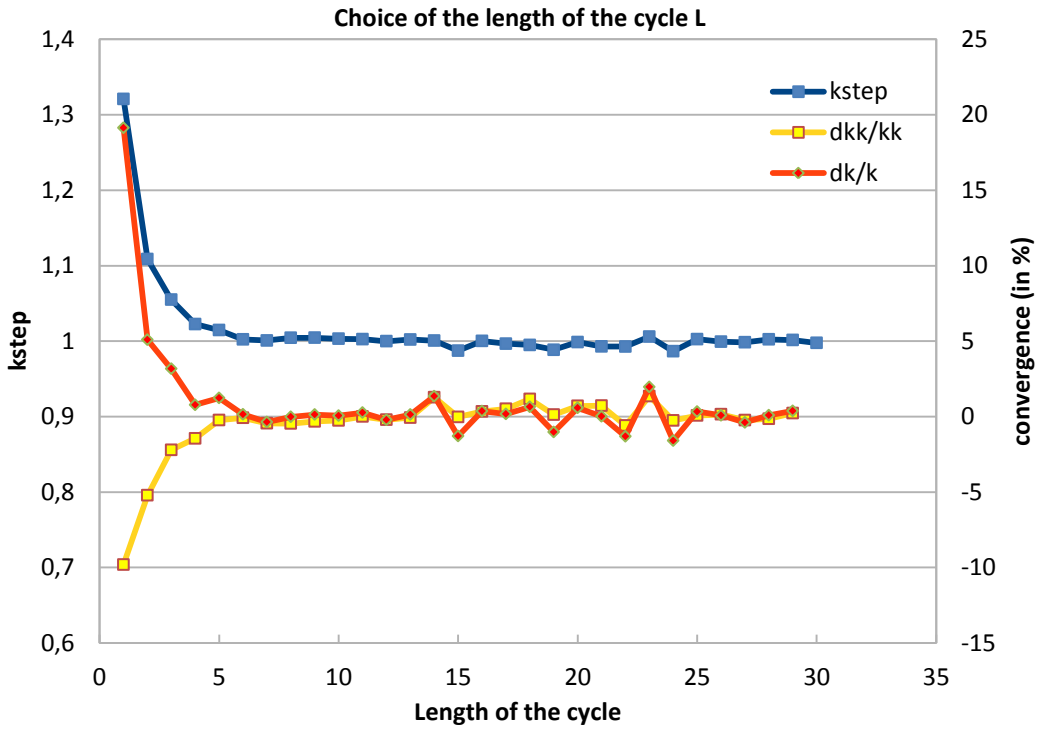

Figure III.4.1: Relative convergence of the k_{step} estimator (in red) and of their products (in yellow)

In blue on this **Figure III.4.1**, we can see the quick convergence of the k_{step} to their asymptotic values (near the critical value), in red the relative convergence $\left(\frac{k_{step}-k_{step-1}}{k_{step-1}}\right)$ and in yellow the relative convergence of the product i.e. the difference between the product at the cycle L and at the cycle L-1. A cycle length of about 10 steps ensures a satisfying statistical convergence (<1%).

III.4.2.2 The ^{252}Cf source method results

The new evaluation of β_{eff} consists in getting P_c with the most recent implementation in the stochastic code TRIPOLI-4®. For this experimental technique, two adjoint integrals have to be calculated for the φ_{sc} term.

$$\varphi_{sc} = \frac{\langle \Phi^{+}, S_1\rangle}{\langle \chi_r \Phi^{+}\rangle \cdot \langle S_1\rangle} = \frac{\langle \chi_{Cf} \Phi^{+}\rangle}{\langle \chi_r \Phi^{+}\rangle} \qquad \textbf{4.8}$$

The two integrals $\langle \chi_{Cf}\Phi^{+}\rangle$ and $\langle \chi_r \Phi^{+}\rangle$ are obtained with the IFP method previously introduced. First by introducing the californium source in the core and then by introducing a source of 1g of ^{235}U at the core centre. The results are presented in the following **Table III.4.1** (with the statistical uncertainty at 1σ).

Table III.4.1: Spectrum importances

	ZONA2	R2 ref	R2 exp
$\langle \boldsymbol{\chi_{Cf}\Phi^{+}} \rangle$	1.7547 (0.0051)	1.6475 (0.0051)	1.6461 (0.0036)
$\langle \boldsymbol{\chi_{r}\Phi^{+}} \rangle$	1.6548 (0.0051)	1.6207 (0.0051)	1.6173 (0.0036)

The last calculated values for this method concern the K_c term that gives the relative importance of the total production of neutrons by fission to the importance of the fission rate of 1g of ^{235}U at the core centre.

$$K_c = \frac{\langle \Phi^{+}, \mathbf{F}\Phi_1 \rangle}{\langle \Sigma_{ref}\Phi_1 \rangle \cdot \langle \chi_r \Phi^{+} \rangle} = \frac{\langle \chi_{ftot}\Phi^{+} \rangle \cdot \langle (\upsilon_d \mathbf{N_d} + \upsilon_p \mathbf{N}_p)\Phi_1 \rangle}{\langle \Sigma_{ref}\Phi_1 \rangle \cdot \langle \chi_r \Phi^{+} \rangle} \quad \textbf{4.9}$$

With: $\upsilon_d \mathbf{N_d} + \upsilon_p \mathbf{N}_p = \mathbf{P}$, $\mathbf{N_p}$ being the number of prompt fission and $\mathbf{N_d}$ the number of events of delayed neutron production. The $\langle \chi_{ftot}\Phi^{+} \rangle$ integral is calculated with the IFP method by introducing a source with the total fission spectrum i.e. a first simulation to get this fission spectrum has to be run with the response "fission spectrum" in TRIPOLI-4®. The integral $\langle (\upsilon_d \mathbf{N_d} + \upsilon_p \mathbf{N}_p)\Phi_1 \rangle$ is also calculated in the first simulation with the responses: "macroscopic reaction rate" allowing to get the "nu delayed fission" and the "prompt fission" in the core. The last factor $\langle \Sigma_{ref}, \Phi_1 \rangle$ can be split into:

$$\langle \Sigma_{ref}, \Phi_1 \rangle = N\big(ref(1g)\big) \langle \sigma_{f,ref}\Phi_1 \rangle \quad \textbf{4.10}$$

Where: $\sigma_{f,ref}$ is the microscopic fission cross-section of the reference nucleus and the microscopic reaction rate is obtained with the response "reaction" in TRIPOLI-4®. To get the macroscopic reaction rate it is necessary to multiply this result by the number of reference atomic nuclei in 1g, in this case the chosen reference nucleus is the ^{235}U, i.e. 2,5618.10^{21} nucleus. All the results needed to get the new evaluation of the K_c term are presented in the following table:

Table III.4.2: Integrals for K_c

	ZONA2	R2 ref	R2 exp
$\langle \boldsymbol{\Phi^{+}\vert\chi_{ftot}} \rangle$	1.7584 (0.0029)	1.6515 (0.0039)	1.6488 (0.0046)
$\langle \boldsymbol{(\upsilon_d \mathbf{N_d} + \upsilon_p \mathbf{N_p})\Phi_1} \rangle$	8.7363 (0.0014)	8.6900 (0.0022)	8.5093 (0.0010)
$\langle \boldsymbol{\sigma_{f,réf}\Phi_1} \rangle$	7.185.10^{-3} (1.4.10^{-5})	6.516.10^{-3} (1.0.10^{-5})	5.926.10^{-3} (1.4.10^{-5})

Then a new evaluation of the experimental β_{eff} can be calculated and the results are given in the following table:

Table III.4.3: Evaluation of β_{eff} with P_c calculated with TRIPOLI-4®

	ZONA2	R2 ref	R2 exp
$\boldsymbol{\beta_{eff}}$ **(pcm)**	326.5	739.8	728.6

The use of TRIPOLI-4® tends to decrease the β_{eff} value for each core in comparison to a previous work done using ERANOS and JEFF-3.1 nuclear data with -8% on ZONA2 and -1.6% on R2 exp. This important discrepancy for the result on ZONA2 is going to be discussed in the section **4.3**.

III.4.2.3 The noise technique results

The noise technique measurements only needs a new evaluation of the K_c factor that is the global fission rate in the core divided by the fission rate of 1g of 235U at the core centre.

$$K_c = \frac{\langle \Sigma_f \Phi \rangle}{\langle \Sigma_{réf} \Phi \rangle} \quad \textbf{4.11}$$

The $\langle \Sigma_f \Phi \rangle$ integral is directly issued from a TRIPOLI-4® simulation using the response "macroscopic reaction rate" which calculates the macroscopic fission rate of all isotopes in the core. This gives a new evaluation of the experimental β_{eff}

Table III.4.4: global fission rate in the cores

	ZONA2	R2 exp
$\langle \Sigma_f \Phi \rangle$	4.2585 (0.0003)	4.8999 (0.0004)
β_{eff}	345.61	757.35

III.4.3 C/E comparisons

The new evaluation of the experimental values of the β_{eff} now can be compared with the calculated values obtained in the section **4.1**. The following tables give the C/E ratio for:

- ERANOS: comparison of the experimental values obtained in a previous work with our calculated results obtained with JEFF-3.1.1 and JEFF3.2 nuclear data.
- TRIPOLI-4®: comparison of our new evaluation of the experimental values (see section **4.2**) with our calculated results obtained with the IFP methods for JEFF-3.1.1 and JEFF-3.2 nuclear data.

The associated uncertainties presented in these tables are the quadratic sum of: experimental uncertainties and nuclear data uncertainties (see section **5**).

Table III.4.5: C/E results for the ^{252}Cf source method

C/E (californium 252 source method)							
Code	Nuclear data	Cores					
		ZONA2		R2 ref		R2 exp	
ERANOS	JEFF-3.1.1	0,9979	± 0,060	0,9360	± 0,045	0,8965	± 0,046
	JEFF-3.2	1,0090	± 0,056	0,9466	± 0,043	0,9066	± 0,045
TRIPOLI-4®	JEFF-3.1.1	1,0620	± 0,051	0,9950	± 0,044	1,0143	± 0,046
	JEFF-3.2	1,0720	± 0,045	1,0035	± 0,043	1,0272	± 0,044

The use of TRIPOLI-4® and the IFP methods gives better C/E for R2 cores compared to the ones obtained with ERANOS with E being measured with the Cf252 source method. However, for the ZONA2 core, the results are consistent within the 2σ uncertainties but ERANOS gives better C/E, this comes from an important increase of the experimental β_{eff} with TRIPOLI-4® which comes from the assessment of the K_c factor, while for the φ_{sc} factor ERANOS and TRIPOLI-4® agreed well.

Table III.4.6: C/E results for the noise method

C/E (Noise method)							
Code	Nuclear data	ZONA2		Cores R2 ref		R2 exp	
ERANOS	JEFF-3.1.1	1,0546	± 0,053	-	-	0,9640	± 0,039
	JEFF-3.2	1,0664	± 0,048	-	-	0,9748	± 0,038
TRIPOLI-4®	JEFF-3.1.1	1,0032	± 0,042	-	-	0,9757	± 0,039
	JEFF-3.2	1,0125	± 0,036	-	-	0,9882	± 0,037

The use of TRIPOLI-4® and the IFP methods gives better C/E for R2 cores compared to the ones obtained with ERANOS, especially for the experimental R2 core that comes from a refined description of its geometry in TRIPOLI-4®.

III.5 Uncertainty analysis

In this chapter, an important focus on the various sources of uncertainties has been made. Indeed the use of new method such as IFP for the evaluation of adjoint flux integrals implies a statistical uncertainty on the results. This uncertainty has to be added to the experimental ones and it has been done in a conservative approach [16]. Furthermore the use of GPT (see Chapter II) allows getting the sensitivities of the β_{eff} to nuclear data and then with recent nuclear data covariances (COMAC V2) [17] and the sandwich formula, it is possible to obtain the associated uncertainty. The delayed neutrons data covariances have also been taken from the JENDL-4.0 library

III.5.1 Statistical uncertainties of the stochastic method

The use of refined geometries in TRIPOLI-4® reduces the calculation bias but it introduces a statistical bias on the results obtained with the stochastic code. Hence, the calculated parameter P_c of each experimental method comes with a statistical uncertainty. The relative uncertainties are presented in the following table:

Table III.5.1: Impact of the statistical uncertainties on P_c

Cores	Relative uncertainties on P_c (in %)	
	P_c Cf 252	P_c Noise
ZONA2	0.58	0.195
R2 ref	0.61	-
R2 exp	0.46	0.24

These statistical uncertainties have a negligible impact on the β_{eff} compared to uncertainties due to nuclear data or experimental ones as we will see in the following sections.

III.5.2 Experimental uncertainties

The experimental uncertainties have been evaluated during the Veronique Zammit thesis [19] and concern for instance the measurements of: the integrated intensity of the ^{252}Cf source, the reactivity, counting rates, etc. In the conservative approach, we consider that these sources of uncertainties are independent [18]. A series of measurements were conducted for each method so we have to take into account the dispersion of this series of measurements. The total experimental uncertainties are the quadratic sum of the method uncertainties and the dispersion. Results in the Table III.5.2 show that the

dispersion of measurements are higher for the R2 experimental core because fewer measurements were conducted than in other cores (7 instead of 22):

Table III.5.2: Relative experimental uncertainties on the effective delayed neutrons fraction

Method	Core	Method uncertainties (in %)	Dispersion of measurements (in %)	Total experimental uncertainties (in %)
Cf 252 source	R2 ref	3.4	0.20	3.41
	R2 exp	3.4	1.24	3.62
	ZONA2	3.5	0.52	3.54
Noise	R2 exp	2.3	1.40	2.69
	ZONA2	2.2	0.42	2.23

The noise method appears as the more accurate one and it can be expected to get information on nuclear data with these noise measurements. That is why a comparison with uncertainties due to nuclear data is needed.

III.5.3 Uncertainties due to nuclear data

The sensitivities of the β_{eff} to nuclear data are obtained with the GPT method (see Chapter II) [20]. The β_{eff} expression needs the forward and adjoint flux:

$$\beta_{eff} = \frac{\langle \Phi^+, \mathbf{F_d}\Phi \rangle}{\langle \Phi^+, \mathbf{F}\Phi \rangle}$$

Then two Lagrange operators are needed:

$$T = \ln(\beta_{eff}) - \langle \Psi^+, \left(\mathbf{A} - \frac{1}{k}\mathbf{F}\right)\cdot\Phi\rangle - \langle\left(\mathbf{A}^+ - \frac{1}{k}\mathbf{F}^+\right)\cdot\Phi^+, \Psi\rangle \qquad \textbf{5.1}$$

We get the sensitivity of the β_{eff} to a parameter σ as follows:

$$S_{\beta_{eff}} = \frac{\sigma}{\beta_{eff}}\cdot\frac{d\beta_{eff}}{d\sigma} = \frac{\sigma}{\beta_{eff}}\left(\underbrace{\frac{d\beta_{eff}}{d\sigma}}_{\text{Direct term}} \underbrace{- \langle \Psi^+, \left(\frac{d\mathbf{A}}{d\sigma} - \frac{1}{k}\frac{d\mathbf{F}}{d\sigma}\right)\cdot\Phi\rangle - \langle \Psi, \left(\frac{d\mathbf{A}^+}{d\sigma} - \frac{1}{k}\frac{d\mathbf{F}^+}{d\sigma}\right)\cdot\Phi^+\rangle}_{\text{Indirect term}}\right) \qquad \textbf{5.2}$$

The direct term takes into account the variation of the parameter σ on the β_{eff} when the indirect term takes into account the impact of its variations on the adjoint and forward flux variation. The importance function Ψ and Ψ^+ have been implemented with :

$$\frac{\mathbf{F_d}\Phi}{\langle \Phi^+, \mathbf{F_d}\Phi\rangle} - \frac{\mathbf{F}\Phi}{\langle \Phi^+, \mathbf{F}\Phi\rangle} = \left(\mathbf{A} - \frac{1}{k}\mathbf{F}\right)\cdot\Psi \text{ and } \frac{\mathbf{F_d^+}\Phi^+}{\langle \Phi^+, \mathbf{F_d}\Phi\rangle} - \frac{\mathbf{F}^+\Phi^+}{\langle \Phi^+, \mathbf{F}\Phi\rangle} = \left(\mathbf{A}^+ - \frac{1}{k}\mathbf{F}^+\right)\cdot\Psi^+ \qquad \textbf{5.3}$$

An ERANOS procedure has been developed by Cyrille Bouret during his PhD Thesis [9] [21] and has been improved during this work. The detailed sensitivities results are given in the Appendix B for benchmark purpose [22]. The results for the R2 cores are not distinguished because the impact of the heterogeneities of the experimental R2 core on the sensitivities can be neglected.

Table III.5.3: Sensitivities of the β_{eff} for R2 cores (in %/%)

	Fission	Capture	Elastic	Inelastic	n.xn	υ_{tot}	υ_p	Fission spectrum	Total
JEFF-3.1.1	-0,0267	0,0365	-0,0064	0,0455	0,0019	-0,0152	0,9997	-0,9609	0,0744
JEFF-3.2	-0,0284	0,0325	-0,0027	0,0524	0,0027	-0,0118	0,9997	-0,9607	0,0836

The sensitivities for the ZONA2 core are presented in the following table:

Table III.5.4: Sensitivities of the β_{eff} for the ZONA2 core (in %/%)

	Fission	Capture	Elastic	Inelastic	n.xn	υ_{tot}	υ_p	Fission Spectrum	Total
JEFF-3.1.1	-0,0923	0,0121	0,0261	0,1136	0,0028	-0,0235	0,9998	-0,9475	0,0911
JEFF-3.2	-0,0981	0,0115	0,0257	0,1216	0,0037	-0,0282	0,9998	-0,9471	0,0888

Using the sandwich rule: $I^2 = S.B.S^t$ and the covariance matrix COMAC-V1 for JEFF-3.1.1 nuclear data and COMAC-V2 for JEFF-3.2 nuclear data we get the uncertainties due to nuclear data on the β_{eff}. The detailed results are given in the Appendix B.

Table III.5.5: Uncertainties due to nuclear data on the β_{eff} of R2 cores.

	Fission	Capture	Elastic	Inelastic	n.xn	υ_{tot}	υ_p	Fission Spectrum	Total
JEFF-3.1.1	**1,26**	**0,73**	0,08	0,25	0,00	0,16	**2,39**	0,33	2,81
JEFF-3.2	**0,61**	**0,58**	0,11	0,30	0,04	0,16	**2,38**	0,32	2,57

Uncertainties for the ZONA2 core are presented in the following table.

Table III.5.6: Uncertainties due to nuclear data on the β_{eff} of ZONA2 core

	Fission	Capture	Elastic	Inelastic	n.xn	υ_{tot}	υ_p	Fission Spectrum	Total
JEFF-3.1.1	**2,81**	0,50	0,16	0,84	0,02	0,35	**2,31**	0,31	3,60
JEFF-3.2	**1,38**	0,16	0,16	0,72	0,09	0,35	**2,31**	0,30	2,82

The main sources of uncertainty are the fission cross section and the delayed neutrons yield for the ZONA2 core, which is based on U-Pu fuel. As expected, the most contributing isotope to the uncertainty is the ^{239}Pu and results in an uncertainty of 2.8% for U-Pu based fuel core. The sources of uncertainty for R2 cores are the same as for the ZONA2 core but the capture has also an important contribution to the uncertainty because the ^{238}U is an important contributor to the β_{eff}.

III.6 Conclusion

The use of Monte-Carlo code TRIPOLI4® and its recent development of the Iterated Fission Probability method allow us to improve the C/E ratio for calculating β_eff. The detailed representation of cores and the use of an energy dependency of the delayed neutron emission to the incident neutron energy are the major contribution to this improvement. Also, the improvement comes from the calculated terms used to derive β_eff from raw experimental measurements. The C/E ratios are greatly improved when using the reliable Noise measurement technique with 1.2% ± 3.6% for the ZONA2 core and -1.2% ± 3.7 % for the R2 experimental core.

The complementary use of the deterministic code ERANOS is fundamental for the uncertainty quantification process, with the sensitivity analysis and uncertainty propagation leading to a 2.82% uncertainty for U-Pu core and 2.57% for enriched uranium cores whose main contributors are the delayed neutron fission yield and the fission cross section of U238.

This work is part of the ASTRID project especially for the ZONA2 core because as we can see in the **Table III.6.1** the breakdown of the β_{eff} on each contributors presents similarities.

Table III.6.1: Contributors to the for ZONA2 and ASTRID core

β_{eff}^{p}(pcm)	ZONA2	ASTRID
Am241	0,8	0,3
Np237	0,0	0,0
Pu238	0,2	2,9
Pu239	150,7	119,0
Pu240	14,2	17,8
Pu241	9,0	54,1
Pu242	1,0	10,0
U234	0,0	0,0
U235	8,3	5,3
U236	0,0	0,0
U238	177,5	173,9
β_{eff}	361,6	383,3

However, since the experimental uncertainties are greater than the nuclear data uncertainties no feedback can be extracted from this programme on nuclear data improvements. Only new experimental techniques (noise method with faster electronic) could reduce current uncertainties of reference codes in calculating β_{eff}.

References

[1] J. Rowlands, 'Delayed neutron data in 8 time groups', JEF/DOC-976, OCDE/NEA, Nov-2003.

[2] S. Massara, 'Etude et amélioration du comportement cinétique de coeur rapides dédiés a la transmutation des déchets a vie longue', thèse, Université Louis Pasteur - Strasbourg I, 2002.

[3] Y. Yamane, 'Review of experimental methods for evaluating effective delayed neutron fraction', *JAERI-Conf-97-005*.

[4] J. Mihalczo, 'New method for measurement of effective fraction of delayed neutrons from fission', *Nucl. Sci. Eng.*, vol. 46, p. 147, 1970.

[5] P. Bertrand *et al.*, 'BERENICE - Inter laboratory comparison of β_{eff} measurement techniques at MASURCA', presented at the PHYSOR 96, Mito, Japan, 1996.

[6] E. Greenspan, 'A generalized source multiplication method', *Trans. Am. Nucl. Soc.*, vol. 14, no. 29, 1971.

[7] G. Perret, 'Amélioration et développement des méthodes de détermination de la réactivité - Maîtrise des incertitudes associées', Université Joseph Fourier de Grenoble, Thèse Chapter 2, section 1, 2003.

[8] A. Gandini, 'A generalized perturbation method for bi-linear functionals of the real and adjoint neutron fluxes', *J. Nucl. Energy*, vol. 21, no. 10, pp. 755–765, 1967.

[9] C. Bouret, L. Buiron, and G. Rimpault, 'Sensitivity and uncertainty analysis on reactor kinetic parameters using perturbation theory', presented at the PHYSOR 2014, Kyoto, Japan, 2014.

[10] G. Rimpault, D. Plisson, J. Tommasi, and R. Jacqmin, 'The ERANOS code and data system for fast reactor neutronic analyses', presented at the PHYSOR 2002, Seoul, KOREA, 2002.

[11] Y. Nauchi and T. Kameyama, 'Proposal of direct calculation of kinetic parameters βeff and based on continuous energy Monte Carlo method', *J. Nucl. Sci. Technol.*, vol. 42, no. 6, pp. 503–514, 2005.

[12] Y. K. Lee and F. X. Hugot, 'Calculation of the effective delayed neutron fraction by TRIPOLI-4 code for IPEN/MB-01 research reactor', in *International Conference on Mathematics and Computational Methods Applied to Nuclear Science and Engineering (MC 2011)*, 2011.

[13] Y. Nauchi and T. Kameyama, 'Development of Calculation Technique for Iterated Fission Probability and Reactor Kinetic Parameters Using Continuous-Energy Monte Carlo Method', *J. Nucl. Sci. Technol.*, vol. 47, no. 11, pp. 977–990, Nov. 2010.

[14] G. Truchet, 'Développements et validation de calculs à énergie continue pondérés par l'importance', thèse, Université Grenoble Alpes, 2015.

[15] A. M. Weinberg, 'Current Status of Nuclear Reactor Theory', *Am. J. Phys. 20*, pp. 401–412, 1952.

[16] G. Rimpault, D. Blanchet, G. Truchet, J. Tommasi, and P. Dufay, 'Uncertainty quantification of delayed neutron fraction of U235 based fuel cores', presented at the PHYSOR 2016, Sun Valley, Idaho, USA, 2016.

[17] P. Archier, C. De Saint Jean, G. Noguere, O. Litaize, P. Leconte, and C. Bouret, 'COMAC: Nuclear Data Covariance Matrices Library for Reactor Applications', presented at the PHYSOR 2014, Kyoto, Japan, 2014.

[18] E. Fort, V. Zammit-Averlant, M. Salvatores, A. Filip, and J.-F. Lebrat, 'Recommended values of the delayed neutron yield for: U-235; U-238 and Pu-239', *Prog. Nucl. Energy*, vol. 41, no. 1–4, pp. 317–359, Jul. 2002.

[19] V. Zammit-Averlant, 'Validation intégrale des estimations du paramètre Beta Effectif pour les réacteurs MOX et incinérateurs', thèse, Aix-Marseille, 1998.

[20] J. Tommasi, 'ERANOS user's manual – applications of perturbation theory with finite difference diffusion and Sn transport flux solvers'. RT 07-003 SPRC/LEPh.

[21] C. Bouret, 'Etudes des contre-réactions dans un réacteur à neutrons rapides à caloporteur sodium. Impact de la conception et de la neutronique sur les incertitudes', *http://www.theses.fr*, 13-Nov-2014. [Online]. Available: http://www.theses.fr/s104600. [Accessed: 17-Nov-2015].

[22] I.-A. Kodeli, 'Sensitivity and uncertainty in the effective delayed neutron fraction (β_{eff})', *Nucl. Instrum. Methods Phys. Res. Sect. Accel. Spectrometers Detect. Assoc. Equip.*, vol. 715, pp. 70–78, Jul. 2013.

Chapter IV: The Sodium Void Reactivity Effect

Abstract

The Sodium Void Reactivity Effect (SVRE) is the difference in reactivity between two configurations of the core, the first one is the nominal configuration of the core and the second one is the voided core. This reactivity effect can be split into two components: the central component (CC) and the leakage component (LC). When the sodium is removed from the core the neutrons are not anymore scattered on sodium nuclei, the neutron spectrum is then shifted to higher energies increasing the probability of getting more fissions on some isotopes (it is the case of ^{239}Pu but also of actinides with fission thresholds like: ^{238}U, ^{240}Pu, etc.) and hence the central component is positive. At the same time, removing the sodium from the core means that the total cross-section is reduced, hence increasing the neutron mean free path. The neutrons in outer areas of the core are more likely to leak out of the core. The leakage component is hence negative. These two antagonistic effects are presented in details in the first section of this Chapter IV. The CFV design maximises the leakage component in order to get a negative SVRE. The experimental programmes studied in this work are presented in the section 2. Two programmes have been conducted in the MASURCA facility at the CEA Cadarache centre: PRE-RACINE studying the impact of inner fertile area in the core and CIRANO studying the substitution of fertile blanket by a sodium-steel reflector. The BFS programme has been done in collaboration with IPPE in Russia, it studies more in detail some characteristics of the CFV design such as the inner fertile slab in the core, the sodium plenum on the core ... The experimental uncertainties on the reactivity measurements are also presented in this section. Some gaps in the experimental data base for validating tools for the CFV design are identified and recommendations for an experimental programme called GENESIS in MASURCA are given at the end of this section. The last section of this Chapter IV is presenting a complementary analysis of the SVRE calculated with refined geometries thanks to the stochastic code TRIPOLI-4® and then both components (the CC and LC) are calculated through perturbation theory with the deterministic code ERANOS using an RZ description of the geometry.

Contents

IV.1 The physical components of SVRE

IV.1.1 The antagonistic components CC and LC

IV.1.1.1 Fertile and fissile isotopes

Some fuel isotopes such as ^{235}U and ^{239}Pu are called "fissile" because whatever the energy of the incident neutrons the probability of fission is non negligible (see **Figure IV.1.1** [1]) due to their nucleus structure, between 1b and 5b at high energy (>100keV) and more than 100b at thermal energies (around 0.025 eV). In Fast Reactors (FR) even the neutron spectrum is centred at 100 keV.

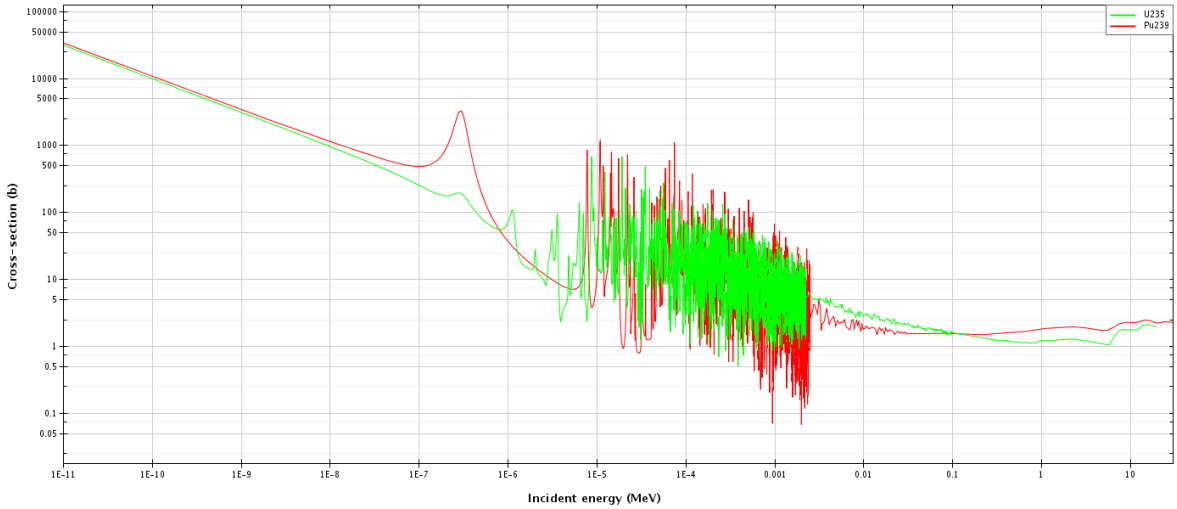

Figure IV.1.1: Fission cross-section of ^{235}U and ^{239}Pu in JEFF-3.1.1 nuclear data

On the contrary, isotopes like ^{238}U and ^{240}Pu are called "fertile" because the fission occurs essentially at high energy with a threshold at around 1 MeV for what concerns U238 and because neutron capture reactions transmute these fertile isotopes into fissile ones. These fertile isotopes have a rather high neutron capture cross sections inducing the creation of new fissile isotopes. The threshold for ^{238}U and ^{240}Pu fission occurs at high energy (see **Figure IV.1.2**) when the incident neutron brings enough energy to break the binding of these nucleus structures.

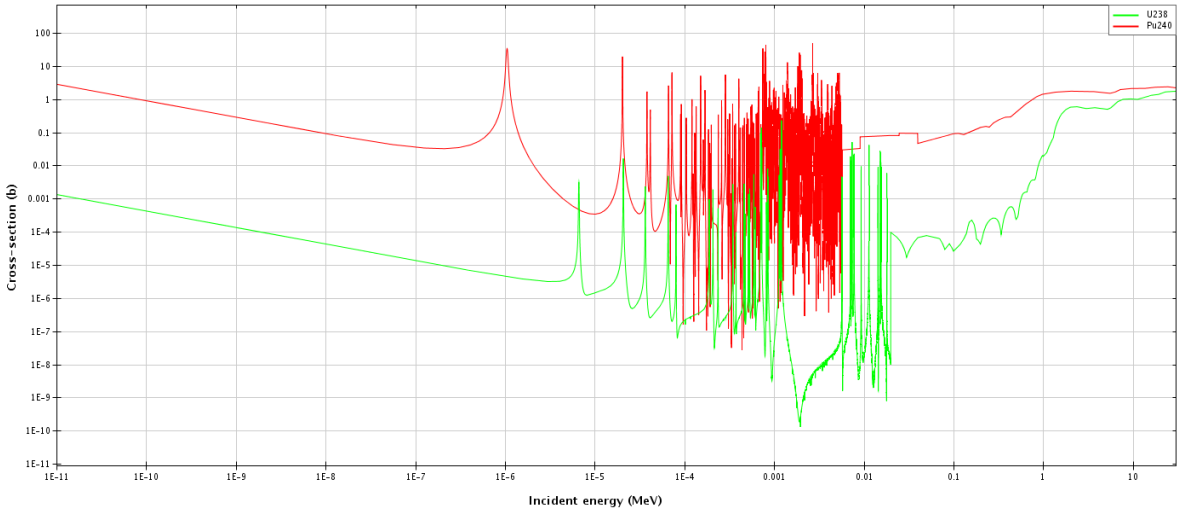

Figure IV.1.2: Fission cross-section of ^{238}U and ^{240}Pu in JEFF-3.1.1 nuclear data

IV.1.1.2 A spectrum effect

As seen in the Chapter I the sodium nuclei have a non-negligible moderator power meaning that the neutron spectrum in the nominal situation is softer due to the scattering of neutrons on sodium nuclei. Furthermore at high energy another moderating phenomenon appears, the inelastic scattering on sodium and uranium due to the nuclei structure and their excited levels [2] [3]. Thus when the sodium is removed from the core there is not anymore inelastic and elastic scattering on sodium nuclei which shifts the neutron spectrum to higher energies. This is presented in the **Figure IV.1.3** where the neutron flux spectrum has been obtained with ERANOS in 33 groups in the nominal and voided case. In blue we see that between 0.1 keV and 60 keV the nominal neutron flux spectrum is more important than the voided one due to the elastic scattering reactions while above 100 keV the voided spectrum is more important because of the lack of scattering.

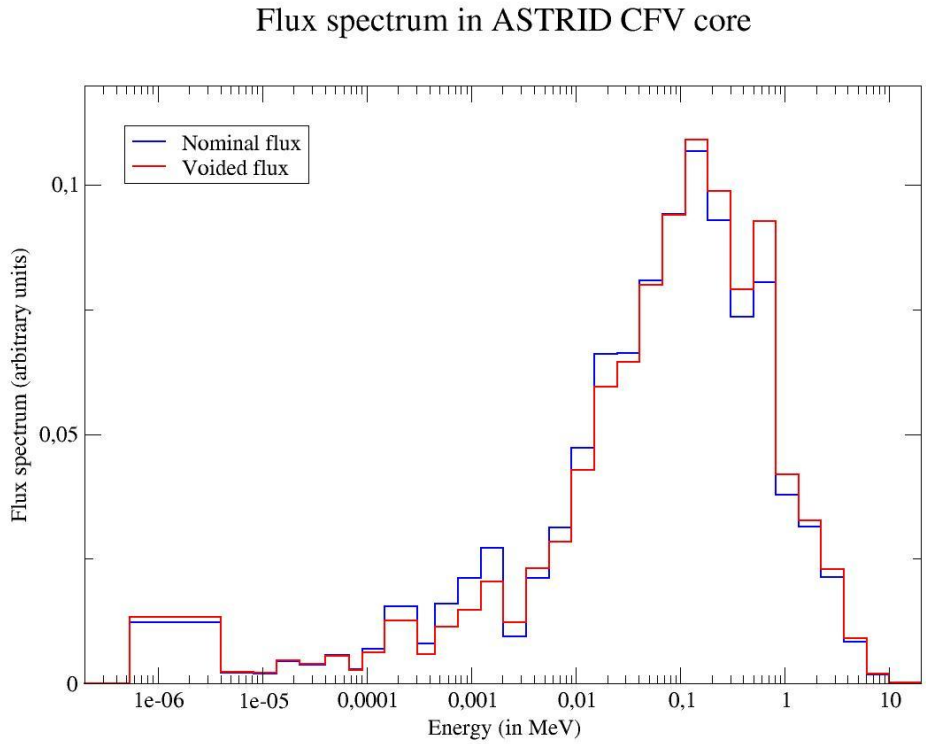

Figure IV.1.3: Neutron flux spectrum in the ASTRID CFV core

The neutrons have more importance at high energy due to the reproduction factor which is the ratio of production over capture ($\nu\Sigma_f/\Sigma_a$), of ^{239}Pu but also of other isotopes and particularly the fertile isotopes with their threshold fissions like ^{240}Pu. For instance the **Figure IV.1.4** presents the adjoint flux spectrum which is related to the importance of the neutrons (see Chapter III, section 1) and this is strongly correlated with the multiplication factor spectrum presented in the **Figure IV.1.5**. It means that neutrons gains importance in the voided configuration which increases the neutron production at high energies.

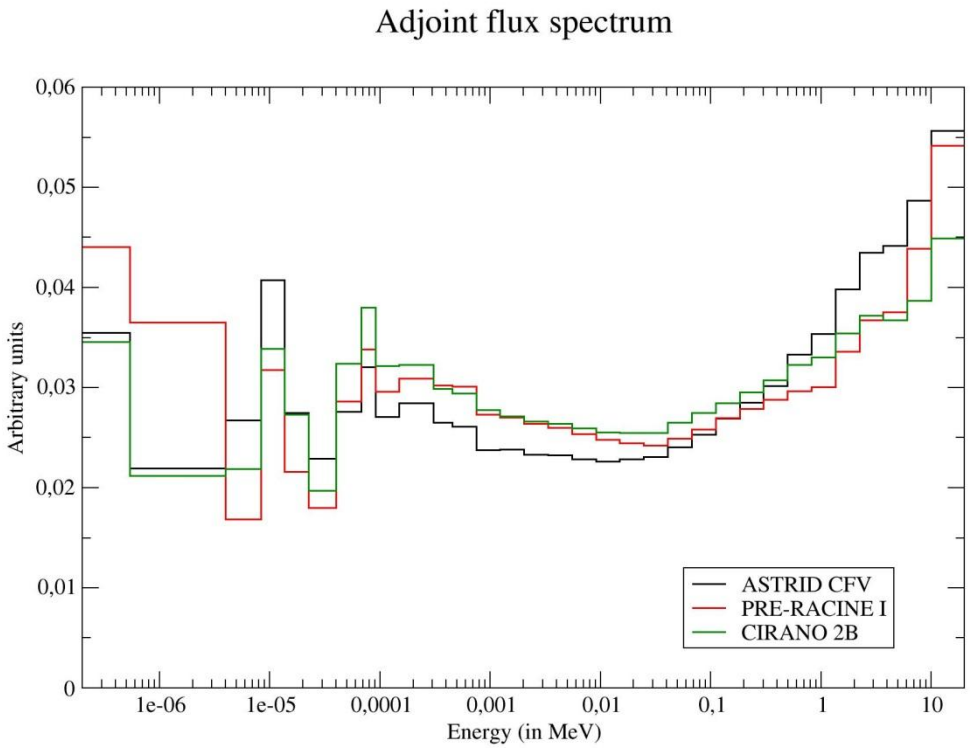

Figure IV.1.4: Adjoint flux spectrum comparison between the ASTRID CFV core and experimental cores

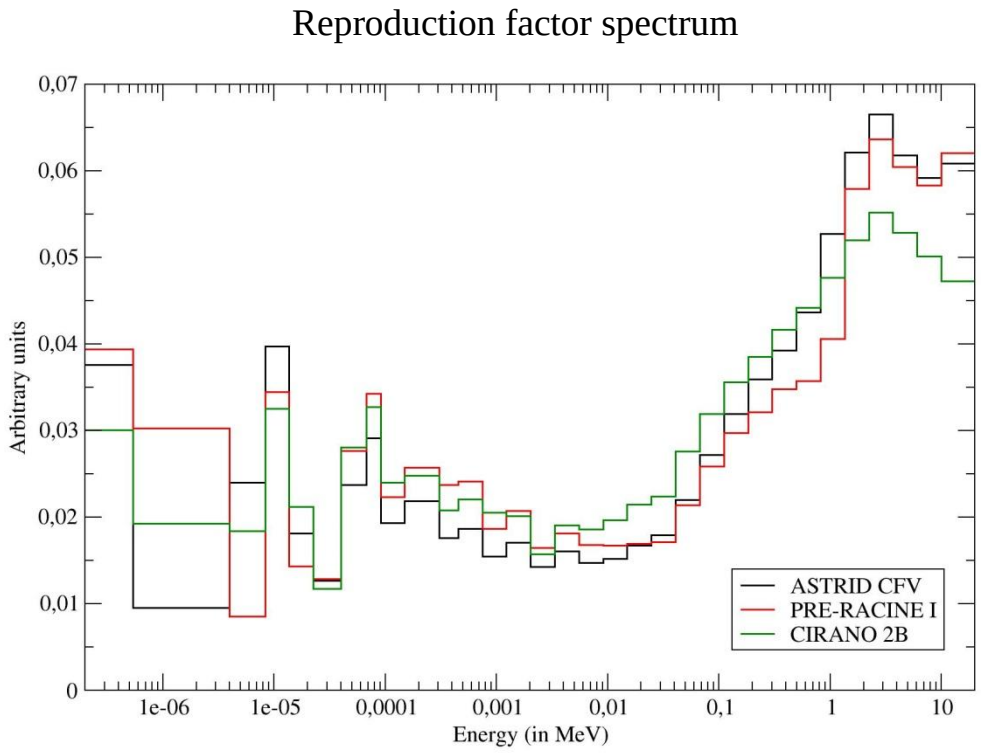

Figure IV.1.5: Reproduction factor spectrum comparison between the ASTRID CFV core and experimental cores

The first impact on reactivity is then positive and it can be break down into different physical components: capture, absorption by fission, production of neutrons by fission, fission spectrum, elastic and inelastic and n,xn scattering removal. These components can be calculated using ERANOS perturbation theory as presented in the **Table IV.1.1** with the adjoint and forward flux and the variation of the concerned macroscopic cross-sections or fission spectrum. The sum of these physical components is called the Central Component (CC) because it is more important in the inner parts of the core but it can also be referred as the "spectral component" in literature.

Table IV.1.1: Expression of physical components

Capture	$C_c^g = -\delta\Sigma_c^g . \int_V \Phi_g^+ . \Phi_g dV$
Fission	$C_f^g = -\delta\Sigma_f^g . \int_V \Phi_g^+ . \Phi_g dV$
Production	$C_\nu^g = \delta(\nu\Sigma_f^g) . \int_V \Phi_g \sum_{g'} \chi_g \Phi_{g'}^+ dV$
Fission Spectrum	$C_{spec}^g = \delta\chi^g \int_V \Phi_g^+ . \sum_{g'} \nu\Sigma_f^{g'} \Phi_{g'} dV$
Scattering	$C_{scatt}^g = \sum_{g'} \delta\Sigma_{scatt}^{g\to g'} \left(\int_V \Phi_{g'}^+ . \Phi_g dV - \int_V \Phi_g^+ . \Phi_g dV \right)$

In the ASTRID CFV core during a total sodium void experiment the reactions of elastic and inelastic reactions are responsible of 85.5% of the reactivity variation.

IV.1.1.3 Neutron leakage

The second impact on reactivity is antagonistic and then negative because when the sodium is removed the total cross-section is less important than in the nominal configuration due to the simple fact that scattering reactions on sodium nuclei are not anymore taken into account in the total cross-section. This implies that the mean free path[1] of neutrons: L, defined as the average length travelled by the neutrons between two interactions, is increased meaning that neutrons in outer parts of the fuel areas can more easily leak out of the core. This negative component is then called the Leakage Component (LC).

During some unprotected accidents i.e. without operation of control rods nor diesels, it is better to have a negative reactivity variation in order to limit the power excursion and improve the intrinsic safety feature of the IVth generation reactors (see chapter I). The only way is to increase the leakage component by specific spatial arrangement (mostly axial) and decrease the central component by reducing the sodium content in the fuel cells since the importance shape cannot be changed as it is due to the nature of the fuel itself.

[1] $L = 1/\Sigma_t$ the mean free path of neutrons in a medium is the inverse of the total macroscopic cross-section of this medium.

IV.1.2 The CFV design maximises the LC

The CFV core [4] (“Coeur à Faible Vidange” : Core with low sodium void reactivity effect in French) design has been proposed by the CEA in 2006 and exhibits a negative SVRE by maximising the leakage component with different geometrical arrangements and reducing the central component by reducing the Na volume fraction (which implies a reduction of the volumic power). The CFV design is composed of an inner core (C1) and of an outer core (C2) using Mixed OXide (MOX based on U-Pu) fuel with an inner fertile slab in the middle of the inner core (FCAM stands for "Fertile Couverture Axiale Médiane" in French) and a lower axial fertile blanket (FCAI stands for "Fertile Couverture Axiale Inférieure" in French). A superior sodium expansion vase (SVES stands for "Sodium Vase d'Expansion Supérieur") and a sodium plenum sits on top of the core with neutronic absorber on it. A radial reflector is also added in order to decrease the radius of the core and hence its overall volume by sending back into the core a fraction of those neutrons leaking out of the core.

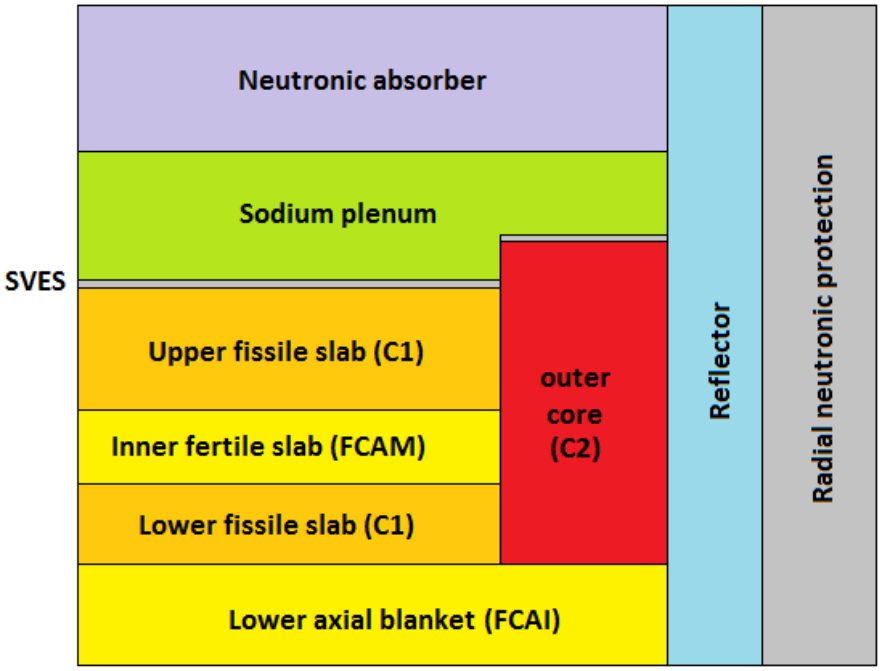

Figure IV.1.6: RZ description of the CFV design

The main innovations concern the objective of maximising the leakage component of the SVRE:

- The neutrons leaking out of the core are quite numerous because of the relative small height of the core (60 cm) and because of the fertile inner blanket increasing the flux level at the top of the inner fuel zone. These leaking neutrons are finding the sodium plenum which send them back into the core before getting to the neutronic absorber which sits on the top of the sodium plenum. When the core temperature increases too much, the sodium starts to boil on the top of the core and in the sodium plenum. Once empty, the sodium plenum no longer acts as a reflector and the leaking neutrons go directly to the neutronic absorber.
- The outer core is higher than the inner core to limit the radius of the core without minimising the sodium plenum role and then the leakage component.

In our studies three configurations of sodium void have been analysed:

- A total void sodium configuration which is the main subject of this PhD, where the C1, C2, FCAM, SVES, sodium plenum areas are voided.

- A core void configuration when only the C1 and C2 areas are voided which maximise the CC.
- A void plenum configuration when only the sodium plenum and the SVES areas are voided which maximise the LC.

The idea is to get configurations matching the experimental ones built in MASURCA and BFS facilities, see Appendix A.

IV.2 Experimental data base

IV.2.1 The reactivity measurements

IV.2.1.1 Introduction to measurements in reactor physics

The measurements in reactor physics are important for validating neutronic tools but also for the operation of nuclear reactors in order to keep an eye on neutron population, power, reactivity... The operators have access to the flux level with detectors such as ionizing chambers placed in the core. In such a system, the neutron flux interacts with a fissile deposit creating fission products which ionized the gas. The electric charges are then amplified and collected to get an electric signal in output. In critical facilities, the use of fission chambers is quite important mainly for getting access to spatial distributions (see Chapter III). In these detectors, the neutrons interact with a fissile deposit placed in the outer part of the detector and the fission products will ionize a gas. The charges are then collected on an electrode and the signal can be amplified by some tools outside of the core. A particular attention has to be given to the fissile deposit because if it is too thick the fission products will be absorbed in it.

The neutron flux interaction with the fission chamber is described by a macroscopic cross-section $\Sigma_d(E)$ depending on the energy of the incident neutron and the counting rate is then:

$$C(t) = \int_{detector} \int_{E} \Sigma_d(E)\Psi(\vec{r}, E, \vec{\Omega}, t) \qquad \textbf{2.1}$$

With: $\Psi(\vec{r}, E, \vec{\Omega}, t)$ the neutron flux through times. As seen in (Chapter III, section 1.2) the neutron flux is factorised such as: $\Psi(\vec{r}, E, \vec{\Omega}, t) = N(t).\Phi(\vec{r}, E, \vec{\Omega}, t)$ in order to split the rapidly changing neutron flux magnitude fluctuation $N(t)$ from a slowly changing shape function $\Phi(\vec{r}, E, \vec{\Omega}, t)$. The counting rate can be expressed as follows, using the detector efficiency: $\epsilon_d(t)$.

$$C(t) = \epsilon_d(t)\, N(t) \qquad \textbf{2.2}$$

$$\epsilon_d(t) = \int_{detector} \int_{E} \Sigma_d(E)\Phi(\vec{r}, E, \vec{\Omega}, t) \qquad \textbf{2.3}$$

If we consider that $\Phi(\vec{r}, E, \vec{\Omega}, t)$ is time-independent then $\epsilon_d(t)$ is constant and the counting rate is faithfully recording the neutron flux magnitude $N(t)$ which is true when the detector is placed far enough from the perturbation source. Otherwise the measurements are spoiled by errors due to:

- the position of the detector, the closer to the perturbation the detector is the greater the error is.
- the magnitude of the perturbation, the more important the perturbation is the more important the error is.
- the sensing range: the more the perturbation affects the flux spectrum in the sensing range of the detector the more important the error is.

IV.2.1.2 The inversion of point kinetics equations

In the MASURCA experiment, the reactivity is measured using a control rod insertion for a given loading. By inverting the point kinetics equations [5] we can directly relate the control rod position to the neutron population and then to the reactivity of the core. Indeed from equations (III-**1.3)** presented in the Chapter III the online reactivity can be deduced from the online measurements of the neutron population.

$$\rho(t) = \beta_{eff} + \frac{\Lambda_{eff}}{N(t)}\left(\frac{\partial N(t)}{\partial t} - \sum_{i=1}^{8} \lambda_i C_{eff,i}\,(t)\right) \qquad \textbf{2.4}$$

Using the evolution equation of each precursor concentration:

$$\frac{\partial C_{eff,i(t)}}{\partial t} = \frac{\beta_{eff,i}}{\Lambda_{eff}} N(t) - \lambda_i C_{eff,i}(t) \qquad \textbf{2.5}$$

The $C_{eff,i}(t)$ can be expressed by solving the 2.5 equation with the variation of constants method where the $C_{eff,i}(t)$ is supposed to get an exponential behaviour:

$$C_{eff,i}(t) = A_i(t)e^{-\lambda_i t} \qquad \textbf{2.6}$$

Integrating the 2.5 equation the "constant" expression of $A_i(t)$ is then:

$$A_i(t) = A_i(0) + \frac{\beta_{eff,i}}{\Lambda_{eff}} \int_0^t N(t')\, e^{\lambda_i t'} dt' \qquad \textbf{2.7}$$

This leads to:

$$C_{eff,i}(t) = \left(C_{eff,i}(0) + \frac{\beta_{eff,i}}{\Lambda_{eff}} \int_0^t N(t')\, e^{\lambda_i t'} dt'\right) e^{-\lambda_i t} \qquad \textbf{2.8}$$

The initial concentration of the precursor can be deduced from the initial neutron population N_0 and by setting the derivate terms to 0 because the perturbation has not been launched yet.

$$C_{eff,i}(0) = \frac{\beta_{eff,i}}{\lambda_i \Lambda_{eff}} N_0 \qquad \textbf{2.9}$$

Using these results in the 2.4 equation we get:

$$\rho(t) = \beta_{eff} + \frac{\Lambda_{eff}}{N(t)}\left(\frac{\partial N(t)}{\partial t} - \sum_{i=1}^{8} \beta_{eff,i} e^{-\lambda_i t}\left(N_0 + \frac{\lambda_i}{\Lambda_{eff}} \int_0^t N(t')\, e^{\lambda_i t'} dt'\right)\right) \qquad \textbf{2.10}$$

The reactivity is then dependent on the effective kinetic parameters and then from adjoint flux, using the expression in dollar of the reactivity and by dividing the **2.10** equation by the effective delayed neutron fraction we get:

$$\rho_{\$}(t) = 1 + \frac{1}{N(t)}\left(\frac{\Lambda_{eff}}{\beta_{eff}} \frac{\partial N(t)}{\partial t} - \sum_{i=1}^{8} a_i e^{-\lambda_i t}\left(N_0 + \frac{\lambda_i}{\Lambda_{eff}} \int_0^t N(t')\, e^{\lambda_i t'} dt'\right)\right) \qquad \textbf{2.11}$$

With $a_i = \beta_{eff,i}/\beta_{eff}$, the relative abundance of each family i of precursors. Thus the step by step integration of the counting rate of a detector gives the online reactivity in dollar of the core after the perturbation. The hypothesis made in **IV.2.1**.1 remains here because the shape function can be affected by the rod drop.

IV.2.1.3 The rod drop calibration

The control rod is then calibrated with the rod drop experiment, the reactivity is recorded during the rod drop giving a typical "S-curve" and the efficiency of the absorption of neutrons by the control rod (see **Figure IV.2.1**).

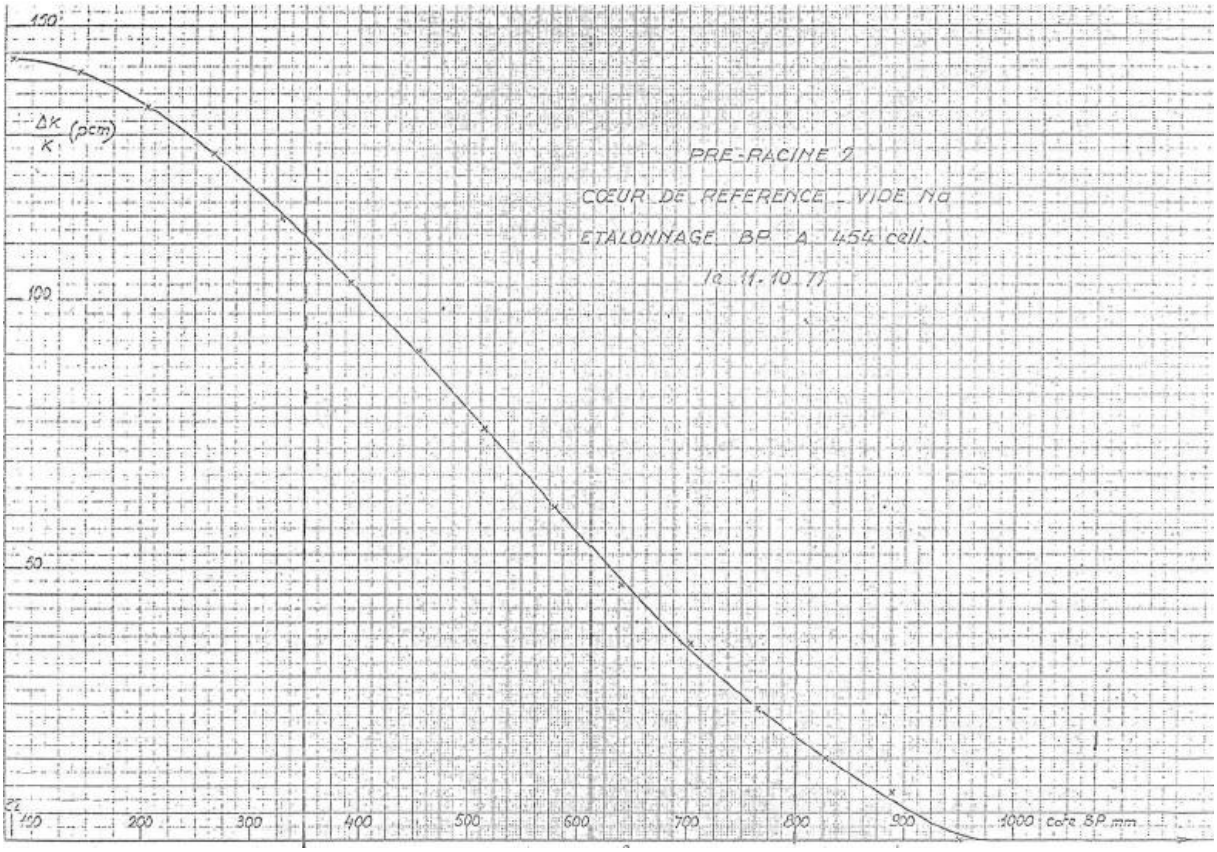

Figure IV.2.1: S-curve of PRE-RACINE IIA core

The magnitude of the control rod is less than 1 $ for safety reasons according to the nuclear safety authority recommendations. Once the control rod is calibrated the small reactivity variations (<1$) are deduced by the control rod position to get back to the criticality and the more important variation are calculated by getting back to the criticality by adding peripheral fuel assemblies. The reactivity is obtained with this loading by adjusting the control rod position.

IV.2.2 Experimental uncertainties on the SVRE

The Sodium Void Reactivity Effect (SVRE) is then the difference between the reactivity measurements of the voided configuration and the reactivity measurement of the reference configuration. The experimental uncertainty associated to the SVRE is the quadratic combination of the uncertainty on each measurement. In such experimental programmes the SVRE measurements takes months because the building of each configurations and the stabilisation (in temperature and reactivity) takes days. Thus the reactivities are measured several times during the programme and the decay of ^{241}Pu (fissile isotope) into ^{241}Am (absorbing isotope) with a period of 14.4 years, has to be taken into account. In the PRE-RACINE and the CIRANO programme the decrease in reactivity due to this decay has been estimated around -0.2 pcm/day [6].

Furthermore the temperature stabilisation is also important because due to Doppler feedback the reactivity comparison is only possible at the same temperature. In the PRE-RACINE programme for

instance a default in the air-cooling system has lead to an overheating (50°C) in the core [7] then two campaigns have been conducted to get the SVRE with a correction in the second campaign for the cooling system (temperature stabilised around 35°C). In the CIRANO programme the decrease of the reactivity with the temperature has been estimated around -3 pcm/°C.

In addition to that the calibration of the control rod is impacted by uncertainties on the kinetic parameters ($\Lambda_{eff}, \beta_{eff}, a_i$) used to invert the point kinetics equations (uncertainties on β_{eff} due to nuclear data have been estimated in the Chapter III) and also by systematic errors due to fission chambers (composition and thickness of the deposit) and by the mechanism to get the position of the control rod.

However in the experimental programme conducted in the MASURCA facility the sources of these biases and uncertainties and the correction of the reactivity measurements due to ^{241}Pu decay have been taken into account but not recorded properly. For instance in the PRE-RACINE programme the reference reactivity measurements are given within a ± 0.7 pcm uncertainty and the voided configuration within ± 1.5 pcm or ± 0.7 pcm if axial blanket have been voided or not.

Another interesting point is the building of voided configurations by replacing the sodium pins by voided pins in MASURCA assemblies (see Appendix A) because when the tubes are removed from the core to be manipulated in the workshop in an ideal world the fuel pins have to be put back at the same position in order to keep exactly the same configuration as the reference one with the exception of the sodium pins. However it is never mentioned in the experimental report if it has been done or not but we will assume this has been done.

In the case of the BFS programme which is the most recent one the uncertainties have been given in details by the Russian part and in dollar allowing to get SVRE values and uncertainties with our own β_{eff} values using recent nuclear data (JEFF-3.2) and methods (IFP see Chapter III).

In the following section are presented the overall uncertainties on SVRE for each voided configuration and experimental programmes.

IV.2.3 Experimental data base

The details on the experimental database are given in the Appendix A. This section just presents the assets of each programme to the experimental qualification of the ASTRID CFV core. In order to do the comparison between these experimental cores and the CFV core we have to select some criteria:

- The presence of a sodium plenum,
- The core surrounding by a reflector or a blanket,
- The presence of an inner fertile area.

These three first criteria are only geometric and based on the innovations in the CFV design so the oldest experimental programme will not meet all these points. Other criteria are based on composition and neutron spectrum.

- The sodium and fuel volume fraction,
- The fuel composition,
- The hardness of the neutron spectrum.

The hardness of the neutron spectrum is defined as the ratio of the average production cross-section to the average slowing down power:

$$r = \frac{\overline{\upsilon\Sigma_f}}{\xi\overline{\Sigma_s}} \qquad \textbf{2.12}$$

The inverse of r is the lethargy interval crossed in average by a neutron during its life: it is the distance in lethargy between the fission spectrum and the disappearance spectrum. The light water reactors (LWR) using thermal neutrons to fission ^{235}U have an spectrum hardness index about 0.15 when in fast reactors (FR) the spectrum hardness index is in a range of 0.3-0.5. This parameter gives information on the neutron spectrum shape which is influenced by the isotopic composition of the fuel and the sodium volume fraction.

The ASTRID CFV Basic Design core uses Pu from reprocessed PWR MOX fuel. This Pu has a highly degraded vector (35% of ^{240}Pu in the Pu content) which can be represented by the P2K fuel which is a 50-50 mix of P4K and PIT Pu based fuel. The PIT fuel has a 18% ^{240}Pu content while the P4K fuel has a 50% ^{240}Pu content and the POA has a 8% of ^{240}Pu content.

Table IV.2.1: Experimental programme features comparison with the ASTRID CFV core

Cores	Sodium plenum	Reflector or Blanket	Inner fertile area	Sodium fraction	Fuel + Fert fraction	Fuel type	Spectrum hardness
PRE-RACINE I	X	Blanket	✓	50%	50%	POA	0.42
PRE-RACINE 2A	X	Blanket	X	50%	50%	POA	0.42
PRE-RACINE 2B	X	Blanket	X	50%	50%	PIT	0.41
CIRANO 2A	X	Blanket	X	50%	50%	PIT	0.51
CIRANO 2B	X	Reflector	X	50%	50%	PIT	0.51
BFS-115-1	✓	Reflector	✓	30%	70%	Military	0.54
ASTRID CFV	✓	**Reflector**	✓	**28%**	**44%**	**P2K**	**0.45**

The fuel compositions are given by fuel type (see Appendix A) for MASURCA core and the ASTRID CFV core is associated to giving the P2K composition. The fuel composition of BFS has a Pu-vector of military quality meaning it is highly enriched in ^{239}Pu which is far from being equivalent to the ASTRID CFV fuel and the spectrum hardness is then much more important than the ASTRID CFV one. Nevertheless the BFS-115-1 core is the only one built with a sodium plenum because the other cores have been built before the CEA proposed the innovations on the CFV design.

IV.2.3.1 PRE-RACINE experimental uncertainties

The PRE-RACINE programme is detailed in Appendix A, this experimental programme is interesting due to the number of voided configurations that have been built with configurations pointing out the LC with only voided in outer axial part of the assemblies and others pointing out the CC with voided areas in the inner part of the tubes. This section presents the overall uncertainties [8] on the SVRE measurements in each core without the detailed breakdown because of a lack of information given in the experimental reports.

Table IV.2.2: Experimental uncertainties of SVRE in PRE-RACINE I

Configuration	Uncertainty (1σ in pcm)
Void V1 R=11.96	5
Void V2 R=11.96	7
Void V3 R=11.96	7
Void V5 R=11.96	7
Void V6 R=11.96	7
Void V7 R=11.96	6
Void V8 R=11.96	5
Void V9 R=11.96	5
Void V5 R=7.33	5

The uncertainties for the PRE-RACINE I core are consistent for small voided areas because only areas with an equivalent radius of 11.96 cm and 7.33 cm have been voided.

Table IV.2.3: Experimental uncertainties of SVRE in PRE-RACINE 2A

Configuration	Uncertainty (1σ in pcm)
Void V1 R=11.96	4
Void V2 R=11.96	3
Void V3 R=11.96	3
Void V4 R=11.96	3
Void V5 R=11.96	3
Void V6 R=11.96	4
Void V7 R=11.96	4
Void V8 R=11.96	4
Void V9 R=11.96	5
Void V5 R=19.83	10
Void V5 R=29.45	7

The uncertainties for the PRE-RACINE 2A and 2B core are also consistent for small voided areas and a bit more important for large voided areas.

Table IV.2.4: Experimental uncertainties of SVRE in PRE-RACINE 2B

Configuration	Uncertainty (1σ in pcm)
Void V1 R=11.96	3
Void V3 R=11.96	3
Void V5 R=11.96	3
Void V5 R=19.83	4
Void V5 R=29.45	8

IV.2.3.2 CIRANO experimental uncertainties

The CIRANO programme is also detailed in the Appendix A and the major asset of these cores are the degraded Pu-vector (using PIT instead of POA type fuel) and the presence of reflector in the ZONA2B core. This section presents the overall uncertainties on the SVRE measurements in each core without the detailed breakdown because of a lack of information given in the experimental reports.

Table IV.2.5: Experimental uncertainties of SVRE in CIRANO 2A

Configuration	Uncertainty (1σ in pcm)
Void V8 R=11.96	1.4
Void V16 R=11.96	1.4
Void V24 R=11.96	1.8
Void V4+4 R=11.96	1.5

Table IV.2.6: Experimental uncertainties of SVRE in CIRANO 2B

Configuration	Uncertainty (1σ in pcm)
Void V8 R=11.96	1.9
Void V16 R=11.96	1.5
Void V24 R=11.96	1.0
Void V4+4 R=11.96	2.5
Void V8 R=20.72	1.5
Void V16 R=20.72	1.4
Void V24 R=20.72	2.5
Void V4+4 R=20.72	2.2

The experimental uncertainties are smaller than the ones of the PRE-RACINE programme due to improvements in the calibration of the control rod method by applying an approximation method for the rod drop record to an online record following the recommendations made after the PRE-RACINE programme [7].

IV.2.3.3 BFS experimental uncertainties

The main asset of the BFS experimental programme [9] is the geometry of the core very similar to the ASTRID CFV core with the axial scheme of the inner fuel and of the outer fuel. The presence of a sodium plenum on the inner fuel, of a steel reflector and of an inner fertile slab (and not anymore an inner radial area such as PRE-RACINE I) are also representative of the innovations of the CFV core. A series of voiding and filling experiments in the inner tubes have been detailed in the experimental reports given by the IPPE[1] to the CEA. The reactivity measurements and uncertainties have been given in cents (1¢=0.01$).

[1] The BFS experimental programme has been done in collaboration between the CEA and the IPPE.

Table IV.2.7: Experimental uncertainties of SVRE in BFS-115-1

Configuration	Uncertainty (1σ in ¢)
Plenum void	3.5 (or 13 pcm)
CSUP and Plenum void	4.3 (or 16 pcm)
Total void	4.8 (or 18 pcm)

The uncertainties are more important than in MASURCA due to the large voided areas.

IV.2.4 The need of GENESIS programme

As seen in the **Table IV.2.1** the features of the experimental programmes do not meet all the innovations implemented for the ASTRID CFV design. Indeed there are some missing features such as:

- The lack of boron neutronic absorber on the core,
- The lack of sodium superior expansion vase (SVES),
- No sodium plenum on the outer core,
- The use of Pressurised Water Reactor (PWR) Mix-Oxyde (MOx) spent fuel Pu-vector (associated to P2K fuel type).

In the BFS experimental programme the boron neutronic absorber have been replaced by neutronic shielding made of depleted uranium using the high absorbing ability of the ^{238}U but this substitution has an important impact on the SVRE when the sodium plenum is voided because it changes the neutron spectrum of "returning" neutrons in the core. Furthermore there is no sodium plenum on outer fuel and no SVES which also impacts the SVRE.

Table IV.2.8: Comparison of the features of a core designed for GENESIS and the ASTRID CFV core

Cores	Sodium plenum	Reflector or Blanket	Inner fertile area	Sodium fraction	Fuel fraction	Fuel type	Spectrum hardness
GENESIS	✓	Reflector	✓	33%	50%	P2K	0.44
ASTRID CFV	✓	**Reflector**	✓	**28%**	**44%**	**P2K**	**0.45**

This GENESIS programme is a real challenge for the CEA because it will bring new and important measurements for the experimental validation of the CFV core [10] as we will see in Chapter V. The skill transfer of experimental experts to the young generation of physicist appointed by the CEA after the halt of the Phénix experimental programme in 2010 has also to be considered.

IV.3 SVRE calculated

In this section, are presented the results obtained with two neutronic codes on the SVRE of each experimental programme. Section **IV.3**.1 presents the results calculated with the Monte-Carlo code TRIPOLI-4® and section **IV.3**.2 with the deterministic code ERANOS (see Chapter II for details).

IV.3.1 Refined geometry with TRIPOLI-4®

The main asset of the Monte-Carlo code TRIPOLI-4® is the ability to implement refined geometries like "as built" and the fact that the results are considered as reference because there is no approximation other than statistics (see Chapter II). In order to get the SVRE a simulation with the refined geometry of the nominal configuration is launched to get the reference reactivity (with the effective multiplication factor) and after that it is needed to launch as many simulations as there are voided configurations. The statistical uncertainty on the reactivity is given by:

$$d\rho = \frac{dk_{eff}}{{k_{eff}}^2} \qquad \textbf{3.1}$$

Then the statistical uncertainty on the SVRE is calculated as the quadratic sum of the uncertainties on each reactivity:

$$d(\Delta\rho) = \sqrt{(d\rho_v)^2 + (d\rho_n)^2} \qquad \textbf{3.2}$$

The following sections present the discrepancies between the TRIPOLI-4® and experimental results (C-E) for JEFF-3.1.1 and JEFF-3.2 nuclear data. The experimental reactivity measurements (made in \$) have been re-evaluated with the calculated β_{eff} using the IFP method with TRIPOLI-4® (see Chapter III).

IV.3.1.1 PRE-RACINE results

The following table presents the discrepancies between the TRIPOLI-4® and experimental results of the SVRE with JEFF-3.1.1 nuclear data for the PRE-RACINE I core in regard of the statistical and experimental uncertainties. All the voided areas are fertile in this core.

Table IV.3.1: C-E in PRE-RACINE I with JEFF-3.1.1

Configuration	C-E (in pcm)	Exp unc (1σ in pcm)	Stat unc (1σ in pcm)
Void V1 R=11.96	-2.2	5	5.6
Void V2 R=11.96	-4.6	7	5.6
Void V3 R=11.96	-2.9	7	5.6
Void V5 R=11.96	0.3	7	5.6
Void V6 R=11.96	4.5	7	5.6
Void V7 R=11.96	7.8	6	5.6
Void V8 R=11.96	3.5	5	5.6
Void V9 R=11.96	4.3	5	5.6
Void V5 R=7.33	3.4	5	5.6

Globally the use of JEFF-3.1.1 estimates well the SVRE for all the voided configurations then the nuclear data of JEFF-3.1.1 implied in the calculations of the SVRE such as ^{238}U and sodium are in good agreement with these measurements.

Table IV.3.2: C-E in PRE-RACINE I with JEFF-3.2

Configuration	C-E (in pcm)	Exp unc (1σ in pcm)	Stat unc (1σ in pcm)
Void V1 R=11.96	-9.5	5	5.6
Void V2 R=11.96	-4.8	7	5.6
Void V3 R=11.96	-0.8	7	5.6
Void V5 R=11.96	8.8	7	5.6
Void V6 R=11.96	10.0	7	5.6
Void V7 R=11.96	5.1	6	5.6
Void V8 R=11.96	14.5	5	5.6
Void V9 R=11.96	7.0	5	5.6
Void V5 R=7.33	9.0	5	5.6

With JEFF-3.2 the discrepancies are more important but the results are consistent within the 3 σ uncertainty.

The following table presents the discrepancies between the TRIPOLI-4® and experimental results of the SVRE with JEFF-3.1.1 nuclear data for the PRE-RACINE 2A core in regard of the statistical and experimental uncertainties. The voided areas are mainly in the fuel in this core and if fertile areas are also voided the results are written in ***bold italic***.

Table IV.3.3: C-E in PRE-RACINE 2A with JEFF-3.1.1

Configuration	C-E (in pcm)	Exp unc (1σ in pcm)	Stat unc (1σ in pcm)
Void V1 R=11.96	-7.2	4	5.6
Void V2 R=11.96	7.2	3	5.6
Void V3 R=11.96	5.0	3	5.6
Void V4 R=11.96	6.4	3	5.6
Void V5 R=11.96	10.1	3	5.6
Void V6 R=11.96	***9.7***	***4***	***5.6***
Void V7 R=11.96	***5.7***	***4***	***5.6***
Void V8 R=11.96	18.3	4	5.6
Void V9 R=11.96	***13.7***	***5***	***5.6***
Void V5 R=19.83	13.0	10	5.6
Void V5 R=29.45	-3.9	7	5.6

Globally the use of JEFF-3.1.1 overestimates the SVRE with an inconsistent result (even at 3σ) for the V8 R=11.96 voided configuration. As this configuration is mainly due to the Leakage Component it seems to indicate a problem with JEFF-3.1.1 nuclear data involved in the LC calculation in the fuel area.

Table IV.3.4: C-E in PRE-RACINE 2A with JEFF-3.2

Configuration	C-E (in pcm)	Exp unc (1σ in pcm)	Stat unc (1σ in pcm)
Void V1 R=11.96	2.0	4	5.6
Void V2 R=11.96	12.7	3	5.6
Void V3 R=11.96	19.3	3	5.6
Void V4 R=11.96	28.2	3	5.6
Void V5 R=11.96	25.2	3	5.6
Void V6 R=11.96	***14.8***	***4***	***5.6***
Void V7 R=11.96	***3.5***	***4***	***5.6***
Void V8 R=11.96	30.8	4	5.6
Void V9 R=11.96	***29.6***	***5***	***5.6***
Void V5 R=19.83	52.0	10	5.6
Void V5 R=29.45	57.6	7	5.6

Here the use of JEFF-3.2 really overestimates the SVRE with many inconsistent results (even at 3σ) for many voided configuration which are mainly voided fuel areas. The nuclear data of fuel isotopes of a U-Pu based fuel in JEFF-3.2 seem not consistent at all for the SVRE in PRE-RACINE 2A.

The following table presents the discrepancies between the TRIPOLI-4® and experimental results of the SVRE with JEFF-3.1.1 nuclear data for the PRE-RACINE 2B core. The voided areas are only in the fuel in this core.

Table IV.3.5: C-E in PRE-RACINE 2B with JEFF-3.1.1

Configuration	C-E (in pcm)	Exp unc (1σ in pcm)	Stat unc (1σ in pcm)
Void V1 R=11.96	-12.7	3	5.6
Void V3 R=11.96	9.7	3	5.6
Void V5 R=11.96	10.6	3	5.6
Void V5 R=19.83	3.7	4	5.6
Void V5 R=29.45	19.1	8	5.6

Globally the use of JEFF-3.1.1 nuclear data gives consistent results for this core within the 3σ range of statistical or experimental uncertainties.

Table IV.3.6: C-E in PRE-RACINE 2B with JEFF-3.2

Configuration	C-E (in pcm)	Exp unc (1σ in pcm)	Stat unc (1σ in pcm)
Void V1 R=11.96	12.9	3	5.6
Void V3 R=11.96	22.5	3	5.6
Void V5 R=11.96	26.7	3	5.6
Void V5 R=19.83	49.5	4	5.6
Void V5 R=29.45	88.9	8	5.6

Here again the use of JEFF-3.2 nuclear data gives inconsistent results for many voided configurations which are voided fuel configurations. Nuclear data of Plutonium and Uranium really become suspect. And as seen in PRE-RACINE 2A core the voided fertile configuration giving consistent results (for 2 out of 3 of them) and the main difference with the fuel being the lack of ^{235}U and Plutonium (in fertile blanket made of depleted Uranium) that seems to save the nuclear data of ^{238}U.

IV.3.1.2 CIRANO results

The following table presents the discrepancies between the TRIPOLI-4® and experimental results of the SVRE with JEFF-3.1.1 nuclear data for the CIRANO 2A core. The voided areas are only in the fuel in this core.

Table IV.3.7: C-E in CIRANO 2A with JEFF-3.1.1

Configuration	C-E (in pcm)	Exp unc (1σ in pcm)	Stat unc (1σ in pcm)
Void V8 R=11.96	0.9	1.4	5.6
Void V16 R=11.96	9.9	1.4	5.6
Void V24 R=11.96	19.6	1.8	5.6
Void V4+4 R=11.96	5	1.5	5.6

Globally the use of JEFF-3.1.1 nuclear data seems to overestimates the SVRE with an inconsistent result for the largest voided configuration (V24 R11.96).

Table IV.3.8: C-E in CIRANO 2A with JEFF-3.2

Configuration	C-E (in pcm)	Exp unc (1σ in pcm)	Stat unc (1σ in pcm)
Void V8 R=11.96	10.0	1.4	5.6
Void V16 R=11.96	15.4	1.4	5.6
Void V24 R=11.96	22.2	1.8	5.6
Void V4+4 R=11.96	5.7	1.5	5.6

In this core, the use of JEFF-3.2 nuclear data increase the discrepancies and the overestimation of the SVRE but it still has only one inconsistent result for the largest voided configuration (V24 R11.96).

The following table presents the discrepancies between the TRIPOLI-4® and experimental results of the SVRE with JEFF-3.1.1 nuclear data for the CIRANO 2B core. The voided areas are only in the fuel in this core.

Table IV.3.9: C-E in CIRANO 2B with JEFF-3.1.1

Configuration	C-E (in pcm)	Exp unc (1σ in pcm)	Stat unc (1σ in pcm)
Void V8 R=11.96	-7	1.9	5.6
Void V16 R=11.96	10.8	1.5	5.6
Void V24 R=11.96	1.6	1.0	5.6
Void V4+4 R=11.96	4.8	2.5	5.6
Void V8 R=20.72	-4.5	1.5	5.6
Void V16 R=20.72	-0.1	1.4	5.6
Void V24 R=20.72	15.1	2.5	5.6
Void V4+4 R=20.72	-6.7	2.2	5.6

Replacing the surrounding fertile blanket by a sodium-steel reflector is not a matter with the Monte-Carlo code TRIPOLI-4® all the SVRE calculated with JEFF-3.1.1 are consistent with experimental results.

Table IV.3.10: C-E in CIRANO 2B with JEFF-3.2

Configuration	C-E (in pcm)	Exp unc (1σ in pcm)	Stat unc (1σ in pcm)
Void V8 R=11.96	-5.5	1.9	8.1
Void V16 R=11.96	11.6	1.5	8.1
Void V24 R=11.96	18.0	1.0	8.1
Void V4+4 R=11.96	2.1	2.5	8.1
Void V8 R=20.72	13.9	1.5	8.1
Void V16 R=20.72	29.4	1.4	7.6
Void V24 R=20.72	47.0	2.5	8.1
Void V4+4 R=20.72	4.7	2.2	8.1

Nevertheless, the use of JEFF-3.2 seems again problematic especially in the largest voided configurations where the CC is important.

IV.3.1.3 BFS results

The following table presents the discrepancies between the TRIPOLI-4® and experimental results of the SVRE with JEFF-3.1.1 nuclear data for the BFS-115-1 core. The voided areas are as well fuel medium or sodium plenum as fertile medium. The configurations selected for this study are detailed in Appendix A.

Table IV.3.11: C-E in BFS-115-1 with JEFF-3.1.1

Configuration	C-E (in pcm)	Exp unc (1σ in pcm)	Stat unc (1σ in pcm)
Plenum void	-65.0	13	5.8
CSUP and Plenum void	-86.7	16	5.8
Total void	-92.8	18	5.8

Globally the use of JEFF-3.1.1 nuclear data for these three voided configurations gives inconsistent results with discrepancies between 12% and 22% to the experimental values. However, the main suspect here is the sodium because if we only consider the configuration where the sodium plenum is voided the discrepancy with experimental result is already representing 65 pcm meaning that 70% of the discrepancy on the total voided configuration comes from this first error if we put apart compensating effect.

Table IV.3.12: C-E in BFS-115-1 with JEFF-3.2

Configuration	C-E (in pcm)	Exp unc (1σ in pcm)	Stat unc (1σ in pcm)
Plenum void	-35.3	13	3.7
CSUP and Plenum void	-41.8	16	3.7
Total void	-36.7	18	3.7

Here the use of JEFF-3.2 nuclear data for these three voided configurations gives consistent results because the discrepancies are reduced and already 30 pcm have been gained on the voided plenum configuration. It tends showing that the sodium of the JEFF-3.2 nuclear data is better than the one of

JEFF-3.1.1. These results also shows compensating effects because the difference between the discrepancies of the voided plenum and the total voided configurations is only about 1 pcm and of course the resulting error due to the fissile medium in JEFF-3.2 is much more than 1 pcm as we have seen with MASURCA cores that ^{235}U and Plutonium have an important impact on these errors.

IV.3.1.4 Conclusion on C-E comparison with TRIPOLI-4®

The first conclusion of this work, thanks to PRE-RACINE and CIRANO experimental programmes is that:

- Voided configurations in fertile areas are well calculated with JEFF-3.1.1 and JEFF-3.2
- Voided configurations in fuel media are not well calculated with JEFF-3.2 and when the LC is important JEFF-3.1.1 is also inconsistent.
- The voided plenum configuration in BFS-115-1 is better calculated with JEFF-3.2 than with JEFF-3.1.1.

Then the main suspects of this work are:

- The JEFF-3.2 nuclear data of ^{235}U and Plutonium are responsible for the discrepancies in the PRE-RACINE and CIRANO cores,
- The sodium nuclear data in JEFF-3.1.1 is the main responsible for the important discrepancies in the BFS results. It is confirmed by the fact that when the LC is important in some sodium voided configurations of the MASURCA cores the results are inconsistent with JEFF-3.1.1 nuclear data because the nuclear data of the sodium (with elastic and inelastic scattering) is the main responsible of the LC.

IV.3.2 RZ geometry with ERANOS

As seen in Chapter II the use of a deterministic code in complement of a stochastic code allows using perturbation theory to get access to the breakdown of the SVRE in physical components and then to calculate the CC and the LC. In the ERANOS code, the RZ model of the core configuration has been chosen for applying the new procedure calculating the sensitivity of the CC to nuclear data (see Chapter V). Then all the results presented in this section are calculated using the RZ model, transport theory and the S_8 angular discretisation. The following tables will present the comparison between the calculated and the experimental results on the SVRE and the proportion: $P_{CC} = CC/(CC + |LC|)$ and $P_{LC} = |LC|/(CC + |LC|)$ for each voided configuration.

IV.3.2.1 PRE-RACINE results

The following table presents the discrepancies between the ERANOS and experimental results of the SVRE with JEFF-3.1.1 nuclear data for the PRE-RACINE I core. All the voided areas are fertile in this core.

Table IV.3.13: C-E in PRE-RACINE I with JEFF-3.1.1

Configuration	C-E (in pcm)	Exp unc (in pcm)	P_{CC} (in %)	P_{LC} (in %)
Void V1 R=11.96	-2.4	5	100	0
Void V2 R=11.96	-2.4	7	97	3
Void V3 R=11.96	2.2	7	91	9
Void V5 R=11.96	13	7	75	25
Void V6 R=11.96	17.3	7	68	32
Void V7 R=11.96	7	6	38	62
Void V8 R=11.96	7	5	55	45
Void V9 R=11.96	11.8	5	49	51
Void V5 R=7.33	-5.5	5	81	19

These results are consistent within the 3σ range of experimental uncertainties with very good agreement where the LC is low and higher discrepancies where the LC becomes relevant.

Table IV.3.14: C-E in PRE-RACINE I with JEFF-3.2

Configuration	C-E (in pcm)	Exp unc (in pcm)	P_{CC} (in %)	P_{LC} (in %)
Void V1 R=11.96	-1.6	5	97	3
Void V2 R=11.96	0.4	7	97	3
Void V3 R=11.96	6.9	7	92	8
Void V5 R=11.96	21.5	7	77	23
Void V6 R=11.96	27.7	7	70	30
Void V7 R=11.96	8.5	6	39	61
Void V8 R=11.96	10.4	5	57	43
Void V9 R=11.96	17	5	50	50
Void V5 R=7.33	-7	5	82	18

Using JEFF-3.2 nuclear data gives inconsistent results with ERANOS for voided fertile areas especially in total voided configurations (V5 and V6) with important contributions of the central component.

The following table presents the discrepancies between the ERANOS and experimental results of the SVRE with JEFF-3.1.1 nuclear data for the PRE-RACINE 2A core. The voided areas are mainly in the fuel in this core and if fertile areas are also voided the results are written in ***bold italic***.

Table IV.3.15: C-E in PRE-RACINE 2A with JEFF-3.1.1

Configuration	C-E (in pcm)	Exp unc (in pcm)	P_{CC} (in %)	P_{LC} (in %)
Void V1 R=11.96	0.6	4	93	7
Void V2 R=11.96	2.4	3	86	14
Void V3 R=11.96	6.4	3	74	26
Void V4 R=11.96	11.4	3	61	39
Void V5 R=11.96	12.5	3	50	50
Void V6 R=11.96	***11.6***	***4***	***44***	***56***
Void V7 R=11.96	***1.8***	***4***	***25***	***75***
Void V8 R=11.96	6.2	4	30	70
Void V9 R=11.96	***4.9***	***5***	***28***	***72***
Void V5 R=19.83	27.4	10	47	53
Void V5 R=29.45	16	7	42	58

Globally the results calculated with ERANOS are consistent within the 3σ range of experimental uncertainties (exception made of the V4 and V5 R=11.96 configurations). ERANOS and JEFF-3.1.1 seems to overestimate the SVRE when the fuel areas are voided.

Table IV.3.16: C-E in PRE-RACINE 2A with JEFF-3.2

Configuration	C-E (in pcm)	Exp unc (in pcm)	P_{CC} (in %)	P_{LC} (in %)
Void V1 R=11.96	1.7	4	93	7
Void V2 R=11.96	5.3	3	87	13
Void V3 R=11.96	11.3	3	76	24
Void V4 R=11.96	18.7	3	63	37
Void V5 R=11.96	22.7	3	52	48
Void V6 R=11.96	***24.6***	***4***	***46***	***54***
Void V7 R=11.96	***4.2***	***4***	***27***	***73***
Void V8 R=11.96	11.4	4	31	69
Void V9 R=11.96	***12.7***	***5***	***29***	***71***
Void V5 R=19.83	55.1	10	49	51
Void V5 R=29.45	77.8	7	43	57

Here the results calculated with ERANOS and JEFF-3.2 are less consistent within the 3σ range of experimental uncertainties than with JEFF-3.1.1 and it concerns as much as the configurations pointing out the CC than the total voided configuration with an important contribution of the LC. ERANOS and JEFF-3.2 overestimate the SVRE when the fuel areas are voided.

The following table presents the discrepancies between the ERANOS and experimental results of the SVRE with JEFF-3.1.1 nuclear data for the PRE-RACINE 2B core. The voided areas are only in the fuel in this core.

Table IV.3.17: C-E in PRE-RACINE 2B with JEFF-3.1.1

Configuration	C-E (in pcm)	Exp unc (in pcm)	P_{CC} (in %)	P_{LC} (in %)
Void V1 R=11.96	-0.1	3	94	6
Void V3 R=11.96	5.3	3	76	24
Void V5 R=11.96	15	3	53	47
Void V5 R=19.83	19.6	4	50	50
Void V5 R=29.45	30.1	8	45	55

The largest voided configurations are not consistent within the 3σ range of experimental uncertainties. This seems to show that in the voided configuration with an important contribution ERANOS and JEFF-3.1.1 nuclear data greatly overestimate the SVRE and the LC.

Table IV.3.18: C-E in PRE-RACINE 2B with JEFF-3.2

Configuration	C-E (in pcm)	Exp unc (in pcm)	P_{CC} (in %)	P_{LC} (in %)
Void V1 R=11.96	1.3	3	94	6
Void V3 R=11.96	11	3	78	22
Void V5 R=11.96	26.5	3	55	45
Void V5 R=19.83	50.5	4	52	48
Void V5 R=29.45	98.7	8	47	53

This is the same conclusion than the one with JEFF-3.1.1 with even greater discrepancies for the largest voided configurations.

IV.3.2.2 CIRANO results

The following table presents the discrepancies between the ERANOS and experimental results of the SVRE with JEFF-3.1.1 nuclear data for the CIRANO 2A core. The voided areas are only in the fuel in this core.

Table IV.3.19: C-E in CIRANO 2A with JEFF-3.1.1

Configuration	C-E (in pcm)	Exp unc (in pcm)	P_{CC} (in %)	P_{LC} (in %)
Void V8 R=11.96	0.8	1.4	86	14
Void V16 R=11.96	4.5	1.4	67	33
Void V24 R=11.96	5.0	1.8	49	51
Void V4+4 R=29.45	5.8	1.5	28	72

The results given by ERANOS with JEFF-3.1.1 nuclear data are quite consistent within the 3σ range of experimental uncertainties even the use of ZONA2 fuel increased the sodium volume fraction the discrepancies are not important.

Table IV.3.20: C-E in CIRANO 2A with JEFF-3.2

Configuration	C-E (in pcm)	Exp unc (in pcm)	P_{CC} (in %)	P_{LC} (in %)
Void V8 R=11.96	5.1	1.4	87	13
Void V16 R=11.96	14.1	1.4	69	31
Void V24 R=11.96	19.8	1.8	51	49
Void V4+4 R=29.45	11.1	1.5	29	81

Otherwise, the use of JEFF-3.2 gives very important discrepancies which is understandable because the fuel fraction is also increased with the use of ZONA2 (50%) cells instead of ZONA1 (37.5%).

The following table presents the discrepancies between the ERANOS and experimental results of the SVRE with JEFF-3.1.1 nuclear data for the CIRANO 2B core. The voided areas are only in the fuel in this core.

Table IV.3.21: C-E in CIRANO 2B with JEFF-3.1.1

Configuration	C-E (in pcm)	Exp unc (in pcm)	P_{CC} (in %)	P_{LC} (in %)
Void V8 R=11.96	-4.0	1.9	84	16
Void V16 R=11.96	4.2	1.5	67	33
Void V24 R=11.96	-0.7	1	48	52
Void V4+4 R=11.96	0.9	2.5	25	75
Void V8 R=20.72	-15.0	1.5	72	28
Void V16 R=20.72	-31.4	1.4	60	40
Void V24 R=20.72	-28.6	2.5	45	55
Void V4+4 R=20.72	-8.2	2.2	24	76

Replacing the surrounding fertile blanket by a sodium-steel reflector seems problematic with ERANOS and JEFF-3.1.1 nuclear data especially for the largest voided areas because for the smaller ones in the centre of the core, the neutron spectrum is not really influenced by the substitution of the fertile blanket by a reflector.

Table IV.3.22: C-E in CIRANO 2B with JEFF-3.2

Configuration	C-E (in pcm)	Exp unc (in pcm)	P_{CC} (in %)	P_{LC} (in %)
Void V8 R=11.96	1.1	1.9	85	15
Void V16 R=11.96	14.4	1.5	68	32
Void V24 R=11.96	16.3	1	50	50
Void V4+4 R=11.96	6.1	2.5	26	74
Void V8 R=20.72	1.0	1.5	73	27
Void V16 R=20.72	-2.3	1.4	62	38
Void V24 R=20.72	14.1	2.5	47	53
Void V4+4 R=20.72	6.0	2.2	26	74

Replacing the surrounding fertile blanket by a sodium-steel reflector seems a bit less problematic with ERANOS and JEFF-3.2 nuclear data because the largest voided areas give more consistent results and the discrepancies are reduced.

IV.3.2.3 BFS results

The following table presents the discrepancies between the ERANOS and experimental results of the SVRE with JEFF-3.1.1 nuclear data for the BFS-115-1 core. The voided areas could be fuel regions or sodium plenum or even fertile medium. The configurations selected for this study are detailed in Appendix A.

Table IV.3.23: C-E in BFS-115-1 with JEFF-3.1.1

Configuration	C-E (in pcm)	Exp unc (in pcm)	P_{CC} (in %)	P_{LC} (in %)
Plenum void	-322	13	7	93
CSUP and Plenum void	-342	16	20	80
Total void	-319	18	29	71

The use of ERANOS and JEFF-3.1.1 nuclear data shows important discrepancies here, this is due to ERANOS trouble with the model of a sodium plenum.

Table IV.3.24: C-E in BFS-115-1 with JEFF-3.2

Configuration	C-E (in pcm)	Exp unc (in pcm)	P_{CC} (in %)	P_{LC} (in %)
Plenum void	-293	13	8	92
CSUP and Plenum void	-302	16	21	79
Total void	-269	18	30	70

The use of ERANOS and JEFF-3.2 nuclear data shows again important discrepancies here even if it is decreased of 30 to 50 pcm according to the configuration, this is due to ERANOS trouble with the model of a sodium plenum with sodium discs.

IV.3.3 Deterministic biases and experimental uncertainties

Once we got the SVRE calculated with ERANOS and TRIPOLI-4® for all these series of voided configurations we want to find a set of parameters (α, β) to adjust the CC anc LC values in order to minimise the difference between the adjusted and experimental values of SVRE.

$$\Delta\rho_{adj} = \alpha.CC + \beta.LC \qquad \textbf{3.3}$$

Using the χ^2 generalised method it is needed to initialise the set of parameter to (1,1) then with two loops it is easy to set α and to vary β. At each step the χ^2 is calculated as follow, taking into account the experimental uncertainties σ_{exp}:

$$\chi^2 = \sum_{experiments} \left(\frac{\Delta\rho_{exp} - \Delta\rho_{adjusted}}{\sigma_{exp}} \right)^2 \qquad \textbf{3.4}$$

Once the χ^2 is minimised the values of (α, β) are kept to get the adjusted values of the series of CC and LC.

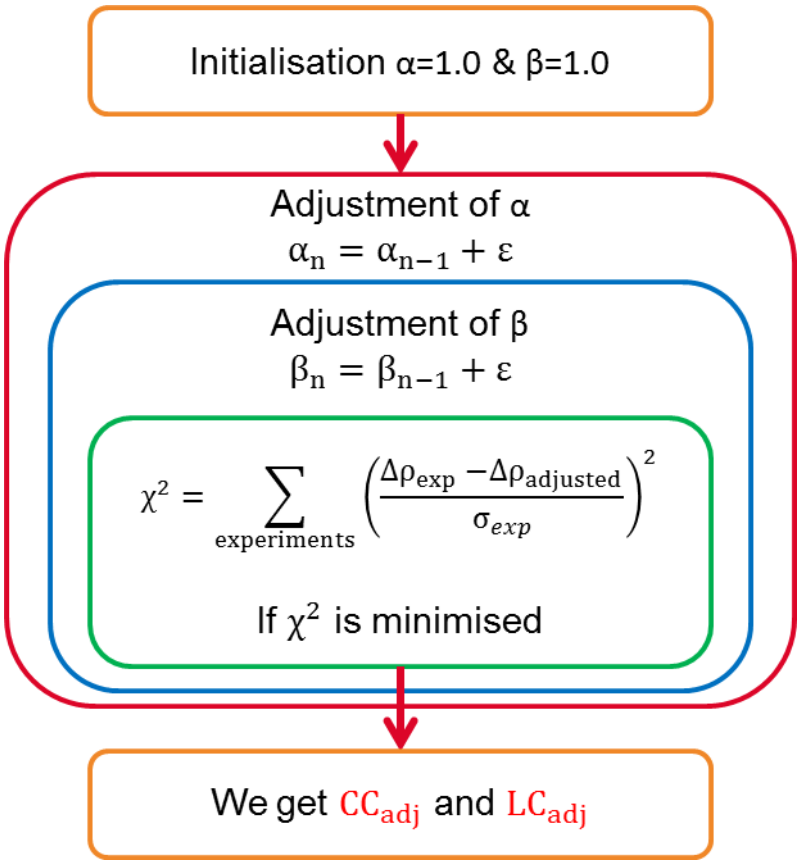

Figure IV.3.1: Adjustment of the set of parameter (α, β)

The convergence of this method to a minimum can be shown on a "map of the χ^2 values" because at each step these values are stored on an output file.

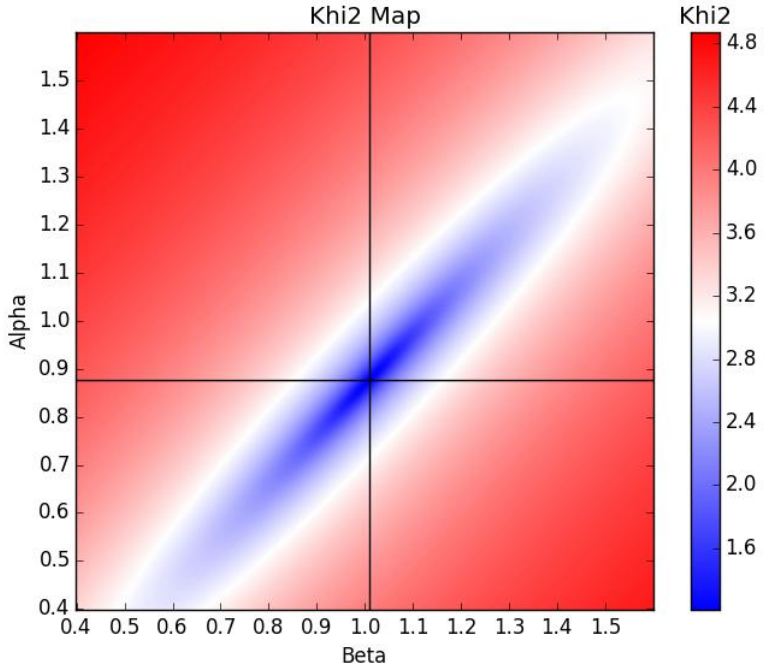

Figure IV.3.2: χ^2 map for the ERANOS-experimental adjustment of the PRE-RACINE 2A&B cores

In **Figure IV.3.2** is presented the "χ^2 map" of the adjustment of the ERANOS (obtained with JEFF-3.2 nuclear data) values of the CC and LC (calculated with JEFF-3.2 nuclear data) to minimise the difference with the experimental SVRE. The two black crossing lines indicate the (α, β) values minimising the χ^2.

This work has to be done between the ERANOS values of CC and LC and the experimental SVRE but also between the ERANOS values of CC and LC and the TRIPOLI-4® SVRE. Indeed as in TRIPOLI-4® has not yet been implemented the ability to break down the SVRE into physical components the discrepancies with experimental results have to be compared with the CC and LC calculated with ERANOS.

The values α and β are meant to be the C/E values for, respectively, the central component (CC) and the leakage component (LC).

IV.3.3.1 Uncertainties in the adjustment

The adjustment takes into account the experimental uncertainties only when the calculation is performed between ERANOS and experimental results and the statistical uncertainties on the TRIPOLI-4® results when it is performed between ERANOS and TRIPOLI-4® results. In order to get the uncertainties of each of the parameters (α, β) the 10000 draws of the experimental/TRIPOLI-4® SVRE value are randomly set according to a Gaussian distribution around the experimental/TRIPOLI-4® SVRE value within a standard deviation equals to the experimental/statistical uncertainty.

Then 10000 adjustments are realised on each series and the mean values of the 10000 set of parameters (α, β) converges to the previous ones calculated with the χ^2 generalised method and the standard deviation gives the uncertainty on α and β associated to these experimental/statistical uncertainties.

IV.3.3.2 Experimental adjustment of the ERANOS CC and LC

In the following table, are presented the results of the adjustment of the ERANOS CC and LC calculated with JEFF-3.1.1 to the experimental SVRE for each core with the uncertainty on each parameter due to the experimental uncertainties.

Table IV.3.25: experimental/ERANOS adjustment with JEFF-3.1.1 nuclear data

Cores	α	dα	β	dβ
PRE-RACINE I	0.993	0.029	1.148	0.054
PRE-RACINE 2A	0.905	0.025	0.964	0.020
PRE-RACINE 2B	0.919	0.033	0.973	0.030
CIRANO 2A	0.994	0.013	1.035	0.015
CIRANO 2B	1.073	0.006	1.019	0.007
BFS-115-1	0.730	0.059	0.640	0.016

ERANOS with JEFF-3.1.1 nuclear data overestimates the CC and the LC when the voided zone concerns the fuel for BFS and PRE-RACINE 2A&B. The magnitude of this overestimation is significantly larger when the voided configuration includes a sodium plenum. In the case of voided fertile areas configurations with PRE-RACINE I, it calculates well the CC with an underestimation of the LC.

In the following table, are presented the results of the adjustment of the ERANOS CC and LC calculated with JEFF-3.2 to the experimental SVRE for each core with the uncertainty on each parameter due to the experimental uncertainties.

Table IV.3.26: experimental/ERANOS adjustment with JEFF-3.2 nuclear data

Cores	α	dα	β	dβ
PRE-RACINE I	0.964	0.025	1.189	0.043
PRE-RACINE 2A	0.873	0.024	1.004	0.020
PRE-RACINE 2B	0.886	0.031	1.019	0.032
CIRANO 2A	0.938	0.012	1.063	0.015
CIRANO 2B	1.010	0.006	1.040	0.007
BFS-115-1	0.716	0.056	0.662	0.017

In most cases the use of ERANOS and JEFF-3.2 nuclear data shows an overestimation of the CC [from 3.6% up to 28.4%], with the exception of the CIRANO 2B results and an underestimation of the LC [from 0.8% up to 18.9%] if we exclude the BFS results which are very specific of the study of the sodium plenum. These adjustments show that, with JEFF-3.2, the CC have to be more adjusted than with JEFF-3.1.1 whereas the detailed analysis of the experimental discrepancies has shown that JEFF-3.2 get better results with voided configuration pointing out the LC due to best sodium nuclear data. These two conclusions seem antagonistic but we will show in Chapter V that the influence of Uranium and Plutonium nuclear data on the LC are not negligible which explains these results for β.

Furthermore a focus on the PRE-RACINE 2A&B results giving indications independently of the Pu type proves that the LC is well calculated for voided fuel areas configurations when the CC is overestimated by 12.4%.

IV.3.3.3 Deterministic bias: TRIPOLI-4® / ERANOS adjustment

In the following table, are presented the results of the adjustment of the ERANOS CC and LC calculated with JEFF-3.1.1 to the calculated SVRE with TRIPOLI-4® for each core with the uncertainty for each parameter due to the experimental uncertainties. In this case the combined adjustment of CIRANO 2A and CIRANO 2B results gave reduced discrepancies with the adjusted values compared to the initial ones.

Table IV.3.27: ERANOS/TRIPOLI4 adjustment with JEFF-3.1.1 nuclear data

Cores	α	dα	β	dβ
PRE-RACINE I	0.961	0.029	1.043	0.064
PRE-RACINE 2A	0.923	0.039	0.963	0.029
PRE-RACINE 2B	0.944	0.030	0.970	0.024
CIRANO 2A	1.045	0.050	0.982	0.052
CIRANO 2B	1.073	0.019	0.998	0.017
BFS-115-1	0.722	0.025	0.710	0.007

For the PRE-RACINE and CIRANO experiments calculated with the JEFF-3.1.1 nuclear data the results on the LC have a good agreement within the adjustment between ERANOS and TRIPOLI-4® (the β is included in the 2σ range). On the other hand for the CC PRE-RACINE and BFS results show an important overestimation [from 5.7% to 27.8%] by ERANOS.

In the following table, are presented the results of the adjustment of the ERANOS CC and LC calculated with JEFF-3.2 to the calculated SVRE with TRIPOLI-4® for each core with the uncertainty on each parameter due to the experimental uncertainties. In this case, the combined adjustment of CIRANO 2A and CIRANO 2B results gave reduced discrepancies with the adjusted values compared to the initial ones.

Table IV.3.28: ERANOS/TRIPOLI4 adjustment with JEFF-3.2 nuclear data

Cores	α	dα	β	dβ
PRE-RACINE I	0.946	0.028	1.031	0.067
PRE-RACINE 2A	1.015	0.038	1.027	0.030
PRE-RACINE 2B	1.109	0.048	1.109	0.044
CIRANO 2A	1.055	0.047	1.056	0.054
CIRANO 2B	1.077	0.025	1.017	0.025
BFS-115-1	0.744	0.017	0.704	0.005

The use of JEFF-3.2 with ERANOS calculations improves the agreement with TRIPOLI-4® for the CC. The results on the LC are also consistent (exception made of BFS results) with a slight overestimation for PRE-RACINE2A&B voided configurations due to the influence of the poor nuclear data of Uranium and Plutonium in JEFF-3.2 since these voided configurations are mainly in the fuel medium.

Then a deterministic bias between ERANOS and TRIPOLI-4® can be estimated with this work for JEFF-3.2 divided by type of voided medium considering that PRE-RACINE I gives information for the voided fertile medium, PRE-RACINE 2A&B and CIRANO 2A&B for the voided fuel configurations and the BFS results for the study of the sodium plenum:

Table IV.3.29: Deterministic bias with JEFF-3.2

Voided configuration	CC	LC
Fertile	-5.4% ±2.8%	3.1% ±6.7%
Fuel	6.0% ±2.8%	3.7%±2.4%
Plenum	-25.6%±1.7%	-29.6%±0.5%

These assumptions are less likely to be done with JEFF-3.1.1 due to the antagonistic conclusions in the results of PRE-RACINE 2A&2B and CIRANO 2A&2B for the voided fuel configurations. Furthermore the important deterministic and modelling bias on the sodium plenum built with sodium discs should be carefully considered as a particular situation indeed as we will see in Chapter V this bias is significantly reduced for the ASTRID CFV core.

IV.3.3.4 Indirect comparison between the experiments and TRIPOLI-4® results

Once these two comparisons have been done (Experience/ERANOS and TRIPOLI-4®/ERANOS) an indirect adjustment between TRIPOLI-4® and the experimental results can be made by dividing the set of values (α, β) of the Experience/ERANOS adjustment by the ones of the TRIPOLI-4®/ERANOS adjustment. This leads to get a virtual CC and LC for TRIPOLI-4®, we can then compare these values to the experimental results.

Table IV.3.30: experimental results / TRIPOLI-4® comparison with JEFF-3.1.1

Cores	α	dα	β	dβ
PRE-RACINE I	1.033	0.041	1.101	0.084
PRE-RACINE 2A	0.980	0.046	1.001	0.035
PRE-RACINE 2B	0.974	0.045	1.003	0.038
CIRANO 2A	0.951	0.052	1.054	0.054
CIRANO 2B	1.000	0.020	1.021	0.018
BFS-115-1	1.011	0.064	0.901	0.017

This comparison erases the overestimated values of ERANOS for the CC and LC of the BFS-115-1 experiments. Then TRIPOLI-4® seems to well calculate the CC with JEFF-3.1.1 nuclear data (~1.1% of error) but the LC mainly due to the voided plenum is overestimated by almost 10%.

Table IV.3.31: experimental results / TRIPOLI-4® comparison with JEFF-3.2

Cores	α	dα	β	dβ
PRE-RACINE I	1.019	0.038	1.153	0.080
PRE-RACINE 2A	0.860	0.045	0.978	0.036
PRE-RACINE 2B	0.799	0.057	0.919	0.054
CIRANO 2A	0.889	0.049	1.007	0.056
CIRANO 2B	0.938	0.026	1.023	0.026
BFS-115-1	0.962	0.059	0.940	0.018

The use of JEFF-3.2 nuclear data reduces the discrepancy on the LC for the BFS-115-1 experiments but the CC is then overestimated by 3.8% due to errors in the nuclear data of fuel isotopes (mainly ^{239}Pu).

IV.4 Conclusion

This Chapter has presented in details the SVRE and its physical components: the CC and the LC due to different phenomena: a spectrum effect by the missing scattering reaction on the sodium nuclei, the increase of the number of fissions due to the increase of neutron importance with energy, etc. The CEA has proposed an innovative design (called CFV) in order to increase the intrinsic safety features of the generation IVth nuclear reactors. This design has a negative SVRE thanks to its innovative geometry which maximises the LC and to its sodium void fraction which reduces as much as possible the CC. The addition of a sodium plenum, an outer core higher than the inner core, neutronic absorber on the sodium plenum increases the LC and the addition of an inner fertile slab also increases the LC and at the same times reduces the CC in the inner core.

In the second section the experimental methods used in the MASURCA facility to measure the reactivity have been detailed, especially the inversion of the point kinetics equations and the rod drop calibration. The uncertainties on the SVRE measurements come from: the temperature stabilisation, uncertainties on the kinetic parameters ($\Lambda_{eff}, \beta_{eff}, a_i$) used to invert the point kinetics equations (uncertainties on β_{eff} due to nuclear data have been estimated in the Chapter III) and by systematic errors due to fission chambers and to the mechanism to get the position of the control rod. The overall uncertainties are given in this section for each core and voided configuration of the experimental data base. Some gaps in the experimental data base for the experimental validation of the CFV design have been found then it justifies the need of a new experimental programme (called GENESIS).

The last section details the comparisons between the experimental results and the simulation made with the Monte-Carlo code TRIPOLI-4® using refined geometry of each core and the JEFF-3.1.1 and JEFf-3.2 nuclear data. These comparisons lead to some conclusions concerning the quality of the nuclear data because:

- Voided configurations in fertile areas are well calculated with JEFF-3.1.1 and JEFF-3.2
- Voided configurations in fuel media are not well calculated with JEFF-3.2 and when the LC is important JEFF-3.1.1 is also inconsistent.
- The voided plenum configuration in BFS-115-1 is better calculated with JEFF-3.2 than with JEFF-3.1.1.

Thus the main sources of errors are:

- In the JEFF-3.2 set of evaluations, nuclear data of ^{235}U and Plutonium are responsible of the SVRE discrepancies in the PRE-RACINE and CIRANO cores,
- The sodium nuclear data in JEFF-3.1.1 is the main responsible of the important discrepancies in the BFS results. It is confirmed by the fact that when the CC is very important in some large voided configurations of the MASURCA cores the results are inconsistent when using the JEFF-3.1.1 evaluation set because the sodium nuclear data (with elastic and inelastic scattering) is the main responsible of the CC.

References

[1] 'http://www.oecd-nea.org/janisweb/'. NEA JANIS database.
[2] R. Capote, A. Trkov, M. Sin, M. W. Herman, and E. S. Soukhovitskiĭ, 'Elastic and inelastic scattering of neutrons on ^{238}U nucleus', *EPJ Web Conf.*, vol. 69, p. 00008, 2014.
[3] P. Leconte and D. Bernard, 'Validation of the U-238 inelastic scattering neutron cross section through the EXCALIBUR dedicated experiment', *EPJ Web Conf.*, vol. 146, p. 06017, 2017.
[4] P. Sciora, D. Blanchet, L. Buiron, B. Fontaine, M. Vanier, and F. Varaine, 'ANALYSE PHYSIQUE DU CONCEPT CFV(SPRC/LEDC/10-406)'. CEA Cadarache, 22-Jul-2010.
[5] B. Richard,'Mesures de perturbations sur le réacteur CALIBAN – Interprétation en terme de qualification de données nucléaires', PhD thesis, University of Paris-Sud(2013) p. 292.
[6] J. Tommasi, 'Expériences de simulation de vidange sodium dans le programme CIRANO de MASURCA: étude critique des valeurs expérimentales et des méthodes de calcul et d'interprétation'. communications personnelles, 2007.
[7] G. Jeanmaire, 'Programme PRE-RACINE II - Etude de vidange sodium dans le coeur de référence.' communications personnelles, 1978.
[8] G. Rimpault, 'Etude de l'effet en réactivité de vidange de sodium dans les expériences critiques à neutrons rapides - Transposition aux réacteurs de puissance', Aix-Marseille, 1979.
[9] V. Dulin, I. Matveenko, E. Rozhikhin, M. Semenov, and A. Tsibulya, 'An Overview of the Experiments Performed at the BFS Facilities and Evaluated for the International Reactor Physics Experiment Evaluation Project', *Nucl. Sci. Eng.*, vol. 178, pp. 377–386, 2014.
[10] G. Rimpault, P. Dufay, J. Tommasi, and F. Mellier, 'Looking forward for a MASURCA experimental programme GENESIS in support to the ASTRID SFR core', presented at the PHYSOR, Cancun, Mexico, 2018.

This page has been left blank intentionally

Chapter V: The Sodium Void Reactivity Effect: nuclear data uncertainties analysis

Abstract

The Sodium Void Reactivity Effect (SVRE) is the difference in reactivity between two configurations of the core, the first one being the nominal configuration of the core and the second one being incidental where the sodium is removed from the core. This reactivity effect is split into two components: the central component (CC) and the leakage component (LC). These components have been presented in the Chapter IV with their physical explanations. Their calculations require the use of the S_n transport theory as it has been shown in the Cyrille Bouret PhD thesis (reference [21] of chapter III).

Now, one of the main concerns in the reactor core design is coming from the nuclear data uncertainties as it represents up to ~959 pcm for the reactivity of the ASTRID CFV core[1] [1]. The SVRE uncertainty due to nuclear data is also of some concerns as it affects the safety of the plant. The uncertainty on the SVRE might be large in relative terms since SVRE is a balance between two antagonistic components: the CC and the LC. The SVRE uncertainty calculation has hence required new developments in ERANOS in addition to the existing equivalent generalised perturbation theory (EGPT) used for the SVRE. This new development concerns the implementation of the generalised perturbation theory (GPT) for the CC in ERANOS. Its validation has been performed on a reflected cell without LC. It was hence possible to get the sensitivities for the CC and LC independently and this was used in the following sections.

In the second section, sensitivities of the CC and the LC of the SVRE of the cores of the experimental database were calculated as well as those of the CC and the LC of the SVRE of the ASTRID CFV core. With these sensitivities and covariances associated to nuclear data, it is hence possible to calculate the representativeness of the SVRE experiments with ASTRID, component per component.

The transferability to the ASTRID SVRE is based on the biases and the representativeness results for each component of the SVRE of the different experimental programmes. This is described in the third section and allows adjusting the CC and the LC of the ASTRID core in order to get discrepancies with experiments on each of the components and their associated experimental uncertainties. These discrepancies are compared to the SVRE uncertainties due to nuclear data of the CFV core of ASTRID which are of 2.4% on the CC, 4.0% on the LC and 16.4% on the SVRE (~100 pcm). It appears these nuclear data uncertainties are underestimated. All these values enable to make recommendations for calculated biases and uncertainties for the SVRE.

[1] Using JEFF-3.2 nuclear data and the covariance matrix COMAC-V2

Contents

V.1 Development of GPT associated to each component

V.1.1 The GPT method implemented in ERANOS for the CC

V.1.1.1 The Legendre polynomial basis

As seen in the Chapter IV, the SVRE in transport S_n theory can be split into several physical components with the positive contribution being the Central Component (CC): the capture, the fission, the production, the spectrum variations and the scattering removal.

Table V.1.1: Physical components of the CC expressions

Capture	$C_c^g = -\delta\Sigma_c^g . \int_V \Phi_g^+ . \Phi_g dV$
Fission	$C_f^g = -\delta\Sigma_f^g . \int_V \Phi_g^+ . \Phi_g dV$
Production	$C_\nu^g = \delta(\nu\Sigma_f^g) . \int_V \Phi_g \sum_{g'} \chi_g \Phi_{g'}^+ dV$
Fission spectrum	$C_{spec}^g = \delta\chi^g \int_V \Phi_g^+ . \sum_{g'} \nu\Sigma_f^{g'} \Phi_{g'} dV$
Scattering	$C_{scatt}^g = \sum_{g'} \delta\Sigma_{scatt}^{g\to g'} \left(\int_V \Phi_{g'}^+ . \Phi_g dV - \int_V \Phi_g^+ . \Phi_g dV \right)$

The LC is then expressed as the transport physical component with the following expression:

Transport

$$C_{trans}^g = \begin{cases} \delta\Sigma_t^g . \left(\int_V \Phi_g^+ . \Phi_g dV - \int_V \sum_{i=1}^{N_\Omega} w(\overrightarrow{\Omega_i}) \Phi_g^+ (\overrightarrow{-\Omega_i}) . \Phi_g(\overrightarrow{\Omega_i}) \, dV \right) \\ + \delta(D_g B_g^2) \int_V \sum_{i=1}^{N_\Omega} w(\overrightarrow{\Omega_i}) \Phi_g^+ (\overrightarrow{-\Omega_i}) . \Phi_g(\overrightarrow{\Omega_i}) \, dV \\ + \sum_{l=1}^{L} \sum_{g'} \delta\Sigma_{scatt,l}^{g\to g'} \left(\int_V \Phi_{g',l}^+ . \Phi_{g,l} dV - \int_V \Phi_{g,l}^+ . \Phi_{g,l} dV \right) \end{cases} \quad \textbf{1.1}$$

with:

- $w(\overrightarrow{\Omega_l})$ the weight associated to the S_n direction $\overrightarrow{\Omega_l}$ and the angular forward flux (or adjoint) associated to this direction: $\Phi_g^{(+)}(\overrightarrow{\Omega_i})$
- D_g the diffusion coefficient in the group g.
- B_g^2 the buckling in the group g

The scattering term and its macroscopic cross-section are developed on the orthogonal Legendre polynomial basis $P_l(\overrightarrow{\Omega_l})$ with:

$$\Sigma_{scatt}(\overrightarrow{\Omega_i} \to \overrightarrow{\Omega_j}) = \frac{1}{4\pi}\sum_{l=0}^{\infty}(2l+1)\Sigma_l\, P_l(\overrightarrow{\Omega_i} \to \overrightarrow{\Omega_j}) \qquad \textbf{1.2}$$

Where Σ_l is the product of the angular scattering cross section and the Legendre polynomial P_l integrated over the angle of deviation.

The neutron flux is developed on the orthonormal basis of the spherical harmonics:

$$\Phi(\overrightarrow{\Omega_i}) = \sum_{l=0}^{\infty}\Phi_l(\overrightarrow{\Omega_i}) \qquad \textbf{1.3}$$

In S_n transport theory, we can take into account the anisotropy of the scattering reaction with Legendre P1 terms. Indeed for l=0 the scattering term represents the removal of neutrons from an energy to another while the higher order of the scattering term represents the anisotropy of the reaction and are part of the leakage component when described in transport theory.

V.1.1.2 The GPT method applied to the CC

As seen in Chapter II the sensitivity to nuclear data of a reactivity variation $\Delta\rho = \rho_2 - \rho_1$, is calculated using the Equivalent Generalised Perturbation Theory (EGPT) but we also have seen that if the two states are closed to each other, the sensitivities values can skyrocket. Another option is to use the Generalised Perturbation Theory with the exact perturbation expression of the reactivity variation:

$$\Delta\rho = -\frac{\langle\Phi_1^+, \left(\Delta\mathbf{A} - \frac{\Delta\mathbf{F}}{k_2}\right)\Phi_2\rangle}{\langle\Phi_1^+, \mathbf{F_1}\Phi_2\rangle} \qquad \textbf{1.4}$$

Using two Lagrange multipliers (see Chapter II section 2.2.2) the expression of the derivation of this reactivity variation is then:

$$\Delta\rho = -\frac{\langle\Phi_1^+, \left(\Delta\mathbf{A} - \frac{\Delta\mathbf{F}}{k_2}\right)\Phi_2\rangle}{\langle\Phi_1^+, \mathbf{F_1}\Phi_2\rangle} - \langle\Phi_1^+, \left(\mathbf{A_1} - \frac{\mathbf{F_1}}{k_1}\right)\Psi_1\rangle - \langle\Psi_2^+, \left(\mathbf{A_2} - \frac{\mathbf{F_2}}{k_2}\right)\Phi_2\rangle \qquad \textbf{1.5}$$

$$d(\Delta\rho) = \begin{cases} -\dfrac{\langle d\Phi_1^+, \left(\Delta\mathbf{A} - \frac{\Delta\mathbf{F}}{k_2}\right)\Phi_2\rangle + \langle\Phi_1^+, \left(d\Delta\mathbf{A} - \frac{d\Delta\mathbf{F}}{k_2}\right)\Phi_2\rangle + \langle\Phi_1^+, \left(\Delta\mathbf{A} - \frac{\Delta\mathbf{F}}{k_2}\right)d\Phi_2\rangle}{\langle\Phi_1^+, \mathbf{F_1}\Phi_2\rangle} \\ -\dfrac{dk_2}{k_2^2}\dfrac{\langle\Phi_1^+, \Delta\mathbf{F}\Phi_2\rangle}{\langle\Phi_1^+, \mathbf{F_1}\Phi_2\rangle} - \Delta\rho\left[\dfrac{\langle d\Phi_1^+, \mathbf{F_1}\Phi_2\rangle}{\langle\Phi_1^+, \mathbf{F_1}\Phi_2\rangle} + \dfrac{\langle\Phi_1^+, d\mathbf{F_1}\Phi_2\rangle}{\langle\Phi_1^+, \mathbf{F_1}\Phi_2\rangle} + \dfrac{\langle\Phi_1^+, \mathbf{F_1}d\Phi_2\rangle}{\langle\Phi_1^+, \mathbf{F_1}\Phi_2\rangle}\right] \\ -\langle d\Phi_1^+, \left(\mathbf{A_1} - \frac{\mathbf{F_1}}{k_1}\right)\Psi_1\rangle - \langle\Psi_2^+, \left(\mathbf{A_2} - \frac{\mathbf{F_2}}{k_2}\right)d\Phi_2\rangle \\ -\langle\Phi_1^+, \left(d\mathbf{A_1} - \frac{d\mathbf{F_1}}{k_1}\right)\Psi_1\rangle - \langle\Psi_2^+, \left(d\mathbf{A_2} - \frac{d\mathbf{F_2}}{k_2}\right)\Phi_2\rangle \end{cases} \qquad \textbf{1.6}$$

The $d\Psi_1$ and $d\Psi_2^+$ terms are not written in **1.6** because the homogeneous equations of the states 1 and 2 are equal to 0. Then by grouping the $d\Phi_1^+$ and $d\Phi_2$ terms, it shows that the generalised importances are the solution of the following equations:

$$\left(\mathbf{A_1}-\frac{\mathbf{F_1}}{k_1}\right)\Psi_1=\underbrace{-\frac{\left(\Delta\mathbf{A}-\frac{\Delta\mathbf{F}}{k_2}\right)\Phi_2+\Delta\rho\mathbf{F_1}\Phi_2}{\langle\Phi_1^+,\mathbf{F_1}\Phi_2\rangle}}_{S_1} \quad \textbf{1.7}$$

$$\left(\mathbf{A_2^+}-\frac{\mathbf{F_2^+}}{k_2}\right)\Psi_2^+=\underbrace{-\frac{\left(\Delta\mathbf{A}^+-\frac{\Delta\mathbf{F}^+}{k_2}\right)\Phi_1^+ +\Delta\rho\mathbf{F_1^+}\Phi_1^+}{\langle\Phi_1^+,\mathbf{F_1}\Phi_2\rangle}}_{S_2} \quad \textbf{1.8}$$

With $\langle\Psi_1^+,\mathbf{F_1^+}\Phi_1^+\rangle=0$ and $\langle\Psi_2^+,\mathbf{F_2}\Phi_2\rangle=0$.

This method has been never used in practice to get the sensitivities of the SVRE because implementing the sources to calculate the generalised importances, is difficult to calculate while the EGPT is much easier to implement.

In the case of the central component, the procedure is the same as presented here but the operator $\Delta\mathbf{A}$ becomes an operator $\Delta\mathbf{A}^{CC}$ without the leakage component i.e. without the scattering terms of higher order than 0 and only the scalar flux are considered (meaning the angular flux of order 0). During this work, some functions have been implemented to get the sources of the inhomogeneous equations of the generalised importances (**1.7** and **1.8**) and others to get the direct and indirect term once we have calculated the generalised importances.

$$\text{Direct term}=-\frac{\langle\Phi_1^+,\left(d\Delta\mathbf{A}^{CC}-\frac{d\Delta\mathbf{F}}{k_2}\right)\Phi_2\rangle}{\langle\Phi_1^+,\mathbf{F_1}\Phi_2\rangle}-\Delta\rho\frac{\langle\Phi_1^+,d\mathbf{F_1}\Phi_2\rangle}{\langle\Phi_1^+,\mathbf{F_1}\Phi_2\rangle}-\frac{dk_2}{k_2^2}\frac{\langle\Phi_1^+,\Delta\mathbf{F}\Phi_2\rangle}{\langle\Phi_1^+,\mathbf{F_1}\Phi_2\rangle} \quad \textbf{1.9}$$

$$\text{Indirect term}=-\langle\Phi_1^+,\left(d\mathbf{A_1}-\frac{d\mathbf{F_1}}{k_1}\right)\Psi_1\rangle-\langle\Psi_2^+,\left(d\mathbf{A_2}-\frac{d\mathbf{F_2}}{k_2}\right)\Phi_2\rangle \quad \textbf{1.10}$$

Then the sensitivity of the CC to the nuclear data σ is expressed as follows:

$$S_{CC}=\frac{\sigma}{CC}\left(\underbrace{\frac{\partial CC}{\partial\sigma}}_{\text{Direct term}}\underbrace{-\langle\Phi_1^+,\left(d\mathbf{A_1}-\frac{d\mathbf{F_1}}{k_1}\right)\Psi_1\rangle-\langle\Psi_2^+,\left(d\mathbf{A_2}-\frac{d\mathbf{F_2}}{k_2}\right)\Phi_2\rangle}_{\text{Indirect term}}\right) \quad \textbf{1.11}$$

This work has been presented with a direct derivation of the CC (but without the details of the direct term) and the same calculation of the indirect term at the PHYSOR 2018 conference [2] and at BEPU 2018 conference [3].

V.1.1.3 The sensitivities of the LC to nuclear data

Once we get the sensitivity of the CC (S_{CC}) and of the SVRE ($S_{\Delta\rho_{Na}}$: using the EGPT procedure) to nuclear data we can calculate the sensitivity of the LC to nuclear data as follows (S_{LC}):

$$S_{\Delta\rho_{Na}}\Delta\rho_{Na}=S_{CC}CC+S_{LC}LC \quad \textbf{1.12}$$

$$S_{LC}=S_{\Delta\rho_{Na}}\frac{\Delta\rho_{Na}}{LC}-S_{CC}\frac{CC}{LC} \quad \textbf{1.13}$$

V.1.1.4 Nuclear data uncertainties

Once sensitivities S are calculated we use the Sandwich formula to get the uncertainty due to nuclear data I [4]:

$$I^2 = S^t . B . S \qquad \textbf{1.14}$$

Where: B is a matrix which is based on the covariance matrix (such as COMAC developed at CEA [5]). The covariance matrix depends on the nuclear data library used: COMAC-V1 for JEFF-3.1.1 [5] and COMAC-V2 for JEFF-3.2. This covariance matrix takes into account the covariance between all neutronic parameters for each isotope.

We can also calculate the representativeness between two sensitivity sets with:

$$R_{1,2} = \frac{{}^tS_1 . B . S_2}{\sqrt{{}^tS_1 . B . S_1 . {}^tS_2 . B . S_2}} \qquad 1.15$$

Then we are able to compare the sensitivity of the CC and of the LC of one core which gives us the correlation between the CC and the LC but it also possible to get the representativeness between the sensitivity set of the CC of one core with the sensitivity set of the CC of another core. Indeed this parameter $R_{1,2}$ varies between -1 to +1 and the closer to $|1|$ the more representative (or correlated) it is.

V.1.2 The case of a reflected cell

These procedures have been validated for the direct term on the case of a reflected cell of fuel. Indeed in this example there is no LC (i.e. no higher order than 0 for the angular flux) when the sodium is removed from the fuel cell and then the direct term of the sensitivity set calculated by our procedure for the CC has to be equal to the sensitivity set calculated by the EGPT for the SVRE. Indeed the reactivity variation expression uses the same forward flux Φ_2 for the variation operator $\left(\Delta\mathbf{A} - \frac{\Delta\mathbf{F}}{k_2}\right)$ and it is normalised by the fission integral: $\langle \Phi_1^+, \mathbf{F_1}\Phi_2 \rangle$. Then the EGPT method has to use the forward flux Φ_2 for the first k_{eff} sensitivity (state 1) and the second k_{eff} sensitivity (state 2) has to be normalised by $\langle \Phi_1^+, \mathbf{F_1}\Phi_2 \rangle$.

$$d(\Delta\rho) = d\rho_2 - d\rho_1 = -\frac{\langle \Phi_1^+, \left(d\mathbf{A_2} - \frac{d\mathbf{F_2}}{k_2}\right)\Phi_2 \rangle}{\langle \Phi_1^+, \mathbf{F_1}\Phi_2 \rangle} + \frac{\langle \Phi_1^+, \left(d\mathbf{A_1} - \frac{d\mathbf{F_1}}{k_2}\right)\Phi_2 \rangle}{\langle \Phi_1^+, \mathbf{F_1}\Phi_2 \rangle} \qquad \textbf{1.16}$$

There are some differences between the two different results as shown in the **Table V.1.2**. There is no difference more important than 0.5%, with the exception of the sensitivity to the n,xn reaction. Since, this last one contributes to less than 0.1% to the total sensitivity, it can be considered as negligible and hence the method is validated.

Furthermore the sources S_1 (**1.7**) and S_2 (**1.8**) are built with the same function used to calculate the direct term then we can assume that the indirect term of the sensitivity is also validated if the condition of convergences of the generalised importances is respected. Another verification that the sources are well built is to calculate the integrals: $\langle \Phi_1^+, S_1 \rangle$ and $\langle S_2, \Phi_2 \rangle$. Indeed the results have to be null:

$$\langle \Phi_1^+, S_1 \rangle = \langle \Phi_1^+, \left(\mathbf{A_1} - \frac{\mathbf{F_1}}{k_1}\right)\Psi_1 \rangle = \underbrace{\langle \left(\mathbf{A_1^+} - \frac{\mathbf{F_1^+}}{k_1}\right)\Phi_1^+ , \Psi_1 \rangle}_{=0} = 0 \qquad \textbf{1.17}$$

$$\langle S_2, \Phi_2 \rangle = \langle \left(\mathbf{A_2^+} - \frac{\mathbf{F_2^+}}{k_2} \right) \Psi_2^+, \Phi_2 \rangle = \langle \Psi_2^+, \underbrace{\left(\mathbf{A_2} - \frac{\mathbf{F_2}}{k_2} \right) \Phi_2}_{=0} \rangle = 0 \qquad \textbf{1.18}$$

Table V.1.2: Discrepancies between the direct term and the EGPT sensitivities

Isotope	Fission	Capture	Elastic	Inelastic	n,xn	ν	Fission spectrum	Sum
B10	0.00%	0.00%	0.00%	0.00%	0.00%	0.00%	0.00%	0.00%
N14	0.00%	0.00%	0.00%	0.00%	0.00%	0.00%	0.00%	0.00%
O16	0.00%	0.00%	0.00%	0.00%	0.00%	0.00%	0.00%	0.00%
Na23	0.00%	0.02%	-0.02%	0.03%	0.52%	0.00%	0.00%	0.00%
Cr50	0.00%	0.00%	0.00%	0.00%	19.49%	0.00%	0.00%	0.08%
Cr52	0.00%	0.00%	0.00%	0.00%	-0.29%	0.00%	0.00%	0.00%
Cr53	0.00%	0.00%	0.00%	0.00%	66.20%	0.00%	0.00%	0.28%
Cr54	0.00%	0.00%	0.00%	0.00%	10.19%	0.00%	0.00%	0.04%
Fe54	0.00%	-0.01%	0.00%	0.00%	0.00%	0.00%	0.00%	0.00%
Fe56	0.00%	-0.02%	0.01%	-0.01%	-2.37%	0.00%	0.00%	-0.01%
Fe57	0.00%	0.00%	0.00%	0.00%	-1.05%	0.00%	0.00%	0.00%
Fe58	0.00%	0.00%	0.00%	0.00%	-0.03%	0.00%	0.00%	0.00%
U234	0.00%	0.00%	0.00%	0.00%	0.00%	0.00%	0.00%	0.00%
U235	0.00%	0.00%	0.00%	0.00%	0.04%	0.00%	-0.01%	0.00%
U236	0.00%	0.00%	0.00%	0.00%	0.00%	0.00%	0.00%	0.00%
U238	0.43%	0.01%	0.00%	0.00%	5.09%	0.27%	0.06%	0.04%
Np237	0.00%	0.00%	0.00%	0.00%	0.00%	0.00%	0.00%	0.00%
Pu238	0.00%	0.00%	0.00%	0.00%	0.00%	0.00%	0.00%	0.00%
Pu239	0.18%	0.00%	0.00%	0.00%	0.55%	0.13%	-0.07%	-0.01%
Pu240	0.02%	0.00%	0.00%	0.00%	0.04%	0.02%	0.02%	0.00%
Pu241	0.00%	0.00%	0.00%	0.00%	0.00%	0.00%	0.00%	0.00%
Pu242	-0.02%	0.00%	0.00%	0.00%	0.00%	-0.01%	0.00%	0.00%
Am241	0.00%	0.00%	0.00%	0.00%	0.00%	0.00%	0.00%	0.00%
Am243	0.00%	0.00%	0.00%	0.00%	0.00%	0.00%	0.00%	0.00%
Part >0	0.18%	0.04%	-0.02%	0.03%	0.78%	0.13%	0.08%	0.02%
Part <0	0.43%	-0.03%	0.01%	-0.01%	97.61%	0.27%	-0.08%	0.41%
Sum	0.61%	0.01%	-0.01%	0.02%	98.39%	0.40%	0.00%	0.42%

V.2 Sensitivity, uncertainty and representativeness analysis

In this section, are presented the results of the application of the procedure presented in the previous section to each experimental configuration to each core. The calculations have been done using the transport theory and a S_8 discretisation for the angle variable.

V.2.1 Results for the experimental data base

V.2.1.1 PRE-RACINE 1

The analysis of the PRE-RACINE 1 void experiments is very interesting because all the voided configurations have been done in the inner fertile medium.

V.2.1.1.1 Sensitivity

In the following table is presented the sensitivity of the CC to nuclear data for the V5 R=11.96cm voided configuration with JEFF-3.2 nuclear data.

Table V.2.1: Sensitivity of the CC to nuclear data for the V5 R=11.96cm voided configuration with JEFF-3.2 nuclear data

Isotope	Fission	Capture	Elastic	Inelastic	n,xn	ν	Fission spectrum	Total
O16	0.000	0.010	**0.378**	0.003	0.000	0.000	0.000	0.391
Na23	0.000	0.082	**0.566**	**0.300**	0.000	0.000	0.000	0.948
Cr50	0.000	-0.001	0.005	0.000	0.000	0.000	0.000	0.004
Cr53	0.000	-0.003	0.006	0.000	0.001	0.000	0.000	0.004
Fe54	0.000	-0.001	0.002	0.002	0.000	0.000	0.000	0.004
Fe56	0.000	-0.051	-0.027	0.042	0.000	0.000	0.000	-0.037
Fe57	0.000	-0.002	0.003	0.006	0.000	0.000	0.000	0.007
U235	**-0.626**	-0.111	-0.005	0.009	0.000	0.136	0.013	-0.584
U238	**-0.272**	**-0.575**	-0.063	**0.295**	0.005	**-0.335**	-0.137	-1.080
Pu239	**-0.735**	**-0.271**	-0.008	0.011	0.000	**-0.459**	**-0.550**	-2.012
Pu240	-0.023	-0.022	-0.001	0.001	0.000	-0.032	-0.009	-0.086
Pu241	-0.003	-0.001	0.000	0.000	0.000	0.001	-0.004	-0.007
Am241	0.000	-0.001	0.000	0.000	0.000	0.000	0.000	-0.001
SUM	-1.660	-0.956	0.855	0.681	0.008	-0.690	-0.687	-2.449

The main contributors to the sensitivity of the CC to nuclear data are the:

- Sodium and oxygen elastic scattering, they are the main responsibles to the moderation of neutrons in the core,
- ^{235}U and ^{238}U with their capture and fission cross sections,

This is not surprising because these are the isotopes of the voided fertile medium but the first contributor is the ^{239}Pu so the influence of spectrum changes due to the sodium void experiment in the inner fertile area on the fuel is strong.

The analysis of the influence of the voided configuration on the sensitivity set is interesting. In order to perform this analysis, we compare a voided configuration with almost no LC (for instance the V3 R=11.96cm configuration with 8% of LC) to a reference one (here the V5 R=11.96 cm with 23% of LC) and also to a configuration with an important LC (for instance the V7 R=11.96cm with 61% of LC) [see Chapter IV section 3.2 for the proportion].

The differences between the V3 and V5 R=11.96 configurations on the sensitivity of the CC to nuclear data are presented in the following table.

Table V.2.2: Differences between the V3 and V5 R=11.96 configurations on the sensitivity of the CC to nuclear data

Isotope	Fission	Capture	Elastic	Inelastic	n,xn	ν	Fission spectrum	Total
O16	0.0%	0.0%	**-4.6%**	0.0%	0.0%	0.0%	0.0%	-1.6%
Na23	0.0%	0.0%	**-2.5%**	-0.2%	0.1%	0.0%	0.0%	-0.9%
Cr50	0.0%	0.0%	0.0%	0.0%	0.0%	0.0%	0.0%	0.0%
Cr53	0.0%	0.0%	0.0%	0.0%	0.1%	0.0%	0.0%	0.0%
Fe54	0.0%	0.0%	-0.1%	0.0%	0.0%	0.0%	0.0%	0.0%
Fe56	0.0%	0.2%	1.0%	-0.3%	0.0%	0.0%	0.0%	0.5%
Fe57	0.0%	0.0%	-0.1%	-0.1%	0.0%	0.0%	0.0%	0.0%
U235	-0.3%	0.3%	0.2%	-0.2%	-0.3%	1.1%	1.3%	-0.7%
U238	0.3%	**4.4%**	**2.1%**	**-2.3%**	**-4.6%**	0.9%	0.3%	3.6%
Pu239	0.0%	1.3%	0.3%	-0.1%	-0.1%	-0.7%	0.3%	0.5%
Pu240	0.1%	0.1%	0.0%	0.0%	0.0%	0.2%	0.0%	0.2%
Pu241	0.0%	0.0%	0.0%	0.0%	0.0%	0.0%	0.0%	0.0%
Am241	0.0%	0.0%	0.0%	0.0%	0.0%	0.0%	0.0%	0.0%
Total	0.0%	6.3%	-11.2%	-3.2%	-4.8%	-0.7%	-0.7%	6.9%

The influence of the size of the voided area on the first contributor (^{239}Pu) is quite negligible but the influence on the ^{238}U, oxygen and sodium sensitivities are important. Indeed the decrease of the size decreases the sensitivity of the CC to the elastic cross-section of the oxygen and sodium and the same conclusion can be drawn for the inelastic of the ^{238}U while the sensitivities to the capture and elastic cross-section of ^{238}U are increased. As less sodium is removed, the scattering removal is less important so it explains the decrease of sodium and oxygen sensitivities but in the non-voided part of the fertile medium, neutrons are scattered and then can be captured by the resonances of the ^{238}U explaining the increase of sensitivity of its capture cross-section.

The differences between the V7 and V5 R=11.96 configurations on the sensitivity of the CC to nuclear data are presented in the following table.

Table V.2.3: Differences between the V7 and V5 R=11.96 configurations on the sensitivity of the CC to nuclear data

Isotope	Fission	Capture	Elastic	Inelastic	n,xn	ν	Fission spectrum	Total
O16	0.0%	-0.5%	**33.4%**	-0.1%	0.0%	0.0%	0.0%	11.4%
Na23	0.0%	-2.1%	**37.3%**	-10.1%	-1.3%	0.0%	0.0%	9.4%
Cr50	0.0%	0.0%	-0.1%	0.0%	-1.6%	0.0%	0.0%	0.0%
Cr53	0.0%	-0.3%	-0.1%	0.0%	-5.4%	0.0%	0.0%	0.0%
Fe54	0.0%	0.1%	0.4%	0.0%	0.0%	0.0%	0.0%	0.3%
Fe56	0.0%	-3.2%	-1.7%	1.2%	0.0%	0.0%	0.0%	0.2%
Fe57	0.0%	-0.2%	0.3%	0.7%	0.0%	0.0%	0.0%	0.4%
U235	2.3%	-5.1%	-0.2%	-0.2%	0.1%	**-19.1%**	**18.2%**	11.5%
U238	-6.4%	**-56.6%**	8.4%	11.0%	**24.6%**	**-23.7%**	-11.7%	-40.6%
Pu239	-0.7%	**-18.9%**	0.3%	0.0%	0.1%	8.5%	-7.0%	-8.2%
Pu240	-0.9%	-1.4%	0.0%	0.0%	0.0%	-3.1%	-0.2%	-2.2%
Pu241	0.1%	-0.1%	0.0%	0.0%	0.0%	0.3%	0.0%	0.2%
Am241	0.0%	-0.1%	0.0%	0.0%	0.0%	0.0%	0.0%	0.0%
Total	-5.6%	-84.4%	103.3%	2.6%	15.7%	2.7%	3.1%	-71.9%

The variations are much more important than in the previous case, mainly due to the difference in the voided size and by its location. Indeed in that case only the outer part of the assembly are voided in the axial fertile blanket then the CC is mainly due to scattering removal than to capture and fission because the faster neutrons are more likely to leak out of the core than to be captured in the core.

V.2.1.1.2 Nuclear data uncertainties

In the following table, are presented the nuclear data uncertainties calculated with the sandwich formula (with JEFF-3.2 nuclear data and the COMAC-V2 covariance matrix) on each component of the SVRE and for each experimental configuration.

Table V.2.4: Nuclear data uncertainties with JEFF-3.2 and COMAC-V2

Configuration	Uncertainties (in pcm)			Relative uncertainties		
	Δρ	CC	LC	Δρ	CC	LC
Void V1 R=11.96	1.4	1.5	6.3	4.4%	4.4%	626.1%
Void V2 R=11.96	4.2	4.2	2.0	4.6%	4.5%	70.5%
Void V3 R=11.96	6.4	6.6	3.3	4.9%	4.5%	24.7%
Void V5 R=11.96	8.9	9.3	5.8	6.2%	4.5%	9.1%
Void V6 R=11.96	9.5	10.1	7.1	7.4%	4.4%	7.2%
Void V7 R=11.96	1.0	0.7	1.3	8.6%	3.5%	4.0%
Void V8 R=11.96	2.7	2.5	2.4	17.3%	4.1%	5.1%
Void V9 R=11.96	3.6	3.5	4.0	360.6%	4.2%	4.9%
Void V5 R=7.33	1.9	2.1	1.4	4.7%	4.0%	12.3%

The absolute uncertainties on each component of the SVRE depend of the size of the voided area. Furthermore, the relative uncertainty on the SVRE is not constant especially for configurations where the CC and the LC almost compensate each other. However, the relative uncertainty on the CC is almost constant and hence much more predictable. For voided inner fertile configurations, the nuclear

data uncertainty is about 3.5-4.5%. For configurations where the LC is important enough (from the V5 to the V9 R=11.96cm for instance) the nuclear data uncertainty is about 4.0-9.1%.

In details the following table presents the breakdown of the nuclear data uncertainty on the CC of the V5 R=11.96cm configuration

Table V.2.5: Nuclear data uncertainties by isotope and by reaction

Isotope	Fission	Capture	Elastic	Inelastic	n,xn	ν	Fission spectrum	Total
O16	0.00	0.20	0.33	0.02	0.00	0.00	0.00	0.39
Na23	0.00	0.08	0.02	0.08	0.00	0.00	0.00	0.11
Fe56	0.00	**0.56**	0.24	0.10	0.00	0.00	0.00	0.62
U235	0.23	**2.46**	0.17	0.12	0.00	0.22	0.16	2.49
U238	0.14	**1.67**	0.18	**1.57**	0.05	0.08	0.15	2.30
Pu239	**2.44**	**1.41**	0.12	0.13	0.00	0.37	0.39	2.88
Pu240	0.16	0.09	0.01	0.02	0.00	0.01	0.04	0.19
TOTAL	2.46	3.35	0.35	1.58	0.05	0.44	0.45	4.51

The main contributors to this uncertainty are:

- The ^{239}Pu with its capture and fission cross section but also with its neutron emission yield per fission and spectrum.
- The ^{235}U with its capture cross-section is also an important contributor
- The ^{238}U with the capture and inelastic cross-sections.

V.2.1.1.3 Representativeness

Once the sensitivities of the CC, LC and SVRE have been calculated for each experimental configuration, we can get the representativeness (see **1.15**) between the CC (or the LC or the SVRE) of the experiment to the CC (or to the LC or to the SVRE) of the ASTRID CFV core for different voided configurations:

- A total sodium void configuration where the fuel (C1 and C2), the inner fertile area (FCAM), the sodium expansion vase (SVES) and the Sodium Plenum areas are voided.
- A fuel void configuration when only the C1 and C2 areas are voided.

A void plenum configuration when only the Sodium plenum and the SVES areas are voided.

Table V.2.6: Representativeness between PRE-RACINE 1 and ASTRID CFV

Configuration	Total void			Sodium plenum voided			Fuel voided		
	Δρ	CC	LC	Δρ	CC	LC	Δρ	CC	LC
Void V3 R=11.96	-0.806	0.745	0.704	-0.476	0.678	0.351	0.836	0.721	0.727
Void V5 R=11.96	-0.841	0.742	0.617	-0.495	0.679	0.302	0.870	0.716	0.637
Void V6 R=11.96	-0.853	0.733	0.577	-0.503	0.676	0.280	0.880	0.704	0.592
Void V7 R=11.96	0.604	0.557	0.398	0.357	0.593	0.184	-0.592	0.506	0.393
Void V9 R=11.96	-0.802	0.677	0.437	-0.469	0.649	0.205	0.817	0.642	0.446

The best results for the representativeness of the SVRE are obtained with the comparison to the CFV fuel voided configuration. Concerning the representativeness between the CC we see that the larger the voided area is, the less representative the CC is and it is the same for the LC. The explanation is that in small voided configurations (V3 R=11.96cm for instance), the CC is more sensitive to fertile and fuel

isotopes and the LC is also strongly related to these isotopes. Furthermore, the representativeness with the sodium plenum void configuration are very low because in that case the CC and LC are more sensitive to sodium than fuel or fertile isotopes.

For PRE-RACINE 1 we also have compared the sensitivity of the experimental components with another CFV voided configuration:

A fertile void configuration where only the FCAM area is voided.

Table V.2.7: Representativeness between PRE-RACINE 1 and fertile void of ASTRID CFV

Configuration	Fertile voided		
	Δρ	CC	LC
Void V3 R=11.96	0.808	0.731	0.717
Void V5 R=11.96	0.850	0.736	0.620
Void V6 R=11.96	0.868	0.735	0.581
Void V7 R=11.96	-0.659	0.669	0.406
Void V9 R=11.96	0.839	0.712	0.434

The representativeness of the CC is better with this configuration than with the CFV fuel voided configuration as expected but the results are similar to the CFV total void configuration for the CC.

V.2.1.2 PRE-RACINE 2A&2B

The analysis of the results on the PRE-RACINE 2A and PRE-RACINE 2B core is done in this section in order to analyse the impact on the sensitivity of the CC (or LC or SVRE) to nuclear data of different fuels. The Pu-vector is more deteriorated in the case of PRE-RACINE 2B which uses a PIT fuel (with 18% of ^{240}Pu/Pu) than the one of PRE-RACINE 2A which uses a POA fuel (with only 8% of ^{240}Pu/Pu). In these two cores, voided V1 to V5 configurations only concern fuel media.

V.2.1.2.1 Sensitivity

In the following table is presented the sensitivity of the CC of the V5 R=11.96cm voided configuration to nuclear data for the PRE-RACINE 2A core.

Table V.2.8: Sensitivity of the CC of the V5 R=11.96cm voided configuration to nuclear data

Isotope	Fission	Capture	Elastic	Inelastic	n,xn	ν	Fission spectrum	Total
O16	0.000	0.027	**0.281**	0.004	0.000	0.000	0.000	0.313
Na23	0.000	0.125	**0.279**	**0.565**	0.000	0.000	0.000	0.968
Cr50	0.000	-0.002	0.006	0.000	0.001	0.000	0.000	0.005
Cr52	0.000	-0.012	-0.025	0.014	0.000	0.000	0.000	-0.024
Cr53	0.000	-0.006	0.011	0.000	0.003	0.000	0.000	0.009
Fe54	0.000	-0.002	0.003	0.003	0.000	0.000	0.000	0.004
Fe56	0.000	-0.074	-0.017	0.045	0.000	0.000	0.000	-0.046
Fe57	0.000	-0.004	0.003	0.006	0.000	0.000	0.000	0.006
U235	**-0.417**	-0.102	-0.004	0.004	0.000	0.117	0.027	-0.376
U238	**-0.561**	**-1.108**	-0.031	**0.257**	0.000	**-0.842**	**0.357**	-1.929
Pu238	-0.001	-0.001	0.000	0.000	0.000	0.000	0.000	-0.002
Pu239	**-0.886**	**-0.729**	0.004	0.027	0.000	-0.263	**-1.409**	-3.257
Pu240	-0.095	-0.063	0.000	0.003	0.000	-0.133	0.050	-0.238
Pu241	-0.014	-0.005	0.000	0.000	0.000	0.013	-0.028	-0.033
Pu242	-0.001	-0.001	0.000	0.000	0.000	-0.001	0.000	-0.003
Am241	-0.002	-0.004	0.000	0.000	0.000	-0.002	0.001	-0.008
SUM	-1.978	-1.963	0.508	0.928	0.005	-1.114	-1.002	-4.616

The main contributor to the sensitivity is ^{239}Pu with its fission and capture cross-sections and neutron emission yield per fission and spectrum that is logical since the voided medium is the POA fuel area. The ^{235}U and ^{238}U isotopes are also in the composition of POA fuel and of the fertile pin of the ZONA1 fuel (see Appendix A) so their contributions are also important. .

The differences with the sensitivity of the CC of the V5 R=11.96cm voided configuration of the PRE-RACINE 2B core are presented in the following table. As the contribution of the ^{240}Pu increases when the ones of the ^{239}Pu decreases, the ones of the ^{235}U and ^{238}U also decreased in order to keep the same level of reactivity. Hence, the PIT U-Pu fuel is a bit more enriched in Pu/(U+Pu) than the POA fuel. The CC of a voided configuration in a PIT fuel area tends to be more sensitive to the elastic scattering cross-section of the sodium as a result of a more important adjoint flux gradient at high energy.

Table V.2.9: Differences between the sensitivity of the CC of the V5 R=11.96cm voided configuration of the PRE-RACINE 2B and PRE-RACINE 2A cores

Isotope	Fission	Capture	Elastic	Inelastic	n,xn	ν	Fission spectrum	Total
O16	0.0%	-0.2%	-2.2%	-0.1%	0.0%	0.0%	0.0%	-0.3%
Na23	0.0%	-0.8%	7.0%	-2.1%	-0.1%	0.0%	0.0%	0.0%
Cr50	0.0%	0.0%	-0.3%	0.0%	-2.2%	0.0%	0.0%	0.0%
Cr52	0.0%	-0.1%	-0.7%	-0.2%	0.0%	0.0%	0.0%	-0.1%
Cr53	0.0%	0.0%	-0.4%	0.0%	-7.3%	0.0%	0.0%	0.0%
Fe54	0.0%	0.0%	-0.1%	0.0%	0.0%	0.0%	0.0%	0.0%
Fe56	0.0%	-0.4%	-1.1%	-0.4%	-0.1%	0.0%	0.0%	-0.2%
Fe57	0.0%	0.0%	-0.1%	-0.1%	0.0%	0.0%	0.0%	0.0%
U235	-2.5%	0.2%	-0.2%	0.0%	0.8%	7.4%	8.9%	-4.7%
U238	-4.2%	-5.8%	-2.2%	-0.9%	13.8%	-11.8%	-3.8%	-6.3%
Pu238	0.1%	0.1%	0.0%	0.0%	0.0%	0.1%	0.0%	0.1%
Pu239	-4.0%	-7.3%	-0.4%	-0.3%	0.7%	1.6%	-6.2%	-5.7%
Pu240	5.8%	2.9%	0.1%	0.4%	1.6%	14.6%	6.1%	5.8%
Pu241	-0.5%	0.8%	0.0%	0.1%	1.1%	6.6%	11.6%	0.8%
Pu242	0.3%	0.2%	0.0%	0.0%	0.1%	0.7%	0.4%	0.3%
Am241	0.5%	1.0%	0.0%	0.1%	0.2%	1.3%	0.5%	0.9%
SUM	-4.9%	-7.7%	7.8%	-3.4%	5.4%	-7.5%	-6.6%	-8.8%

The same work has been done for the LC. The following table presents the sensitivity of the LC of the V5 R=11.96cm voided configuration to nuclear data of the PRE-RACINE 2A core. The reader has to be careful with the sign of these sensitivities as the LC is negative a **negative sensitivity** will in fact **increase the LC**.

Table V.2.10: Sensitivity of the LC of the V5 R=11.96cm voided configuration to nuclear data

Isotope	Fission	Capture	Elastic	Inelastic	n,xn	ν	Fission spectrum	Total
O16	0.000	0.058	1.057	0.011	0.000	0.000	0.000	1.126
Na23	0.000	0.010	-0.020	0.128	0.000	0.000	0.000	0.118
Cr50	0.000	-0.004	0.014	0.000	0.003	0.000	0.000	0.012
Cr52	0.000	-0.025	0.023	0.054	0.000	0.000	0.000	0.052
Cr53	0.000	-0.010	0.025	0.000	0.009	0.000	0.000	0.024
Fe54	0.000	0.004	0.022	0.012	0.000	0.000	0.000	0.038
Fe56	0.000	-0.142	0.216	0.198	0.000	0.000	0.000	0.272
Fe57	0.000	-0.007	0.012	0.019	0.000	0.000	0.000	0.024
U235	-1.042	-0.077	0.006	0.021	0.000	-0.745	-0.836	-2.673
U238	-1.127	-2.200	0.374	0.815	0.005	-1.803	-0.683	-4.619
Pu238	-0.002	-0.001	0.000	0.000	0.000	-0.002	-0.001	-0.006
Pu239	0.073	-1.734	0.053	0.067	0.000	1.659	0.621	0.739
Pu240	-0.178	-0.148	0.005	0.007	0.000	-0.253	-0.079	-0.645
Pu241	-0.005	-0.010	0.000	0.001	0.000	0.036	-0.016	0.005
Pu242	-0.003	-0.002	0.000	0.000	0.000	-0.004	-0.001	-0.009
Am241	-0.003	-0.009	0.000	0.000	0.000	-0.005	-0.002	-0.019
SUM	-2.288	-4.300	1.788	1.335	0.018	-1.117	-0.998	-5.563

The LC is very sensitive to neutron emission yield per fission and fission spectrum as it leads to the production of fast neutrons. The main contributors are ^{235}U, ^{238}U and ^{239}Pu of the fuel. The capture cross-section is the main source of negative sensitivity as an increase of the capture cross-section will shift the neutron spectrum to higher energy and then increase the LC. The sensitivity of the LC to the elastic scattering is positive or very low as an increase of this cross-section would decrease the LC.

The differences with the sensitivity of the LC of the V5 R=11.96cm voided configuration of the PRE-RACINE 2B core are presented in the following table.

Table V.2.11: Differences between the sensitivity of the CC of the V5 R=11.96cm voided configuration of the PRE-RACINE 2B and PRE-RACINE 2A cores

Isotope	Fission	Capture	Elastic	Inelastic	n,xn	ν	Fission spectrum	Total
O16	0.0%	0.0%	4.1%	0.0%	0.0%	0.0%	0.0%	0.4%
Na23	0.0%	0.0%	-3.0%	1.5%	0.0%	0.0%	0.0%	0.8%
Cr50	0.0%	0.0%	-0.2%	0.0%	0.2%	0.0%	0.0%	0.0%
Cr52	0.0%	0.0%	0.4%	0.1%	0.0%	0.0%	0.0%	0.0%
Cr53	0.0%	0.0%	-0.3%	0.0%	0.5%	0.0%	0.0%	0.0%
Fe54	0.0%	0.0%	-0.2%	0.0%	0.0%	0.0%	0.0%	0.0%
Fe56	0.0%	0.1%	1.1%	0.5%	0.0%	0.0%	0.0%	0.2%
Fe57	0.0%	0.0%	-0.1%	0.0%	0.0%	0.0%	0.0%	0.0%
U235	-7.0%	1.8%	0.0%	0.0%	0.8%	-28.4%	-31.4%	-15.9%
U238	-2.8%	0.4%	0.0%	4.1%	28.0%	-7.8%	-4.6%	-4.7%
Pu238	0.1%	0.2%	0.0%	0.0%	0.0%	0.1%	-0.1%	0.1%
Pu239	-3.6%	-8.4%	-1.0%	0.0%	1.1%	-19.3%	-26.2%	-8.5%
Pu240	12.6%	9.1%	1.4%	1.3%	4.4%	32.0%	11.5%	19.0%
Pu241	7.0%	2.1%	0.3%	0.3%	1.8%	26.8%	7.6%	11.2%
Pu242	0.6%	0.5%	0.1%	0.1%	0.1%	1.5%	0.5%	0.9%
Am241	1.0%	2.9%	0.1%	0.1%	0.5%	2.5%	0.8%	2.4%
SUM	0.6%	8.7%	10.6%	7.9%	35.4%	-7.6%	-7.9%	-2.4%

Here again the contribution of ^{240}Pu is increased when the contribution of ^{235}U, ^{238}U and ^{239}Pu are decreased for the same reasons than for the CC. However the variations are much more important especially for the sensitivity of the LC to the neutron emission yield per fission and spectrum, this is due to the more important gradient of the adjoint flux at high energy.

V.2.1.2.2 Nuclear data uncertainties

The nuclear data uncertainties on each component and for each voided configuration of the PRE-RACINE 2A core are presented in the following table. The conclusion on the behaviour of the relative uncertainties is the same as for PRE-RACINE 1 results but the figures are a bit different. Indeed for fuel voided configurations, the nuclear data uncertainty on the CC is more important between 5.6% and 7.5% and on the LC the uncertainty is about 3.6-7.6% for voided configuration where the LC is important enough to consider the uncertainty.

Table V.2.12: Nuclear data uncertainties with JEFF-3.2 and COMAC-V2 for PRE-RACINE 2A

Configuration	Uncertainty (in pcm)			Relative uncertainty		
	Δρ	CC	LC	Δρ	CC	LC
Void V1 R=11.96	1.8	1.6	0.8	9.0%	7.5%	53.3%
Void V2 R=11.96	5.1	4.6	2.4	9.8%	7.4%	25.1%
Void V3 R=11.96	8.0	7.1	3.9	12.2%	7.4%	12.6%
Void V4 R=11.96	10.2	8.9	5.5	20.1%	7.2%	7.6%
Void V5 R=11.96	12.3	10.0	7.2	141.6%	7.1%	5.4%
Void V6 R=11.96	12.4	10.6	8.4	45.1%	6.6%	4.5%
Void V7 R=11.96	1.1	2.8	36.0	42,8%	6,3%	5,6%
Void V8 R=11.96	4.1	2.9	3.5	7.7%	6.6%	3.6%
Void V9 R=11.96	5.4	3.4	4.7	6.0%	5.6%	3.1%
Void V5 R=19.83	28.7	25.8	20.0	169.6%	7.1%	5.3%
Void V5 R=29.45	58.5	48.7	45.4	28.8%	7.2%	5.2%

The following table presents the nuclear data uncertainties for each component of all the voided configurations of PRE-RACINE 2B core. The values of the uncertainty on the CC are even less spread than for PRE-RACINE 2A and it is about 6.3-6.7% when for the LC the uncertainty vary between 5.3% and 5.6%.

Table V.2.13: ND uncertainties with JEFF-3.2 and COMAC-V2 for PRE-RACINE 2B

Configuration	Uncertainty (in pcm)			Relative uncertainty		
	Δρ	CC	LC	Δρ	CC	LC
Void V1 R=11.96	1.7	1.6	0.8	7.7%	6.7%	57.1%
Void V3 R=11.96	7.7	7.1	3.9	10.0%	6.6%	12.8%
Void V5 R=11.96	11.3	9.9	7.3	42.8%	6.3%	5.6%
Void V5 R=19.83	29.5	25.2	20.4	96.8%	6.3%	5.5%
Void V5 R=29.45	55.8	48.5	45.7	51.1%	6.5%	5.3%

More in details, the following table presents the breakdown of the nuclear data uncertainty on the CC for the V5 R=11.96cm voided configuration of the PRE-RACINE 2A core.

Table V.2.14: ND uncertainties on the CC with JEFF-3.2 and COMAC-V2 for PRE-RACINE 2A

Isotope	Fission	Capture	Elastic	Inelastic	n,xn	ν	Fission spectrum	Total
O16	0.0	0.6	0.4	0.0	0.0	0.0	0.0	0.7
Na23	0.0	0.1	0.3	0.1	0.0	0.0	0.0	0.3
Cr52	0.0	0.1	0.0	0.0	0.0	0.0	0.0	0.1
Fe54	0.0	0.1	0.1	0.0	0.0	0.0	0.0	0.1
Fe56	0.0	0.8	0.9	0.1	0.0	0.0	0.0	1.2
U235	0.3	2.0	0.2	0.1	0.0	0.2	0.1	2.0
U238	1.2	2.7	0.6	1.0	0.2	0.4	0.2	3.1
Pu239	4.9	2.8	0.2	0.1	0.0	1.0	1.1	5.8
Pu240	0.7	0.4	0.0	0.1	0.0	0.0	0.1	0.8
Pu241	0.0	0.1	0.0	0.0	0.0	0.0	0.1	0.1
Total	5.1	4.5	0.9	1.0	0.2	1.1	1.1	7.1

The main source of uncertainty on the CC is the ^{239}Pu once again and the capture cross-sections with important contributions of ^{235}U and ^{238}U, the main isotopes of the fuel composition.

The next table presents the differences on the uncertainty of the CC between the V5 R=11.96cm voided configuration of PRE-RACINE 2A and PRE-RACINE 2B core.

Table V.2.15: Differences between ND uncertainties of PRE-RACINE 2A and PRE-RACINE 2B on the CC

Isotope	Fission	Capture	Elastic	Inelastic	n,xn	ν	Fission spectrum	Total
O16	0.0%	-1.8%	-2.8%	-0.3%	0.0%	0.0%	0.0%	-1.1%
Na23	0.0%	-0.4%	-4.8%	1.1%	0.0%	0.0%	0.0%	-0.6%
Cr52	0.0%	-0.2%	-0.3%	-0.2%	0.0%	0.0%	0.0%	-0.1%
Fe54	0.0%	-0.2%	-1.9%	-0.2%	0.0%	0.0%	0.0%	-0.3%
Fe56	0.0%	-1.8%	-15.9%	-0.4%	0.0%	0.0%	0.0%	-2.2%
U235	0.4%	4.8%	-0.7%	-0.4%	0.1%	0.4%	2.5%	3.1%
U238	-3.8%	-7.8%	-7.9%	8.1%	-19.3%	-6.5%	-3.0%	-4.9%
Pu239	-16.8%	-12.3%	-5.0%	-1.0%	-1.2%	-16.8%	-17.4%	-14.8%
Pu240	16.2%	10.1%	3.0%	9.2%	0.8%	2.7%	12.6%	13.3%
Pu241	2.9%	3.8%	0.6%	0.9%	1.0%	6.0%	14.9%	4.0%
Total	-12.8%	-8.3%	-13.7%	6.8%	-19.2%	-17.1%	-12.1%	-10.6%

As expected the contribution of ^{240}Pu is increased by the use of PIT-fuel instead of POA and it is also the case for ^{241}Pu contribution while the ^{239}Pu, ^{235}U and ^{238}U contributions are reduced. A more deteriorated Pu-vector tends to get less uncertainty on the CC from the structural materials such as ^{56}Fe but its contribution in PRE-RACINE 2A already was almost negligible.

The following table presents the uncertainty on the LC for the V5 R=11.96cm voided configuration of the PRE-RACINE 2A core.

Table V.2.16: ND uncertainties on the LC with JEFF-3.2 and COMAC-V2 for PRE-RACINE 2A

Isotope	Fission	Capture	Elastic	Inelastic	n,xn	ν	Fission spectrum	Total
O16	0.0	0.1	0.8	0.0	0.0	0.0	0.0	0.8
Na23	0.0	1.7	0.9	1.5	0.0	0.0	0.0	2.5
Cr52	0.0	0.0	0.1	0.0	0.0	0.0	0.0	0.1
Fe54	0.0	0.1	0.1	0.0	0.0	0.0	0.0	0.1
Fe56	0.0	0.2	1.4	0.3	0.0	0.0	0.0	1.4
U235	0.5	3.9	0.3	0.0	0.0	0.3	0.4	4.0
U238	0.4	0.4	0.1	2.0	0.1	0.1	0.4	2.0
Pu239	0.7	0.4	0.2	0.1	0.0	0.2	0.3	0.8
Pu240	0.1	0.0	0.0	0.0	0.0	0.0	0.1	0.2
Pu241	0.0	0.0	0.0	0.0	0.0	0.0	0.0	0.0
Total	0.7	4.4	1.8	2.5	0.1	0.4	0.7	5.4

The main uncertainty source for the LC are the capture cross-section of ^{235}U, the inelastic cross-section of ^{238}U and the capture cross-section of sodium.

The next table presents the differences on the uncertainty of the LC between the V5 R=11.96cm voided configuration of PRE-RACINE 2A and PRE-RACINE 2B core.

Table V.2.17: Differences between ND uncertainties of PRE-RACINE 2A and PRE-RACINE 2B on the LC

Isotope	Fission	Capture	Elastic	Inelastic	n,xn	ν	Fission spectrum	Total
O16	0.0%	0.2%	0.1%	0.0%	0.0%	0.0%	0.0%	0.0%
Na23	0.0%	-0.2%	8.2%	4.2%	0.0%	0.0%	0.0%	2.1%
Cr52	0.0%	0.0%	0.1%	0.0%	0.0%	0.0%	0.0%	0.0%
Fe54	0.0%	0.1%	0.1%	0.0%	0.0%	0.0%	0.0%	0.0%
Fe56	0.0%	0.2%	0.3%	0.3%	0.0%	0.0%	0.0%	0.1%
U235	-0.3%	3.2%	-0.1%	0.3%	0.1%	1.0%	1.0%	2.5%
U238	1.3%	2.3%	0.8%	-1.5%	-4.7%	1.6%	1.1%	-0.2%
Pu239	-7.1%	-1.6%	-0.7%	-0.4%	-0.2%	-4.5%	6.3%	-1.1%
Pu240	36.3%	3.5%	1.0%	1.3%	1.6%	2.3%	30.3%	5.3%
Pu241	2.6%	0.3%	0.6%	0.1%	1.9%	4.3%	42.5%	5.1%
Total	2.7%	2.8%	4.8%	1.5%	-4.8%	-0.6%	22.5%	3.1%

As expected the contribution of ^{240}Pu is increased by the use of PIT-fuel instead of POA and it is also the case for ^{241}Pu contribution as the (^{241}Pu+^{241}Am)/(Pu+Am) concentration goes for 1% to 4% when the ^{239}Pu, ^{235}U and ^{238}U contributions are reduced.

V.2.1.2.3 Representativeness

The following table presents the representativeness between the sensitivity set of the CC (or of the LC or of the SVRE) of an experimental configuration with the sensitivity set of the CC (or of the LC or of the SVRE) of a voided configuration of the ASTRID CFV core.

Table V.2.18: Representativeness of PRE-RACINE 2A (and 2B) with ASTRID CFV

Core	Configuration	Total void			Sodium plenum voided			Fuel voided		
		Δρ	CC	LC	Δρ	CC	LC	Δρ	CC	LC
PRE-RACINE 2A	Void V3 R=11.96	-0.778	0.839	0.351	-0.778	0.839	0.351	0.850	0.846	0.487
	Void V5 R=11.96	-0.782	0.845	0.354	-0.782	0.845	0.354	0.845	0.850	0.449
	Void V6 R=11.96	-0.784	0.854	0.380	-0.784	0.854	0.380	0.840	0.855	0.454
	Void V5 R=29.45	0.759	0.824	0.303	0.455	0.660	0.134	-0.814	0.832	0.385
PRE-RACINE 2B	Void V3 R=11.96	-0.840	0.844	0.377	-0.560	0.659	0.123	0.886	0.868	0.534
	Void V5 R=11.96	**0.886**	**0.871**	**0.482**	-0.564	0.670	0.144	-0.846	0.849	0.369
	Void V5 R=29.45	0.812	0.823	0.314	0.534	0.642	0.119	-0.850	0.844	0.412

As expected the PRE-RACINE 2B is more representative than the PRE-RACINE 2A core when it is compared to the CFV total void or fuel voided configuration due to the use of PIT fuel instead of POA as the CFV core is using a very deteriorated Pu-vector. More in details the representativeness of the CC reaches 0.871 and the best representative experiment is the V5 R=11.96cm configuration in the PRE-RACINE 2B core.

V.2.1.3 CIRANO cores

In this section, the influence of the reflector on the sensitivity of the CC, LC and SVRE to nuclear data is analysed. Indeed the two cores of the CIRANO programme have the same fuel composition (with this exception of a small POA fuel zone in the outer assemblies of the ZONA2A core). The ZONA2A core is surrounded by fertile blanket while the ZONA2B is surrounded by a reflector made of steel and sodium.

V.2.1.3.1 Sensitivity

The following table presents the sensitivity of the CC to nuclear data of the CIRANO ZONA2A core calculated with JEFF-3.2 for the V24 R=11.96cm voided configuration.

Table V.2.19: Sensitivity of the CC of CIRANO 2A for the V24 R=11.96cm configuration

Isotope	Fission	Capture	Elastic	Inelastic	n,xn	ν	Fission spectrum	Total
O16	0.000	0.022	**0.196**	0.003	0.000	0.000	0.000	0.222
Na23	0.000	0.084	**0.370**	**0.509**	0.000	0.000	0.000	0.963
Fe56	0.000	-0.043	0.007	0.033	0.000	0.000	0.000	-0.003
U235	-0.031	-0.009	0.000	0.001	0.000	0.014	-0.052	-0.076
U238	**-0.482**	**-0.772**	0.051	0.163	-0.001	**-0.665**	**0.320**	-1.386
Pu238	-0.002	-0.001	0.000	0.000	0.000	-0.001	0.000	-0.004
Pu239	**-1.272**	**-0.575**	0.012	0.021	0.000	-0.182	**-1.497**	-3.494
Pu240	-0.213	-0.120	0.003	0.006	0.000	**-0.295**	**0.188**	-0.431
Pu241	-0.012	-0.009	0.000	0.001	0.000	0.039	-0.078	-0.059
Pu242	-0.007	-0.004	0.000	0.000	0.000	-0.009	0.006	-0.014
Am241	-0.030	-0.064	0.000	0.001	0.000	-0.041	-0.003	-0.136
Total	-2.049	-1.508	0.646	0.755	0.003	-1.142	-1.115	-4.410

In comparison with PRE-RACINE core, the sensitivity of the elastic cross-section of sodium is more important (37% for CIRANO ZONA2A compared to respectively 25% and 15% for PRE-RACINE 2A and PRE-RACINE 2B). This is due to the fact that neutron flux spectra are harder than the ones of

PRE-RACINE core since the U-Pu fuel volume has increased between the two programmes from 18.75% to 25%, by replacing the fertile pin of the ZONA1 scheme by a U-Pu fuel pin. Then the sensitivities of Pu isotopes have increased and the ones of ^{235}U and ^{238}U have decreased. However, the ^{238}U stays a main contributor to the sensitivity.

The next table compared the sensitivity of the CC of the V24 R=11.96cm configuration of the CIRANO 2A core with the one of the V24 R=11.96cm configuration of the CIRANO 2B core.

Table V.2.20: Differences of the sensitivity of the CC between CIRANO 2A and 2B for the V24 R=11.96 cm configuration

Isotope	Fission	Capture	Elastic	Inelastic	n,xn	ν	Fission spectrum	Total
O16	0.0%	0.1%	-2.4%	0.0%	0.0%	0.0%	0.0%	-0.2%
Na23	0.0%	0.7%	**-20.1%**	4.7%	-0.1%	0.0%	0.0%	-1.0%
Fe56	0.0%	1.4%	**15.4%**	0.9%	2.2%	0.0%	0.0%	2.4%
U235	-1.4%	-0.1%	0.0%	0.0%	0.0%	0.6%	-0.8%	-0.9%
U238	-0.5%	-2.9%	**-6.6%**	5.1%	-7.0%	3.5%	**22.2%**	-5.7%
Pu238	0.0%	0.0%	0.0%	0.0%	0.0%	0.0%	0.0%	0.0%
Pu239	**23.7%**	2.4%	0.1%	0.5%	0.6%	**22.3%**	**63.4%**	**30.2%**
Pu240	1.7%	0.6%	-0.1%	0.2%	0.3%	4.0%	10.3%	-0.3%
Pu241	0.8%	0.1%	0.0%	0.0%	0.1%	-0.4%	3.6%	1.2%
Pu242	0.1%	0.0%	0.0%	0.0%	0.0%	0.1%	0.3%	0.0%
Am241	0.2%	0.4%	0.0%	0.0%	0.1%	0.5%	0.1%	0.4%
SUM	24.6%	1.9%	-51.4%	11.9%	23.9%	30.3%	33.4%	29.2%

The main differences are concerning the sensitivity the CC to the ^{239}Pu as it is greatly increased (30.2%) with a major contribution of the fission spectrum sensitivity (63.4%) since the reflector has an important influence on the neutron spectrum changes. There is also a decrease of the sensitivity of CC to the elastic scattering of sodium. An explanation is that the substitution of the blanket made of depleted uranium by a reflector decreases the capture reaction rate in the blanket then the elastic scattering of neutrons on sodium nuclei is less important.

V.2.1.3.2 Nuclear data uncertainties

The next table presents the nuclear data uncertainties on each component for each experimental configuration of the CIRANO 2A core calculated with JEFF-3.2 and COMAC-V2.

Table V.2.21: Nuclear data uncertainties with JEFF-3.2 and COMAC-V2 for CIRANO 2A

Configuration	Uncertainty (in pcm)			Relative uncertainty		
	Δρ	CC	LC	Δρ	CC	LC
Void V4+4 R=11.96	2.8	2.0	2.0	4.5%	4.6%	1.8%
Void V24 R=11.96	12.1	9.2	6.1	137.2%	5.0%	3.5%
Void V16 R=11.96	8.4	7.3	4.3	11.0%	5.3%	6.9%
Void V8 R=11.96	4.6	4.0	2.2	7.3%	5.4%	19.3%

The following table presents the nuclear data uncertainties on each component for each experimental configuration of the CIRANO 2B core calculated with JEFF-3.2 and COMAC-V2.

Table V.2.22: Nuclear data uncertainties with JEFF-3.2 and COMAC-V2 for CIRANO 2B

Configuration	Uncertainty (in pcm)			Relative uncertainty		
	Δρ	CC	LC	Δρ	CC	LC
Void V4+4 R=20,72	8.6	7.0	7.1	4.1%	6.4%	2.2%
Void V24 R=20.72	32.9	28.5	20.3	48.9%	5.5%	3.5%
Void V16 R=20.72	25.6	14.2	13.3	17.1%	5.7%	5.4%
Void V8 R=20.72	14.2	12.3	6.9	10.2%	5.7%	8.9%
Void V4+4 R=11.96	3.1	2.5	2.5	4.3%	6.4%	2.3%
Void V24 R=11.96	37.9	10.4	7.1	1995.0%	5.7%	3.9%
Void V16 R=11.96	9.5	8.6	4.8	12.2%	6.0%	7.3%
Void V8 R=11.96	5.2	4.5	2.5	8.1%	5.8%	18.1%

The conclusion on the behaviour of the relative uncertainties is the same as for PRE-RACINE results but the figures are a bit different. Indeed, for configuration where the sodium is removed from the fuel medium, the nuclear data uncertainty on the CC is about 5.5-6.4% and on the LC the uncertainty is about 2.2-8.9% for voided configuration where the LC is important enough to consider the uncertainty.

V.2.1.3.3 Representativeness

The following table presents the representativeness between the sensitivity set of the CC (or of the LC or of the SVRE) of an experimental configuration with the sensitivity set of the CC (or of the LC or of the SVRE) of a voided configuration of the ASTRID CFV core.

The results could be a bit surprising as the presence of a radial reflector in CIRANO 2B like in the ASTRID CFV core seems more representative than a fertile blanket. In fact, the presence of an axial reflector deteriorates the flux by sending back to the core, neutrons at lower energy than the ones leaking out. This is very different from a sodium plenum for which once voided, neutrons are leaking out and are absorbed in neutronic shielding. Hence, this is a bit similar to the behaviour of the fertile blanket that is absorbing neutrons in ^{238}U.

Table V.2.23: Representativeness of CIRANO 2A (and 2B) with ASTRID CFV

Core	Configuration	Total void			Sodium plenum voided			Fuel voided		
		Δρ	CC	LC	Δρ	CC	LC	Δρ	CC	LC
CIRANO 2A	V16 R=11.96	-0.842	0.842	0.511	-0.609	0.625	0.254	0.865	0.877	0.626
	V24 R=11.96	-0.862	0.856	0.592	-0.652	0.644	0.371	0.866	0.888	0.635
	V4+4 R=11.96	-0.853	0.903	0.687	-0.720	0.723	0.569	0.807	0.919	0.581
CIRANO 2B	V16 R=11.96	-0.829	0.839	0.449	-0.607	0.625	0.196	0.852	0.874	0.592
	V24 R=11.96	0.839	0.837	0.506	0.644	0.619	0.274	-0.847	0.872	0.600
	V4+4 R=11.96	0.792	0.866	0.522	0.685	0.681	0.369	-0.756	0.890	0.517
	V16 R=20.72	-0.835	0.842	0.453	-0.625	0.621	0.218	0.850	0.879	0.583
	V24 R=20.72	0.841	0.835	0.518	0.657	0.614	0.295	-0.842	0.871	0.599
	V4+4 R=20.72	0.792	0.867	0.525	0.690	0.681	0.379	-0.754	0.891	0.514

V.2.1.4 BFS cores

V.2.1.4.1 Sensitivity

The following table presents the sensitivity of the SVRE to nuclear data of the BFS-115-1 core calculated with JEFF-3.2 for the total voided configuration.

Table V.2.24: Sensitivity of the SVRE for the total voided configuration in BFS-115-1

Isotope	Fission	Capture	Elastic	Inelastic	n,xn	ν	Fission spectrum	Total
O16	0.000	0.021	**0.456**	0.007	0.000	0.000	0.000	0.485
Na23	0.000	-0.055	**-0.523**	-0.283	0.000	0.000	0.000	-0.862
Cr52	0.000	0.000	0.030	0.015	0.000	0.000	0.000	0.045
Fe54	0.000	0.006	0.011	0.004	0.000	0.000	0.000	0.021
Fe56	0.000	0.005	0.153	0.070	0.000	0.000	0.000	0.228
Fe57	0.000	0.001	0.006	0.004	0.000	0.000	0.000	0.011
U235	-0.027	-0.008	0.001	0.002	0.000	-0.019	-0.011	-0.062
U238	**-0.493**	-0.239	0.250	**0.562**	0.012	**-0.770**	**-0.793**	-1.470
Pu239	**-0.530**	-0.307	0.023	0.031	0.001	-0.179	-0.162	-1.124
Pu240	-0.025	-0.016	0.001	0.002	0.000	-0.030	-0.031	-0.099
Pu241	0.000	0.000	0.000	0.000	0.000	0.000	0.000	0.001
Am241	-0.001	-0.002	0.000	0.000	0.000	-0.001	-0.001	-0.006
Total	-1.076	-0.590	0.418	0.414	0.015	-0.999	-0.999	-2.817

The next table presents the difference in sensitivity of the SVRE between the total voided configuration and the voided sodium plenum voided configuration.

Table V.2.25: Differences of the sensitivity of the SVRE between the plenum voided configuration and the total voided configuration in BFS-115-1

Isotope	Fission	Capture	Elastic	Inelastic	n.xn	ν	Fission spectrum	Total
O16	0.0%	12.0%	231.1%	2.0%	0.0%	0.0%	0.0%	-15.2%
Na23	0.0%	-32.7%	-232.5%	-108.6%	0.1%	0.0%	0.0%	26.7%
Cr52	0.0%	-0.7%	8.5%	3.2%	0.0%	0.0%	0.0%	-0.8%
Fe54	0.0%	1.7%	3.6%	0.8%	0.0%	0.0%	0.0%	-0.4%
Fe56	0.0%	-3.7%	45.1%	14.2%	0.1%	0.0%	0.0%	-4.0%
Fe57	0.0%	0.2%	1.7%	1.1%	0.0%	0.0%	0.0%	-0.2%
U235	-1.0%	-7.0%	0.4%	0.6%	0.3%	-2.4%	-3.1%	-2.3%
U238	22.9%	-322.6%	99.7%	148.6%	140.8%	41.0%	49.6%	41.6%
Pu239	-15.4%	-198.3%	10.4%	9.0%	8.5%	-40.6%	-48.9%	-33.8%
Pu240	1.1%	-10.0%	0.5%	0.5%	0.6%	1.6%	2.1%	2.4%
Pu241	0.0%	0.0%	0.0%	0.0%	0.0%	0.0%	0.0%	0.0%
Am241	0.0%	-1.5%	0.0%	0.0%	0.0%	0.1%	0.1%	0.2%
Total	7.5%	-561.2%	172.2%	71.5%	172.6%	-0.3%	-0.3%	13.8%

The main difference concerns the fuel isotope as the fuel medium is not voided in this last configuration. Also, the sodium has less impact than in the total voided configuration however the elastic scattering of sodium and elastic and inelastic of ^{238}U has an increased sensitivity due to spectrum effect in the top of the superior fuel area.

V.2.1.4.2 Nuclear data uncertainty

The next table presents the nuclear data uncertainties on each component for each experimental configuration of the BFS-115-1 core calculated with JEFF-3.2 and COMAC-V2.

Table V.2.26: Nuclear data uncertainties with JEFF-3.2 and COMAC-V2 for BFS-115-1

Configuration	Uncertainty (in pcm)			Relative uncertainty		
	Δρ	CC	LC	Δρ	CC	LC
Total void	23.3	34.3	52.4	4.9%	6.4%	5.2%
Sodium plenum void	9.8	5.5	52.2	1.6%	7.2%	7.8%

The differences on the relative uncertainty of the SVRE are less important than in the other experiments due to high negative values of these SVRE.

V.2.1.4.3 Representativeness

For the BFS experiments, the calculation of the generalised importance needed for the indirect sensitivity did not converge. Hence, the sensitivity of the CC is only built with the direct term and the representativeness with the ASTRID CFV CC is calculated with the direct sensitivity of the CC of the CFV to keep a consistent comparison.

Table V.2.27: Representativeness of PRE-RACINE 2A (and 2B) with ASTRID CFV

Configuration	Total void			Sodium plenum voided			Fuel voided		
	Δρ	CC	LC	Δρ	CC	LC	Δρ	CC	LC
BFS Total void	0.763	0.721	0.722	0.540	0.719	0.720	-0.755	0.726	0.726
BFS sodium plenum void	0.555	0.730	0.731	0.535	0.733	0.734	-0.475	0.736	0.737

The main important result there is the higher values of representativeness between the LC of the experiments and the one of the CFV reflecting a more representative geometry. Even if we expected to get more difference in representativeness with the CFV but as the direct term only takes into account the macroscopic variations and not their influence on the flux (and then their spatial impact) the impact of a more representative geometry is limited.

V.2.2 Results on ASTRID core

V.2.2.1 Sensitivity

In this section, are presented the sensitivity of the CC, LC and SVRE to the nuclear data in different sodium void configurations (see Chapter IV):

- A total sodium void configuration where the fuel (C1 and C2), the inner fertile area (FCAM), the sodium expansion vase (SVES) and the Sodium Plenum areas are voided.
- A void plenum configuration when only the Sodium plenum and the SVES areas are voided.

The following table presents the sensitivity of the SVRE of the total sodium void configuration calculated with the EGPT method and the JEFF-3.2 nuclear data.

The SVRE is very sensitive to the elastic cross-section of the sodium that is coming from the presence of a sodium plenum on the top of the core. The contribution of the oxygen elastic scattering is not negligible. The fuel isotopes ^{238}U, ^{239}Pu, ^{240}Pu and ^{241}Pu are also major contributors to the sensitivity of the SVRE with their fission cross-section and neutron emission yield per fission and fission spectrum.

Table V.2.28: Sensitivity of the SVRE of the total voided configuration of the ASTRID CFV

Isotope	Fission	Capture	Elastic	Inelastic	n,xn	ν	Fission spectrum	Total
B10	0.000	-0.489	0.060	0.000	0.000	0.000	0.000	-0.428
O16	0.000	0.047	1.158	0.008	0.000	0.000	0.000	1.213
Na23	0.000	-0.247	-3.189	-1.420	0.000	0.000	0.000	-4.856
Cr50	0.000	-0.004	0.008	0.000	0.002	0.000	0.000	0.006
Cr52	0.000	-0.032	0.058	0.047	0.000	0.000	0.000	0.073
Cr53	0.000	-0.014	0.015	0.000	0.006	0.000	0.000	0.007
Fe54	0.000	0.008	0.037	0.017	0.000	0.000	0.000	0.063
Fe56	0.000	-0.235	0.383	0.293	0.000	0.000	0.000	0.441
Fe57	0.000	-0.008	0.012	0.025	0.000	0.000	0.000	0.029
Fe58	0.000	-0.001	0.002	0.001	0.000	0.000	0.000	0.002
U235	0.019	-0.012	0.001	0.002	0.000	0.032	0.057	0.099
U238	-0.925	-1.510	0.285	0.903	0.007	-1.495	-1.653	-4.389
Pu238	-0.017	-0.074	0.003	0.003	0.000	-0.016	-0.021	-0.122
Pu239	0.724	-0.827	0.025	0.037	0.000	1.180	1.331	2.470
Pu240	-0.831	-0.563	0.024	0.037	0.001	-1.173	-1.276	-3.781
Pu241	0.591	-0.102	0.005	0.007	0.000	0.868	0.983	2.353
Pu242	-0.260	-0.166	0.009	0.014	0.000	-0.363	-0.387	-1.154
Am241	-0.015	-0.037	0.001	0.001	0.000	-0.020	-0.023	-0.094
Total	-0.713	-4.267	-1.103	-0.023	0.016	-0.989	-0.989	-8.068

The next table presents the sensitivity of the CC of the total sodium void configuration calculated with our GPT method and the JEFF-3.2 nuclear data.

Table V.2.29: Sensitivity of the CC of the total voided configuration of the ASTRID CFV

Isotope	Fission	Capture	Elastic	Inelastic	n,xn	ν	Fission spectrum	Total
B10	0.000	0.005	0.001	0.000	0.000	0.000	0.000	0.006
O16	0.000	0.006	0.369	0.002	0.000	0.000	0.000	0.377
Na23	0.000	0.055	0.568	0.347	0.000	0.000	0.000	0.969
Cr50	0.000	0.003	0.001	0.000	0.000	0.000	0.000	0.005
Cr52	0.000	-0.005	0.010	0.007	0.000	0.000	0.000	0.013
Cr53	0.000	0.004	0.003	0.000	0.001	0.000	0.000	0.008
Fe54	0.000	0.000	0.008	0.003	0.000	0.000	0.000	0.011
Fe56	0.000	-0.043	0.073	0.053	0.000	0.000	0.000	0.083
Fe57	0.000	-0.002	0.004	0.007	0.000	0.000	0.000	0.009
Fe58	0.000	0.000	0.001	0.000	0.000	0.000	0.000	0.001
U235	-0.012	-0.003	0.000	0.000	0.000	0.003	-0.030	-0.041
U238	-0.155	-0.356	0.045	0.187	0.003	-0.191	0.154	-0.312
Pu238	-0.016	-0.014	0.000	0.001	0.000	-0.010	-0.003	-0.042
Pu239	-1.301	-0.157	0.004	0.011	0.000	-0.502	-0.997	-2.942
Pu240	-0.132	-0.104	0.004	0.011	0.000	-0.174	0.213	-0.182
Pu241	-0.309	-0.021	0.001	0.002	0.000	-0.052	-0.386	-0.764
Pu242	-0.042	-0.032	0.002	0.005	0.000	-0.055	0.068	-0.055
Am241	-0.002	-0.008	0.000	0.000	0.000	-0.003	0.000	-0.012
Total	-1.968	-0.669	1.095	0.636	0.005	-0.983	-0.982	-2.866

The CC in the total sodium void configuration is very sensitive to the elastic sodium scattering and the main contributor is the ^{239}Pu. Then the CC is strongly related to the sodium nuclear data.

The next table presents the differences between the sensitivity set of the CC of the total sodium void configuration and the sensitivity set of the CC of the sodium plenum void configuration calculated with JEFF-3.2 nuclear data.

The difference between the two configurations is the increase of the sensitivity of the sodium elastic cross-section due to the sodium plenum and as the sodium is not removed from the fuel media there is less influence of a spectral component so the sensitivity of the fission spectrum is reduced in the sodium plenum void configuration.

Table V.2.30: Differences of the sensitivity of the CC between the sodium plenum void configuration and the total voided configuration of the ASTRID CFV

Isotope	Fission	Capture	Elastic	Inelastic	n,xn	ν	Fission spectrum	Total
B10	0.0%	5.4%	0.4%	0.0%	0.0%	0.0%	0.0%	1.4%
O16	0.0%	-0.8%	3.2%	-0.2%	0.0%	0.0%	0.0%	0.9%
Na23	0.0%	-3.1%	32.5%	-0.9%	-0.6%	0.0%	0.0%	11.5%
Cr50	0.0%	2.0%	0.1%	0.0%	-0.4%	0.0%	0.0%	0.5%
Cr52	0.0%	-0.3%	1.0%	0.9%	0.0%	0.0%	0.0%	0.7%
Cr53	0.0%	3.3%	0.1%	0.0%	-1.0%	0.0%	0.0%	0.8%
Fe54	0.0%	0.4%	0.3%	0.5%	0.0%	0.0%	0.0%	0.3%
Fe56	0.0%	-1.0%	2.3%	10.2%	-0.1%	0.0%	0.0%	3.4%
Fe57	0.0%	-0.1%	0.2%	0.8%	0.1%	0.0%	0.0%	0.3%
Fe58	0.0%	0.0%	0.0%	0.0%	0.0%	0.0%	0.0%	0.0%
U235	0.2%	0.0%	0.0%	0.0%	0.0%	-0.2%	-2.2%	-0.5%
U238	-5.8%	-6.6%	0.3%	-9.5%	-19.1%	-18.8%	-13.1%	-3.7%
Pu238	0.4%	-0.5%	0.0%	0.0%	0.0%	0.9%	1.2%	0.9%
Pu239	14.7%	-4.3%	0.2%	0.0%	-0.1%	36.1%	-14.4%	16.4%
Pu240	-2.2%	-5.5%	0.2%	0.1%	-0.7%	-6.3%	-15.8%	4.4%
Pu241	5.3%	-1.0%	0.1%	0.0%	0.3%	13.4%	-16.1%	2.5%
Pu242	-1.0%	-1.1%	0.1%	0.0%	0.1%	-2.7%	-5.4%	1.0%
Am241	-0.1%	-0.4%	0.0%	0.0%	0.0%	-0.2%	0.1%	-0.2%
SUM	11.5%	-28.6%	40.9%	1.7%	-22.3%	22.7%	22.9%	0.9%

The next table presents the sensitivity of the LC of the total sodium void configuration calculated with JEFF-3.2 nuclear data.

Table V.2.31: Sensitivity of the LC of the total voided configuration of the ASTRID CFV

Isotope	Fission	Capture	Elastic	Inelastic	n,xn	ν	Fission spectrum	Total
B10	0.000	-0.075	0.010	0.000	0.000	0.000	0.000	-0.064
O16	0.000	0.013	0.497	0.003	0.000	0.000	0.000	0.512
Na23	0.000	0.006	-0.039	0.061	0.000	0.000	0.000	0.028
Cr50	0.000	0.002	0.002	0.000	0.001	0.000	0.000	0.005
Cr52	0.000	-0.009	0.018	0.014	0.000	0.000	0.000	0.022
Cr53	0.000	0.001	0.005	0.000	0.002	0.000	0.000	0.008
Fe54	0.000	0.001	0.013	0.005	0.000	0.000	0.000	0.019
Fe56	0.000	-0.074	0.123	0.092	0.000	0.000	0.000	0.141
Fe57	0.000	-0.003	0.005	0.010	0.000	0.000	0.000	0.013
Fe58	0.000	0.000	0.001	0.000	0.000	0.000	0.000	0.001
U235	-0.007	-0.004	0.000	0.001	0.000	0.007	-0.016	-0.019
U238	-0.279	-0.543	0.084	0.303	0.004	-0.402	-0.138	-0.971
Pu238	-0.016	-0.024	0.001	0.001	0.000	-0.011	-0.006	-0.055
Pu239	-0.974	-0.265	0.008	0.015	0.000	-0.230	-0.621	-2.067
Pu240	-0.245	-0.178	0.007	0.015	0.000	-0.335	-0.027	-0.764
Pu241	-0.163	-0.034	0.002	0.003	0.000	0.097	-0.165	-0.260
Pu242	-0.077	-0.053	0.003	0.006	0.000	-0.105	-0.006	-0.232
Am241	-0.004	-0.013	0.000	0.000	0.000	-0.006	-0.004	-0.026
SUM	-1.765	-1.251	0.740	0.530	0.007	-0.984	-0.983	-3.707

The next table presents the differences between the sensitivity set of the CC of the total sodium void configuration and the sensitivity set of the CC of the sodium plenum void configuration calculated with JEFF-3.2 nuclear data.

Table V.2.32: Differences of the sensitivity of the LC between the sodium plenum void configuration and the total voided configuration of the ASTRID CFV

Isotope	Fission	Capture	Elastic	Inelastic	n,xn	ν	Fission spectrum	Total
B10	0.0%	2.7%	0.3%	0.0%	0.0%	0.0%	0.0%	0.8%
O16	0.0%	-0.8%	-42.8%	-0.4%	0.0%	0.0%	0.0%	-8.9%
Na23	0.0%	0.0%	-0.8%	-4.8%	-0.5%	0.0%	0.0%	-0.7%
Cr50	0.0%	-0.1%	-0.2%	0.0%	-5.5%	0.0%	0.0%	-0.1%
Cr52	0.0%	-0.5%	-1.0%	-1.4%	0.0%	0.0%	0.0%	-0.2%
Cr53	0.0%	0.0%	-0.4%	0.0%	-17.1%	0.0%	0.0%	-0.1%
Fe54	0.0%	-0.1%	-0.9%	-0.5%	0.0%	0.0%	0.0%	-0.3%
Fe56	0.0%	-4.1%	-9.4%	-8.3%	0.0%	0.0%	0.0%	-1.7%
U235	0.3%	-0.3%	0.0%	-0.1%	0.0%	0.2%	-0.3%	0.5%
U238	-6.4%	-36.0%	-6.9%	-38.6%	-40.6%	-19.9%	0.5%	-13.4%
Pu238	0.9%	-1.4%	-0.1%	-0.1%	0.0%	1.9%	2.4%	1.1%
Pu239	-17.4%	-15.5%	-0.6%	-2.0%	-1.1%	26.0%	-4.3%	-7.4%
Pu240	-6.1%	-10.9%	-0.6%	-1.9%	-3.1%	-18.0%	6.9%	-9.1%
Pu241	0.0%	-2.0%	-0.1%	-0.4%	-0.6%	0.2%	-1.2%	4.4%
Pu242	-2.1%	-3.2%	-0.2%	-0.8%	-0.1%	-6.0%	1.9%	-3.0%
SUM	-30.9%	-70.3%	-62.5%	-60.5%	-70.0%	5.5%	5.6%	-14.2%

The difference on the sensitivity of the LC in the sodium plenum void configuration compared to the total void configuration is mainly due to the ^{238}U. Indeed the capture reaction rate is quite similar to the nominal situation when the sodium plenum is voided. Neutrons with the lowest energy stay in the core. However in the total sodium void configuration there are less neutrons at low energy due to the lack of scattering in the fuel.

V.2.2.2 Correlation between CC and LC

Thanks to the sensitivity of the CC and of the LC to nuclear data it is possible to calculate the representativeness (see **1.15**) between the two set of sensitivity for the same voided configuration which gives the correlation between the CC and LC sensitivity profiles.

Table V.2.33: Correlation between the CC and the LC sensitivity sets of the ASTRID CFV

Configuration	$R_{CC,LC}$
ASTRID CFV total void	0.002
ASTRID CFV fuel void	-0.14
ASTRID CFV sodium plenum void	-0.05
ASTRID CFV fertile void	-0.26

The results are near 0 meaning that the two components have an almost independent behaviour. This justifies a posteriori the independent study of the CC and LC in sodium void experiments. Indeed as experimental configurations highlight the LC when other ones emphasise the CC. It seems obvious to do it even if a perturbation in one part of the core can have effect on the opposite side by perturbing the harmonics of the neutron flux but this needs dedicated tools to characterise it [6].

V.3 Prediction for ASTRID core

After getting the representativeness between the sodium void experiments and the different ASTRID CFV sodium void configurations the experimental results can be transferred. The CC and LC of the SVRE calculated by TRIPOLI-4® are then corrected by taking into account the TRIPOLI-4®-experiments adjustment results of the Chapter IV.

V.3.1 Nuclear data uncertainties

The sensitivities on each component of the SVRE of each voided configuration for the ASTRID CFV core presented in the section 2.2 enable calculating the nuclear data uncertainties thanks to **1.14**. In the following table, are presented the nuclear data uncertainties obtained with JEFF-3.2 and the covariance matrix COMAC-V2 for the four voided configurations:

- A total sodium void configuration where the sodium is removed from: the fuel (C1 and C2), the inner fertile area (FCAM), the sodium expansion vase (SVES) and the Sodium Plenum areas.
- A void plenum configuration when only the Sodium plenum and the SVES areas are voided.
- A fuel voided configuration where the sodium is removed from only the fuel (C1 and C2) media.
- A fertile voided configuration where the sodium is removed from the inner fertile slab (FCAM) is voided.

The relative uncertainties on the CC are about 2.1% to 3.0% according to the configuration when the relative uncertainties on the LC is included between 1.4% and 5.1% when the LC is enough important as 17.3%.

Table V.3.1: Nuclear data uncertainties for ASTRID CFV SVRE

Configuration	Uncertainty (in pcm)			Relative uncertainty		
	Δρ	CC	LC	Δρ	CC	LC
CFV Total Void	96.8	71.0	65.7	18.1%	2.6%	2.0%
CFV Sodium plenum Void	35.6	9.9	34.7	1.9%	2.1%	1.4%
CFV Fuel Void	60.5	54.2	35.3	5.3%	3.0%	5.1%
CFV Fertile Void	10.1	8.7	8.4	3.1%	2.3%	17.3%

V.3.2 Corrections of the components of the SVRE

In this section, the CC and the LC of the total voided configuration of the ASTRID CFV core calculated with ERANOS are corrected of the modelling and deterministic bias with the TRIPOLI-4® comparison and then each experimental programme is used to correct the CC and the LC medium by medium.

V.3.2.1 Correction process

V.3.2.1.1 Deterministic and modelling bias

First, the values of CC and LC calculated with ERANOS for the total voided configuration of the CFV core have to be corrected from the deterministic and modelling bias.

Table V.3.2: Discrepancies between TRIPOLI-4® and ERANOS for different voided configuration of the CFV core with JEFF-3.2 nuclear data

Sodium removed from	Δρ(TRIPOLI-4®)-Δρ(ERANOS)
Fuel: C1 and C2 media	-56
Fertile: FCAM medium	-25
Sodium plenum	-8
Total voided (Fuel, Fertile and Plenum)	-67

These results show that the deterministic and modelling bias from the sodium plenum is significantly reduced for the CFV core in comparison to an average discrepancy of -250 pcm between TRIPOLI-4® and ERANOS results of SVRE for different voided configurations of the BFS core (see Chapter IV). Thanks to these results we can adjust a set of parameters (α_d, β_d). The uncertainty given takes into account the statistical uncertainty on the TRIPOLI-4® results:

$$(\alpha_d \pm d\alpha_d, \beta_d \pm d\beta_d) = (0.969 \pm 0.006\,, 0.995 \pm 0.005\,) \qquad \textbf{3.1}$$

Now the nuclear data uncertainties calculated in **section 3.1** have to be considered. Indeed different voided configurations have been calculated in order to get the impact of each medium on the values of the SVRE and its components (CC and LC) and their uncertainties. These values have been calculated with nuclear data uncertainties and then it has an impact on the adjustment with TRIPOLI-4® results. The correction of the deterministic and modelling bias has to take into account the nuclear data uncertainty impact, this has been done by introducing the nuclear data uncertainty on the CC and LC

of the different voided configurations of the CFV in the adjustment process which lead to an overall uncertainty on each parameter (α_d, β_d) presented in equation **3.2**:

$$(\alpha_d \pm d\alpha_d, \beta_d \pm d\beta_d) = (0.969 \pm 0.030\ , 0.995 \pm 0.020\ ) \quad \textbf{3.2}$$

Then by adding the statistical uncertainty presented in the equation **3.1** to the nuclear data uncertainty we get the overall uncertainty on the adjustment with the results:

$$(\alpha_d \pm d\alpha_d, \beta_d \pm d\beta_d) = (0.969 \pm 0.031\ , 0.995 \pm 0.021\ ) \quad \textbf{3.3}$$

These results show that the deterministic and modelling bias is consistent within the nuclear data and statistical uncertainties.

V.3.2.1.2 Experimental validation

The use of the deterministic code ERANOS allows calculating the CC and LC in each medium of the core, the breakdown of the CC and LC by medium is presented in the following table for a total SVRE of -535 pcm:

Table V.3.3: SVRE breakdown by medium in the total voided configuration of the ASTRID CFV core

	CC (pcm)	LC (pcm)	$\Delta\rho_{Na}$
C1	1092.6	-359.7	732.9
C2	759.4	-371.6	387.8
FCAM	407.4	-40.9	366.5
SPLN	514.5	-2537.7	-2023.2
Total	2774.1	3309.9	-535.8

The idea is to correct these values with the set of parameters (α_i, β_i) of each experimental programme. This is done by taking into account the representativeness between the CC of the experiments and the one of the total voided configuration of the CFV core (through the use of the α_i parameter) and the representativeness of the LC of the experiments and the one of the total voided configuration of the CFV core (through the use of the β_i parameter).

Indeed, three experimental programmes (PRE-RACINE, CIRANO and BFS-115-1) give information on the CC and the LC of the C1 and C2 medium because in these programmes there are fuel voided zones. The PRE-RACINE 1 and the BFS-115-1 experimental cores give information on the CC and LC of the inner fertile slab (FCAM medium) because in these two cores an inner fertile area has been voided and only the BFS programme gives information on the CC and LC of the sodium plenum.

Then for each medium the CC and LC are multiplied by a predicted set of parameters (α_p, β_p) calculated as the mean of the set of parameters (α_i, β_i) weighted by the representativeness $(R_{CC,i}, R_{LC,i})$

$$(\alpha_p, \beta_p) = \frac{\sum_i (\alpha_i . R_{CC,i}, \beta_i . R_{LC,i})}{\sum_i (R_{CC,i}, R_{LC}, i)} \quad \textbf{3.4}$$

First the deterministic and modelling bias is corrected from these values using the set of parameters: (α_d, β_d) giving the breakdown into the CC and LC fitting the best with the TRIPOLI-4® results giving a total SVRE of -605 pcm which is a more negative effect than calculated by ERANOS.

Table V.3.4: SVRE in the total voided configuration of the ASTRID CFV corrected of the deterministic and modelling bias

	CC (pcm)	LC (pcm)	$\Delta\rho_{Na}$
C1	1058.7	-357.9	700.8
C2	735.9	-369.7	366.2
FCAM	394.8	-40.7	354.1
SPLN	498.6	-2525.0	-2026.4
Total	2688.0	3293.3	-605.3

Then, these values are corrected using the adjustment between the experiments and TRIPOLI-4®. Values have been obtained with the following experiments:

- PRE-RACINE 2A, PRE-RACINE-2B, CIRANO-2A, CIRANO-2B and BFS-115-1 results for the fuel set (α_p, β_p),
- PRE-RACINE 1 and BFS-115-1 results for the fertile set (α_p, β_p),
- BFS-115-1 results for the plenum set (α_p, β_p).

Table V.3.5: Set of parameter (α_p, β_p) by medium

	α_p	β_p
Fuel (C1 and C2)	0.8875	0.9817
Fertile (FCAM)	0.9901	1.0921
Sodium Plenum (SPLN)	0.9624	0.9403

These sets of parameters give predicted values for the CC and LC presented in the following table for a total SVRE of -670 pcm which is again more negative than calculated with TRIPOLI-4®.

Table V.3.6: SVRE in the total voided configuration of the ASTRID CFV corrected of the deterministic and modelling bias

	CC (pcm)	LC (pcm)	$\Delta\rho_{Na}$
C1	939.6	-351.4	588.2
C2	653.0	-363.0	290.0
FCAM	390.9	-44.4	346.5
SPLN	479.8	-2374.4	-1894.6
Total	2463.3	-3133.2	-669.9

Indeed the corrections on the CC are very important for the fuel medium when the corrections on the LC are quite negligible for the fuel medium. There is a need of a 9.2% increase in the fertile area for the LC but this component is very small (-40 pcm) making it negligible. For the plenum medium the correction is only about 6% but this does not compensate the previous corrections on the CC. The experimental feedback on the SVRE shows an overestimation of the CC by TRIPOLI-4® and once corrected the CFV design is then well labelled with a SVRE more negative than calculated.

V.3.2.2 Uncertainties of the corrections

In the process of calculating the experimental-calculation discrepancy on the central component and the leakage component (see Chapter IV), the experimental uncertainties associated to the reactivity measurements and the statistical uncertainties due to TRIPOLI-4® are transferred to the CC and LC. In such a process the conservative way is the easiest one to implement:

$$\left(d\alpha_p, d\beta_p\right) = \frac{\sqrt{\sum_i \left(\left(d\alpha_i . R_{CC,i}\right)^2, \left(d\beta_i . R_{CC,i}\right)^2\right)}}{\sqrt{\sum_i \left(R_{CC,i}, R_{LC}, i\right)^2}} \quad \textbf{3.5}$$

which gives us the following uncertainties on the set of parameters of each medium:

Table V.3.7: Experimental and statistical uncertainties on the set of parameter (α_p, β_p)

	$d\alpha_p$	$d\beta_p$
Fuel (C1 and C2)	0.048	0.045
Fertile (FCAM)	0.050	0.074
Sodium Plenum (SPLN)	0.059	0.018

V.3.3 Conclusion

The experimental feedback of the PRE-RACINE, CIRANO and BFS programmes show that ERANOS and TRIPOLI-4® when using the JEFF-3.2 nuclear data, overestimates the CC, especially in the fuel medium. While the LC is well calculated for inner fertile and fuel areas exception made of a small overestimation for the LC of the sodium plenum but this compensating effect is not enough to balance the decrease of the CC in the fuel. But only one experiment has been taken into account for this result and it will be better to corroborate this one with other experiments (for instance in the future GENESIS experimental programme in MASURCA see Chapter IV section 2.4). The results of the experimental feedback are summed up in the following table:

Table V.3.8: Set of parameter (α_p, β_p) by medium and its associated uncertainties

	α_p	$d\alpha_p$	β_p	$d\beta_p$
Fuel (C1 and C2)	0.8875	0.048	0.9817	0.045
Fertile (FCAM)	0.9901	0.050	1.0921	0.074
Sodium Plenum (SPLN)	0.9624	0.059	0.9403	0.018

This shows a good agreement with TRIPOLI-4® on the LC (ERANOS gives similar results) and a slight overestimation of the CC but this is included in 1σ uncertainty.

In addition to the experimental uncertainty (and statistical due to the use of TRIPOLI-4®) presented in the previous table 3.7, the nuclear data uncertainty on each component has to be considered as seen in **section 3.1**

Table V.3.9: Nuclear data relative uncertainties on each component of the SVRE of the CFV

Configuration	Relative uncertainty		
	Δρ	**CC**	**LC**
CFV Total Void	18.1%	2.6%	2.0%
CFV Sodium plenum Void	1.9%	2.1%	1.4%
CFV Fuel Void	5.3%	3.0%	5.1%
CFV Fertile Void	3.1%	2.3%	17.3%

Since, correction factors and experimental uncertainties are available for each medium and not for the overall total void reactivity effect, we use the adjustment procedure as described in **section 3.2.1.1** to get the uncertainties on the total void reactivity effect with equation 3.5.

$$(\alpha_d \pm d\alpha_d, \beta_d \pm d\beta_d) = (0.969 \pm 0.031\,, 0.995 \pm 0.021\,) \qquad \textbf{3.6}$$

These uncertainties of 3.1% and 2.1% on the components (α_d, β_d) of the total void reactivity effect have been calculated by taking into account the nuclear data uncertainty on each component of the SVRE of 4 different voided zones of the ASTRID CFV core.

This shows a good agreement between TRIPOLI-4® on the LC and a slight overestimation of the CC by TRIPOLI-4® but this is included in 1σ uncertainty.

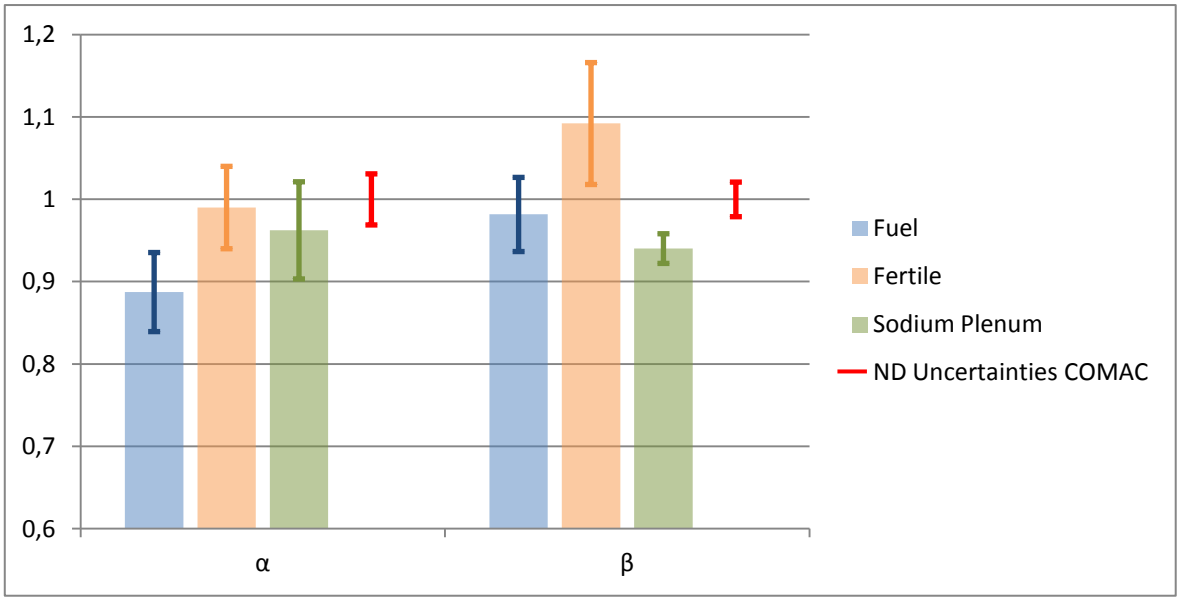

Figure V.3.1: Comparison of the predicting set of parameters (α_p, β_p) by media in regard of the nuclear data and experimental uncertainties

This **Figure V.3.1** shows that the JEFF-3.2 nuclear data and "experimental" uncertainties (also taking into account the statistical ones) do not explain all the discrepancies given by the bias on the CC of the fuel medium and on the LC of the sodium plenum. It appears obvious that an underestimation of the nuclear data uncertainties with COMAC-V2 is occurring. For the LC as only one experiment has been used, this discrepancy could be due to an underestimation of the experimental uncertainty.

References

[1] V. Huy, 'Contribution to nuclear data improvement by assimilation of integral experiments for the ASTRID core neutronic characterization', Aix-Marseille, 2018.
[2] P. Dufay and G. Rimpault, 'A new approach for analysing the impact of nuclear data uncertainties on the ASTRID sodium void reactivity effect', presented at the PHYSOR 2018: Reactor Physics paving the way towards more efficient systems, Cancun, Mexico, 2018.
[3] P. Dufay, 'Development of the nuclear data sensitivity calculations with the GPT method of SVRE central components. Transferability from the PRE-RACINE cores to the ASTRID core', in *BEPU2018-254*, Real Collegio, Lucca, Italy, 2018.
[4] T. Frosio, P. Blaise, and T. Bonaccorsi, 'Impact of correlations between core configurations for the evaluation of nuclear data uncertainty propagation for reactivity', *EPJ Nucl. Sci. Technol.*, vol. 3, p. 6, 2017.
[5] P. Archier, C. De Saint Jean, G. Noguere, O. Litaize, P. Leconte, and C. Bouret, 'COMAC: Nuclear Data Covariance Matrices Library for Reactor Applications', presented at the PHYSOR 2014- The Role of Reactor Physics toward a Sustainable Future, Kyoto, Japan, 2014.
[6] M. Maxence, 'Caractérisation des Effets Spatiaux dans les Grands Cœurs RNR : Méthodes, Outils et Etudes', Thèse, Université d'Aix Marseille, 2016.

This page has been left blank intentionally

Chapter VI: General conclusions and Perspectives

Introduction

This chapter compiles the conclusions of this PhD work on nuclear data, uncertainty quantifications and corrections for the effective delayed neutron fraction (Chapter III) and on the Sodium Void Reactivity Effect (SVRE) (Chapter IV and V). It outlines the progresses of this PhD work and gives perspectives for further work on these both topics.

The objective of this PhD thesis is to master the different sources of uncertainties in calculating the sodium void reactivity effect and use the integral experiments to predict the sodium void reactivity effect of the CFV core of ASTRID as well as its uncertainty.

In the various experimental programmes considered, the sodium void reactivity effect (SVRE) is measured for zones of different sizes in order to vary the relative importance of central and leakage components. This reactivity is measured on a β_{eff} scale which is the effective delayed neutron fraction of the reactor. A new analysis of β_{eff} measured in the BERENICE programme (in the MASURCA facility) has been made using the TRIPOLI4® Monte Carlo with the newly Iterated Fission Probability (IFP) method for calculating integrals. It allows revisiting more precisely the experiments dedicated to sodium void reactivity measurements.

For analysing the sodium void reactivity effect, we split it into two components: the central component (CC) which is a positive reactivity effect due to spectrum changes and the leakage component (LC) which is a negative reactivity effect due to the increase of the neutron mean free path and, thus, neutron leakage. In order to study in detail the uncertainty associated to the SVRE, a development of an innovative generalized perturbation theory procedure for computing sensitivities of the CC and the LC has been conducted. Using both a deterministic and a stochastic approach, is mandatory because even if the Monte-Carlo code such as TRIPOLI-4® gives reference results by using "as-built" geometry of the core the generalized perturbation has not been implemented yet in this code [1].

Once simulations have been run for each experimental programme it is possible to adjust the results from ERANOS and TRIPOLI-4® to experimental ones. Independent adjustment according to the fuel composition and the core geometry lead to a set of parameter (α,β) to correct the CC and LC of the SVRE of the CFV core of the ASTRID plant. This SVRE best-estimate value is associated to certified uncertainties.

Contents

VI.1 Conclusion on nuclear data

VI.1.1 For the delayed neutron fraction

The analysis of the measurements made during the BERENICE programme (see Chapter III) using the latest developments in the stochastic code TRIPOLI-4® has lead to new C/E (with JEFF-3.2 nuclear data):

- with improvements for Uranium fuel based cores for the results with the ^{252}Cf source method, the C/E ratio goes from: 0.9466 to 1.0035 for the R2 reference core
- with improvements for U-Pu fuel based cores for the results with the noise method, the C/E ratio goes from: 1.0664 to 1.0125 for the ZONA2 core.

The experimental uncertainties have been studied during V. Zammit PhD and have been updated in this one taking into account the statistical uncertainty on the series of measurements, the following table summarises up the results according to the method used and for each core of the experimental programme:

Table 1.1: experimental relative uncertainties on the β_{eff}

Cores	Relative uncertainties on β_{eff} (in %)	
	Cf 252 method	**Noise method**
ZONA2	3.54	2.23
R2 ref	3.41	-
R2 exp	3.62	2.69

Furthermore the sensitivity and uncertainty analysis on the effective delayed neutron fraction using the deterministic code ERANOS has lead to an uncertainty of:

- 2.6% on the β_{eff} for Uranium fuel based cores with JEFF-3.2 nuclear data and COMAC-V2 covariance data.
- 2.8% on the β_{eff} for U-Pu fuel based cores with JEFF-3.2 nuclear data and COMAC-V2 covariance data

The main source of uncertainty due to nuclear data are the ones on the fission cross-section and on neutron emission yield per fission especially the one of ^{238}U and ^{239}Pu.

VI.1.2 For the Sodium Void Reactivity Effect

The analysis of PRE-RACINE, CIRANO and BFS experimental programmes where many different voided configurations have been built to allow a critical analysis on the quality of some nuclear data (see Chapter IV). Indeed some voided configurations emphasise the Leakage Component (LC) whereas others emphasise the Central Component (CC) which are not sensitive to the same nuclear data. The LC is more sensitive to fission neutron spectrum, capture cross-section when the CC is also sensitive to these nuclear data but even more to elastic scattering cross-section especially the one of the sodium. The comparison of calculated results (with TRIPOLI-4® and ERANOS) to experimental results show that:

- Voided configurations in fertile areas are well calculated with JEFF-3.1.1 and JEFF-3.2

- Voided configurations in fuel media are not well calculated with JEFF-3.2 and when the LC is important JEFF-3.1.1 is also inconsistent.
- The voided plenum configuration in BFS-115-1 is better calculated with JEFF-3.2 than with JEFF-3.1.1.

Thus the main sources of errors are:

- In the JEFF-3.2 set of evaluations, nuclear data of ^{235}U and Plutonium are responsible of the SVRE discrepancies in the PRE-RACINE and CIRANO cores,
- The sodium nuclear data in JEFF-3.1.1 is the main responsible of the important discrepancies in the BFS results.

VI.2 Corrections and uncertainties for the Sodium Void Reactivity Effect

VI.2.1 Uncertainties quantifications

The sensitivity and uncertainty analysis have shown that independent analysis of the CC and LC can be conducted because the correlation between the two sensitivity sets is almost null or very low. Indeed according to the voided configuration for the ASTRID CFV core the correlation vary between: 0.002 and -0.26 (see Chapter V).

The results on the relative uncertainty due to nuclear data on the CC or the LC (when their values are significant) shows a nearly constant behaviour according to the voided configuration in opposition to the behaviour of the relative of the uncertainty due to nuclear data on the SVRE.

The nuclear data uncertainties calculated with JEFF-3.2 nuclear data and the COMAC-V2 covariance matrix, on the ASTRID CFV core are summed up in the following table according to the voided configuration:

Table 2.1: Nuclear data uncertainties for ASTRID CFV SVRE

Configuration	Uncertainty (in pcm)			Relative uncertainty		
	Δρ	CC	LC	Δρ	CC	LC
CFV Total Void	96.8	71.0	65.7	18.1%	2.6%	2.0%
CFV Sodium plenum Void	35.6	9.9	34.7	1.9%	2.1%	1.4%
CFV Fuel Void	60.5	54.2	35.3	5.3%	3.0%	5.1%
CFV Fertile Void	10.1	8.7	8.4	3.1%	2.3%	17.3%

VI.2.2 Corrections for the SVRE

The series of adjustment of the CC and LC calculated with ERANOS with the experimental SVRE and of the CC and LC calculated with ERANOS with the SVRE calculated with TRIPOLI-4® made in the Chapter IV for each experimental programme allow to get a set of parameters (α_p, β_p) to correct the TRIPOLI-4® SVRE of the total voided configuration of the ASTRID CFV core by taking into account the representativity of each experimental core with the CFV core. Firstly the deterministic and modelling bias has to be corrected and this is done by getting a set of parameters (α_d, β_d) with the adjustment of the CC and LC calculated with ERANOS for different voided configuration of the ASTRID CFV core with the SVRE calculated with TRIPOLI-4®:

$$(\alpha_d \pm d\alpha_d, \beta_d \pm d\beta_d) = (0.969 \pm 0.031\,, 0.995 \pm 0.021\,) \qquad \textbf{2.1}$$

The uncertainty given for the set of parameters takes into account the statistical uncertainty on the TRIPOLI-4® results and the uncertainty due to nuclear data. Then the SVRE of the total voided configuration of the CFV core is broken down by medium: fuel, fertile and plenum. Indeed in the different experimental cores the voided configurations have been made in different media then each experimental core bring different information on the CC and LC according to the medium voided. Thus a set of parameter (α_p, β_p) is calculated for each medium: fuel, fertile and plenum, using the:

- PRE-RACINE 2A, PRE-RACINE-2B, CIRANO-2A, CIRANO-2B and BFS-115-1 results for the fuel set (α_p, β_p),
- PRE-RACINE 1 and BFS-115-1 results for the fertile set (α_p, β_p),
- BFS-115-1 results for the plenum set (α_p, β_p).

These sets are given in the following table:

Table 2.2: Predicting set of parameter according to the experimental feedback

	α_p	$d\alpha_p$	β_p	$d\beta_p$
Fuel (C1 and C2)	0.8875	0.048	0.9817	0.045
Fertile (FCAM)	0.9901	0.050	1.0921	0.074
Sodium Plenum (SPLN)	0.9624	0.059	0.9403	0.018

and the predicted values for the CC and LC presented in the following table give a total SVRE of -670 pcm which is more negative than the one calculated with TRIPOLI-4®. The overall uncertainty on each set of parameter takes into account the experimental uncertainties of each configuration of each core of each programme.

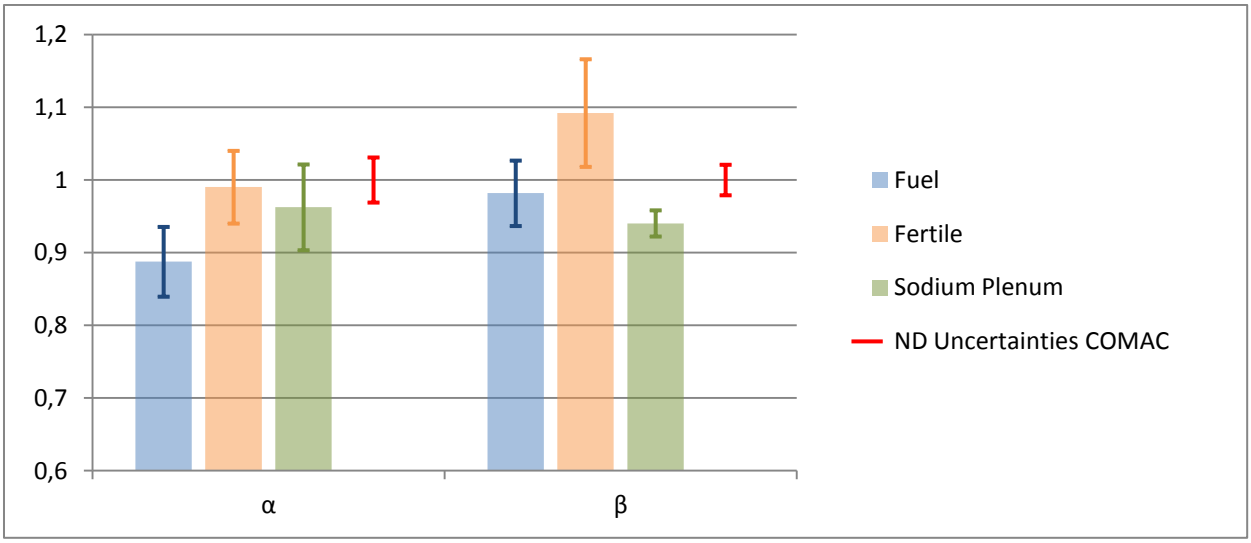

Figure 2.1: Comparison of the predicting set of parameters (α_p, β_p) by media in regard of the nuclear data and statictical uncertainties

This **Figure 2.1** shows that the nuclear data and "experimental" uncertainties (also taking into account the statistical ones) do not fully explain the discrepancies given by the bias on the CC of the fuel medium and on the LC of the sodium plenum. It appears obvious that an underestimation of the nuclear data uncertainties with COMAC-V2 is occurring. For the LC as only one experiment has been used, this discrepancy could be due to an underestimation of the experimental uncertainty.

VI.3 Perspectives

VI.3.1 For the delayed neutron fraction

Currently the delayed neutron covariances used in COMAC-V2 are coming from the covariance matrix of the Japanese library JENDL4. A work is ongoing at the LEPh of Cadarache by a PhD student Daniela FOLIGNO in order to get a new evaluation of the delayed neutrons constants of each family of precursors (see Chapter III) but also to evaluate their uncertainty and to produce covariances.

The need of other integral experiments with β_{eff} measurements is also outlined since experimental uncertainties with the noise technique are larger than the uncertainty induced by the nuclear data uncertainties. Also, the Cf252 technique remains reliable but the noise technique produces better results with less experimental uncertainties. An improved noise technique is under study at Cadarache in order to reduce the experimental uncertainty and it could be used in the GENESIS programme.

VI.3.2 For the SVRE

The experimental data base for this work includes the PRE-RACINE, CIRANO experimental programmes from the MASURCA facility and the BFS-1 experimental programme. An extension to other experimental programmes has been considered such as SNEAK 9B and 9C2 programmes, ZPR6, ZPPR2 and ZPPR10 programmes. This could bring information on the SVRE, CC and LC of the fuel area but not on the sodium plenum. For the sodium plenum, new measurements are planned at the BFS facility in another experimental configuration. Also the GENESIS programme in support of the CFV core design has been drawn and would possibly take in the MASURCA facility refurbished.

A work has been performed at LEPh by the PhD student Virginie HUY on the nuclear data for improving actinides nuclear data by assimilation of integral experiments. And a future work could be to calculate the feedback of this assimilation work on the SVRE and evaluate the nuclear data uncertainty after this assimilation. Since this assimilation work has been using critical mass and spectral indices, it might be interesting to supplement it with sodium void reactivity experiments. Then new assimilation work could be done so as to better predict the sodium void reactivity coefficient both on ^{23}Na but also on actinides whose contribution is mainly due to the energy slope of the fission and capture cross sections at high energy.

CEA is also moving from the deterministic code ERANOS to the APOLLO3-RNR code. APOLLO3 will replace ERANOS (deterministic code for fast reactors) and APOLLO2 (deterministic code for thermal reactors) in the same solver platform. The specificities of SFR computational tools are studied with the PhD student Bastien FAURE. When sensitivity procedures will be available in APOLLO3, the same work of experimental validation and of uncertainty quantification of the SVRE for the ASTRID CFV core will be possible.

References

[1] G-H Nuria and al, ‘Nuclear data sensitivity and uncertainty assessment of sodium voiding reactivity coefficients of an ASTRID-like sodium fast reactor’, ND 2016

Appendix A: Experimental programmes

1 MASURCA

1.1 The experimental facility

Figure 1.1: MASURCA reactor buildings

The experimental facility of MASURCA has been commissioned in 1966 in order to conduct experimental programmes in support of Fast Reactors development. Located in the CEA Cadarache centre this facility has a thermal power of 5 kW, the in-core temperature is about 25°C and it is cooled by air. The main asset of this facility is its high flexibility indeed the steel assemblies of a square base of 10.6x10.6 cm dimension can be filled with discs or rodlets according to a defined pattern. Studies on different: fuel (Uranium; Plutonium, …), diluant (Sodium, graphite, …), core configurations (fertile blanket, reflector, …), kinetic parameters, etc have been performed until the beginning of its refurbishment in 2006. Furthermore the fuel inventory is important and very diversified which combined with the ability to put different moderator allows getting different neutron spectrum. Since 2011 the facility has been refurbished in order to match the new safety standard since the Fukushima accident [1].

The assemblies of MASURCA (see **Figure 1.3**) have defined patterns with 64 rodlets, it exists three series of fuel patterns (see **Figure 1.2**): the R series made of metallic enriched uranium with sodium and ferrite diluent, the Z series is the twin of the R series but with metallic U-Pu fuel and the ZONA series is made of oxide U-Pu fuel with sodium. The first fuel cell of each series has fertile rodlets made of depleted uranium with a ratio of 1 fertile rodlet for 3 fuel rodlets. In the fuel inventory there some different U-Pu vector, three are used in the studied programmes: the POA, PIT and P2A which are made of:

- ZONA-POA: with 8% of ^{240}Pu/Pu and less than 1% of (^{241}Pu+^{241}Am)/(Pu+Am),
- ZONA-PIT: with 18% of ^{240}Pu/Pu and about 4% of (^{241}Pu+^{241}Am)/(Pu+Am),
- ZONA-P2A: with 18% of ^{240}Pu/Pu and about 8% of (^{241}Pu+^{241}Am)/(Pu+Am),
- ZONA-P4K: with 45% of ^{240}Pu/Pu and about 8% of (^{241}Pu+^{241}Am)/(Pu+Am).

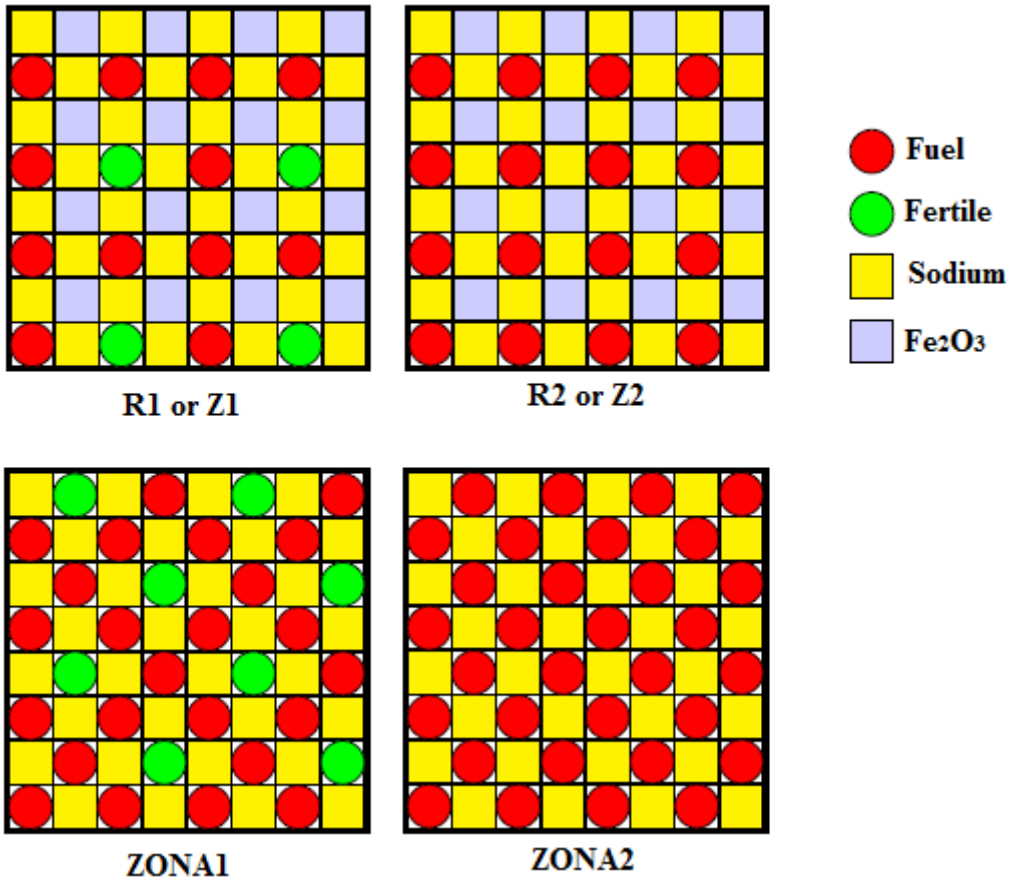

Figure 1.2: Fuel cells used in MASURCA

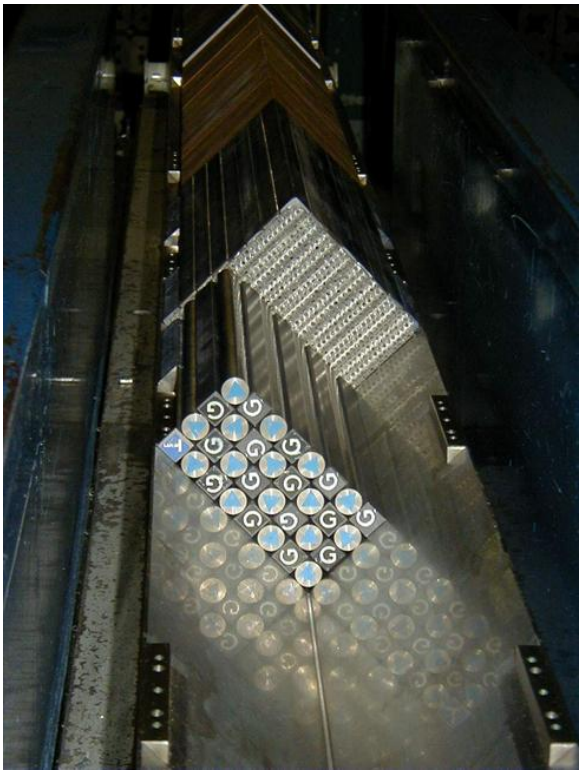

Figure 1.3: Steel assembly of MASURCA with 32 rodlets at the forefront on a diffusor

1.2 The BERENICE programme

The Beta Effective Reactor Experiment for a New International Collaborative Evaluation (BERENICE) programme has been conducted between 1993-1994 for experimental measurements of β_{eff} with two different fuels:

- R2 cores with enriched uranium
- ZONA2 core with 90.7% of PIT cells and 9.3% of POA cells.

Two cores with R2 fuel cells have been built, the first one is called "reference" because it is an homogeneous core surrounded by fertile blanket. The other one is the twin of the "R2 ref" core but it has four big axial channels in the fuel area (see **Figure 1.4**) and is called the "R2 experimental core".

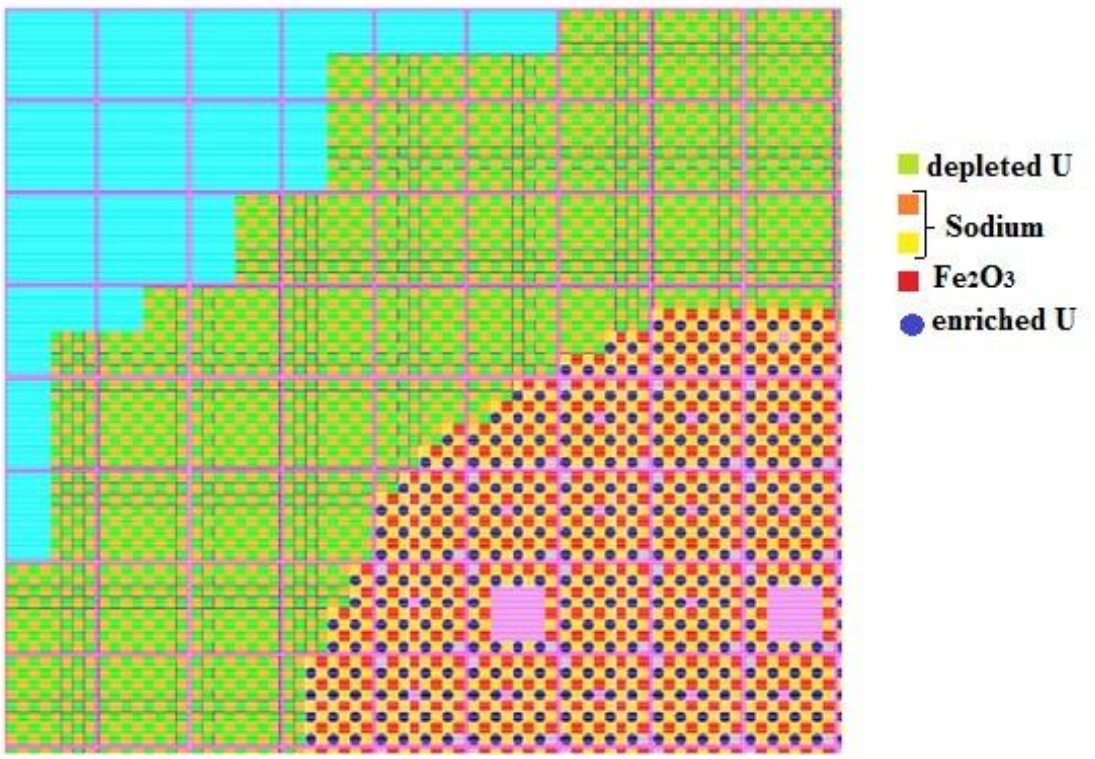

Figure 1.4: ¼ of the R2 experimental core with two axial channels (rose squares)

As descripted in Chapter III three experimental methods have been used, the ^{252}Cf source method, the Noise method and the α-Rossi method but only the results of first two are presented in this Chapter III because the α-Rossi method gave poor results (a discrepancy greater than 7% with no consistency within the 3σ confidence interval).

These three cores have been modeled in RZ geometry: the four axial channels have been homogenized meaning that a greater radius of the fuel area is needed to get enough reactivity reserve with this core. The diffusor with placed at the top and the bottom of the fuel area is also represented (between Z 30.48 and 31.28 cm) this piece is here to improve the air circulation in the core.

1.2.1 R2 reference and experimental cores

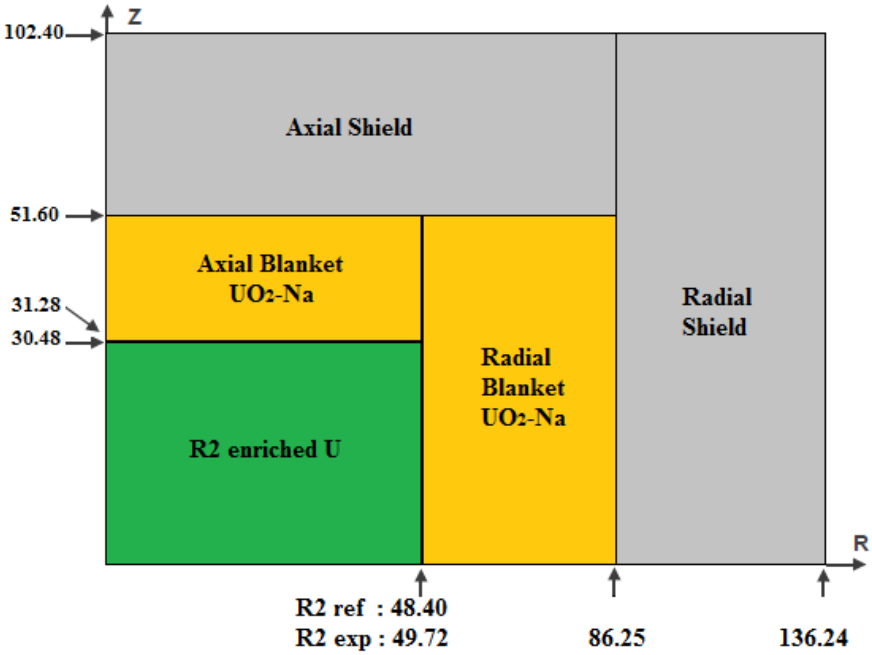

Figure 1.5: RZ model of R2 cores (dimensions in cm)

These two cores have been built using enriched Uranium fuel and are surrounded fertile blanket of sodium and depleted uranium.

1.2.2 ZONA2 core

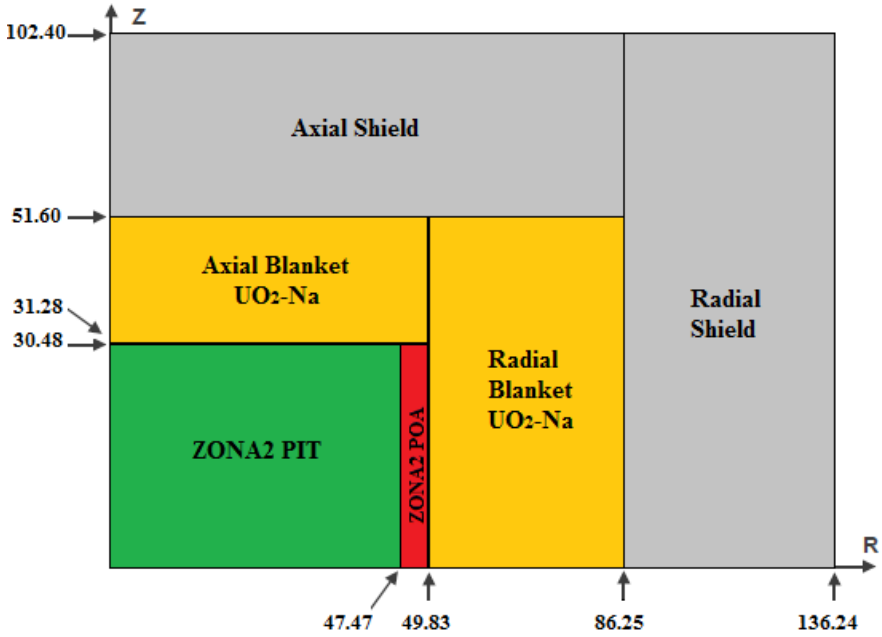

Figure 1.6: RZ model of ZONA2 core (dimensions in cm)

The ZONA2 core is using U-Pu fuel of mainly PIT type and a bit of POA type and it is also surrounded by fertile blanket of sodium and depleted uranium.

1.3 The PRE-RACINE programme

The first programme studied from the MASURCA experiments is the PRE-RACINE programme, conducted between the years 1976 and 1979 it studied the design of heterogeneous cores with inner fertile block and fertile blankets. Numerous voided configurations have been made during this programme the idea is to get different contributions from the central and the leakage components. The axial configurations are presented in the following **Figure 1.7**.

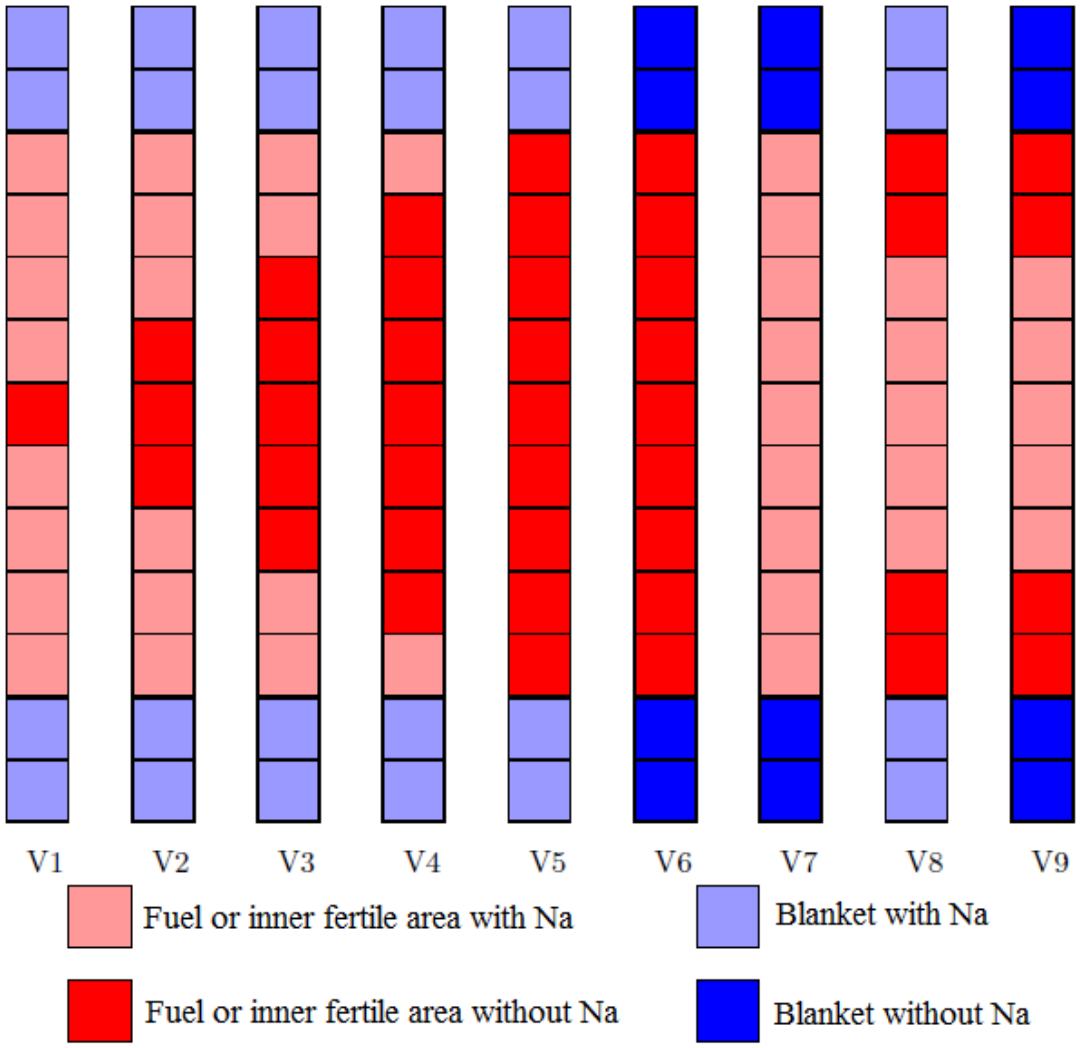

Figure 1.7: Axial voided configuration

The V1-V4 points out the central component when the V6-V9 points out the leakage one; with the V5 configuration a rather balanced situation is reached between these two components.

1.3.1 PRE-RACINE I

The first core built during the PRE-RACINE programme is very heterogeneous because it has an inner fertile area composed of depleted uranium plus a fuel area of U-Pu fuel of POA type and an outer area of enriched uranium fuel R1. The core is surrounded by fertile blanket using depleted uranium mixed with sodium or not. Two radial voided configurations have been done in this core: the first one the sodium is removed in a radius between 0 and 7.33 cm and the last one the sodium is removed in a radius between 0 and 11.96 cm.

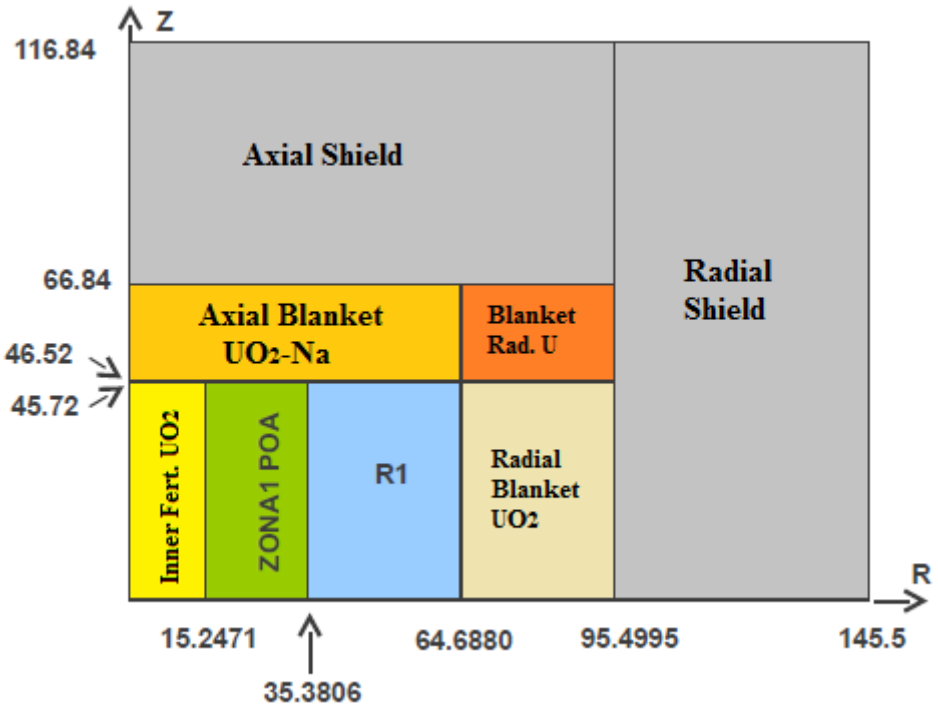

Figure 1.8: RZ model of the PRE-RACINE I core (dimensions in cm)

1.3.2 PRE-RACINE 2A

The second core built during this programme is also heterogeneous like the previous one and it is composed of an inner fuel area of U-Pu of POA and P2A type plus an outer fuel area of enriched uranium R1. The core is surrounded by fertile blanket using depleted uranium mixed with sodium or not.

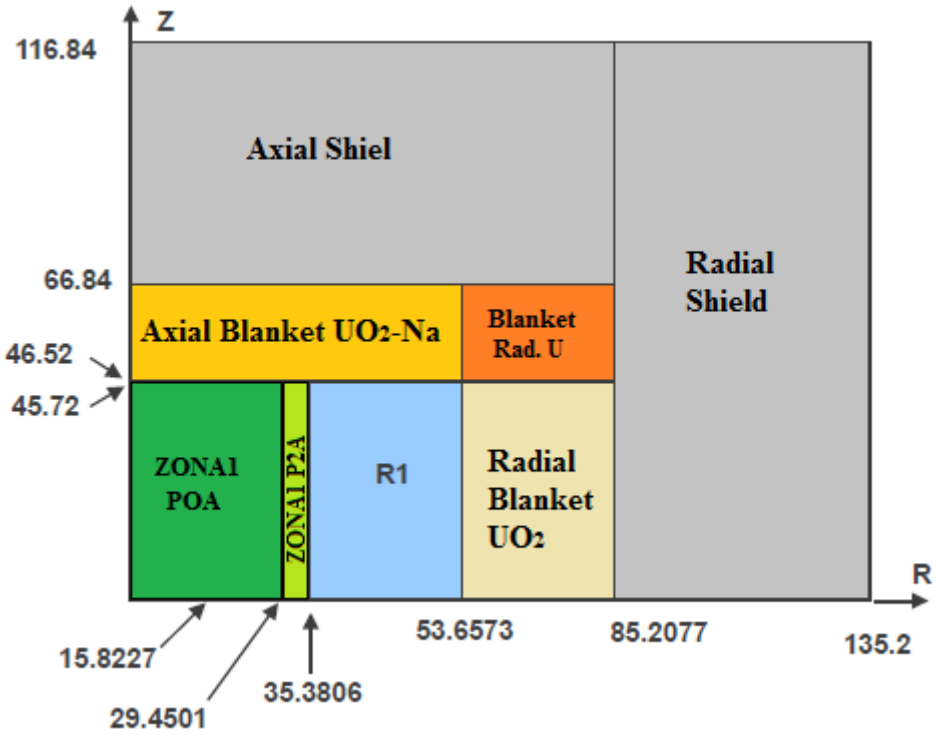

Figure 1.9: RZ model of PRE-RACINE 2A core (dimensions in cm)

Three radial voided configurations have been studied in this core: the first one the sodium is removed in a radius between 0 to 11.96 cm, the second one the sodium is removed in a radius between 0 to 19.83 cm and the last one the sodium is removed in a radius between 0 and 29.45 cm.

1.3.3 PRE-RACINE 2B

The third core built during this programme is the twin of the previous one and it composed of an inner fuel area of U-Pu of PIT and P2A type plus an outer fuel area of enriched uranium R1. The core is surrounded by fertile blanket using depleted uranium mixed with sodium or not.

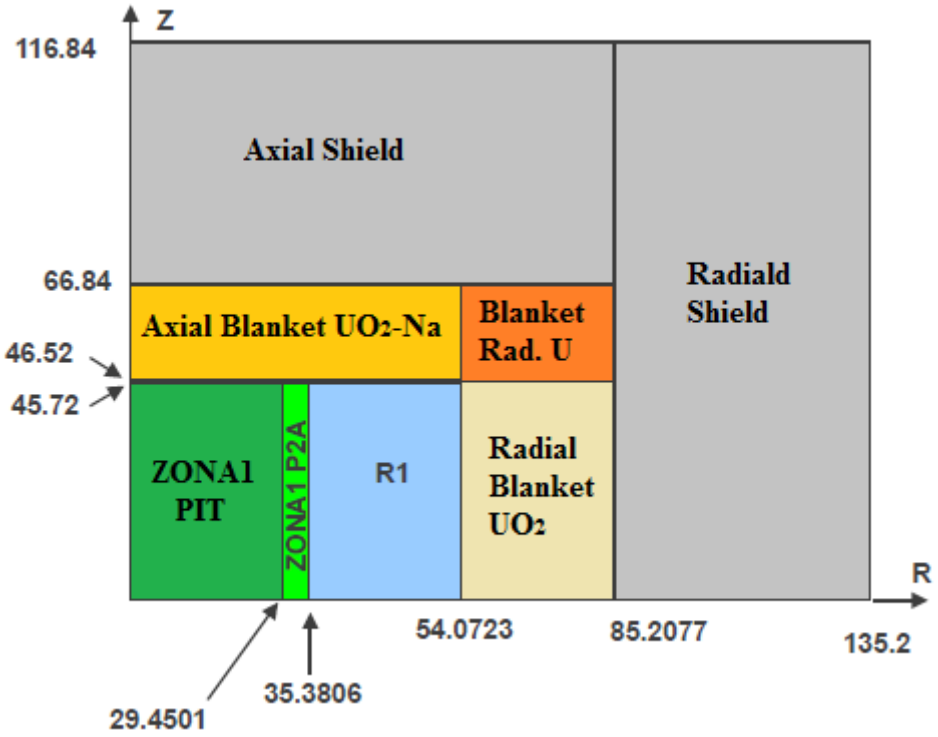

Figure 1.10: RZ model of PRE-RACINE 2B core (dimensions in cm)

Three radial voided configurations have been studied in this core: the first one the sodium is removed in a radius between 0 to 11.96 cm, the second one the sodium is removed in a radius between 0 to 19.83 cm and the last one the sodium is removed in a radius between 0 and 29.45 cm.

1.4 The CIRANO programme

The CIRANO programme has been conducted between 1994 and 1997 to study cores having the ability to burn plutonium because since 1992 and the French adhesion to the Non Proliferation Treaty (non proliferation treaty), MASURCA cannot produce more plutonium than it can burn. Then during this programme:

- one core have a steel reflector instead of fertile blanket (where ^{239}Pu is produced from ^{238}U),
- the fuel used is highly enriched in plutonium with ZONA2 cells fuel,
- the cores built have smaller heights than before.

The height goes from 45.72 cm to 30.48 cm which decreases the number of possible axial voided configurations (see **Figure 1.11**) and only fuel areas have been voided.

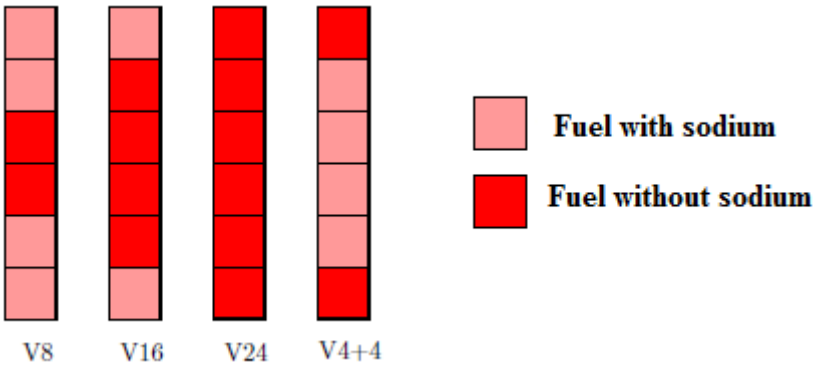

Figure 1.11: Axial voided configurations in CIRANO

1.4.1 ZONA2A

The first core built during this programme is ZONA2A and it is composed of U-Pu fuel of PIT (90.4% of the tubes) and POA (9.6% of the tubes) type and it is surrounded by fertile blanket made of depleted uranium and sodium.

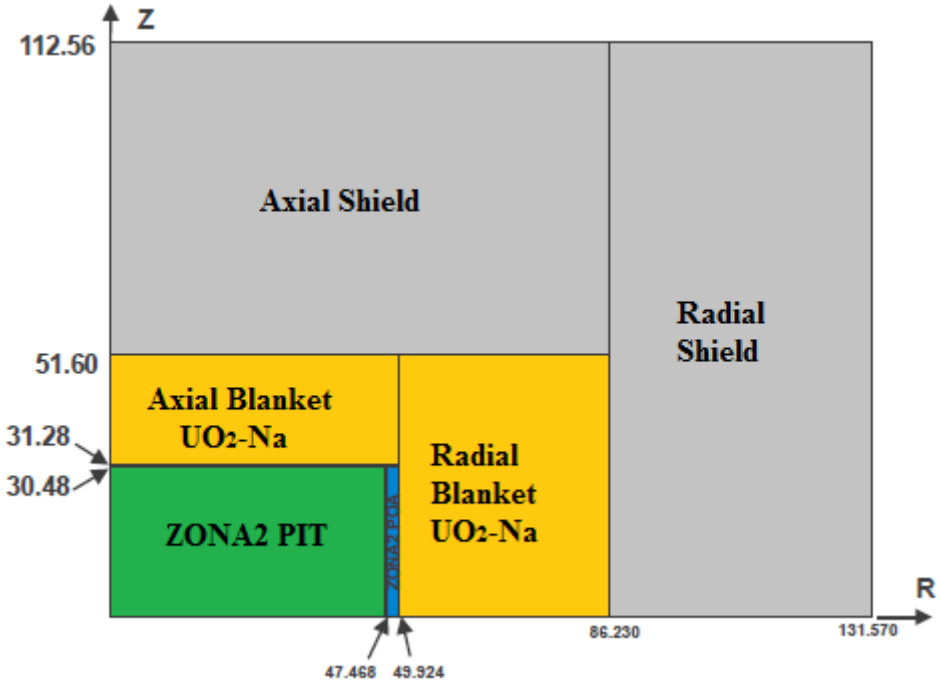

Figure 1.12: RZ model of ZONA2A core (dimensions in cm)

In this core only one radial voided configuration have been made: it was the four central tubes which have been voided and this is equivalent to remove the sodium from 0 to 11.96 cm.

1.4.2 ZONA2B

The first core built during this programme is ZONA2A and it is composed of U-Pu fuel of PIT type and it is surrounded by a reflector made of steel and sodium.

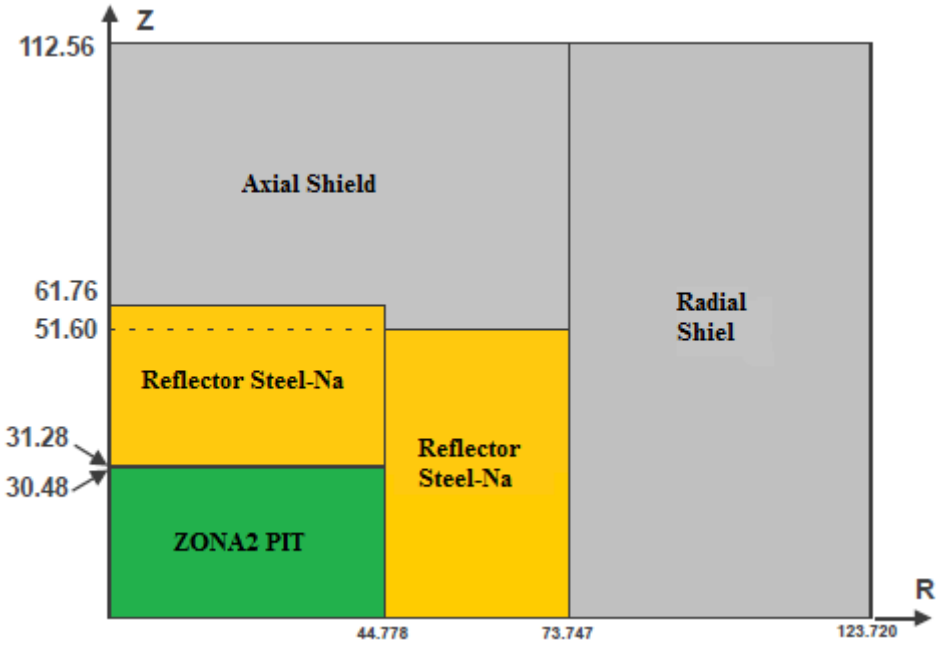

Figure 1.13: RZ model of ZONA2B core (dimensions in cm)

In this core only two radial voided configurations have been made: it was the four central tubes which have been voided and this is equivalent to remove the sodium from 0 to 11.96 cm and the 12 central tubes and this is equivalent to remove the sodium from 0 to 20.72 cm.

2 BFS

2.1 The experimental facility

The collaboration between the CEA and the IPPE[1] has lead to a common experimental programme conducted in the BFS[2] facility at Obninsk between 2013 and 2017. The BFS facility has been operational in 1969 and the facility is very flexible then experiments can be designed with many different configurations and measurements of kinetic parameters are also easily implemented [2]. The BFS facility used hexagonal assemblies made with cells which are built by stacking discs (see **Figure 2.2**) [3]. The fuel discs used during this collaboration are very thin and it can induce heterogeneities effects on the multiplication factor or on axial reaction rate traverses.

The objective of this collaboration is to study some of the innovations of the CFV design, in first place the addition of a plenum sodium on the core and of an inner fertile slab in the core.

[1] Institute for Physics and Power Engineering named after A. I. Leypunsky
[2] From the Russian for « Big Physical Facility »

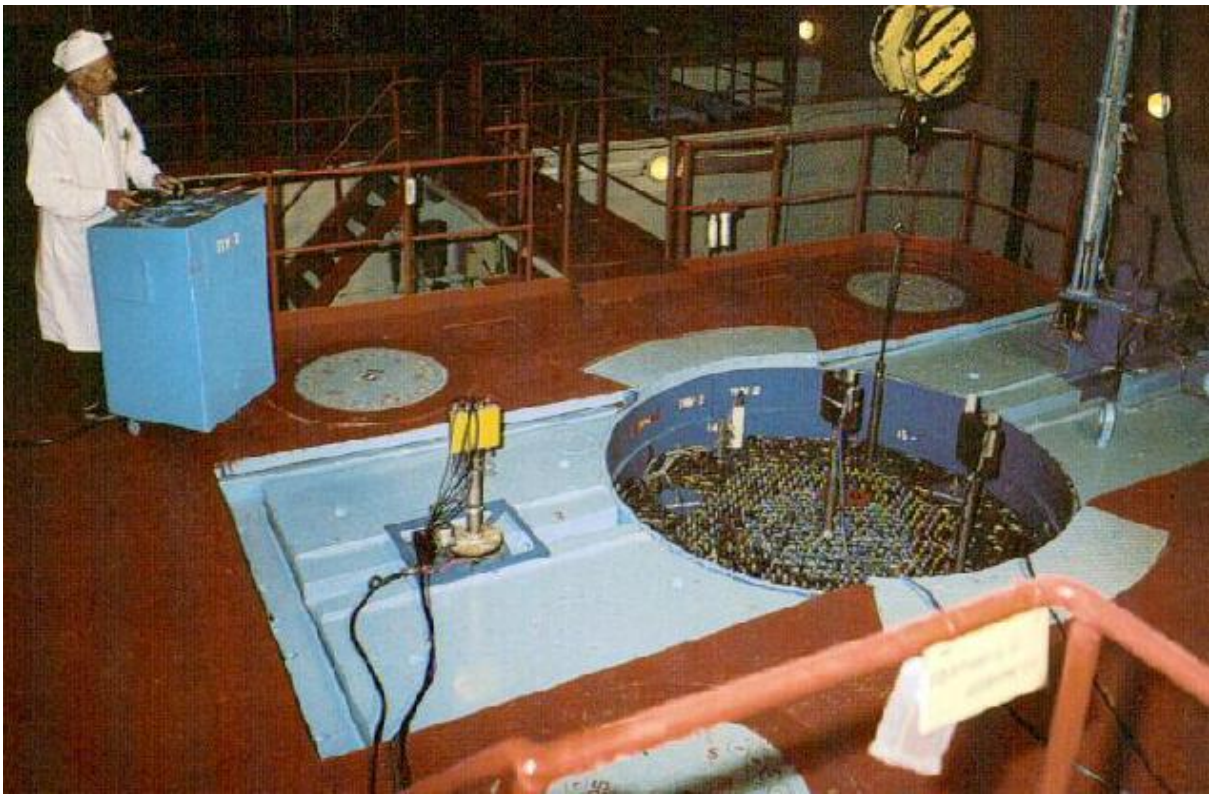

Figure 2.1: View from the top of the core of BFS-1

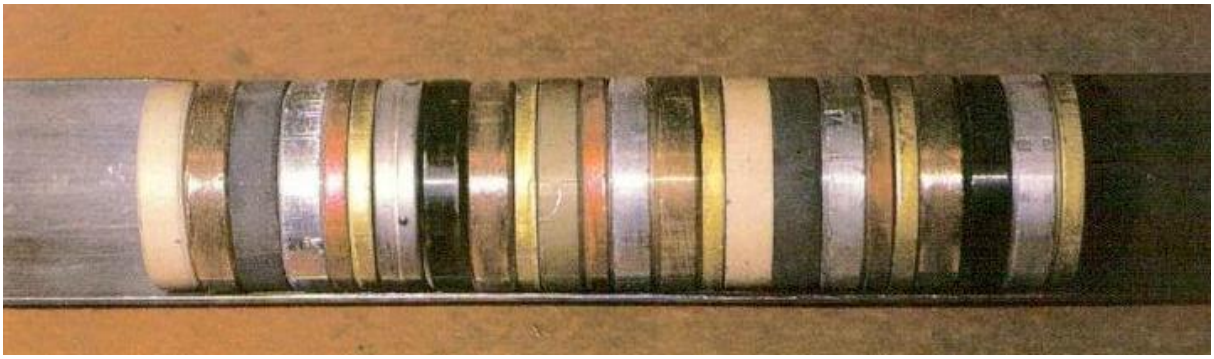

Figure 2.2: stacking of discs in an assembly of BFS

2.2 The BFS-115-1 core

The BFS-115-1 core is made of an inner core composed of U-Pu fuel (highly enriched in ^{239}Pu/Pu) with an inner fertile slab made of depleted uranium and sodium, a plenum sodium sits on top of this inner core, an outer core higher than the inner one (as in CFV design see Chapter IV) but without plenum sodium on it and only fertile shielding made of depleted uranium and the outer core is surrounded by a steel reflector (see **Figure 2.3**). Three different axial voided configurations have been studied in it (see **Figure 2.4**):

- A total voided configuration in the 91 inner tubes (which is equivalent to remove the sodium between a radius of 0 and 25.5 cm).
- A voided plenum configuration in the 91 inner tubes.
- A voided plenum and voided superior fuel configuration in the 91 inner tubes.

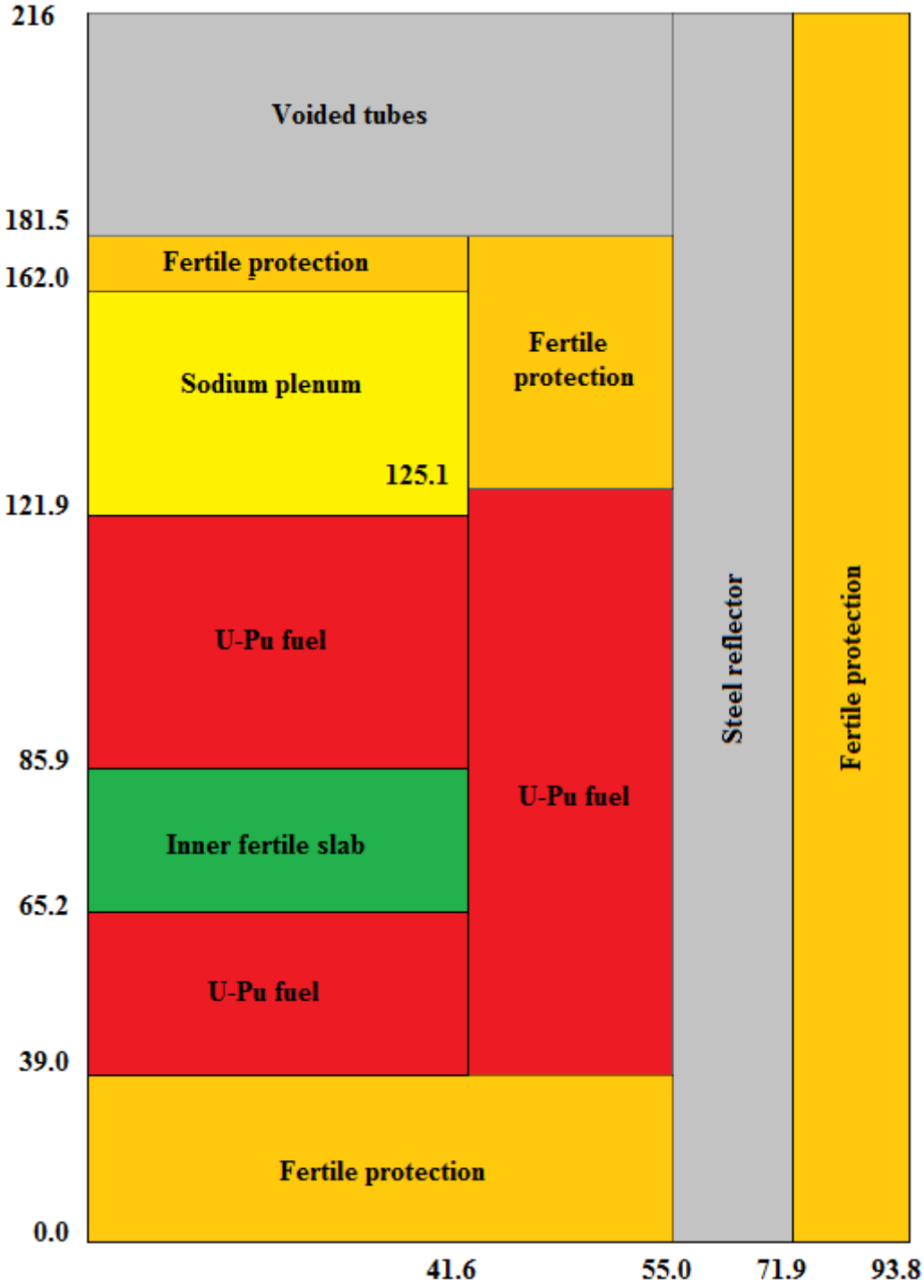

Figure 2.3: RZ model of the BFS-115-1 core (dimensions in cm)

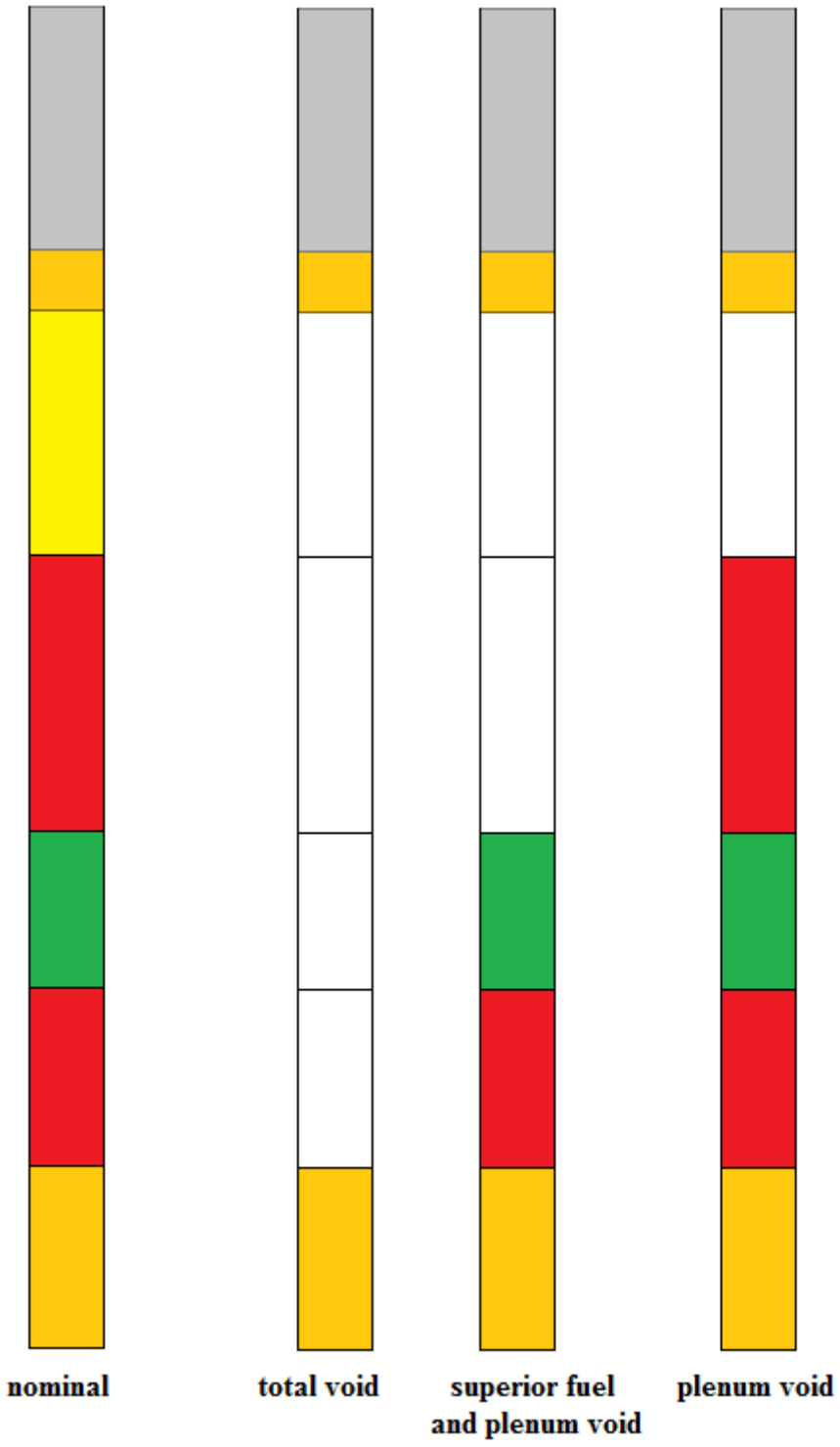

Figure 2.4: axial void configurations in BFS-115-1 core compared to the nominal configuration

The blank areas are the ones where the sodium has been removed compared to the nominal configuration.

References

[1] CEA/DEN/CAD/DIR/CSN, 'Installation MASURCA – INB 39, Evaluation complémentaire de la sûreté au regard de l'accident survenu à la centrale nucléaire de Fukushima Daiichi.' Autorité de Surêté Nucléaire.

[2] V. Dulin, I. Matveenko, E. Rozhikhin, M. Semenov, and A. Tsibulya, 'An Overview of the Experiments Performed at the BFS Facilities and Evaluated for the International Reactor Physics Experiment Evaluation Project', *Nucl. Sci. Eng.*, vol. 178, pp. 377–386, 2014.

[3] 'BFS-62-3A experiment: fast reactor core with U and Pu fuel of 17% enrichment and partial stainless steel reflector'. NEA/NSC/DOE, 2006.

Appendix A

This page has been left blank intentionally

Appendix B: Detailed sensitivities and nuclear data uncertainties on the delayed neutrons fraction

1 Sensitivities

Table 1.1: Sensitivities on the β_{eff} in R2 cores with JEFF-3.1.1 nuclear data

Isotope	Fission	Capture	Elastic	Inelastic	n.xn	Nu total	Nu delayed	Total Fission Spectrum	Total
U235	-0.219320	0.021939	-0.002418	0.006470	0.000423	-0.243128	0.780889	-0.884586	-0.539731
U238	0.192575	0.015961	-0.008638	0.024847	0.001453	0.227933	0.218814	-0.076274	0.596670
Na23	0.000000	-0.000101	0.001188	0.003811	0.000001	0.000000	0.000000	0.000000	0.004898
Fe56	0.000000	0.000410	0.000665	0.008767	0.000011	0.000000	0.000000	0.000000	0.009852
O16	0.000000	-0.001836	0.001854	-0.000056	0.000000	0.000000	0.000000	0.000000	-0.000038
Cr52	0.000000	0.000170	0.000923	0.001687	0.000002	0.000000	0.000000	0.000000	0.002782
TOTAL	-0.026745	0.036543	-0.006426	0.045526	0.001889	-0.015196	0.999703	-0.960859	0.074434

Table 1.2:Sensitivities on the β_{eff} in r R2 cores with JEFF-3.2 nuclear data

Isotope	Fission	Capture	Elastic	Inelastic	n.xn	Nu total	Nu delayed	Total Fission Spectrum	Total
U235	-0.222915	0.019723	-0.002125	0.007255	0.000762	-0.241979	0.778873	-0.886046	-0.546451
U238	0.194483	0.013938	-0.007878	0.027780	0.001883	0.230225	0.220827	-0.074702	0.606555
Na23	0.000000	-0.000093	0.000718	0.005403	0.000001	0.000000	0.000000	0.000000	0.006030
Fe56	0.000000	0.000262	0.001366	0.009758	0.000010	0.000000	0.000000	0.000000	0.011396
O16	0.000000	-0.001401	0.003980	-0.000047	0.000000	0.000000	0.000000	0.000000	0.002532
Cr52	0.000000	0.000098	0.001251	0.002235	0.000002	0.000000	0.000000	0.000000	0.003585
TOTAL	-0.028431	0.032527	-0.002689	0.052385	0.002658	-0.011755	0.999700	-0.960748	0.083648

Sensitivities for ZONA2 core are presented in the following tables:

Table 1.3: Sensitivities on the β_{eff} in ZONA2 core with JEFF-3.1.1 nuclear data

Isotope	Fission	Capture	Elastic	Inelastic	n.xn	Nu total	Nu delayed	Total Fission Spectrum	Total
U235	0.003355	0.000022	-0.000014	0.000144	0.000007	0.003809	0.013725	-0.007658	0.013391
U238	0.425221	0.002013	-0.004971	0.065215	0.002562	0.458471	0.446905	-0.057317	1.338097
Pu238	-0.000793	0.000020	-0.000003	0.000011	0.000000	-0.000707	0.000484	-0.001174	-0.002161
Pu239	-0.524822	0.010694	-0.001656	0.006810	0.000197	-0.499507	0.465296	-0.805964	-1.348951
Pu240	0.001243	0.002183	-0.000442	0.002065	0.000032	0.010663	0.042692	-0.054858	0.003578
Pu241	0.001448	0.000138	-0.000021	0.000140	0.000017	0.001389	0.027683	-0.019125	0.011668
Pu242	0.002044	0.000081	-0.000015	0.000095	0.000002	0.002344	0.003018	-0.001397	0.006171
Na23	0.000000	-0.000182	0.009951	0.011700	0.000001	0.000000	0.000000	0.000000	0.021471
Fe56	0.000000	-0.000342	0.003662	0.022234	0.000021	0.000000	0.000000	0.000000	0.025575
O16	0.000000	-0.002514	0.017490	0.000330	0.000000	0.000000	0.000000	0.000000	0.015306
Cr52	0.000000	-0.000018	0.002099	0.004873	0.000003	0.000000	0.000000	0.000000	0.006957
TOTAL	-0.092304	0.012095	0.026080	0.113617	0.002842	-0.023537	0.999802	-0.947494	0.091100

Table 1.4: Sensitivities on the β_{eff} in ZONA2 core with JEFF-3.2 nuclear data

Isotope	Fission	Capture	Elastic	Inelastic	n.xn	Nu total	Nu delayed	Total Fission Spectrum	Total
U235	0.003275	0.000010	-0.000010	0.000140	0.000012	0.003746	0.013746	-0.007731	0.013187
U238	0.429162	0.001577	-0.004711	0.065140	0.003308	0.462393	0.451687	-0.055880	1.352677
Pu238	-0.000772	0.000019	-0.000003	0.000011	0.000000	-0.000686	0.000480	-0.001144	-0.002093
Pu239	-0.534791	0.010135	-0.001637	0.007152	0.000289	-0.508501	0.460062	-0.807821	-1.375111
Pu240	0.001253	0.002074	-0.000437	0.002253	0.000065	0.010778	0.043250	-0.054483	0.004753
Pu241	0.001717	0.000129	-0.000020	0.000145	0.000016	0.001688	0.027585	-0.018712	0.012548
Pu242	0.002043	0.000075	-0.000015	0.000097	0.000002	0.002339	0.002990	-0.001358	0.006174
Na23	0.000000	-0.000182	0.007454	0.017215	0.000002	0.000000	0.000000	0.000000	0.024489
Fe56	0.000000	-0.000383	0.003957	0.023188	0.000021	0.000000	0.000000	0.000000	0.026783
O16	0.000000	-0.001876	0.018846	0.000328	0.000000	0.000000	0.000000	0.000000	0.017299
Cr52	0.000000	-0.000046	0.002233	0.005886	0.000003	0.000000	0.000000	0.000000	0.008076
TOTAL	-0.098113	0.011534	0.025658	0.121556	0.003719	-0.028242	0.999799	-0.947129	0.088781

These sensitivities are given for comparative purpose, they are calculated with RZ modelisation of the core and with S_4 transport in ERANOS-2.4.

2 Nuclear data uncertainties

Uncertainties results for R2 cores:

Table 2.1: Uncertainties on the β_{eff} with JEFF-3.1.1 and COMAC-V1 in R2 cores

Isotope	Fission	Capture	Elastic	Inelastic	n.xn	Nu total	Nu delayed	Total Fission Spectrum	Total
U235	0.1516	**0.6531**	0.0600	0.0392	0.0017	0.0721	**2.2698**	0.3089	2.3868
U238	**1.2517**	0.3170	0.0504	0.2583	0.0069	0.1721	**0.7400**	0.1039	1.4785
Na23	0.0000	0.0031	0.0214	0.0134	0.0001	0.0000	0.0000	0.0000	0.0254
Fe56	0.0000	0.0135	0.0563	0.0269	0.0000	0.0000	0.0000	0.0000	0.0639
O16	0.0000	0.0510	0.0425	0.0004	0.0000	0.0000	0.0000	0.0000	0.0664
Cr52	0.0000	0.0054	0.0029	0.0024	0.0000	0.0000	0.0000	0.0000	0.0066
TOTAL	1.2609	0.7279	0.0807	0.2535	0.0071	0.1563	2.3874	0.3259	2.8093

Table 2.2: Uncertainties on the β_{eff} with JEFF-3.2 and COMAC-V2 in R2 cores

Isotope	Fission	Capture	Elastic	Inelastic	n.xn	Nu total	Nu delayed	Total Fission Spectrum	Total
U235	0.1538	**0.5844**	0.0544	0.0434	0.0031	0.0727	**2.2642**	0.3001	2.3625
U238	**0.5865**	0.1024	0.0635	0.2982	0.0447	0.1734	**0.7474**	0.1031	1.0138
Na23	0.0000	0.0027	0.0197	0.0173	0.0001	0.0000	0.0000	0.0000	0.0264
Fe56	0.0000	0.0121	0.0561	0.0297	0.0000	0.0000	0.0000	0.0000	0.0646
O16	0.0000	0.0381	0.0442	0.0004	0.0000	0.0000	0.0000	0.0000	0.0583
Cr52	0.0000	0.0052	0.0029	0.0031	0.0000	0.0000	0.0000	0.0000	0.0067
TOTAL	0.6064	0.5768	0.1118	0.3033	0.0448	0.1575	2.3843	0.3173	2.5724

Uncertainties results ZONA2 core:

Table 2.3: Uncertainties on the β_{eff} with JEFF-3.1.1 and COMAC-V1 in ZONA2 core

Isotope	Fission	Capture	Elastic	Inelastic	n.xn	Nu total	Nu delayed	Total Fission Spectrum	Total
U235	0.0013	0.0019	0.0003	0.0008	0.0000	0.0018	0.0377	0.0046	0.0381
U238	**2.6538**	**0.4860**	0.0880	**0.8504**	0.0161	0.3456	**1.5090**	0.2022	3.0002
Pu238	0.0005	0.0003	0.0001	0.0001	0.0000	0.0022	0.0071	0.0007	0.0075
Pu239	**0.9100**	0.0796	0.0070	0.0942	0.0018	0.0121	**1.7325**	0.2169	1.9728
Pu240	0.0509	0.0093	0.0064	0.0236	0.0009	0.0048	0.2058	0.0769	0.2242
Pu241	0.0032	0.0039	0.0003	0.0039	0.0005	0.0016	0.1372	0.0196	0.1387
Pu242	0.0038	0.0006	0.0002	0.0012	0.0001	0.0026	0.0287	0.0026	0.0292
Na23	0.0000	0.0036	0.0451	0.0427	0.0001	0.0000	0.0000	0.0000	0.0620
Fe56	0.0000	0.0069	0.0533	0.0662	0.0000	0.0000	0.0000	0.0000	0.0852
O16	0.0000	0.0701	0.1085	0.0023	0.0000	0.0000	0.0000	0.0000	0.1292
Cr52	0.0000	0.0039	0.0035	0.0068	0.0000	0.0000	0.0000	0.0000	0.0086
TOTAL	2.8060	0.4974	0.1562	0.8418	0.0162	0.3459	2.3113	0.3070	3.6046

Table 2.4: Uncertainties on the β_{eff} with JEFF-3.2 and COMAC-V2 in ZONA2 core

Isotope	Fission	Capture	Elastic	Inelastic	n.xn	Nu total	Nu delayed	Total Fission Spectrum	Total
U235	0.0013	0.0016	0.0003	0.0008	0.0000	0.0018	0.0379	0.0045	0.0383
U238	**1.3243**	0.1767	0.0948	**0.7080**	0.0865	0.3480	**1.5263**	0.2023	2.1753
Pu238	0.0005	0.0002	0.0001	0.0001	0.0000	0.0021	0.0070	0.0023	0.0077
Pu239	0.3913	0.0440	0.0135	0.0809	0.0018	0.0213	**1.7111**	0.2148	1.7709
Pu240	0.0443	0.0074	0.0054	0.0213	0.0008	0.0049	0.2086	0.0685	0.2230
Pu241	0.0033	0.0039	0.0003	0.0040	0.0005	0.0020	0.1367	0.0127	0.1375
Pu242	0.0038	0.0006	0.0002	0.0012	0.0001	0.0025	0.0285	0.0004	0.0289
Na23	0.0000	0.0050	0.0431	0.0577	0.0002	0.0000	0.0000	0.0000	0.0718
Fe56	0.0000	0.0065	0.0538	0.0693	0.0000	0.0000	0.0000	0.0000	0.0879
O16	0.0000	0.0509	0.1127	0.0024	0.0000	0.0000	0.0000	0.0000	0.1237
Cr52	0.0000	0.0037	0.0035	0.0084	0.0000	0.0000	0.0000	0.0000	0.0098
TOTAL	1.3816	0.1634	0.1622	0.7180	0.0866	0.3487	2.3070	0.3032	2.8226

Uncertainties due to nuclear data are reduced with JEFF-3.2 nuclear data thanks to a great work on U238 and Pu239 fission cross section. These results show that uncertainties on ν_d data must be improved.

Appendix B

This page has been left blank intentionally

Publications

G. RIMPAULT, D. BLANCHET, P. DUFAY, J. TOMMASI, G. TRUCHET, “
“Uncertainty Quantification of Delayed Neutron Fraction of U235 Bases Fuel Cores”,
PHYSOR 2016, Unifying Theory and Experiments in the 21st Century, May 1-5, 2016 Sun Valley, Idaho, US

G. RIMPAULT, P. DUFAY, V. HUY,
“**Analysis of Material Buckling Experiments Performed in the MASURCA Facility in Support of the Astrid SFR Prototype Core Balance”,**
PHYSOR 2016, Unifying Theory and Experiments in the 21st Century, May 1-5, 2016 Sun Valley, Idaho, US

P. DUFAY, G. RIMPAULT, J.TOMMASI, G. TRUCHET
“Evaluation of beff measurements from BERENICE programme with TRIPOLI4® and uncertainty qualification”
Progress in Nuclear Energy 101 (2017) 312-320

P. DUFAY, G. RIMPAULT,
“Evaluation of βeff measurements from BERENICE programme with TRIPOLI4® and uncertainties quantification”, IAEA-CN-245-218,
International Conference on Fast Reactors and Related Fuel Cycles: Next Generation Nuclear Systems for Sustainable Development (FR17), Monday 26 June 2017 - Thursday 29 June 2017, Yekaterinburg, Russia

I.-A. KODELI, G. RIMPAULT, P. DUFAY, Y. PENELIAU, J. TOMMASI, E. FRIDMAN, W. ZWERMANN, A. AURES, E. IVANOV, K. IVANOV, Y. NAKAHARA, T. IVANOVA, J. GULLIFORD, **“Uncertainty Analysis of Kinetic Parameters for Design, Operation and Safety Analysis of SFRs”, IAEA-CN-245-136,**
International Conference on Fast Reactors and Related Fuel Cycles: Next Generation Nuclear Systems for Sustainable Development (FR17), Monday 26 June 2017 - Thursday 29 June 2017, Yekaterinburg, Russia

P. DUFAY, G. RIMPAULT
“Development of the nuclear data sensitivity calculations with the GPT method of SVRE central components. Transferability from the PRE-RACINE cores to the ASTRID core.”, Paper BEPU2018-254,
ANS Best Estimate Plus Uncertainty International Conference (BEPU 2018) Real Collegio, Lucca, Italy, May 13-19, 2018

P. DUFAY, G. RIMPAULT
“A new approach for analyzing the impact of nuclear data uncertainties on the ASTRID sodium void reactivity effect”
PHYSOR 2018 - 22/04/2018 - 26/04/2018, Cancun, Mexique

G. RIMPAULT, P. DUFAY, J. TOMMASI, F. MELLIER
“Looking forward for a MASURCA experimental programme GENESIS in support to the ASTRID SFR core”
PHYSOR 2018 - 22/04/2018 - 26/04/2018, Cancun, Mexique

G. RIMPAULT, P. DUFAY, G. TRUCHET, P. LECONTE, I. KODELI
“Assessing the Uncertainty of Reactivity Worth Scale Measurements”
NENE 2018 - 10/09/2018 - 13/09/2018, Portoriz, Slovenia

P. DUFAY, G. RIMPAULT
“A new approach for analyzing the impact of nuclear data uncertainties on the ASTRID sodium void reactivity effect”
Annals of Nuclear Energy, Publication in Progress

Quantification des biais et incertitudes sur l'effet en réactivité de vidange sodium dans le cœur d'ASTRID à l'aide des mesures intégrales

Résumé en français

L'énergie nucléaire est l'une des plus propres en matière d'émission de gaz à effet de serre et, malgré ses atouts, elle n'est développée que dans quelques pays du monde. La sûreté reste une question ouverte pour l'avenir de cette énergie après l'accident de Fukushima. En France, la loi de 2006 sur la gestion des déchets soutient le développement d'une nouvelle génération de réacteurs nucléaires et du prototype de Réacteur Technologiquement Avancé au Sodium pour la Démonstration Industrielle (projet ASTRID) qui vise à apporter une réponse industrielle et technologique à de nombreux enjeux de ce siècle.

L'une des préoccupations de la technologie du Réacteur à Neutrons Rapides et caloporteur sodium (RNR Na) est la perte de ce dernier car elle pourrait entraîner un emballement de la réaction en chaîne si l'effet en réactivité de vidange sodium (SVRE) est positif. Lorsque le sodium est retiré du cœur, deux effets antagonistes se produisent qui affectent l'équilibre neutronique: l'un augmente la réactivité du cœur et est appelé la composante centrale (CC) et l'autre est la composante de fuite (LC) avec un effet négatif sur la réactivité. Maximiser la dernière composante est l'une des réponses pour augmenter la sûreté inhérente aux RNR-Na. C'est pourquoi le CEA a développé un concept de cœur innovant: le «Cœur à Faible Vidange» (CFV) qui donne une SVRE négatif. Cependant, de telles innovations doivent être validées expérimentalement et l'incertitude sur cet effet en réactivité doit être maîtrisée. En soutien au développement des RNR Na : la base de données expérimentale existante est assez importante (PRE-RACINE, CIRANO).

Dans les différents programmes expérimentaux considérés, la réactivité est mesurée sur une échelle en β_{eff} qui est la fraction neutronique retardée du cœur. Une nouvelle analyse des β_{eff} mesurés dans le programme BERENICE (dans l'installation MASURCA) a donc été faite en utilisant le code Monte Carlo TRIPOLI4® avec la méthode de probabilité de fission (IFP) nouvellement implémentée dans le code pour le calcul des intégrales d'importance.

L'effet de réactivité de vidange sodium se décompose en une composante centrale positive (dû à un effet de spectre) et une composante de fuites négative (dû à l'augmentation du libre parcours moyen des neutrons). Afin d'étudier en détail l'incertitude associée au calcul du SVRE, on a développé une procédure innovante basée sur la théorie des perturbations généralisées pour calculer les sensibilités de la CC et de la LC indépendamment. Avec de telles sensibilités et l'utilisation de la matrice de covariance COMAC-V2, on peut calculer les incertitudes dues aux données nucléaires sur chaque composante en utilisant des données nucléaires JEFF-3.2.

Le code Monte-Carlo TRIPOLI-4® donne des résultats de référence en utilisant les géométries «exactes » des cœurs mais la méthode des perturbations généralisées n'a pas encore été implémentée dans ce code. Le code déterministe ERANOS du CEA est donc utilisé en complément pour le calcul des sensibilités et incertitudes sur l'effet de vidange global mais aussi sur la composante centrale (CC) et la composante de fuites (LC). Une fois les simulations effectuées pour chaque configuration des divers programmes expérimentaux, il est possible d'ajuster les résultats d'ERANOS et de TRIPOLI-4 avec l'expérience grâce à un jeu de paramètre (α,β) et d'obtenir des incertitudes sur ces paramètres. Ce travail a été conduit pour l'ensemble des programmes expérimentaux considérés et a permis l'obtention de corrections à apporter aux composantes du cœur CFV en fonction de la représentativité des diverses zones y compris le plénum sodium et les incertitudes dues aux données nucléaires qui leur sont associées.

Cette thèse a donc permis de maîtriser les différentes sources d'incertitudes dans le calcul de la SVRE et d'utiliser les expériences intégrales pour prédire l'effet de réactivité de vidange sodium du cœur CFV d'ASTRID ainsi que son incertitude.

Quantification of biases and uncertainties on the sodium void reactivity effect in the ASTRID core using integral measurements

Abstract in english

The nuclear energy is one of the cleanest energy in regard of greenhouse gas emission and despite its assets is only developed in few countries in the world. Safety remains an open issue for the future of this energy after the Fukushima accident[1]. In France the 2006 law on the waste management ensures the development of a new generation of nuclear reactor and has lead to the Advanced Sodium Technology Reactor for Industrial Demonstration (ASTRID) which aims to bring an industrial and technological advanced answer to many issues of this century.

One of the concerns in the sodium cooled fast reactor (SFR) technology is the loss of sodium coolant accident because it might lead to a snowball effect in the chain reaction if the sodium void reactivity effect (SVRE) is positive. When the sodium is removed from the core, two antagonistic effects arise that affect the neutron balance: one increases the reactivity of the core and is called the central component (CC) and the other is the leakage component (LC) with a negative feedback on the reactivity. Maximizing the last component is one of the answer to increase the inherent safety of the SFRs. That is why the CEA has developed an innovative core design: the "Cœur à Faible Vidange" (CFV : Core with low void effect) which exhibits a negative SVRE. However, such innovations have to be experimentally validated and the uncertainty on this reactivity effect has to be mastered. In support of SFRs the existing experimental data base is quite large (PRE-RACINE, CIRANO, …).

In these experimental programme the reactivity have been measured by the position of shim rod or/and the addition of peripheral assemblies. A rod drop and the use of the Nordheim equation insures calibration of the reactivity. This reactivity is measured on a β_{eff} scale which is the delayed neutron fraction of the core. A new analysis of β_{eff} measured in the BERENICE programme (in the MASURCA facility) has been made using the TRIPOLI-4® Monte Carlo with the newly Iterated Fission Probability (IFP) method for calculating integrals of importance.

For analysing the sodium void reactivity effect, we split it into two components: the central component (CC) which is a positive reactivity effect due to spectrum changes and the leakage component (LC) which is a negative reactivity effect due to the increase of the neutron mean free path. In order to study in details the uncertainty associated to the SVRE, a development of an innovative generalized perturbation theory procedure for computing sensitivities of the CC and the LC to nuclear data has been conducted. With such sensitivities and the use of the COMAC-V2 covariance matrix, we are able to calculate the uncertainties due to nuclear data on each component using JEFF-3.2 nuclear data.

The Monte-Carlo code such as TRIPOLI-4® gives reference results by using "as-built" geometry of the core the generalized perturbation have not been implemented yet in this code that is why ERANOS the deterministic code for SFR at CEA is used in complement. Once simulations have been run for each experimental programme it is possible to adjust the results from ERANOS and TRIPOLI-4® to experimental ones. Independent adjustment according to the fuel composition, the core geometry lead to a set of parameter (α,β) to correct the CC and LC. This work provide a set dedicated to the CFV core of

[1] ranked at the level 7 of the INES scale

ASTRID to take into account the experimental feedback on the SVRE and it also gives the uncertainties associated to each component and to the set of parameter

This PhD thesis has been mastering the different sources of uncertainties in calculating the sodium void reactivity effect and use the integral experiments to predict the sodium void reactivity effect of the CFV core of ASTRID as well as its uncertainty.